The Importance of Pattern Recognition Receptors in Mycobacterial Immunity and Pathogenesis

Jean-Yves Dubé

Department of Microbiology & Immunology

McGill University, Montreal

Submitted September 2021.

A thesis submitted to McGill University in partial fulfillment of

the requirements of the degree of Doctor of Philosophy

ABSTRACT

Mycobacterium tuberculosis (*Mtb*) has afflicted humankind over centuries and continues to be one of the most lethal infectious agents globally. Although a clear role for host genetics during *Mtb* infection has defied decades of research efforts, some genes have been linked to altered immunity and to other mycobacterial infections, like the pattern recognition receptor (PRR) gene *NOD2*. Previous studies by our group demonstrated that NOD2 is important for innate and adaptive immune responses to mycobacteria. Mycobacteria have a unique cell wall modification, *N*-glycolylation of muramic acid, that renders the corresponding NOD2 ligand, muramyl dipeptide (MDP), more potent. Other groups have pointed to the unique mycobacterial molecule trehalose dimycolate (TDM) and its host PRR Mincle as key drivers of the mycobacterial immune response.

In this thesis, I aimed to measure the sufficiency and essentiality of NOD2 and Mincle signalling in innate and adaptive immune responses to mycobacteria, plus determine the importance of these pattern recognition receptors, alone and together, during mycobacterial infection. I hypothesize that NOD2 and Mincle are major pattern recognition receptors of mycobacteria and thus contribute to immunity and the outcome of infection.

We studied mycobacterial immunity in the context of Complete Freund's adjuvant (CFA, essentially dead *Mtb* in mineral oil). By using mycobacterial and murine knockouts plus chemical complementation, we demonstrated that the NOD2/MDP and Mincle/TDM pathways were essential for the mycobacterial adjuvant effect. Dendritic cell effector functions were synergistically augmented with a combination of synthetic *N*-glycolyl MDP and TDM. This

wholly synthetic adjuvant also induced experimental autoimmunity qualitatively similar to but quantitatively less than CFA, demonstrating that much of innate mycobacterial signalling comes from the NOD2 and Mincle pathways and that the reactogenic CFA can be substituted with a molecularly-defined adjuvant for future pharmacological optimization.

We next sought to define the importance of NOD2 and Mincle singly and in combination during infection with live *Mtb*. Aerosol infection of mice deficient in NOD2, Mincle or both receptors showed minor or insignificant differences in bacterial burden compared to wildtype controls. Mice without NOD2 (regardless of Mincle status) survived around 290 days post infection while wildtype counterparts survived longer than 363 days; Mincle deficiency alone was intermediate. Hastened mortality in NOD2 deficient mice was accompanied by weight loss, increased bacterial burden plus distinct pulmonary necrotic cell death. Using an established model of murine intraperitoneal *Mycobacterium avium paratuberculosis* infection, we similarly showed maintained bacterial control in PRR deficient mice with the trend of altered immunity, compared to wildtype controls.

We have demonstrated that PRRs are essential for the immune response elicited by mycobacteria in different contexts, yet their benefit to the host during infection is subtle. NOD2 was more important than Mincle in terms of survival, indicating that an immune response elicited by a PRR *per se* does not correlate with control or tolerance of infection. Acting as immune modifiers, the contribution of genetic variation in PRRs will need to be investigated with a nuanced approach.

RESUMÉ

Mycobacterium tuberculosis (*Mtb*) a affligé l'humanité au cours des siècles et continue d'être l'un des agents infectieux les plus mortels au monde. Bien que le rôle clair de la génétique de l'hôte au cours de l'infection par *Mtb* ait défié des décennies d'efforts de recherche, certains gènes ont été liés à une immunité altérée et à d'autres infections mycobactériennes, comme le gène du récepteur de reconnaissance de motifs moléculaires (PRR) *NOD2*. Des études antérieures de notre groupe ont démontré que NOD2 est important pour les réponses immunitaires innées et adaptatives aux mycobactéries. Les mycobactéries ont une modification de la paroi cellulaire unique, la *N*-glycolylation de l'acide muramique, qui rend le ligand de NOD2 correspondant, muramyl dipeptide (MDP), plus puissant. D'autres groupes ont postulé que la molécule mycobactérienne unique tréhalose dimycolate (TDM) et son PRR Mincle sont les principaux moteurs de la réponse immunitaire mycobactérienne.

Dans cette thèse, j'avais pour objectif de mesurer la suffisance et l'essentialité de la signalisation NOD2 et Mincle dans les réponses immunitaires innées et adaptatives aux mycobactéries, ainsi que de déterminer l'importance de ces récepteurs de reconnaissance de formes, seuls et ensembles, lors d'une infection mycobactérienne. J'ai émis l'hypothèse que NOD2 et Mincle sont des récepteurs majeurs de reconnaissance de formes de mycobactéries et contribuent ainsi à l'immunité et au résultat de l'infection.

Nous avons étudié l'immunité mycobactérienne dans le contexte de l'adjuvant complet de Freund (CFA, *Mtb* essentiellement mort dans l'huile minérale). En utilisant des mycobactéries et souris transgéniques ainsi que deux substitutions chimiques, nous avons démontré que les voies

NOD2/MDP et Mincle/TDM étaient essentielles pour l'effet adjuvant mycobactérien. Les fonctions effectrices des cellules dendritiques ont été augmentées de manière synergique avec une combinaison de *N*-glycolyl MDP et de TDM synthétiques. Cet adjuvant entièrement synthétique a également induit une auto-immunité expérimentale qualitativement similaire mais quantitativement inférieure à celle observée avec CFA, démontrant qu'une grande partie de la signalisation mycobactérienne innée provient des voies NOD2 et Mincle et que le CFA réactogène peut être remplacé par un adjuvant moléculairement défini pour une future optimisation pharmacologique.

Nous avons ensuite cherché à définir l'importance de NOD2 et de Mincle seuls et en combinaison lors d'une infection par *Mtb* vivant. L'infection par aérosol de souris déficientes en NOD2, Mincle ou les deux récepteurs a montré des différences mineures ou insignifiantes dans la charge bactérienne par rapport aux témoins de type sauvage. Les souris sans NOD2 (indépendamment du statut Mincle) ont survécu environ 290 jours après l'infection, tandis que leurs homologues de type sauvage ont survécu plus de 363 jours ; le déficit en Mincle seul était intermédiaire. La mortalité accélérée chez les souris déficientes en NOD2 était accompagnée d'une perte de poids, d'une augmentation de la charge bactérienne et d'une mort cellulaire nécrotique pulmonaire distincte. En utilisant un modèle établi d'infection intrapéritonéale murine à *Mycobacterium avium paratuberculosis*, nous avons également montré un contrôle bactérien maintenu chez des souris déficientes en PRR avec une tendance à une immunité altérée, par rapport aux témoins de type sauvage.

Nous avons démontré que les PRR sont essentiels pour la réponse immunitaire déclenchée par les mycobactéries dans différents contextes, mais leur bénéfice pour l'hôte pendant l'infection est subtile. NOD2 était plus important que Mincle en termes de survie,

indiquant qu'une réponse immunitaire déclenchée par un PRR en soi n'est pas corrélée avec le contrôle ou la tolérance de l'infection. Agissant comme des modificateurs immunitaires, la contribution de la variation génétique dans les PRR devra être étudiée avec une approche nuancée.

ACKNOWLEDGEMENTS

I thank my supervisor, Marcel Behr, for allowing me to mess around in his laboratory for several years. Marcel's has thoroughly encouraged me to pursue whichever direction, methodology or hypothesis was of interested to me, while ensuring that my activities were producing interpretable, quality data and were framed in the larger context. Generating useless knowledge with your guidance has been wonderful, especially when the accumulated results eventually moved the field forward. You are a rare teacher of an excellent level of science. I hope you find the adjectives are acceptable; I think they are warranted in this paragraph.

I have been lucky to also have many other remarkable teachers during my studies. Entering among such good company was admittedly intimidating, but I was firmly supported by Damien Montamat-Sicotte, a mentor of immunology and life for me in my first two years, and a remarkable individual. Once established, I was only able to continue being productive because of Fiona McIntosh, lab manager but also much more, without whom little of this research would be possible. Damien and Fiona, together with Marwan Ghanem, Joyce Wang, and many other Behr lab alumni: the environment created in our team was amazing! Thank you for these years.

I am very grateful to Sam David and the members of his lab for very generously instructing and assisting me in the methods of neuroscience. I thank Jérôme Nigou for making Chapter II possible. For the useful feedback on my research, I also express my gratitude to my advisory committee members Samantha Gruenheid, Connie Krawczyk and Joyce Rauch. To members of the Schurr, Sheppard and Divangahi labs who have been vital, I am appreciative. I thank my parents and brothers for their continued support and outside perspective.

TABLE OF CONTENTS

LIST OF FIGURES

LIST OF TABLES

LIST OF ABBREVIATIONS

ADP	adenosine diphosphate
Ag	antigen
AIDS	acquired immunodeficiency syndrome
AIM2	absent in melanoma 2
APC	allophycocyanin
ATP	adenosine triphosphate
BCG	bacille Calmette-Guérin
BMDC	bone marrow-derived dendritic cell
BMDM	bone marrow-derived macrophage
BUV	brilliant ultraviolet
BV	brilliant violet
CARD	caspase activation and recruitment domain
CDC	Centers for Disease Control and Prevention
cDC	conventional dendritic cell
c-di-AMP	cyclic-di-adenosine monophosphate
CFA	complete Freund's adjuvant

CFU	colony-forming unit
cGAS	cyclic GMP–AMP synthase
CIA	collagen-induced arthritis
CLR	C-type lectin receptor
CMI	cell-mediated immunity
CNS	central nervous system
COVID-19	coronavirus disease 2019
Cy	cyanine
DC	dendritic cell
DC-SIGN	DC-specific intercellular adhesion molecule-3-grabbing non-integrin
Dectin	dendritic cell-associated C-type lectin
DKO	double knockout
DNA	deoxyribonucleic acid
DTH	delayed-type hypersensitivity
EAE	experimental autoimmune encephalomyelitis
ELISA	enzyme-linked immunosorbent assay
ELISpot	enzyme-linked immunosorbent spot assay
ESAT-6	6-kDa early secretory antigenic target

ESX-1	ESAT-6 secretion system 1
FcRγ	Fc receptor γ chain
FITC	fluorescein isothiocyanate
FSC	forward scatter
HIV	human immunodeficiency virus
H&E	hematoxylin and eosin
IFA	incomplete Freund's adjuvant
IFN	interferon
IGRA	interferon gamma release assay
IL	interleukin
ITAM	immunoreceptor tyrosine-based activation motif
KO	knockout
LAM	lipoarabinomannan
LPS	lipopolysaccharide
LRR	leucine-rich repeat
MAC	*Mycobacterium avium* complex
MAMP	microbe-associated molecular pattern
ManLAM	mannose-capped lipoarabinomannan

Map	*Mycobacterium avium* subspecies *paratuberculosis*
MAPK	mitogen-activated protein kinase
MARCO	macrophage receptor with collagenous structure
MCL	macrophage C-type lectin
MDP	muramyl dipeptide
MFI	median fluorescence intensity
MHC	major histocompatibility complex
Mincle	macrophage-inducible C-type lectin
Mip	*Mycobacterium indicus pranii*
MOG	myelin oligodendrocyte glycoprotein
Mtb	*Mycobacterium tuberculosis*
MTBC	*Mycobacterium tuberculosis* complex
NamH	*N*-acetyl muramic acid hydroxylase
NBD	nucleotide-binding domain
NF-κB	nuclear factor κ-light-chain-enhancer of activated B cells
NIH	National Institutes of Health
NLR	NOD-like receptor
NLRP	NLR family pyrin domain-containing

NOD	nucleotide-binding oligomerization domain-containing
NTM	non-tuberculous mycobacteria
OVA	ovalbumin
PBS	phosphate buffered saline
PBMCs	peripheral blood mononuclear cells
pDC	plasmacytoid dendritic cell
PE	phycoerythrin
PGN	peptidoglycan
PIM	phosphatidylinositol mannoside
PPD	purified protein derivative
PRR	pattern recognition receptor
RD	region of difference
RIPK2	receptor-interacting serine/threonine-protein kinase 2
RNA	ribonucleic acid
RPMI	Roswell Park Memorial Institute
RR-EAE	relapsing-remitting EAE
SARS-CoV-2	severe acute respiratory syndrome coronavirus 2
SNP	single nucleotide polymorphism

spp.	species (plural)
SSC	side scatter
STING	stimulator of interferon genes
SYK	spleen tyrosine kinase
TB	tuberculosis
TBVI	TuBerculosis Vaccine Initiative
TDB	trehalose-6,6'-dibehenate
TDM	trehalose-6,6'-dimycolate
Th	T-helper
TLR	Toll-like receptor
TNF	tumor necrosis factor
TST	tuberculin skin test
UDP	uridine diphosphate
UNAIDS	Joint United Nations Programme on HIV/AIDS
USDA	United States Department of Agriculture
UTP	uridine triphosphate
WHO	World Health Organisation
WT	wildtype

CONTRIBUTIONS TO ORIGINAL KNOWLEDGE

The major original findings presented in this thesis are summarized below:

1. First to systematically review and present the literature results on PRR KOs during *Mtb* infection of mice:
    a. PRRs are largely dispensable for bacteriologic control and survival
    b. PRR KOs result in immunologic changes that should be sought in human studies
2. First to demonstrate synergy between NOD2 and Mincle pathways in DCs stimulated with *N*-glycolyl MDP and GlcC14C18:
    a. In DC expression of MHC (signal 1), costimulatory molecules (signal 2) and cytokine (signal 3)
    b. *N*-glycolyl MDP was more potent and efficacious than *N*-acetyl MDP in DCs
3. Rationally deconstructed CFA, identifying essential MAMPs, and formulated a wholly synthetic adjuvant with corresponding MAMPs, *N*-glycolyl MDP and GlcC14C18:
    a. *namH*, *Nod2* and *Mincle* were essential for CFA adjuvancy
    b. *N*-glycolyl MDP plus GlcC14C18 upregulated DC effector functions *in vivo*
    c. *N*-glycolyl MDP plus GlcC14C18 generated T-cell immunity *in vivo*
    d. *N*-glycolyl MDP plus GlcC14C18 produced EAE comparable to CFA
4. First to cross C57BL/6 *Mincle*-/- mice with C57BL/6 *Nod2*-/- mice to generate *Mincle*-/-*Nod2*-/- double knockout (DKO) mice:
    a. DKO mice did not have severe immune deficiency compared to single knockouts
    b. DKO mice controlled mycobacterial infection similar to single knockouts

5. First to quantify survival of *Mincle*-/- and DKO mice during *Mtb* infection:
    a. *Mincle*-/- survival was intermediate between *Nod2*-/- and WT
    b. DKO survival was indistinguishable from *Nod2*-/-
6. First to show pathology associated with *Nod2* deficiency at *Mtb*-caused mortality in mice
    a. Altered pulmonary immunity manifested as increased volume of cell death
    b. Distinct necrotic foci in the lungs

CONTRIBUTIONS OF AUTHORS

This thesis was written by Jean-Yves Dubé with assistance and editing from Dr. Marcel A. Behr. It was prepared according to the guidelines provided by McGill University's Graduate and Postdoctoral Studies unit. The format of the thesis is "manuscript-based". The work presented herein was conducted entirely under the supervision of Dr. Marcel A. Behr. Below is a chapter-by-chapter breakdown of contributions.

Chapter I – General Introduction

Jean-Yves Dubé created the entirety of this chapter with the assistance of Dr. Marcel A. Behr save for the inset adapted manuscript:

Dubé J-Y, Fava VM, Schurr E and Behr MA. Underwhelming or Misunderstood? Genetic Variability of Pattern Recognition Receptors in Immune Responses and Resistance to Mycobacterium tuberculosis. *Front. Immunol*. 2021 June 30; 12:714808.

In this manuscript, Drs. Vinicius Medeiros Fava and Erwin Schurr wrote the original draft for the sections concerning human genetic associations with TB (Chapter I, sections 2.5 and 2.7). Jean-Yves Dubé jointly created the figure with Dr. Vinicius Medeiros Fava. Jean-Yves Dubé drafted the remainder of the manuscript, including the table. All four authors were involved in editing the manuscript for publication. All authors contributed to its conceptualization.

Chapter II – Dubé J-Y, McIntosh F, Zarruk JG, David S, Nigou J, Behr MA. Synthetic mycobacterial molecular patterns partially complete Freund's adjuvant. *Sci Rep.* 2020 April 3;10(1):5874.

Jean-Yves Dubé wrote the original manuscript and adapted it to this thesis. With input from Dr. Marcel A. Behr, all experiments and assays were designed, performed and analyzed by Jean-Yves Dubé with the following exceptions: in harvesting of lymph nodes and extracting their cells, Jean-Yves Dubé was assisted by one or two others per experiment including Fiona McIntosh, Damien Montamat-Sicotte, Daniel Houle, Sarah Danchuck and Andréanne Lupien; in EAE work, Juan G. Zarruk, performed animal injections and spinal cord extractions, and Orania Tsatas plus Laura Curan assisted Jean-Yves Dubé with spinal cord sectioning and staining. GlcC14C18 was prepared by Alexiane Decout with Jérôme Nigou. Writing of the manuscript was mostly accomplished by Jean-Yves Dubé, with assistance from Dr. Marcel A. Behr and suggestions on revision from all co-authors.

Chapter III – Dubé J-Y, McIntosh F, Duffy SC, Behr MA. Respective and combined disruption of *Mincle* and *Nod2* distinctly alter mycobacterial immunity and resistance. (Manuscript in preparation).

Jean-Yves Dubé wrote the original manuscript and adapted it to this thesis. With input from Dr. Marcel A. Behr, all experiments and assays were designed, performed and analyzed by Jean-Yves Dubé with the following exceptions: in various aspects of the work with *Mtb*-infected mice, JYD was assisted by Fiona McIntosh, Andréanne Lupien, Helena Strand Clemmensen and Sarah Danchuck. Shannon Duffy and Fiona McIntosh assisted with methodology and executing experiments with *Map*-infected mice. Writing of the manuscript was mostly accomplished by

Jean-Yves Dubé, with assistance from Dr. Marcel A. Behr and suggestions on revision from all co-authors.

Chapter IV – Discussion

Jean-Yves Dubé wrote the entirety of this chapter with input from Dr. Marcel A. Behr.

CHAPTER I – General Introduction

1 – The Mycobacteria-Human Interaction

Throughout history, humans and microorganisms have had a tumultuous relationship. The benefits provided by microbes to our lifestyles are innumerable, from food and digestion to making entire ecosystems possible. However, a minority of microorganisms are pathogenic and the resulting negative impacts on our species are substantial. The legacy of infectious diseases on the development and trajectory of humankind is hard to grasp, but we can vaguely sense its significance in considering some major events: plagues of *Yersinia pestis* claimed an estimated 200 million lives in the middle ages alone and continues to cause occasional but dangerous outbreaks [1]. Endemic since at least the Middle Ages, smallpox killed approximately 30% of those infected and left a similar proportion of survivors blind, up until eradication was declared in 1980 [2,3]. In two years, the pandemic of the 1918 strain of Influenza claimed 17 million lives globally, possibly more [4]. Many infectious diseases continue to flourish despite advances in medicine: Malaria kills 400,000 people annually (WHO); AIDS has killed around 36 million since the beginning of the HIV pandemic and just under one million per year in the last few years (UNAIDS); COVID-19 has killed over 4 million since SARS-CoV-2 was discovered at the end of 2019 (WHO). One disease in particular has both a bloodied past and present: tuberculosis (TB), caused by *Mycobacterium tuberculosis* (*Mtb*), is estimated to have killed over 1 billion people in the last 130 years alone and continues to kill over 1 million annually (NIH, WHO). This thesis addresses the immunological interactions between *Mtb* and humankind which influence our relationship with this deadly pathogen.

1.1 – The mycobacteria

The genus *Mycobacterium* belongs to the actinobacteria phylum. Other notable genera of actinobacteria are *Streptomyces*, *Nocardia*, *Corynebacterium*, and *Rhodococcus*. Mycobacteria are bacilli (rod-shaped), typically under 5 μm in length. Most mycobacteria species are soil or water dwelling, and their unique structural features evolved in such environments [5]. However, a few mycobacterial species have used their unique attributes for pathogenesis and a subset of these have evolved to be obligate pathogens. In a non-host environment, many mycobacteria are saprophytic and resemble fungal hyphae in that they grow in fibres, hence the prefix 'myco' in the name *Mycobacterium*, dubbed by Lehmann and Neumann in the 19th century [6]. Some mycobacteria, like *Mtb*, form distinct rough colonies when grown on solid media [7], while others are smooth [8]. Many of the mycobacteria are considered slow-growing, requiring hours to days to complete one replication. In contrast, *Escherichia coli* replicates in as fast as 20 minutes.

While they do not properly stain Gram-positive like certain other actinobacteria, mycobacteria stain acid-fast, and this criterium is used in the diagnosis of infection. The rationale of acid-fast-staining is based on the distinct cell envelope of *Mycobacterium* species (fig. 1). Like other bacteria, a cell wall of peptidoglycan (PGN) is located around the plasma membrane of the cell. However, beyond this, mycobacteria possess a unique second membrane called a 'mycomembrane'. Unlike the outer membrane of Gram-negative species (e.g. *E. coli*), the mycomembrane is anchored with arabinogalactan to the cell wall [5,9]. The mycomembrane is a highly hydrophobic barrier around the cell, making mycobacteria impermeable to Gram stains, but also retain the carbol fuchsin dye during *acid* alcohol washing in the Ziehl-Neelsen technique which renders the cells 'acid-fast' [10]. Mycobacteria also have a carbohydrate capsule forming the outermost surface of the cell which varies in composition across the genus [11,12].

1.1.1 – Mycobacterium tuberculosis complex

Mtb was established as the causative agent of TB by Robert Koch in 1882 by transferring material with the 'tubercule bacillus' from infected animals, to *in vitro* culture medium, and back into naïve animals to reproduce the disease. He announced his discovery to the Berlin Physiological Society on March 24th, 1882, and then in writing shortly after [7,13,14]. In the many years since Koch's momentous discovery, different subspecies and lineages of *Mtb* have been defined. The *Mycobacterium tuberculosis* complex (MTBC) comprises multiple different species that cause TB in humans and various animal hosts. They are highly genetically similar at the nucleotide level; over 99.9 % between lineages [15] and 97 % between subspecies [8]. However, genomic differences potentially contain or regulate virulence factors. It is not yet clear whether macroscopic (environmental/human-animal proximity) barriers limit zoonosis or whether interspecies transmission is limited by pathogen-host specialization. Nonetheless infection of non-traditional hosts occurs occasionally.

Hitherto, nine different lineages of *Mtb* have been described that infect humans, based on genetic phylogeny, where lineages 2, 3 and 4 cause most human TB. Along with 2, 3 and 4, linage 1 and 7 comprise "*Mtb sensu stricto*". Linages 5 and 6 are restricted geographically to west Africa, are referred to as *Mtb* subspecies africanum, and are less capable of causing disease [16,17]. Lineage 8 was recently defined from isolates in the African Great Lakes region as a 'sister lineage' of the MTBC, having certain genetic regions more similar to the smooth, divergent *Mycobacterium canettii* [18]. A lineage 9 was yet more recently described and is also restricted to Africa [19]. The global distribution of lineages 2, 3 and 4 was partly explained by greater virulence in animal models from deletion of the TbD1 region of the genome, which is retained in the other 'ancestral' (i.e. less human-adapted) linages [20]. In the laboratory, one of the most common

strains used is the H37Rv strain, which was the first *Mtb* strain to have its genome sequenced and assembled [21]. H37Rv is from linage 4 and was first isolated at the Trudeau Institute at Saranac Lake in upstate New York [22].

TB can be caused by other MTBC species for which the reservoirs are in animals. A notable example is *M. bovis*, which causes bovine TB in cattle, zoonotic TB in humans, and is the source species for the Bacille Calmette-Guérin (BCG) vaccine developed by French microbiologists Calmette and Guérin a century ago [23]. Interestingly, *M. orygis* (MTBC isolated from the oryx [24]) was recently detected in multiple TB cases in India, while zero *M. bovis* isolates were detected from the same sampling, suggesting that bovine TB and/or zoonotic TB in the region may be caused by *M. orygis* than *M. bovis* [25]. There are a handful of other MTBC species, including *M. caprae* (the goat bacillus), *M. microti* (infects rodents and shrews) and *M. pinnipedii* (seal bacillus), which occasionally also infect humans.

1.1.2 – *M. leprae and M. lepromatosis*

Mycobacterium leprae is another important mycobacterium in terms of human disease. Leprosy has afflicted the human body and conscience for millennia and continues to newly infect about 200,000 people per year, causing physical disability in the untreated. By infecting the skin, peripheral nerves, mucosa and eyes, *M. leprae* causes immunopathology, neuropathy and eventually deformity and disability. Leprosy occurs along a spectrum from tuberculoid (paucibacillary, small bacterial burden) to lepromatous (multibacillary, large bacterial burden) [26]. Additionally, the host can react differently to the infection in what are well defined as lepra reactions: type 1 involves increased cell-mediated inflammation of existing lesions; type 2

involves sudden antibody and immune complex formation with widespread inflammation [27]. These differences in disease presentation have been defined as endophenotypes of leprosy, which is the exophenotype [28]. Treating leprosy requires a combination of drugs (dapsone, rifampicin and clofazimine) for 6 to 12 months (WHO).

M. leprae DNA has been detected and sequenced with impressive coverage from human remains approximately 1,000 years old around Europe [29,30]. The *M. leprae* genome is degenerate in comparison to *Mtb* [31], indicative of an obligate pathogen that has acquired a specific, restricted lifestyle. *M. leprae* spreads between people, but transmission between the nine-banded armadillo (a natural *M. leprae* reservoir) and humans is also probable [32]. A new similar species, *M. lepromatosis,* was recently described in from two people with lepromatous leprosy [33]. Recently, Red squirrels in the British Isles were shown to uniquely carry both *M. leprae* and *M. lepromatosis* and hence two animal reservoirs are known [34,35]. *M. leprae* is uncultivable in standard laboratory animals or culture medium, making the study of its virulence difficult.

1.1.3 – *Non-tuberculous mycobacteria (NTM)*

Mycobacterium spp. which are neither part of the MTBC nor *M. leprae* nor *M. lepromatosis* are called non-tuberculous mycobacteria (NTM). NTM include *bona fide* pathogens and opportunists. The difference in ability for the various NTM and MTBC to cause pathology has aided research into the mechanisms of mycobacterial disease, using comparative genomics combined with molecular biology and immunology.

Mycobacterium kansasii is an opportunistic NTM that is relatively genetically similar to the MTBC [36]. It was first described in the 1950s as the “yellow bacillus” because of its

pigmentation before being officially renamed "the mycobacterium of Kansas" [37,38]. It can be found in tap water and cause TB-like lung disease in the immunocompromised or those who have prior lung dysfunction. Because of its relatedness to the MTBC, it has been used to model the pathoevolution of *Mtb* by heterologous expression of *Mtb*-specific-genes in *M. kansasii* [39]. A "*M. kansasii* complex" (MKC) was recently described by sequencing hundreds of globally isolates from water and clinical sources, along with the suggestion that the MKC's success in infecting humans can be explained by its relative genetic homology to *Mtb* [40].

Mycobacterium marinum was first isolated from saltwater fish of a Philadelphia fish tank by Aronson in the 1920s [41]. Human *M. marinum* infection is often acquired from exposure to a contaminated fish tank [42], and hence the term "fish tank granuloma" is used to describe the ensuing pathology that forms in the infected skin. *M. marinum* is a useful model organism for studying macrophage granulomas in the zebrafish (*Danio rerio*), where mechanisms of mycobacterium-macrophage biology can be directly visualized [43,44].

Mycobacterium ulcerans is relatively closely related to *M. marinum*. *M. ulcerans* causes Buruli ulcer, a lesion afflicting the skin, and sometimes bone, which can grow to debilitating size. The disease was first described by Cook in Uganda at the end of the 19th century, and the organism was first isolated by MacCallum with samples from Bairnsdale, Australia, in the 1930s (WHO). It is a very slow-growing mycobacterium (replication time of 1-3 days when cultured *in vitro* [45]) and therefore difficult to study. Possibly its most unique feature is the production of mycolactone, which is responsible for the distinct pathology *M. ulcerans* causes [46].

The *Mycobacterium avium* complex (MAC) may include the (sub)species *avium*, *intracellulaire* and *chimaera*, or others depending on the field [47]. These opportunistic pathogens are found in the environment or animal hosts (e.g. livestock), but also cause disease in

immunocompromised humans. Persons with bronchiectasis, chronic obstructive pulmonary disease or cystic fibrosis are vulnerable to pulmonary MAC. The spread of HIV resulted in a MAC epidemic: people with low CD4+ T cell counts as a result of AIDS are particularly vulnerable but restoring T-cell numbers with antiretroviral therapy helps [48]. MAC can be treated with clarithromycin, azithromycin, ethambutol or rifabutin. However, the five-year all-cause mortality rate is approximately 27 % in developed countries [49].

Mycobacterium avium paratuberculosis (*Map*) is a subspecies of *M. avium* that infects ruminants. As established by Twort and Ingram in 1912, it is the cause of Johne's disease in cattle, often presenting as an infection of the small intestine that causes diarrhoea, emaciation, and death [50]. Most herds in the USA contain at least one infected animal (USDA). *Map* has been detected by polymerase chain reaction and culture from raw milk as well as pasteurized or processed dairy around the world, including developed countries, indicating that human *Map* infection is possible through food products [51]. Because of similarities in intestinal pathology and details of mycobacterial genetic susceptibility that are discussed later, *Map* has and continues to be hypothesized to play a role in Crohn's disease [52]: Crohn's disease most often afflicts the terminal ileum of the small intestine, but can manifest anywhere along the digestive tract, typically as chronic granulomatous inflammation [53,54]. It is commonly experienced as abdominal pain, diarrhea, fatigue, and malnutrition.

Phylogenetically close to MAC species, *Mycobacterium indicus pranii* (*Mip*, formerly known as *Mycobacterium w*) was selected from a collection of atypical mycobacteria in the 1970s for its useful immunomodulatory effects against *M. leprae* [55,56]. This non-pathogenic mycobacterium is being studied as an immunotherapeutic agent for various conditions (discussed later in section 3 of this chapter).

The mycobacteria described hitherto are slow-growing species, with replication times over 12 hours. The *Mycobacterium abscessus* complex (MABC) comprises three species of fast-growing mycobacteria: *abscessus, bolletii* and *massiliense* [57]. MABC species most often cause lung and skin disease (CDC). They are common infections in people with cystic fibrosis due to compromised function of the respiratory tract (~15% of patients) and are naturally resistant to known-antimycobacterial drugs, making MABC treatment difficult [58].

Another well-studied fast-growing mycobacterium is *Mycobacterium smegmatis*. It is a completely non-pathogenic species, making it a convenient model organism for mycobacteria. It was first isolated and characterized by Alvarez and Tavel in normal smegma while looking to confirm the reports from Lustgarten of an acid-fast bacillus in syphilitic secretions [59]. *M. smegmatis* is useful for developing mycobacterial molecular biology methods because of its safety, speed of growth and thorough characterization.

1.2 – Tuberculosis (TB)

TB is an ancient disease, known to have afflicted humans for millennia. Scientific efforts have aimed to describe the pathogenesis of TB for centuries. Over this time TB has gone by many names, including 'phthisis,' 'consumption' and the 'white plague'. Descriptions of illness consistent with TB were reported by Hippocrates [60], and the Greek historian Herodotus nearly 2,500 years ago [61]. Laënnec suspected the "tubercule" was the common feature of the disease, and the name "tuberculosis" was subsequently coined by Schönlein in 1839 [14]. Recently, traces of mycolic acids and MTBC-specific DNA sequences were found in a now-submerged 9,000 year-old settlement on the coast of Israel in the skeletal remains of a woman and ill infant [62]. *Mtb*-specific DNA was also found on a 3,000 year-old Egyptian mummy [63] and a 1,000 year-old

Peruvian mummy [64] with pathological features of TB. Based on genomic sequencing, the most recent common ancestor of the MTBC is estimated to have existed between 2,000 and 6,000 years ago [65,66].

1.2.1 – *Modern TB in humans*

Most people (>90%) who inhale *Mtb* to become infected never experience TB. Of those that do, the majority (~90%) progress to TB within 2-3 years of the primary infection [67]. Progression to TB more than three years after infection is exceptional, an extreme example being 33 years after primary infection [68,69]. TB is best known as a lung disease, but *Mtb* can afflict any part of the body. The most common symptoms of human pulmonary TB are persistent coughing, fever, night sweats and weight loss. Coughing up sputum and/or blood is also common (CDC and WHO). Occasionally, *Mtb* disseminates to different organs. *Mtb* infection in the spine (tuberculous spondylitis), especially the thoracic vertebrae, is called Pott's disease and can result in mechanical and/or neurological impairment [70]. Tuberculous cervical adenitis, also called scrofula, is another possibility [71], as are tuberculous meningitis or miliary (widely disseminated) TB. A surge of TB was observed concurrent with the spread of HIV at the end of the 20th century: HIV+ people are at a higher risk of developing TB. AIDS-associated TB is more often extrapulmonary and pulmonary cavitation is less frequent on radiological examination. Detection of AFB positive sputum is less likely and immune anergy is also possible, complicating testing [72]. While HIV+ people can have TB with normal CD4+ T cell counts, the risk of TB increases as CD4 counts decline with AIDS [73].

1.2.2 – Early stages of Mtb infection

Mtb infection involves numerous tissues over extended amounts of time. Additionally, the host's response can be varied by genetic and environmental factors. There are however defining elements of the host response to *Mtb*. After *Mtb* is inhaled, the first host cell to meaningfully interact with the bacillus is the alveolar macrophage, along with possibly a few epithelial cells [74]. Infection can be established with a single bacterium in both mouse [75] and primate models [76]. Within the first two weeks of infection, most *Mtb* in the lungs resides in alveolar macrophages, and their migration from the alveolar space into the lung interstitium provides a mechanism for *Mtb* to spread [74]. By three weeks post infection, with the recruitment of myeloid cells, monocyte-derived cells and PMNs become the predominant cell types to harbour *Mtb* in the lungs [74,77]. A few weeks pass before the adaptive immune response becomes detectable. Immune-based testing for infection is not recommended until 8-10 weeks post probable infection due to this delay (CDC). Dendritic cells (DCs) carry bacilli to the lymph nodes where the adaptive immunity can be instructed, but this also establishes a second site of infection [78-80]. The Ghon complex, composed of a primary, pulmonary lesion (Ghon focus) plus lymphadenopathy of the infected regional lymph node, demonstrates that *Mtb* is present in the lymphatic system. The Ranke complex is the healed, calcified Ghon complex, visible with radiology and indicative of a past primary infection.

1.2.3 – The Granuloma: Containment and Transmission

The characteristic pathology caused by mycobacteria is the granuloma. It is formed of macrophages that surround the bacteria in an attempt to destroy, or at least contain the invader.

In humans, these macrophages become activated and 'epithelioid-like': enlarged with elongated nuclei. A layer of lymphocytes surrounds the macrophages where adaptive immunity is present and the granuloma can form a fibrotic shell. Other cells in the area include a few neutrophils, DCs and giant multinucleated cells [43]. Over time, macrophages become 'foamy' in appearance (by H&E) owing to the accumulation of lipid drops within. Necrosis of the granuloma can also occur, and a granuloma can become 'caseous'. The caseum is a lipid-rich environment formed largely of necrotized foamy macrophages and supports extracellular *Mtb* [81]. The granuloma is a proinflammatory environment while the living tissue buttressing caseum is relatively anti-inflammatory [82]. Interestingly, the formation of a granuloma and subsequently a necrotic cavity is essential for efficient transmission of *Mtb* via aerosolization [83], and thus the immune response to *Mtb* is also necessary for its lifecycle.

While animals are useful to model human TB, mice for example do not produce 'true' granulomas with activated macrophages. Common mouse strains like C56BL/6 and BALB/C have little pulmonary necrosis, while the C3HeB/FeJ (Kramnik) mouse develops 'necrotic microfoci' [84,85]. Guinea pigs, rabbits and non-human primates produce necrotic granulomas. As lesions mature, they may calcify and sterilize, or they may become caseous and cavitary. Comparing FDG-PET-CT scans over time, human pulmonary TB lesions were shown to be highly dynamic, diverse and greatly fluctuated in size and inflammatory activity over just two months [84]. More of these features of human granulomas were recapitulated in the mouse when the inoculum of infection was representative of the human infection (one to three founding bacilli, as opposed to the common 50 to 100 dose) [75].

1.2.4 – Diagnosis and treatment of Mtb infection

Mtb infection is easily diagnosed with the tuberculin skin test (TST, also called Mantoux or PPD test). Purified protein derivative (PPD) derived from *Mtb* is injected intradermally and the diameter of induration is read 48-72 hours later to permit the development of a delayed-type hypersensitivity (DTH) immune reaction. Induration equates to pre-existing DTH to *Mtb* antigens, indicating a mycobacterial infection [86]. However, caveats with this test include: 1) the immune response indicates a past infection which may or may not be ongoing (i.e. risk of false positive for live infection); 2) past NTM infection or BCG vaccination can sometimes cause an immune response to the mixture of proteins in PPD (false positive for *Mtb* infection) [87] ; 3) a severely immunocompromised individual may not mount a strong enough immune response (false negative). The interferon-gamma release assay (IGRA) utilizes pure *Mtb* antigens: 6-kDa early secretory antigenic target (ESAT-6), 10-kDa culture filtrate protein (CFP-10) and TB-7.7 (Rv2654). These antigens stimulate IFN-γ release from the patient's antigen-specific T cells *ex vivo*, giving a more specific result than PPD. IGRAs might also contain a mitogen positive control, to indicate that sufficient IFN-γ can be made from the individual's cells (e.g. QuantiFERON-TB Gold Plus). Thus the IGRA improves upon caveats 2 and 3 of the TST.

The diagnosis of TB often includes a chest roentgenogram to see if the lungs have abnormal densities indicative of infection (e.g. granulomas, scarring, cavitation, etc.). Definitive criteria for a TB diagnosis are acquired from the sputum. Observation of acid-fast bacilli under the microscope, growth of *Mtb in vitro*, or detection of *Mtb*-specific nucleic acids (e.g. via GeneXpert® (Cepheid)) from sputum demonstrates an individual is infected and contagious, and therefore should be treated.

Drug susceptible *Mtb* is typically cured with combinations of drugs: isoniazid, rifampin pyrazinamide and ethambutol are first-line antibiotics. However, drug resistant TB requires the use of second-line antibiotics, which generally have worse side-effects [88]. The course of antibiotic therapy is typically 6 to 9 months in duration (CDC). Over this extended period of time, liver toxicity, neuropathy, discoloration of skin and secretions, and other adverse effects can occur.

Because most people who are TST positive do not develop TB in their lifetime, a diagnostic that accurately predicts risk of developing TB is of immense interest. Currently, blood transcriptional signatures are being investigated for their predictive value, with some promising leads, but as yet are deemed only predictive enough for triage, not confirmation [89]. Signatures are limited to usefully predicting imminent conversion of incipient TB to active TB (i.e. within a 3-6 month range) [90]. Ideally, antimycobacterials could be given only to those who are highly likely develop TB or already have TB, which would be more efficient and ethical than treating all TST positive individuals (vis-à-vis costs and drug toxicity).

A vaccine that reliably prevents or treats adult pulmonary TB would be also ideal. However, TB vaccine development is hampered by the lack of knowledge of correlates of protection [91]. Although possessing a strong immunological profile in terms of antigen-specific T cell development, the experimental MVA85A vaccine failed to demonstrate protection in humans in a phase 2b study [92]. Current promising candidates include the M72/AS01$_E$ (which showed 50% protection against TB over three years [93]), BCG modified to express listeriolysin (which uniquely elicited IL-17+ CD8+ T cells compared to BCG) [94] and *Mip* (discussed in section 3 of introduction) (TBVI). Host-directed therapies to treat TB are also under development. Such treatments will need to appropriately promote or supress inflammatory

processes at the right time to increase bacterial clearance while limiting collateral lung damage from host effectors [95].

1.3 – Molecular Mechanisms of Mycobacterial Disease

Not all mycobacteria cause disease. By comparing genomes of pathogenic mycobacteria with harmless ones, genes encoding virulence factors have been discovered over the last few decades. Comparisons of extracts of different mycobacteria have also revealed unique molecules in pathogenic species. These studies have revealed that *Mtb* manipulates the phagosomal environment of the macrophage to avoid phagosomal maturation and the associated microbial killing mechanisms like low pH, reactive oxygen species and antimicrobial peptides. It is also becoming apparent that *Mtb* evades and manipulates aspects of the immune response by controlling its recognition by immune sensors.

Possibly the most well-studied virulence factor in *Mtb* is the type VII secretion system called ESX-1 (ESAT-6 secretion system 1). ESX-1 is composed of genes named esxA to esxW encoding various proteins, where esxA (encoding ESAT-6) and esxB (encoding CFP10) are relatively well studied. ESAT-6 participates in disruption of host cell membranes, creating admixture of phagosomal and cytosolic content, and is essential for a *Mtb*-host-membrane contact-dependent mechanism of phagosomal rupture [44]. ESAT-6 is a major secreted antigen of *Mtb* to which immunity is readily relatively rapidly generated [96], and thus it is used in the IGRA. ESX-1-dependent phagosomal permeabilization has a distinct effect on the recognition of the invading mycobacterium and ensuing cellular response, favouring type I IFN production [97].

Mycobacteria contain many lipid virulence factors. Phthiocerol dimycoserates (PDIM) are lipids found in the mycomembrane and were associated with virulence in the mouse model [98,99]. PDIM may mask other elements (like microbe-associated molecular patters, MAMPs) on the surface of *Mtb* to evade immunity [100], and aid in phagosomal and cellular escape [101]. A screen for *Mtb* mutants unable to prevent phagosome acidification identified loci for lipid synthesis, one of which encodes genes for the synthesis of the terpene-nucleoside 1-tuberculosinyladenosine (1-TbAd) [102,103], which aids in phagosomal disruption through a pH mechanism [39,104]. *Mtb* also produces a sulfolipid that stimulates nociceptive neurons in the airways to induce cough: this is technically a case of a transmission factor, not a virulence factor *per se* [105].

Mtb produces products that alert the immune system. This might seem surprising; however, the mammalian innate immune system has evolved to sense microbe-associated molecular patterns (MAMPs) which are common between large groups of microbes. At some point in the past, the ancestor of *Mtb* was not an obligate pathogen, and therefore its MAMPs evolved without host selective pressure. What is interesting however, are MAMPs or MAMP modifications which are seemingly unnecessary for *Mtb* survival but are retained in all *Mtb* isolates. For example, mycobacterial PGN contains a distinct, *N*-glycolyl group, rather than the common *N*-acetyl group, on muramic acid,[106,107] and this makes the bacteria more immunogenic [108,109]. This modification is non-essential for survival, since it can be deleted from *M. smegmatis* and *Mtb* [108,109], and is degenerate in the *M. leprae* genome [110]. It is seemingly retained by purifying selection. In the following section of the General Introduction, I discuss the role of MAMPs and their host receptors in *Mtb* infection from an evolutionary standpoint.

2 – Underwhelming or misunderstood? Genetic Variability of Pattern Recognition Receptors in Immune Responses and Resistance to *Mycobacterium Tuberculosis*

(This section is adapted from a review article published in *Frontiers in Immunology*)

Jean-Yves Dubé [1, 2, 3], Vinicius M. Fava [2, 3], Erwin Schurr [1, 2, 3, 4, 5], Marcel A. Behr [1, 2, 3, 5]

1. Department of Microbiology and Immunology, McGill University, Montreal, Quebec, Canada
2. Program in Infectious Diseases and Immunity in Global Health, The Research Institute of the McGill University Health Centre, Montreal, Quebec, Canada
3. McGill International TB Centre, Montreal, Quebec, Canada
4. Department of Human Genetics, Faculty of Medicine, McGill University, Montreal, Quebec, Canada
5. Department of Medicine, Faculty of Medicine, McGill University, Montreal, Quebec, Canada

2.1 – Abstract

Human genetic control is thought to affect a considerable part of the outcome of infection with *Mycobacterium tuberculosis* (*Mtb*). Most of us deal with the pathogen by containment (associated with clinical "latency") or sterilization, but tragically millions each year do not. After decades of studies on host genetic susceptibility to *Mtb* infection, genetic variation has been discovered to play a role in tuberculous immunoreactivity and tuberculosis (TB) disease. Genes encoding pattern recognition receptors (PRRs) enable a consistent, molecularly direct interaction between humans and *Mtb* which suggests the potential for co-evolution. In this review, we explore the roles ascribed to PRRs during *Mtb* infection and ask whether such a longstanding and intimate interface between our immune system and this pathogen plays a critical role in determining the outcome of *Mtb* infection. The scientific evidence to date suggests that PRR variation is clearly implicated in altered immunity to *Mtb* but has a more subtle role in limiting the pathogen and pathogenesis. In contrast to 'effectors' like IFN-γ, IL-12, Nitric Oxide and TNF that are critical for *Mtb* control, 'sensors' like PRRs are less critical for the outcome of *Mtb* infection. This is potentially due to redundancy of the numerous PRRs in the innate arsenal, such that *Mtb* rarely goes unnoticed. Genetic association studies investigating PRRs during *Mtb* infection should therefore be designed to investigate endophenotypes of infection – such as immunological or clinical variation – rather than just TB disease, if we hope to understand the molecular interface between innate immunity and *Mtb*.

2.2 – Introduction

Tuberculosis (TB) was the number one cause of death due to a single infectious agent, *Mycobacterium tuberculosis* (*Mtb*), in the year 2019 according to the WHO. SARS-CoV-2 has surpassed *Mtb* in the last year; however, deployment of vaccines and experience with containment measures should blunt the death rate from COVID-19 in the years to come, such that TB may reprise its role as the most important cause of infectious mortality. Near 40 million people have died from TB in the last 20 years while treatment has saved 60 million (WHO). Yet, in the same interval, an estimated 10- to 20-fold more people were infected but did not progress to disease [67,111]. Together, this suggests broad host control or tolerance of this pathogen, despite the important minority who progress to disease each year.

Our time together with *Mtb* has potentially spurred human adaptation to allow us as a population to subsist with this obligate pathogen. *Mtb* has been evolving to parasitize humans for millennia and within that time the relationship has possibly changed us too, when and where *Mtb* was endemic [65,66,112]. Current and past abundance of human genetic diversity allows researchers to test the importance of genetic variation in *Mtb* infection outcomes and infer an evolutionary response by our species to survive the *Mtb* pandemic. One example where *Mtb* has potentially exerted a purifying selection on humans is that of the *TYK2* P1104A variant, which was calculated to have decreased in western Europeans concomitant with endemic TB over the last two millennia [113,114]. The *TYK2* P1104A variant is known to disrupt IL-23-dependent IFN-γ production [113] and was associated with a 5-fold increased risk for developing TB in the contemporary UK biobank [115]. We are not aware of any evidence of positive selection of a TB resistance gene to date.

Is every case of TB a situation where the host genetic combination is vulnerable to *Mtb*? We can hypothesize a genetic combination impervious to *Mtb*. We may not have to extend our imagination very far, as there are documented cases of people who remain TST negative in high-burden settings, such that it is statistically unlikely that they have never inhaled *Mtb* (recently reviewed in [116]). Therefore, developing TB is, in part, a result of genetics, and not just being a human exposed to *Mtb*, a postulate supported by the 21% heritability estimate for household contacts in Peru progressing from TST positivity to TB [117]. Environmental parameters can also have an effect (e.g. level of exposure, lung damage, HIV co-infection) and thus in theory identical twins could have different outcomes with *Mtb* infection. *Mtb* also has variation which might contribute to a different outcome for the bacterium and the host: there are 9 lineages described to date [18,19,118] with some being deemed more virulent in experimental models [20].

Genetic variation creates differences that can fine tune a host-pathogen interaction, or abrogate it completely, resulting in altered immunity. One modality where there is a direct opportunity for co-evolution is in physical interactions between host molecules and *Mtb* molecules. These interactions can be placed into a few camps including: 1) between classical T-cell receptors and MHC molecules presenting microbial epitopes [119]; 2) between antibodies and cognate microbial ligands [120]; 3) between donor-unrestricted T cells and their respective mycobacterial epitopes presented on invariant host molecules operating analogously to MHC [121,122]; 4) between inborn sensors of microbial products, otherwise known as pattern recognition receptors (PRRs), and their cognate microbe-associated molecular patterns (MAMPs). By their nature as structural molecules, MAMPs are subjected to a stronger purifying selection than many proteins. Unlike T-cell receptors, PRRs cannot generate diversity within an individual, yet there is variability amongst human population PRR gene pools as discussed further below. Most of

all, should we even expect strong selective pressure on host PRRs to recognize *Mtb* MAMPs? In this paper, we sought to review what is known about the relative importance of the MAMP-PRR interaction for the mammalian host during *Mtb* infection primarily through two sources of data: 1) controlled animal experiments using engineered genetic knockouts (KOs) of PRRs; 2) natural experiments in humans where genetic diversity permits us to seek associations between polymorphisms and the course of *Mtb* infection. We later place this in perspective with genes known to have strong effects on animal outcomes and lastly discuss how to approach human genetic studies of PRRs in the years to come.

2.3 – PRRs and their functions against *Mtb* at the cellular level

The interactions between many PRRs, *Mtb* and *Mtb* MAMPs have been described over the last few decades and are summarized in figure 2. Various mechanisms have been uncovered by which PRR recognition of *Mtb* leads to a cellular effect. Immediately below, we briefly review the molecular functionality of the PRRs which have been demonstrated to mediate an immune response to mycobacteria. Whether these molecular and/or cellular effects translate to protection or pathology in the whole animal is examined in the subsequent section.

2.3.1 – Toll-like receptors

Toll-like receptors (TLRs) were the prototypical PRR fitting the hypothesis proposed earlier by Janeway Jr. [123] that there existed inborn sensors in animals for products common among groups of microbes but absent from the host, allowing host recognition of non-self invading microbes – a form of antibody or T-cell receptor for innate immunity. The discoveries

in the 1990s on the Toll gene of *Drosophila*, followed by work exploiting mutant forms of TLR4 in human cells and mice demonstrated that mammalian TLR4 was a sensor of Gram-negative endotoxin (a.k.a. lipopolysaccharide, LPS) [124-127]. In total there are 10 TLRs in humans (13 in mice), each with different microbial ligands and slightly varying effects. TLR2 cooperates with TLR1 or TLR6, as well as other PRRs like CD14, to sense mycobacterial lipoproteins and lipoglycans. Identified mycobacterial TLR2 ligands include LAM (non-capped araLAM and not ManLAM) [128,129], 19 kDa lipoprotein (LpqH), 38 kDa lipoprotein (PstS1) [130], PIMs (with differing activities) [131,132], 27 kDa lipoprotein (LprG) [133], and LprA [134] to name a few [135]. Mycobacteria including *Mtb* shed membrane vesicles containing TLR2 ligands that are sufficient to generate a TLR2-dependent immune response [136]. More recently *Mtb* sulfoglycolipids have been shown to be competitive TLR2 antagonists [137]. TLR4's mycobacterial ligands are less clear, but *Mtb* extracts have TLR4-dependent stimulatory activity; many proteins have been proposed as TLR4 agonists, with GroEL1 and 2 being examples [138]. TLR5, which recognizes flagellin, does not have a known mycobacterial ligand (mycobacteria do not swim – they float). TLR3, TLR7 and TLR8 recognize RNA, and recent reports revealed that they may respond to host and/or mycobacterial RNA during infection [139-141]. TLR9 recognizes CG-rich DNA (i.e. CpG motifs) and has been shown to contribute to the cellular response to *Mtb*'s CG-rich genomic DNA [142,143]. TLR10 has no known ligands, mycobacterial or otherwise. Murine TLR11, 12, and 13 are not reviewed here because they have no direct relevance to human health.

A complete review of TLR signalling, not specific to mycobacteria, has been recently published elsewhere [144]. Briefly, when TLRs are engaged and oligomerize on the membrane, adaptor proteins MyD88 or TRIF are recruited to the cytoplasmic side to form 'myddosomes' or 'triffosomes', respectively. These supramolecular platforms direct signalling events that lead to

activation of MAPK and NF-κB pathways, for example. Such signalling begins an inflammatory response by the cell which includes upregulation of costimulatory molecules and antigen presentation by MHC molecules, plus secretion of soluble factors like cytokines, in the cases of macrophages and dendritic cells (DCs).

2.3.2 – C-type lectin receptors

C-type lectin receptors (CLRs) are a large, diverse category of receptors of which some members function as PRRs by binding to MAMPs; other CLRs bind endogenous ligands or non-microbial exogenous ligands. The etymology of the name originates from some members requiring calcium (Ca^{++}, hence "C") to bind their respective carbohydrate ligands (hence "lectin"). There are both membrane-bound and soluble forms of CLRs. A full review of this complex category of PRRs has recently been published and provides more mechanistic detail than is presented here [145].

The mannose receptor (CD206) expressed on macrophages was shown to assist these phagocytes in uptake of the tubercule bacillus [146] with ManLAM being the mycobacterial ligand for CD206 [147]. The ManLAM-CD206 interaction was later demonstrated to uniquely induce IL-8 and cyclooxengenase expression via PPARγ, while PPARγ knockdown was associated with reduced bacterial growth and increased TNF production during monocyte-derived macrophage infection [148]. *Pparg*-KO mice had about half the pulmonary bacterial burden and reduced lung pathology than WT counterparts when aerosol infected with *Mtb* [149].

The CLR called DC-SIGN (Dendritic Cell-Specific Intercellular adhesion molecule-3-Grabbing Non-integrin, a.k.a. CD209) is a main receptor on DCs for binding to *Mtb* [150]. DC-

SIGN expressed on DCs has been show to interact with ManLAM [151], PIM6 [152] and capsular alpha-glucan [153]. The DC-SIGN homologues L-SIGN (human) and SIGNR1 (mouse, one of five homologues), have been shown to interact with ManLAM too [154]. DC-SIGN ManLAM ligation modulated TLR-induced signalling (e.g. NF-κB pathway) via Raf-1 [155,156].

MINCLE (Macrophage inducible Ca^{++}-dependent lectin receptor, encoded by *CLEC4E*) associates with FcRγ to bind mycobacterial cord factor trehalose-6,6'-dimycolate (TDM) and TDM is sufficient to induce granuloma formation in murine lungs if functional MINCLE and FcRγ are present [157]. MINCLE signals via the SYK-CARD9 pathway to lead to the production of proinflammatory cytokines [158]. *Card9*-KO mice succumb more quickly to *Mtb* than WT, associated with defective anti-inflammatory signalling presumably leading to lethal immunopathology [159]. MINCLE expression is low in resting macrophages, and first requires induction via signalling through MCL (encoded by *Clec4d* and not to be confused with MCL-1). MCL is also a FcRγ-coupled and TDM CLR but cannot mediate the same pro-inflammatory response on its own [160]. MINCLE and MCL expression are co-dependent [161,162].

Dectin-1 was shown to mediate part of the immune response of splenic DCs to *Mtb* [163]. *Mif*-KO mice have impaired survival and immunity compared to WT during aerosol infection with *Mtb* HN878 strain, while bacterial killing and cytokine production were nearly restored when *Mif*-KO cells were complemented with Dectin-1 (overexpressed). These results suggest the MIF defect mostly manifests in defective Dectin-1 signalling [164]. The mycobacterial ligand for Dectin-1 remains unknown. Dectin-2 was reported to recognize ManLAM [165,166], but pathogenesis studies have yet to be done with this CLR.

Recently, DCAR (dendritic cell immunoactivating receptor; encoded by *Clec4b1*), also a FcRγ-coupled CLR, was demonstrated to be a receptor of PIMs. DCAR is expressed on

monocytes and macrophages. *Clec4b1*-KO mice had partially defective immune responses and bacterial control during BCG infection [167].

2.3.3 – Soluble CLRs

Collectins are soluble, non-cell-bound proteins; they are CLRs in that they specifically associate with sugars on the surface of microbes to mediate an effect. Surfactant proteins (SP) are collectins that exist in pulmonary surfactant. SP-A promoted attachment and phagocytosis of *Mtb* by alveolar macrophages by a mechanism that required mannose receptor but not SP-A contacting *Mtb* [168,169]. SP-A supressed nitrite production from alveolar macrophages preventing *Mtb* killing and controlling bacterial growth [170]. SP-A was shown to bind to ManLAM [171] and APA, the alanine- and proline-rich antigenic glycoprotein [172]. SP-D binds to ManLAM and agglutinates *Mtb*, but in contrast to SP-A, SP-D reduced *Mtb* binding to macrophages [173]. Reduced uptake occurred without agglutination using a modified SP-D [174]. However, SP-D increased phagosome-lysosome fusion, but did not alter the respiratory burst [175].

The collectin mannan-binding lectin (MBL) and ficolins are serum-borne receptors that bind to microbes to initiate the complement cascade. MBL was first demonstrated to interact with *Mtb* and *M. leprae* sonicate [176]. Ficolins, of which there are at least three in humans and two in mice, are also part of the lectin-complement system. Ficolin-2 was shown to bind to *Mtb* to play a protective role involving opsonization and inflammatory signalling in macrophages [177]. Another group suggested ficolin-3 was important for agglutination and phagocytosis of *Mtb* [178]. MBL and ficolins were suggested to bind to ManLAM and/or Ag85 [179,180].

2.3.4 – NOD-like receptors

Nucleotide-binding oligomerization domain-containing (NOD)-like receptors (NLRs) are a group of cytoplasmic sensors. Reviews with more detail on their mechanisms of action than presented here have been published, for example [181]. Its members NOD1 and NOD2 are essential in the detection of peptidoglycan fragments D-glutamyl-meso-diaminopimelic acid (iE-DAP) and muramyl dipeptide (MDP), respectively [182-185]. Both NOD1 and NOD2 signal through the adaptor protein RIPK2 to reach NF-κB and MAPK pathways. Few reports have been published on an important role for NOD1 during *Mtb* infection, one showing NOD1 plays a role in cytokine production only in the absence of NOD2 or after LPS-pretreatment of BMDMs [186]. Mycobacteria do posses the iE-DAP moiety in their peptidoglycan [110]. In contrast, NOD2 has been well-studied in *Mtb* infection (Pubmed searches of "Mycobacterium tuberculosis AND NOD1" or "…NOD2" yielded 7 and 57 hits, respectively, at the time of writing (15-2-2021)).

Mycobacteria produce a distinct NOD2 ligand, *N*-glycolyl MDP, while most other bacteria produce *N*-acetyl MDP [106,107]. *N*-glycolylated peptidoglycan and MDP were shown to be better inducers of immune responses compared to the *N*-acetylated forms by comparing with mycobacterial KOs and synthetic MDPs [108,109,187]. The absence of NOD2 during *Mtb* infection was accompanied by reduced nitric oxide and cytokine production from mouse macrophages [188,189] and reduced iNOS from human macrophages [190]. NOD2 signalling has been called "non-redundant" in that although there are shared pathways with TLR and CLR signalling (e.g. NF-κB), NOD2 signalling appears to work synergistically with other MAMPs and little immune response is produced with MDP stimulation alone [108,187,191].

Only one other NLR has been significantly studied in the context of *Mtb* infection: NLRP3 (NLR family pyrin domain-containing 3). There is no known mycobacterial ligand for

this NLR – it has been suggested that NLRP3 can sense specific host products in the context of infection [181]. Recently, ESX-1-mediated membrane damage has been tied to caspase-1 activation, NLRP3 oligomerization, inflammasome formation and finally IL-1β release [192].

2.3.5 – Nucleic acid cytosolic surveillance receptors

AIM2 (absent in melanoma 2) appears to play a role in *Mtb* infection. This cytosolic DNA receptor was necessary for full caspase-1 cleavage/activation and IL-1β release during *Mtb* infection and *Mtb* DNA transfection [193]. STING (Stimulator of interferon genes), part of a cytosolic DNA sensing system, was essential for autophagy targeting of ESAT-6-producing mycobacteria in mouse bone marrow-derived macrophages [194] and zebrafish embryos [195]. cGAS (cyclic guanosine monophosphate–adenosine monophosphate (cGAMP) synthase), a DNA sensor that works with STING, was required for *Mtb* autophagy in addition to STING [196]. Type I IFN production during *Mtb* infection elicited by cGAS-produced, STING-sensed cGAMP was dependent on RD-1[197,198]. *Mtb*-produced c-di-AMP was also shown to contribute to type I IFN production through STING [199]. It has been suggested that *Mtb* DNA engagement of the AIM2 inflammasome leads to the inhibition of host cell-protective STING functions [200].

2.3.6 – Scavenger receptors and complement

Scavenger receptors (SR) are a diverse and poorly defined group of cell surface receptors that interact with endogenous and microbial ligands. Details of these receptors have been recently reviewed elsewhere [201,202]. Inhibitors of scavenger receptors reduced *Mtb* binding to macrophages [203].

MARCO is a scavenger receptor that was suggested to bind and "tether" *Mtb* to a macrophage's surface by interacting with TDM [204], and zebrafish lacking MARCO expression had reduced macrophage uptake of *M. marinum* [205]. Similarly, blocking MARCO on human mesenchymal stems cells reduced *Mtb* uptake [206].

KO of the gene encoding scavenger receptor A (SR-A) did not affect inflammatory gene transcription during *Mtb* infection [207]. The KO increased TNF and MIP-1α production from alveolar macrophages treated with TDM [208]. Overexpression of Scavenger receptor B1 (SR-B1) in immortal cells was associated with increased BCG and *Mtb* binding to the cells, but the corresponding KO in murine macrophages had no effect on BCG binding [209]. SR-B1 was essential for EsxA-mediated transcytosis of *Mtb* across M cells [210]. A related SR-B family member, CD36, was identified with a *Drosophila* RNAi screen to be essential for uptake of *M. fortuitum* [211]. CD36 knockdown in human monocyte-derived macrophages reduced surfactant lipid uptake as well as intracellular growth of *Mtb*, suggesting CD36 normally promotes intracellular *Mtb* growth or survival [212]. Another group showed *Cd36* KO macrophages control *Mtb*, BCG and *M. marinum* infections better, independent of phagocytosis rate, nitric oxide and ROS production. Similarly, mice receiving BCG i.p. had lower bacterial loads with *Cd36* KO vs WT [213]. Homologues of SR-BII and CD36 in *Dictyostelium discoideum* (a social amoeba) are similarly involved in phagocytosis of *M. marinum* [214].

2.4 – Consequences of PRR KOs in mice

The overall importance of individual genes during *Mtb* infection is best addressed in two ways: observing what happens to individuals with diverse expression or functionality of the gene

of interest who perchance become infected with *Mtb* (the natural experiment); alternatively, individuals of known or controlled gene status can be intentionally infected with *Mtb* – unethical in humans and therefore animal models are necessary. As mentioned above, many PRRs are important for specific cellular processes relevant to *Mtb* infection. It is therefore hypothesized that in the absence of a PRR, certain aspects of the host-*Mtb* interaction are lost, which should result in a phenotype in the whole animal. We have also assumed that the animal would suffer most from the aberrant immune response. This assumption is perhaps too simplistic: *Mtb* is a professional, obligate pathogen, and although it is perceived as hard-to-kill, it might also suffer from a host environment that does not behave as *Mtb* has evolved to 'expect'. Additionally, we have suggested that the potential coevolution of humans and *Mtb* has shaped the PRR-MAMP interaction, which clearly would not apply in infections of animals like mice, which are not natural hosts for *Mtb*. However, one can still use mice to generate testable hypotheses for human studies and validate genetic effects observed first in humans. Numerous KO mouse studies of *Mtb* infection have been performed over the years with hypotheses of defective immunity in the animal that should manifest as decreased survival, increased bacterial burden and/or detectable differences in the immune response (e.g. bronchoalveolar lavage cytokines or T-cell defects).

2.4.1 – Systematic literature search of Mtb *and PRRs*

To non-biasedly form a conclusion as to the importance of PRRs during *Mtb* infection in animal models, we used the Medline database via Pubmed to repeatedly search every known PRR and its role in *Mtb* infection in a living animal with the term below (where "[PRR]" was changed in each search):

"Mycobacterium tuberculosis AND [PRR]"

Where PRR names were ambiguous, we searched multiple times using the different names. After removing duplicates, this search produced over 1100 papers, which were screened for data using KO animals during *Mtb* infection. The results of this *in silico* exercise are summarized in table 1. We have added a few studies of which we were aware but that were missed by the screen (noted in table 1). It is possible that other appropriate data are absent; however the non-biased approach reinforces the validity of our subsequent conclusions.

In table 1, we summarized the results of individual experiments presented in the literature on murine *Mtb* infections comparing a PRR KO to the 'WT' control animal. All data found were exclusive to the mouse. We have included the dose, *Mtb* strain and route of infection per experiment. *Mtb* can establish an infection via the lungs with just a few bacilli [75,215], and therefore models using large doses and atypical routes may represent different aspects of *Mtb* disease but not necessarily follow the normal mode of infection. The magnitude of disease in mice also changes with the strain of *Mtb*, where for example the H37Rv strain is expected to be less virulent than the related Erdman strain and the HN878 strain. It is possible that some of the different outcomes across different studies addressing the same PRR knockout were due to differences in the infection model. However, our review of the data did not reveal an obvious effect of dose, strain nor route (table 1).

Where survival data were present, it was clear that PRRs can have an effect on survival, although in most cases there was either no significant difference in survival from WT to KO, or it was quantitatively small. There were two instances where KO mice survived longer than WT (CD14 [216] and SR-A [217]), demonstrating that some host systems are detrimental to *Mtb* tolerance.

2.4.2 – TLR KOs resulted in small and inconsistent effects on survival and Mtb *burden*

For TLR2, two of four experiments showed reduced survival in KOs. A single *Tlr6*-KO study did not show a difference in bacterial burden nor immune response [218]. For TLR4, two of seven experiments showed reduced survival in KOs. Note that many TLR4 studies took advantage of the C3H/HeJ mouse (having a spontaneous *Tlr4* loss-of-function mutation) employing other only somewhat related C3H strains as wildtype control. The maximum difference in pulmonary bacterial burden observed in most of these papers was approximately one log more in *Tlr2* or *Tlr4* KOs vs WT. Defects in immune responses were observed in a majority of *Tlr2* KO experiments and a minority of *Tlr4* KO experiments. Two experiments with *Tlr9* KO from one study showed more rapid death with high dose infection compared to low dose, and only the high-dose resulted in a statistically significant increase in pulmonary bacterial burden [219]. No survival data for other TLRs have been published. Interestingly, most experiments with combination KOs of *Tlr2*, *4* and/or *9* resulted in no differences in bacterial burden nor immunologic responses. Two of seven experiments (*Tlr2/9* double KOs) resulted in shortened survival times, but with small or unreported differences in bacterial burden. Together, mutations in TLRs, even multiple, had only modest or negligible effects on the host's survival and bacterial control but were frequently associated with altered immune responses. In particular, TLR2 and 9 stood out.

Of note, *Myd88*-KO mice succumbed rapidly (all dead within 1-2 months) to *Mtb* infection, despite TLRs seeming to be largely dispensable. This was attributed to the necessity of MyD88 for IL-1R signalling (*Il1r1* KO mice are equally susceptible) and intrinsic macrophage function requiring MyD88 [220-222]. An earlier report with *Myd88*-KO mice showed a

nearly 2-log increase in pulmonary colony-forming units (CFU) compared to WT but mice survived at least 12 weeks with limited immunological changes; no survival was presented [223].

2.4.3 – Few CLR KOs resulted in small reductions in survival and bacterial control

For CLRs, only MCL and Dectin-1 were found by us to have been disrupted in *Mtb* survival challenges. In one report, MCL (*Clec4d*)-KO caused a significant difference in survival, but specifically this was 20% mortality by 6 weeks, after which no *Clec4d*-KO mice died to week 10 (when the experiment was ended) [224]. However, in the same study, pulmonary bacterial burden was less than half a log higher in the KO at four months (no significant difference at 2 months). Proinflammatory immunologic responses were elevated in the KO. Thus, MCL might play a role early in infection to control the immune response, but not so much for bacterial control.

Another lone report showed Dectin-1 (*Clec7a*)-KO mice did not have changed mortality after infection with *Mtb*, and in fact had slightly lower bacterial burdens compared to WT at 2 and 4 months post infection [225]. Therefore, Dectin-1 is likely not required by the host during *Mtb* infection. No survival data was found for murine DC-SIGN homologues, mannose receptor, nor MINCLE. Only one of three studies reported a difference in bacterial burden with SIGNR1 (*Cd209b*)-KO at one- and nine-months post infection, but by scoring Ziehl-Neelsen-stained lung sections rather than directly counting CFUs [226]. When assessed, altered immunity was consistently observed with this KO. A single study found a difference in bacterial burden and immunological response with a SIGNR3 (*CD209d*)-KO but not a SIGNR5 (*Cd209a*)-KO [227]. Another lone study addressing the mannose receptor showed no bacterial or immunologic effect

with KO [226]. Two studies on MINCLE presented opposing data on pulmonary bacterial burden (more or less a half log compared to WT) and only one identified significant immunological changes with KO. Double KO of the genes encoding mannose receptor plus SIGNR1 showed no bacterial or immunologic differences. KOs of other membrane-bound CLRs have not been tested during *in vivo Mtb* infection.

KOs of genes encoding collectins SP-A and SP-D had no long-term effect on bacterial burden during *Mtb* infection – survival was not tested/presented. Immunologic responses were similar to WT but with decreased neutrophil numbers in the lung. Double KO for SP-A and SP-D genes was similar to the SP-A single KO [228]. KO of the gene encoding ficolin-A (homologue of human ficolin-2 and/or 3) decreased the survival of mice given one million CFU H37Rv strain i.v. compared to WT, but survival was enhanced compared to WT when KO mice were given a plasmid containing ficolin-A or ficolin-2 by i.m. electroporation on the day of infection [177]. This suggests ficolins might help control systemic or bloodborne *Mtb*. Thus, as with TLRs, CLRs are generally dispensable for *Mtb* immunity. The few exceptions seem to suggest an early, minor role in *Mtb* infection for CLRs like MCL and SP-A/D.

2.4.4 – KOs of certain cytosolic PRRs worsened Mtb infection outcome

NOD2 disruption produced a late survival phenotype: KO mice died faster than WT near 6 months post *Mtb* infection. Bacterial burden was slightly higher and immunological responses were also reduced in KO mice in this study [189]. A separate study did not find significant differences in bacterial burden nor immunological responses with *Nod2*-KO nor *Nod2-Tlr2*-double KO, but survival was not evaluated [188]. In contrast, *Nlrp3*-KO had no effect on bacterial

burden in three studies. Immunological responses with *Nlrp3*-KO can be altered, but survival did not change.

Aim2-KO mice succumbed rapidly to infection with one million CFU H37Rv strain delivered i.t. compared to WT. The KO had greater bacterial burden and pathology and altered immunity [193]. However, no other independent studies were found besides this one, and the high dose delivery makes the result difficult to compare to other PRR-KO survival studies with the more physiological low-dose aerosol infection. The importance of AIM2 during mycobacterial infection is supported by data with BCG, where repeated infection of WT and *Aim2*-KO mice vial the tail vein showed KO mice were defective in controlling bacterial burden which was associated with altered immunity (enhance type I IFN, reduced type II IFN) [200]. Additionally, the adaptor protein ASC (a.k.a. PYCARD) was also shown to be important for survival in at least two separate studies [229,230]. This supports the importance of AIM2 and/or another inflammasome sensor for *Mtb* infection, with NLRP3 seemingly dispensable.

Pulmonary burden of *Mtb* in *Cgas*-KO and *Sting1*$^{gt/gt}$ mice was unchanged from WT at 3 and 6 weeks post aerosol infection of 200 CFU of the Erdman strain, although *Cgas*-KO mice had late reduced survival (deaths between 100 and 200 days p.i.) while the STING mutant did not differ from WT [196]. In another study, an Erdman-strain aerosol experiment running 100 days did not reveal a difference between WT and *Cgas*-KO mice in terms of survival and bacterial burden, but less type I IFN was present in the lungs and serum [198]. In a third study with i.n. infection with 1000 CFU H37Rv strain, cGAS and STING mutations did not affect survival past 250 days (no mice died as with WT), although *Cgas*-KO mice did not maintain weight as well. Bacterial burden and immunology were the same as WT too [231]. Together, these studies suggest cGAS plays a minor role during *Mtb* infection (that emerged as a death phenotype late in one

study), while STING is dispensable. These findings are difficult to reconcile with the proposed model where cGAS functions upstream of STING as the mycobacterial DNA sensor; accordingly a STING mutant should be defective for cGAS functions. Furthermore, *Mtb* CDC1551 mutants that either lack their own c-di-AMP production, or overexpress it, significantly decreased and increased survival relative to WT, respectively [199], contributing further confusion regarding the importance of STING. It is possible that the importance of cGAS during mouse survival of *Mtb* infection is related to a STING-independent function of cGAS, and that the STING phenotype with mutant *Mtb* is more valuable as a mechanistic lesson than a biologically relevant one.

2.4.5 – No other PRR KOs were detrimental to the host during Mtb *infection*

No data was found showing scavenger receptor KOs were detrimental to *Mtb* control. A difference in bacterial burden during *Mtb* infection of *Marco*-KO mice was only detected by scoring Ziehl-Neelsen-stained lungs, not by CFU enumeration, at 6 and 9 months post infection [226]. KOs for SR-A and SR-B genes did not result in increased bacterial burdens nor were they consistently associated with immunological changes. Two independent studies examining the complement receptor CR3/*Cd11b* KO during *Mtb* infection found no evidence that they play a role in *Mtb* control nor survival [232,233].

In summary, most PRR KO experiments presented did not show reduced survival compared to WT. Control of bacterial burden was either unaffected or just slightly increased by PRR KOs in most experiments. We suspect that publication bias against negative data would also mean that PRR KO effects are, if anything, over-represented in the literature. In contrast, altered immunity was found often in PRR KOs during *Mtb* infection. It is possible that the

effects on immunity with some PRR KOs are not large or relevant enough to result in changes in survival and bacterial burden that are sufficiently robust to be statistically detectable with a practical number of animals.

2.5 – PRR diversity in humans and outcomes of *Mtb* infection

Selective pressure caused by human-microbe interactions coupled with population admixture has helped shape the response of modern humans to pathogens [234]. A recent example is a locus controlling COVID-19 severity in modern humans that can be traced to Neanderthal introgression [235]. *Mtb* and humans have coexisted for an estimated 2,000 – 6,000 years [65,66] and purifying selection of human genes by *Mtb* was traced to the bronze age for the *TYK2* P1104A mutation. Similarly, as members of the first line of host innate immune defense PRRs have been subjected to purifying selection [236]. PRR diversity in humans may explain, at least in part, the variable susceptibility to *Mtb* across populations.

For example, humans express 10 functional TLRs which are subdivided in two categories: cell surface (TLR1, 2, 4 – 6 and 10) and intracellular endolysosomal (TLR3, 7 – 9). The intracellular TLRs underwent strong purifying selection and have poor tolerance to loss of function mutations [237]. Conversely, cell surface TLRs are more permissive to genetic variation across human populations [238]. This difference may be attributed to the nature of ligands. Bacterial antigens detected by cell surface TLRs are clearly distinct from host molecules while nucleic acids detected by intracellular TLRs (RNA or DNA with CpGs) can resemble host endogenous factors. It has been proposed that mutations in intracellular TLRs are less tolerated to prevent "autoimmunity" [239-241]. *Mtb* is detected by heterodimers of TLR1, 2 and 6, therefore

presenting redundancy in the host response. Interestingly, mutations in the *TLR1* (S248N, I602S), *TLR6* (P249S) and *TLR10* (I775V) genes clustered on chromosome 4p14 have shown signs of recent positive selection in Europeans [237]. It has been suggested, although not confirmed, that TB and leprosy epidemics in Europe have played a role in this selective pressure [242]. Of particular interest is the TLR1 I602S mutation which has been associated with both TB and leprosy [243-247]. The TLR1 602S amino acid was shown to impair NF-κB activity in response to *Mtb* and decrease IL-6 production [246]. Studies evaluating TLR2 mutations in TB have provided inconsistent results, which limited the interpretation of its role in TB pathogenesis [248,249]. Moreover, TLR4 and TLR9 have also been suggested to contribute to TB susceptibility [250-252]

NLR is another group of PRRs that shows signs of diversity between populations. NLRs encompass three families of cytosolic PRRs (NOD receptors, NLRPs and IPAFs) involved in viral and intracellular bacterial pathogen recognition. An excess of rare *NOD1* non-synonymous variants segregating in the human population provided evidence for weak negative selection against these variants [253]. In contrast, there was evidence among Asians and Europeans of positive selection for rare variants in *NOD2* [253]. In a meta-analysis, the NOD2 R702W amino acid change was associated with protection from TB [254,255]. Curiously, the same NOD2 R702W mutation is one of the strongest known genetic risk factors for Crohn's disease, suggesting a pivotal role for NOD2 in balancing host inflammatory responses [256]. Most NLRPs shows signs of strong selective constrains emphasizing their essential function in the human innate immune response [253]. Macrophages challenged with *Mtb* or *M. marinum in vitro* showed a NLRP3-dependent increase in IL1β production [248]. In a small population of cases with HIV/*Mtb* co-infection a non-coding variant in NLRP3 had a weak association with early mortality [257].

DC-SIGN (CD209), a member of CLR family, is a major DC receptor of *Mtb* [150]. In ancient humans a duplication of *CD209* gave origin to the *CD209L* gene. Interestingly, natural selection has prevented accumulation of amino acid changes in CD209 while the closely related *CD209L* gene was permissive [258]. This discrepancy in selective pressures highlights the importance of function for CD209 while diversity in CD209L might have benefitted human adaptation to pathogens. Two promoter variants in CD209 are associated with TB in multiple African populations [259-261], South Asians [262] and Brazilians [263]. Other PRRs, such as ficolins, have been evaluated for association with TB [264,265], while studies with genes encoding proteins of the complement and PRRs for the RIG-1 family have not yet been reported.

2.6 – How some non-PRR KOs compare

Through animal experimentation, certain genes and associated pathways have been shown to be major determinants of the host outcome upon *Mtb* infection. Here, we define how some of these pathways compare to PRR pathways at the molecular level, and the level of importance to *Mtb* infection, as internal positive controls to our review.

For the sake of controls, similar systems to the PRR-MAMP interaction would include endogenous receptor-ligand systems. Receptor-cytokine interactions are an example which includes mechanisms that are even functionally related to PRR signalling pathways (e.g. the IL-1R/IL-1 system, which uses MyD88 like the TLRs as mentioned above).

IL-1R deficient mice were more susceptible to *Mtb* after intranasal infection with 10^5 CFU H37Rv strain, with a median survival of around 110 days, while no WT had died by 140 days; the remaining KO mice had 4 logs more pulmonary CFU than WT at 140 days post

infection [266]. Another study by a different group showed that with 100 CFU Kurono strain aerosol infection *Il1r1* KO mice had died after 45 days (KO mice had 3 logs more pulmonary CFU than WT at 35 days) [267]. During another H37Rv strain infection (200 CFU i.n.), *Il1r1* KO mice phenocopied *Myd88* KO mice (died around 4 weeks post infection) [220]. There have been variable phenotypes with IL-1α and IL-1β deficiency: in one study *Il1b* KO was sufficient to phenocopy *Il1r1* KO [229]; in another study the double cytokine KO only reduced pulmonary *Mtb* CFU control [268]; in a third study only double cytokine KO, not single, shortened survival like *Il1r1* KO [269]. Lastly, heterozygous deficiency of IL-1R antagonist, overexpressed in mice carrying the *Sst1* (super susceptibility to tuberculosis 1) locus, almost completely rescued these mice from their type-I IFN driven early mortality and excessive pulmonary CFU burden during *Mtb* Erdman strain infection, again highlighting the protective effect of IL-1R signalling [270]. Thus, MyD88-dependent cytokine-receptor systems can be critical for *Mtb* control in mice.

In mice lacking TNF receptor, or treated with anti-TNF antibodies, mice succumbed to uncontrolled *Mtb* Erdman strain i.v. infection in about a month while WT controls all survived past 125 days [271]. This result has been replicated in *Tnf* KO mice in numerous studies over the years [222,269,272]. TNF receptor deficient mice died approximately as rapidly as *Tnf* KO, even if the receptor KO was only on myeloid cells; lymphoid cell receptor KO did not differ from WT [273]. Thus, the TNF pathway is critical for *Mtb* control in mice to prevent rapid death. The importance of TNF with *Mtb* infection in humans was demonstrated when anti-TNF treatment was associated with the emergence of TB in patients receiving this treatment for other reasons [274].

Similarly, IFN-γ signalling has been known to be critical for control of *Mtb* in animal models for decades [275,276]. IFN-γ from CD4+ T cells in particular is necessary for survival, and

animals lacking IFN-γ from just CD4+ T cells succumb after two months post aerosol infection; however IFN-γ's role was mostly extrapulmonary with a limited role in the lungs [277]. IL-12p40, upon which IFN-γ is partly dependent, has also been knocked-out in mice and resulted in uncontrolled replication of *Mtb* (Erdman strain, administered i.v.) and mortality within 1.5 months compared to WT mice which lived "to old age" [278]. Human mutations in IFN-γ or IL-12 pathway genes causing impaired IFN-γ-mediated immunity result in Mendelian Susceptibility to Mycobacterial Disease, which manifests as childhood BCG dissemination or non-tuberculous mycobacterial infection, and occasionally *Mtb* infection later in those who live [279].

Cytokine and PRR signalling on their own do not have direct bactericidal effects – they are thought to modulate innate defense mechanisms and instruct adaptive immunity. The endgame of bacteriologic control is the host's killing mechanisms, which in macrophages include low phagosomal pH, digestive enzymes like lysozymes, and reactive oxygen species. As an example, the well-studied nitric oxide is produced by NOS2 to attack *Mtb*. Mice lacking NOS2 all died within 50 days of i.v. infection with 10^5 CFU Erdman strain while WT median survival was about 150 days [280]. In a separate study, aerosol infection with 100 CFU H37Rv strain similarly resulted in death before day 50 associated with increased *Mtb* burden [281]. Thus, effectors like nitric oxide are irreplaceable for control of *Mtb* and host survival.

2.7 – Why have genetic studies of TB in humans been underwhelming?

Genetic epidemiology studies have provided only a handful of PRR and non-PRR genes as global risk factors for TB. This lack of success is in striking contrast to leprosy, the second most common mycobacterial disease in humans [282]. Strain diversity of *Mtb* compared to *M.*

leprae might have played a role; however, the most likely cause for the lack of consistent results is phenotypic heterogeneity among TB cases. Most studies define TB as a single entity combining cases regardless of their clinical and biological characteristics. While this approach has worked for leprosy [283,284], in other instances combining all leprosy cases has proven troublesome due to the presence of well-defined endophenotypes [285,286]. Common endophenotypes in leprosy are excessive host inflammatory responses, so-called lepra reactions, that sub-divide the overall group of patients. Endophenotypes can result in misclassification of genetic effects [286,287]. Indeed, the genetic associations can be in opposite direction between endophenotype and disease *per se* [285,288].

Genetic modulators with opposing effects on unrecognized endophenotypes and clinically defined TB might be difficult to detect even in studies with very large sample sizes. This raises the question if similar, perhaps more complex endophenotypes, underlie the disappointing results from TB genetic studies. Specifically, considering the impact of PPR genes on intermediary immune phenotypes in the mouse, it is conceivable that PPR polymorphism may yet have a role to play in the genetics of TB pathogenesis. Heterogeneity among cases appears to be predominant in large scale genetic studies in TB and the existence of TB endotypes has been proposed [289]. Recent advances in molecular and analytical techniques have allowed the identification of at least two TB endotypes through unbiased clustering of transcriptional changes in distinct molecular pathways [290]. One endophenotype presented immune exhaustion resulting in poor prognosis compared to the second endophenotype.

What remains unclear is to what extent TB endophenotypes represent the continued progression of TB pathogenesis or if they are distinct forms of the same disease. More studies will be necessary to settle this question. Such future studies need to focus on defining

endophenotypes with the full weight of omics approaches, keeping in mind that these better-resolution phenotypes may represent kinetic entities. Such a 'systems-medicine' definition of TB, in excess of clinical and microbiological data, is expected to improve power for efficient mapping of endophenotypes. Molecular (RNA, proteins and metabolites) and immune (cellular) phenotyping using blood can provide information for dissociating TB cases into endophenotypes. This is a two-step approach, where first identification of interindividual molecular/cellular similarities is done prior to the genetic study. How to deal with the genetic study in the second step would depend on the groups, but could be either a continuous phenotype or stratified by endophenotype. Using an omics signature would overcome the limitations where patients are clinically similar but the genetic cause of TB is not the same. Clinical heterogeneity with *Mtb* infection that is ambiguous (e.g. placement on a spectrum from TST positive to active TB) can be better-defined or bypassed with non-biased omics data. However, independently of the nature of TB endotypes, it is now clear that heterogeneity may impact on genetic studies of TB and perhaps shed new light on the role of PPR polymorphisms.

2.8 – Final thoughts and conclusion

PRRs appear to be important for immunologic responses but have a more subtle role in control of *Mtb* and the course of TB. We hypothesize that this is partly due to the redundancy of many PRRs sensing different *Mtb* MAMPs. Amongst this redundancy, however, there may be unique immunological adjustments performed by specific PRRs. In contrast, genes that produce products mediating distinct effects, like IFN-γ, IL-12, nitric oxide and TNF are clearly essential to the host's survival. Although we can consider PRRs 'less important' than effectors, this prompts an interesting question: Is this a situation of reduced selective pressure, which explains

human PRR diversity? It is imaginable that the immunological outcome performed by an orchestra of PRRs can be quite varied as individual PRR activities are tuned differently by genetics. By contrast, altering the potency of an effector like IFN-γ would directly correlate with *Mtb* control, and therefore selection would be purifying.

Human genetic association studies of TB have yielded but a few promising leads. Animal and cellular human data clearly demonstrate that PRRs affect immunity during *Mtb* infection, despite small and/or delayed survival and bacteriologic phenotypes in PRR KO mice. Thus, PRR mutation in humans might manifest in endophenotypes of *Mtb* infection – states of altered immunity wherein the progression of TB may possess subtly different parameters. Defining such endophenotypes of *Mtb* infection through molecular and immunological profiling of patients may provide a roadmap on which to trace the effects of PRR variation on the course of TB.

Acknowledgements

J.Y.D. is supported by a Canadian Institutes of Health Research (CIHR) Canada Graduate Scholarship – Master's Program, Fonds de Recherche du Québec – Santé (FRQ-S) Doctoral Training Award, RI-MUHC studentships and scholarships from the McGill Department of Microbiology and Immunology. M.B.'s research is funded by a CIHR foundation grant (FDN-148362) and a Tier 1 Canada Research Chair. E.S. is funded by a CIHR foundation grant (FDN-143332) and a grant by NIH (1R01AI124349).

Data collection, processing and presentation

Literature searches were performed on the Medline database with Pubmed and results were collected and curated using Endnote X9 (Clarivate Analytics, USA). The text, table and figure were created with Microsoft Word, Excel and PowerPoint, respectively.

Author contributions

All authors listed have made a substantial, direct, and intellectual contribution to the work, and approved it for publication.

3 – Immunity & Mycobacterial Microbe-Associated Molecular Patterns

Many MAMPs of mycobacteria are distinct. Some of the exotic lipids produced by mycobacteria are MAMPs, including TDM, PIMs, lipoarabinomannanas and lipoproteins. As mentioned previously, common MAMPs like PGN and DNA are also unusual in mycobacteria.

3.1 – Mycobacteria as Immunological Agents

Despite their role in disease, mycobacteria and their component are increasingly recognised for having potential as therapeutic and/or immunologic agents. Beginning with Koch's tuberculin, which he had first mistakenly proposed as a treatment for TB, this or a similar extract of *Mtb* is used in one of the most common medical tests globally: the TST, thanks to Clemens von Pirquet and Charles Mantoux. BCG is also one of the most common vaccines distributed globally and, along with *Mip*, are being studied for non-mycobacteria-specific effects. In the research setting, mycobacteria-based adjuvants have distinct properties that made them invaluable reagents. Their unique capacity to cause disease may be related to potentially useful biological effects of mycobacterial products which communicate with our immune system through mechanisms such as PRRs.

3.1.1 – Bacille Calmette-Guérin (BCG)

Albert Calmette and Camille Guérin extensively passaged *M. bovis* on glycerin-potato medium to make their attenuated, eponymous vaccine strain Bacille Calmette-Guérin (BCG). BCG was first administered to children in Paris with great acclaim, while controlled clinical trials followed decades later [23,91,291]. A century later, BCG is administered to millions of infants

each year across the world. The utility of BCG is nuanced: although it is accepted that BCG provides protection from TB meningitis and miliary TB in children, its protective effect against *Mtb* infection or pulmonary TB in adults is less clear, where studies in some populations had shown protection but others not [91]. Various strains have evolved from the BCG of Calmette and Guérin and it is not clear if they differ significantly in protective effect. What separates BCG strains from virulent MTBC and each other are "regions of difference" (RD) and point mutations accumulated from repeated *in vitro* passaging, which have resulted in absent or altered expression of major MTBC antigens, such as ESAT-6 and MPT70/83, respectively [292-294].

Calmette had thought of BCG as an innocuous vehicle for the delivery of antigens for the purpose of generating immunity to *Mtb* [23]. Today, we know BCG produces an immune response in the form of antigen-specific T-cells. Although we know that T cells are essential to controlling human *Mtb* infection (as evidenced by persons with AIDS and TB), no data has shown that T-cell mediated immunity is sufficient for sterilization. People with TB are TST positive, indicating T-cell immunity in the presence of sickness. T-cell immunity is also critical in the murine model [295], where interestingly T-cell immunity (specifically IFN-γ) is of greater importance for extrapulmonary than pulmonary control of *Mtb* [277]. BCG was estimated to offer 10-fold protection against miliary TB and TB meningitis in infants, while protection was harder to detect for other forms of TB or demographics [296]. The role of BCG-induced T-cell mediated immunity in *Mtb* infection may be limited to non-sterilizing bacteriologic control.

In recent years, attention has been given to the possibility that trained innate immunity elicited by BCG may be key to the utility of the bacillus. Trained innate immunity is a form of immunological memory maintained in leukocytes and their progeny through epigenetic changes in their chromosomes. This form of genomic rewiring can result in more robust production of

immune mediators upon a future, unrelated microbial insult [297]. Some studies pointed to BCG being useful for the prevention of various childhood infectious diseases through non-specific immune activation, a potential serendipitous effect of BCG immunization in children [298,299]. However, after more than 10 years of negative or inconclusive clinical studies the effect is small at best [300,301]. BCG is also used to treat bladder cancer by repeated intravesical instillation of the bacilli. The mechanism of this treatment is hypothesized to include trained innate immunity because BCG does not contain cancerous antigens itself but augments the immune response against the cancer [302]. The role of trained innate immunity in natural human TB is unclear. BCG appeared to result in elevated immune responses from human monocytes and lymphocytes to *Mtb* and heterologous pathogens for months to a year after BCG administration, which may be depended on PRRs, notably NOD2 [297,303]. In the mouse, BCG that has access to the bone marrow instils epigenetic changes in myeloid progenitors, making differentiated myeloid cells better at killing *Mtb* [304], while *Mtb* has the opposite effect on myeloid precursors [305].

3.1.2 – Mycobacterium indicus pranii (Mip)

Mip was hypothesized to assist leprosy treatment by eliciting cross-reactive mycobacterial immunity to similar *M. leprae* antigens (an inactivated *M. leprae* would be impossible to mass produce for a vaccine and *M. leprae* is thought to induce immunological tolerance to its antigens) [306]. Currently, *Mip* has been approved as an adjunct therapy to treat leprosy in India, along with the usual antibiotics. *Mip* is currently being tested in the treatment of TB. A randomized trial found that adjunct *Mip* accelerated sputum conversion rate in category II TB patients (those who failed a first attempt of treatment, for any reason) [307]. However, *Mip* with or without prednisolone corticosteroid as adjunctive therapy did not

demonstrate any benefit to treating tuberculous pericarditis in a large randomized trial [308]. A clear use for *Mip* in adjunctive TB therapy is yet unclear. *Mip* is also being studied as an immune potentiator in cancer therapy [309,310], based on utility of mycobacteria for non-specific immune system activation.

3.1.3 – Complete Freund's Adjuvant (CFA)

Jules Freund's eponymous adjuvant is composed of liquid paraffin (a mineral oil), aracel A (a surfactant, also called mannide monooleate) and heat-killed desiccated *Mtb* (or on occasion a different mycobacterium). This oily part is mixed with a saline solution containing antigen(s) of interest to produce a water-in-oil emulsion to be injected for the purpose of immunization. While researching in New York, by 1937 Freund had begun combining heat-killed, dried *Mtb* with mineral oil, based on work from Abelardo Saenz [311], a collaborator of Calmette, Guérin and Canetti of the Pasteur Institute in Paris. Freund had begun experimenting with the vaccination of animals with heat-killed tubercule bacilli to prevent TB, where it became apparent through survival and antigen-sensitization experiments that tubercule bacilli drive a strong immune response [312,313]. Later, he developed the method of producing water-in-oil emulsions [314] and began testing mycobacteria-adjuvanted immunization against various antigens and other infectious agents [315-319]. The function of the water-in-oil emulsion results in a slow release of the aqueous materials, as noted too by Freund [314].

At the same time at the Rockefeller Institute in Manhattan, Merrill Chase and Karl Landsteiner were utilizing the adjuvant of Freund to immunize guinea pigs against picryl chloride, and then transferring the peritoneal exudates to naïve guinea pigs and conducting skin

tests with antigen to measure the immune response in the recipient animal. First with picryl chloride and later with tuberculin, they observed DTH in the guinea pigs receiving cells from the immunized animals. DTH was only transferable through the cellular fraction of peritoneal exudates and was sensitive to heating at 48^{o}C for 15 minutes as well as freezing or overnight refrigeration (conditions that would harm cells but not proteins) [320,321]. These experiments demonstrated for the first time the cellular nature of DTH and marked the discovery of cell-mediated immunity (CMI), as opposed to humoral (antibody) immunity. These experiments are key evidence that *Mtb* distinctively elicits CMI, in the form of CFA.

Currently, CFA has numerous uses in experimental animal models but is too reactogenic for human use [322]. CFA is often used in animal models to induce autoimmunity. In this context, an autoantigen relevant to a specific tissue is emulsified with CFA for immunization. There are CFA-driven mouse models for encephalomyelitis, arthritis and uveitis as examples [323-325]. CFA can also be used as a model adjuvant for immunization against an infectious agent, and to generate an immune response against a purified antigen solely to harvest antibodies afterwards for other applications. Without mycobacteria, the oil fraction by itself is called incomplete Freund's adjuvant (IFA), and is sufficient to boost antibody titers while lacking the ability to generate CMI [326]. The ability of the mycobacteria in CFA to elicit robust immune responses to even autoantigens has drawn attention to uncovering what properties of mycobacteria make them good adjuvants. In Chapter II, I present data wherein we addressed this point of interest by deconstructing CFA into some of its essential MAMPs.

3.1.4 – Mycobacteria-induced autoimmunity

Autoimmune-mediated neuropathy has been described in various natural and laboratory contexts over decades. Early versions of Pasteur's rabies vaccine, made from dried rabbit spinal cords, would occasionally result in paralysis of variable severity in the recipients. Just a few decades later, scientists investigating the causes of paralysis showed that it would sometimes occur in rabbits or monkeys repeatedly injected with central nervous system (CNS) tissue of different animals [327]. More recently in 2006-2008, 24 workers from two pork processing plant in Minnesota and Indiana developed autoimmune polyradiculoneuropathy where a machine using highly pressurized air was being used to remove pigs' brains from the skull, creating aerosols [328]. Thus, exposure to exceptional amounts of CNS antigens can cause autoimmune neuropathy. In the 1940s, Kabat and Morgan first demonstrated that adjuvating injections of CNS tissue with CFA made the induction of experimental autoimmune encephalomyelitis (EAE) in monkeys far quicker and more efficient [329,330]. Thus, EAE was born.

EAE can be induced in mice by immunization with myelin oligodendrocyte glycoprotein (MOG) mixed with CFA. Different degrees of intensity can be achieved based on the concentration of mycobacteria and MOG at immunization: a relapsing-remitting (RR)-EAE is achieved with lower-dose injection while a progressive EAE ensues with high-dose [331]. Pertussis toxin is also administered at MOG/CFA immunization intravenously. The inclusion of pertussis toxin was classically thought increase vascular permeability in the central nervous system to leukocytes, but direct activation of leukocytes is also possible, although this rationale is confounded by the chance of endotoxin contamination [332-336]. The inclusion of pertussis toxin increases the efficiency of inducing EAE [325].

EAE is characterized by inflammation and demyelination in the central nervous system. Myelin-reactive T cells infiltrate the CNS and attack the myelin sheath around the axons of neurons resulting in demyelination, reduced conductivity of electrical signals and axonal death. The ensuing paralysis is ascending, affecting the lower body/limbs of the animal before the upper ones. Because of the many similarities to multiple sclerosis, EAE has been used extensively to model this disease although it is not a perfect surrogate: an obvious difference being that EAE is achieved by adjuvants and a known antigen, resulting in a rapid disease, while multiple sclerosis occurs without a known adjuvant nor autoantigen and proceeds more slowly [331,337].

3.2 – MDP and NOD2

The adjuvant effect of the mycobacteria in CFA has been attributed to the mycobacterial cell wall for decades, and specifically MDP since the 1970s. It was not until the mid-2000s that NOD2 was discovered to be essential for the recognition of MDP by immune cells and NOD2 was deemed the PRR for MDP. NOD2 and MDP are well-studied components of immunity and both have a distinct relationship with mycobacteria. These aspects are further described in the following sections.

3.2.1 – Muramyl Dipeptide (MDP)

In the 1970s, Lederer and colleagues showed that the minimal adjuvant-active motif of the mycobacterial cell wall was "*N*-acetyl-muramyl-L-alanyl-D-isoglutamine" (i.e. *N*-acetyl MDP) [338]. Since then, various MDP derivatives have been synthesized for experimental and

clinical purposes. Many MDP derivatives are approved in certain countries as an adjuvant or to treat infections, cancer or inflammatory conditions [339]. The most widely authorized MDP derivative is mifamurtide, which is approved in the European Union in combination with chemotherapy for the treatment of osteosarcoma.

PGN is highly studied in part because of its ability to be targeted by many antibiotics; thus, the steps in its biological synthesis are well-known. PGN monomers originate in the cytoplasm. Firstly, *N*-acetyl glucosamine (GlcNAc) is synthesized and then reacted with UTP to form UDP-GlcNAc. The muramic acid (Mur) moiety is generated by reacting phosphoenoyl pyruvate with UDP-GlcNAc to form UDP-MurNAc. In mycobacteria, some of this intermediate becomes *N*-glycolylated by the enzyme *N*-acetyl muramic acid hydroxylase (NamH) using molecular oxygen to form UDP-MurNGlyc [106,107,110]. Of the actinobacteria, *Nocardia* spp. and *Rhodococcus* spp. also have *namH* and *N*-glycolylated PGN, while *Streptococcus* spp. and *Corynebacterium* spp. have neither [106]. Next, the amino acids L-alanine, D-iso-glutamine and meso-diaminopimelic acid are added one-by-one, and lastly the D-alanine dimer is added to form the pentapeptide attached to muramic acid. UDP is released from MurNAc (or MurNGlyc) as it is reacted with decaprenyl phosphate to anchor the muropeptide to the inner leaflet of the plasma membrane, forming a molecule called lipid I. GlcNAc is reacted with lipid I to form the complete basic PGN subunit (GlcNAc-MurN(Ac/Glyc)-pentapeptide, called lipid II). A flippase orients the PGN subunit to the periplasmic side of the plasma membrane. Transglycosylase and transpeptidase (3-3 and 3-4 linkages of pentapeptides) activity forms the PGN polymer from the monomers and the decaprenyl bond is broken (reviewed in [340]).

Different processes have been used to chemically synthesize synthetic muramyl dipeptides with modifications at different parts of the molecule [341-344]. *N*-glycolyl MDP is better

than *N*-acetyl MDP in stimulating the NOD2 pathway [108,341-343]. Substitutions at different parts of the molecule modestly increase or completely ablate activity [341-343], suggesting the natural versions, particularly *N*-glycolyl, are the evolutionary preference for the host receptor. Large additions such as lipids have been attached to the end of the peptide, and the molecule remains active (e.g. mifamurtide) [345]. Others have functionalized carbon 6 of the muramic acid ring [346,347]. Most immunological studies on MDP are conducted with chemically synthesized MDP, rather than purified PGN fragments, ruling out the possibility of contamination by other MAMPs and ruling in that MDP is a *bona fide* MAMP. MDP alone is often insufficient to provoke a measurable immune response and requires the presence of another MAMP with which to synergize [108,348]. This was explained with a block to translation of MDP-induced TNF transcripts which needed to be alleviated by MAMP (e.g. LPS) costimulation [349].

When bacteria are taken up by a phagocyte, PGN must be digested in the phagosome by lysozyme to release muropeptides [350]. MDP is then thought to traverse a transporter (such as the small peptide transporters of the SLC15A family [351-353]) to gain access to the cytosol, where NOD2 resides. Soluble synthetic MDP requires clathrin-, dynamin- and pH-dependent endocytosis for NOD2 sensing [354,355]. NOD2 requires localization to the cellular membrane for MDP recognition, presumably to be in proximity to MDP upon cytoplasmic ingress [356-358].

The physical binding of MDP to NOD2 has not been irrefutably demonstrated. Surface plasmon resonance was used by the same researchers in two studies to show an interaction between NOD2 and MDP, although true negative controls were lacking (e.g. the biologically inactive stereoisomer of MDP also interacted with NOD2, albeit less than the active MDP) [347,359]. Another study showed detection of tagged NOD2 from a pull-down with biotin-MDP, enhanced when NOD2 also bound ATP rather that ADP (NOD2 is an ATPase) [360]. The increased

biological activity of *N*-glycolyl MDP was explained by it stabilizing NOD2 from proteolysis for a longer period of time than *N*-acetyl MDP [343]. The physiological muropeptide that interacts with NOD2 has not been demonstrated. MDP is the minimal biologically active PGN fragment, but the part of PGN that naturally interacts with NOD2 is unknown, whether it is a larger fragment than MDP or modified by host factors first.

Besides NOD2, muropeptides are thought to interact with other host proteins. Muramyl di-, tri- and penta-peptide were shown to interact with PGN recognition proteins (PGLYRPs) [361-363] and the amidase activity of PGLYRP-2 can cleave the peptide from PGN, removing the MDP motif and NOD2-mediated recognition [364]. In contrast, lysozyme cleaves PGN polymers between muramic acid and glucosamine residues, leaving muropeptides intact. NLRP1 was also suggested to interact with MDP for inflammasome formation [365], but its crystal structure did not contain an obvious MDP binding site in the expected domain [366]. The metabolism of muropeptides in mammalian cells is not well studied, but presumably humans and other mammals have evolved to be able to utilize or excrete muropeptides given that we house many bacteria in our guts. MDP is detectable in the circulation too [367]. Exactly how these elements contribute to the immune response to muropeptides is not well understood.

3.2.2 – Nucleotide-binding Oligomerization Domain-containing 2 (NOD2)

NOD2 first received major attention in 2001 when single nucleotide polymorphisms (SNPs) in the gene were associated with Crohn's disease [368-370] and Blau syndrome [371]. By 2003, it was shown that NOD2 was essential for the innate immune response to the common bacterial PGN motif MDP [182,183]. Soon after, *Map* had been reported in multiple patients with NOD2

polymorphisms and/or Crohn's disease [372,373] and NOD2 was shown to be necessary for full recognition of *Mtb* [191] and *Map* [374] by PBMCs. NOD2 is clearly expressed in myeloid cells but has also been reported in many other cell types, such as epithelial cells [375-378].

NOD2 has four domains: two *N*-terminal caspase activation and recruitment domains (CARDs), a nucleotide-binding domain (NBD) and a *C*-terminal leucine rich repeat (LRR) domain. The CARDs mediate interactions with other proteins (e.g. through CARD-CARD interactions). The NBD binds ATP, which was proposed to provide a conformational change that enhances the MDP interaction and oligomerization, while ATP hydrolysis to ADP has the opposite effect [360]. The LRRs are thought to compose the ligand (MDP) binding domain [359,379].

Mutations in *NOD2* have been associated with various diseases, but most strongly with Crohn's disease: especially the common LRR domain mutations 2104CT (R702W), 2722GC (G908R) and 3020insC (1007FS) [368-370,380,381]. For these three mutations, the increased risk of Crohn's disease is 2.0, 3.1 and 4.6 in heterozygotes, respectively, and 3.3, 12.1 and 34.7 in homozygotes, respectively [382]. These are all recessive loss-of-function mutations (i.e. loss of MDP responsiveness) [182,183]. A 1001GA (R334Q) mutation in the NBD was associated with Blau syndrome [371], a chronic and systemic inflammatory disease with granulomatous pathology. Contrary to initial hypothesis that *NOD2* polymorphisms associated with Blau syndrome are gain-of-function mutations (i.e. greater NOD2 activation) [379], data have shown neutral or defective MDP signalling [383-386]. However, one study using overexpression of NOD2 with various Blau-associated NBD polymorphisms unanimously showed higher, MDP-independent, basal levels of NF-κB activation compared to unmutated NOD2, complicating the NOD2 mechanism in Blau [387] (this phenotype was not seen in patient-derived cells [384,385]). *NOD2* and *RIPK2* SNPs (synonymous or non-coding) have been associated with leprosy [284,388-391]. In one

study, the R702W mutation was linked with a decreased risk of active TB while the A725G mutation was associated with increased risk [255]. Intronic SNPs in *NOD2* were associated with a *Mtb* resistor phenotype (perpetually negative TST) but not TB *per se* in another study [392].

NOD2 signalling begins when NOD2 molecules are recruited to the membrane where bacterial sensing takes place and NOD2 molecules oligomerize. Signalling continues with the recruitment of the RIPK2 (aka RICK) to the membrane with NOD2 through CARD-CARD interactions [393,394]. RIPK2 is an adaptor kinase specific for NOD1 and NOD2 signalling [395]. RIPK2 forms filaments that recruit IAPs and TRAFs, which in turn leads to the ubiquitination of RIPK2 and recruitment of the linear ubiquitin assembly complex (LUBAC). TAK1 and TAK1-binding proteins are assembled at RIPK2, forming the complete "nodosome". The IKK complex is ubiquitinated, phosphorylated, and in turn phosphorylates Inhibitor of κB (IκB) molecules, leading to their degradation and release of NF-κB molecules which become free to translocate into the nucleus and activate transcription of various genes of immunity. Additionally, the nodosome can activate MAPK pathways (p38, c-Jun, JNK) to phosphorylate and activate AP-1 transcription factor components (reviewed in [376,396]).

NOD2 has been linked to other cellular processes. One study showed an essential interaction between NOD2 and MAVS for the IRF3 response to viral RNA [397]. This may be related to a NOD2 interaction with the viral RNA sensor RIG-1 [398]. NOD2 expression in T cells was reported in 2009 to be essential to the immune response to *Toxoplasma gondii* [399], but this phenotype was subsequently contradicted [400] and never replicated. Autophagy is enhanced by MDP and functional NOD2 is required for proper recruitment of autophagy machinery (e.g. ATG16L1) as well as autophagy-dependent bacterial control and antigen processing/presentation in DCs [401,402]. Interestingly, *ATG16L1* polymorphisms are linked to Crohn's disease like *NOD2*

[403,404]. Reports have also linked NOD2 to LRRK2-dependent intestinal homeostasis and RIPK2 phosphorylation [405-407] (*LRRK2* polymorphisms are also associated with Crohn's disease and leprosy susceptibility [256,284,408-411]). A few other reports have linked NOD1/2 and/or RIPK2 to the endoplasmic reticulum stress response [412-415]. These studies suggest a broader role for NOD2 than simply a sensor of MDP, but which requires further study.

3.3 – TDM and Mincle

TDM, the molecule associated with the "cording" phenotype of mycobacteria, was isolated and described in the 1950s. It was sought after to explain mycobacterial virulence but was later recognized to also possess adjuvant properties. In 2009, Mincle was discovered to be a receptor for TDM. Thus, TDM and by extension Mincle continue to be of interest in understanding the mycobacteria-host interaction.

3.3.1 – Trehalose-6,6'-dimycolate (TDM)

The "cord factor" was hypothesized by Dubos and Middlebrook in the 1940s as a molecular entity driving the cord-like fashion in which virulent mycobacteria grow in culture media [416,417]. The structure of a lipid deemed responsible for cording was first isolated by Bloch in 1950 and reported by Bloch and Lederer as trehalose-6,6'-dimycolate by 1956 [417,418]. The toxic effects associated with cording and cord factor (cytolytic effects and animal weight-loss/mortality [416,417]) labeled this mycomembrane lipid as a virulence factor [419]. However, its adjuvant properties have resulted in the use of TDM analogues in research and vaccines. For example, trehalose-6,6'-dibehenate (TDB) is a synthetic analogue of TDM and is the adjuvant

active part of the CAF01 adjuvant which has been tested in multiple phase I vaccine trials against different infectious agents with a good safety and immunogenicity profile [420-423].

TDM synthesis in mycobacteria begins with mycolic acid synthesis. Fatty acids are assembled *de novo* from acetyl-CoA and energy from NADH and NADPH, using the enzyme FAS-I and the enzyme complex FAS-II. FAS-I and II products are linked and combined to trehalose with polyketide synthase 13 (Pks13) to form trehalose monomycolate (TMM). MmpL3 (mycobacterial membrane proteins large 3) with TtfA (TMM transport factor A [424]) transport TMM into the periplasmic space. Two TMM molecules combine to form TDM in the mycomembrane (reviewed in [425,426]). Trehalose lipids are also produced by a few other actinobacteria, including *Corynebacterium* spp., *Nocardia* spp. and *Rhodococcus* spp. [427]

The natural structure of TDM is difficult to reproduce synthetically, thus synthetic TDM analogues with simplified structures have been created for experimentation and adjuvants. TDB has simplified acyl chains attached to trehalose, instead of complex mycolic acids. A rationally designed minimal Mincle-active motif was described by reverse-engineering TDM down to a single glucose and simplified acyl group, called GlcC14C18, which also lacks the cytotoxicity associated with purified TDM [428].

In 2009, Ishikawa *et al*. demonstrated that Mincle was an essential receptor for cellular recognition of TDM and TDM-induced granuloma formation in mice [157]. Prior to this, Marco had been proposed to assist in TDM adherence to immune cells in one study [204]. Mincle was also confirmed to be the receptor for TDB [429]. The similar C-type lectin MCL also interacts with TDM and is thought to be the first TDM sensor that, while not driving the immune response itself, upregulates Mincle expression for immune activation [160].

3.3.2 – Macrophage-inducible C-type lectin (Mincle)

Mincle was first described in 1999 as a NF-IL6-dependent C-type lectin having inducible expression from LPS, TNF, IL-6 or IFN-γ stimulation [430], and next shown as a sensor of dead cells via the endogenous small nuclear riboprotein SAP130 [431]. In the same study, the dependence of Mincle on FcRγ for signalling was demonstrated. Besides mycobacteria, Mincle was described as a sensor of the fungi *Candida albicans* [432,433] and *Malassezia* spp. [434]. Polymorphisms in *MINCLE* have only recently been associated with TB in a single study [435]. Mincle expression is low on resting myeloid cells, requiring induction as its name suggests (e.g. through MCL, TLR4 or cytokine signalling as previously mentioned) [160,430].

Mincle has a small *N*-terminal cytoplasmic tail, a transmembrane domain that spans the plasma membrane, and a *C*-terminal carbohydrate recognition domain outside of the cytoplasm. Mincle interacts with TDM trough its carbohydrate recognition domain, binding each glucose of trehalose in distinct pockets, one with an adjacent hydrophobic groove to accommodate the attached mycolic acid [428,436]. Mincle does not have its own cytoplasmic signalling domain but is coupled to FcRγ which contains an immunoreceptor tyrosine-based activation motif (ITAM) [431]. When Mincle molecules bind ligand, the cytoplasmic ITAM tyrosine residues of FcRγ molecules are phosphorylated by SRC kinases. This recruits and activates Spleen Tyrosine Kinase (SYK), leading to activation of phospholipase Cγ which in turn leads to calcineurin and Protein Kinase Cδ (PKCδ) activation. Calcineurin dephosphorylates the transcription factor NFAT. PKCδ phosphorylates CARD9 for the formation of a CARD9-BCL10-MALT1 signalling complex, which activates NF-κB and MAPK pathways. MALT1 also has "paracaspase activity" which cleaves various regulators of immune signalling, including mRNA binding proteins (reviewed in [437,438]).

That *Card9* was critical to *Mtb* control in a knockout mouse study [159] reveals little about Mincle's importance during TB, since CARD9 is an adaptor molecule shared by many pathways [438]. However, TDM-Mincle signalling accounted for most of the *Card9*-dependent adjuvant effect of the mycobacteria in CFA, which was further enhanced with purified PGN [439]. Notably, NOD2 also interacted with overexpressed CARD9 and the murine macrophage immune response to MDP was *Card9*-dependent [440]. In Chapter III, I present data which specifically addressed the importance of both Mincle and NOD2, singly and in combination, during infection with *Mtb* and *Map*.

4 – Hypothesis and Objectives of the Research

Mycobacteria are important agents of disease. In addition, they are historically, genetically and biochemically linked to our understanding of immunity. Healthcare and research are major consumers of BCG and CFA, respectively; however, we do not fully understand how these mycobacterial entities work to stimulate innate and adaptive immune responses. Genetics have pointed to a pivotal role for NOD2 in inflammatory diseases, as well as a relationship to mycobacterial infection. The NOD2-mycobacteria connection is also supported by the fact that mycobacteria produce a distinct NOD2 ligand, namely *N*-glycolyl MDP. Mycobacteria produce many unique molecules, including the glycolipid of many properties, TDM. Given that *N*-glycolyl MDP and TDM are unique MAMPs recognized by human PRRs, **I hypothesize that MDP/NOD2 and TDM/Mincle play important roles in mycobacterial immunity affecting the host outcome**. This hypothesis was investigated through two distinct research aims:

1. To measure the essentiality and sufficiency of NOD2 and Mincle ligands in the adjuvancy of CFA. This was done with mycobacterial plus murine KOs and chemical complementation using two mouse models: one of antigen-specific T-cell immunity after immunization; another of adjuvant-driven autoimmunity (EAE).
2. To determine the importance of Mincle and NOD2 during infection with *Mtb*. This was accomplished using KO mice infected with virulent *Mtb* with measures of bacterial burden, immunity and survival.

5 – Figures of Chapter I

Chapter I, Figure 1. The mycobacterial cell envelope.

A cross-sectional cartoon of the mycobacterial envelope, with major components shown in approximate relative depth. Mycobacteria have an inner plasma membrane plus an outer 'mycomembrane'. Between these membranes are a periplasmic space, PGN and arabinogalactan. A capsule surrounds the bacterium [5,9].

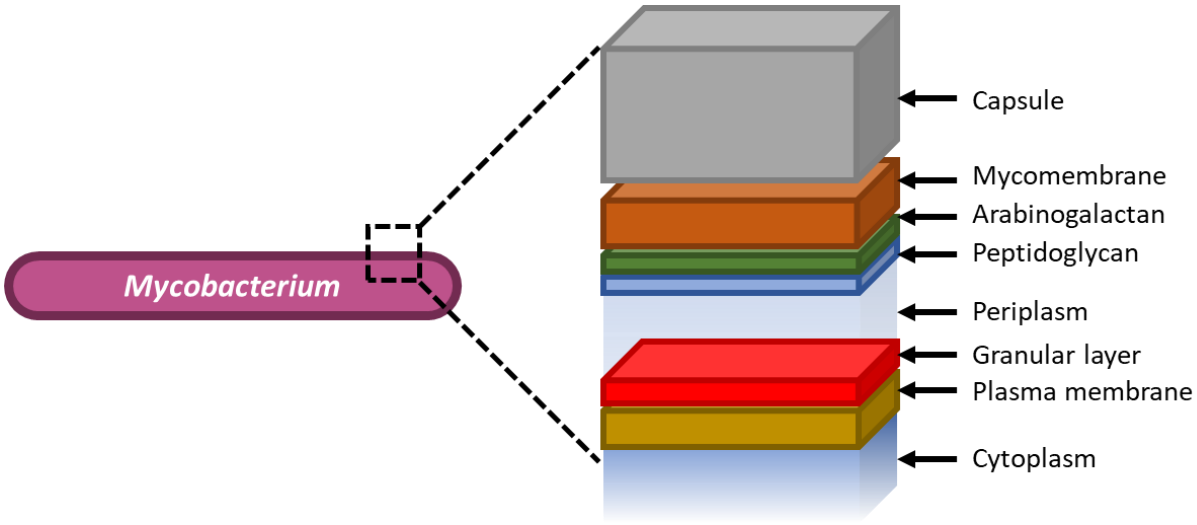

Chapter I, Figure 2. The various host PRR and *Mtb* MAMP interactions.

Representative MAMP-PRR interaction are depicted in their approximate cellular locations highlighting the numerous ways in which *Mtb* announces its arrival to a phagocyte.

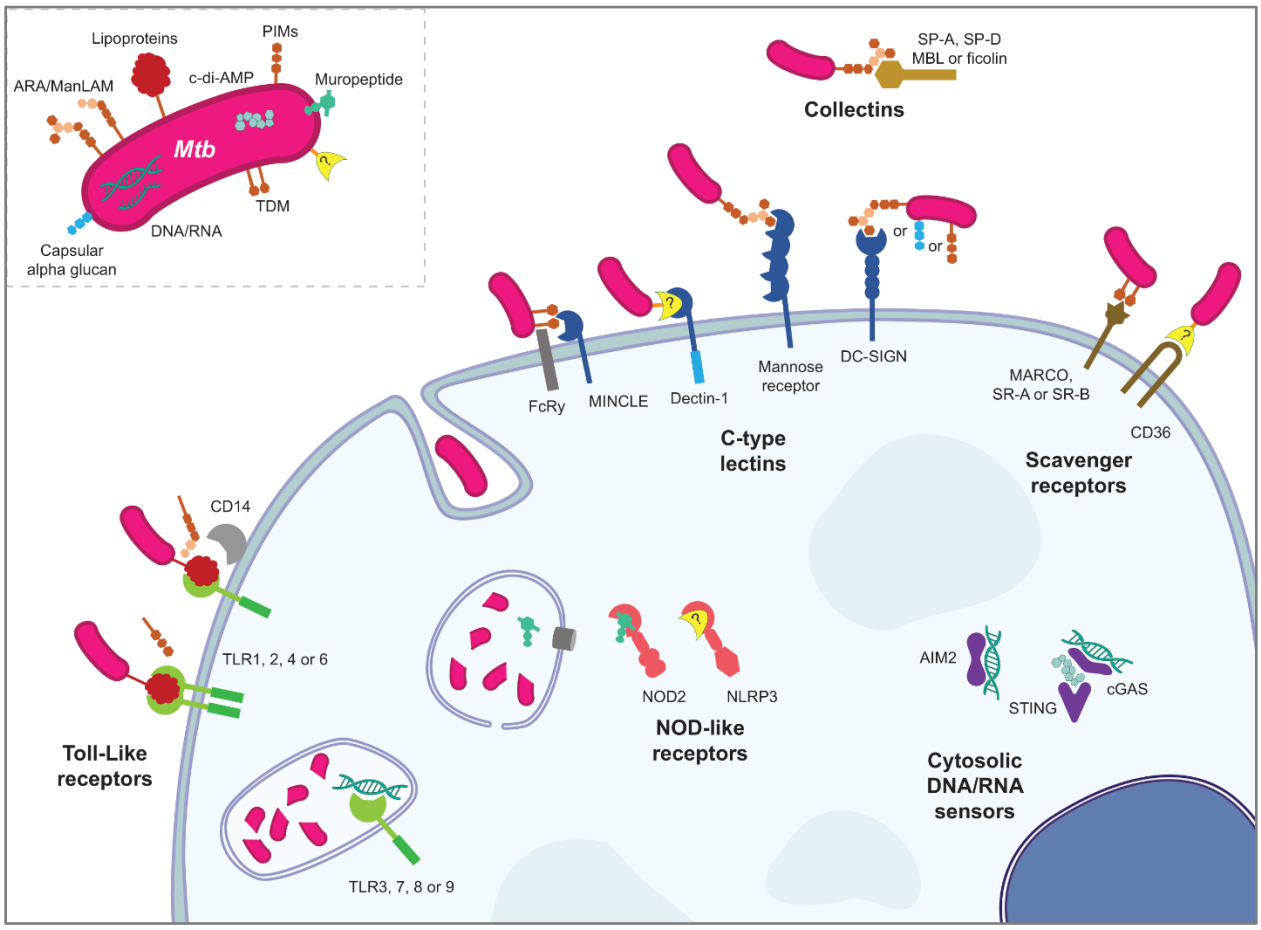

6 – Tables of Chapter I

Chapter I, Table 1. Results of KO mouse studies of *Mtb* infection.

PRR KO(s)	*Dose, CFU*	*strain*	*route*	*Δ Survival* [A]	*Δ Mtb* [B]	*Δ Imm* [C]	*Notes* [D]	*Source*
Tlr2	100	H37Rv	aero	-	N	N		[441] Reiling
	2,000	H37Rv	aero	Y (60/150)	-	Y		[441] Reiling
	100	Kurono	aero	-	Y (1)	Y		[218] Sugawara
	100	H37Rv	aero	N	Y (1)	-		[272] Drennan
	500	H37Rv	aero	Y (100/>155)	Y (1)	Y		[272] Drennan
	75	H37Rv	aero	N	N	N	manual	[442] Bafica
	20	H37Rv	aero	-	Y (<1)	Y		[443] Tjärnlund
	100	H37Rv	aero	-	N	-		[221] Hölscher
	100,000	H37Rv	i.t.	-	Y (1)	Y		[444] Carlos
	150	H37Rv	i.n.	-	-	Y		[445] Teixeira-Coelho
	10,000,000	H37Rv	i.v.	-	-	Y		[446] Choi
	75	Erdman	aero	-	Y (1)	-		[447] McBride
	10	Erdman	aero	-	Y (2)	-		[448] McBride
	100	Erdman	aero	-	Y (2)	Y		[448] McBride
	150	Erdman	aero	-	Y (1)	-		[448] McBride
	100	Erdman	aero	-	Y (<1)	Y	chimera	[449] Konowich
	20	HN878	aero		Y (3)	Y		[450] Gopalakrishnan
RP105	200	H37Rv	aero	-	Y (<1)	Y		[451] Blumenthal
TLR4	100	H37Rv	aero	Y (180/>250)	Y (1)	Y	HeJ/HeN	[452] Abel
	100	H37Rv	aero	-	N	N	HeJ/HeN	[441] Reiling
	2,000	H37Rv	aero	N	-	N	HeJ/HeN	[441] Reiling
	144	Erdman	aero	N	N	-	HeJ/other C3H	[453] Kamath
	472	Erdman	aero	N	N	N	HeJ/other C3H	[453] Kamath
	75	H37Rv	aero	N	Y (-1)	N	HeJ/OuJ	[454] Shim
	100,000	H37Rv	i.n.	Y (90/>110)	Y (<1)	Y	HeJ/HeN	[455] Branger
	500,000	H37Rv	i.n.	N	-	-	HeJ/HeN	[455] Branger
	20	H37Rv	aero	-	Y (<1)	Y		[443] Tjärnlund
	100	H37Rv	aero	-	N	-		[221] Hölscher
	150	K strain	aero	-	Y (2)	Y	HeJ/HeN and B6	[456] Park

CD14	100	H37Rv	aero	-	N	N		[441] Reiling
	100,000	H37Rv	i.n.	Y (>224/210)	N	Y		[216] Wieland
LBP	100,000	H37Rv	i.n.	N	N	Y		[457] Branger
TLR6	100	Kurono	aero	-	N	N		[218] Sugawara
TLR9	75	H37Rv	aero	Y (90/>150)	N	Y	manual	[442] Bafica
	500	H37Rv	aero	Y (45/>90)	Y (<1)	Y (not shown)	manual	[442] Bafica
	100	H37Rv	aero	-	N	-		[221] Hölscher
	75	Erdman	aero	-	N	N		[458] Gopalakrishnan
SIGNR1	100,000	H37Rv	i.n.	-	N	Y		[459] Wieland
	1,000	H37Rv	i.n.	-	N	-		[227] Tanne
	200	H37Rv	i.n.	-	Y (score)	Y		[226] Court
SIGNR3	1,000	H37Rv	i.n.	-	Y (1)	Y		[227] Tanne
SIGNR5	1,000	H37Rv	i.n.	-	N	-		[227] Tanne
CD206(MR)	200	H37Rv	i.n.	-	N	N		[226] Court
Mincle	100	H37Rv	aero	-	Y (>-1)	N		[460] Heitmann
	100	Erdman	aero	-	Y (<1)	Y		[461] Lee
MCL	100	H37Rv	aero	Y	Y (<1)	Y	N>30 in survival	[224] Wilson
Dectin-1	100	H37Rv	aero	N	Y, (>-1)	N		[225] Marakalala
Ficolin-A/2	1,000,000	H37Rv	i.v.	Y (10/22)	-	-		[177] Luo
SP-A	50	Erdman	aero	-	N	Y		[228] Lemos
	6,000	Erdman	aero	-	Y (<1)	-		[228] Lemos
SP-D	50	Erdman	aero	-	N	Y		[228] Lemos
	6,000	Erdman	aero	-	Y (<1)	-		[228] Lemos
Nod2	35	1254	aero	-	N	N		[188] Gandotra
	1,500	H37Rv	aero	-	N	N		[188] Gandotra
	400	H37Rv	aero	Y (200/>230)	Y (<1)	Y		[189] Divangahi
NLRP3	300	H37Rv	aero	N	N	Y		[230] McElvania TeKippe
	100	H37Rv	aero	-	N	Y		[462] Walter
	300	H37Rv	aero	-	N	N		[463] Dorhoi
NLRP12	300	H37Rv	aero	N	N	N	manual	[464] Allen
NLRC3	200	H37Rv	aero	-	Y (-1)	Y	manual	[465] Hu
NLRC4	300	H37Rv	aero	N	-	-		[230] McElvania TeKippe
cGAS	200	Erdman	aero	Y (150/210)	N	-		[196] Collins
	100	Erdman	aero	N (100)	N	Y	manual	[198] Watson
	1,000	H37Rv	i.n.	N	N	N		[231] Marinho

STING	200	Erdman	aero	N	N	-	gt/gt STING	[196] Collins
	1,000	H37Rv	i.n.	N	N	N		[231] Marinho
AIM2	1,000,000	H37Rv	i.t.	Y (45/>56)	Y (1)	Y		[193] Saiga
Marco	200	H37Rv	i.n.	-	Y (score)	Y		[226] Court
SR-A	200	H37Rv	i.n.	-	N	N		[226] Court
	75	H37Rv	aero	Y (>430/230)	Y (-1, ns)	Y		[217] Sever-Chroneos
SR-B1	100	H37Rv	aero	-	N	N		[209] Schafer
	1,000	H37Rv	aero	-	N	Y		[209] Schafer
CD11b(CR3)	200,000	Erdman	i.v.	N	N	-	3 back-grounds	[232] Hu
	100,000	Erdman	i.v.	-	Y (<1, ns)	-		[233] Melo
TLR-2/4	60	H37Rv	aero	-	N	N		[207] Shi
	600	H37Rv	aero	-	N	N		[207] Shi
	100	H37Rv	aero	-	N	-		[221] Hölscher
TLR2/4/9	100	H37Rv	aero	-	N	N		[221] Hölscher
TLR2/9	75	H37Rv	aero	Y (90/>150)	Y (<1)	Y	manual	[442] Bafica
	75	H37Rv	aero	Y (120/>280)	-	-	manual	[229] Mayer-Barber
	75	Erdman	aero	-	N	N		[458] Gopalakrishnan
Nod2/TLR2	100	H37Rv	aero	-	N	-		[188] Gandotra
CD206/SIGNR1	200	H37Rv	i.n.	-	N	N		[226] Court
SR-A/CD36	200	H37Rv	i.n.	-	N	N		[226] Court
SP-A/D	50	Erdman	aero	-	N	Y		[228] Lemos
	6000	Erdman	aero	-	Y (<1)	-		[228] Lemos

A, change in survival (Yes/No) (median survival KO / median survival control). **B**, change in pulmonary Mtb CFU burden (Yes/No) (maximum log KO/control). **C**, change in immune response observed (Yes/No). **D**, any irregularities from other studies (manual means source was not found in systematic search and was added manually afterwards).

PREFACE TO CHAPTER II

In Chapter I, I have highlighted the history shared between mycobacteria and cell-mediated immunity through CFA, and how PRRs are known to contribute to the immune response to mycobacteria. Through the work presented in Chapter II, we sought to determine the precise contributions of NOD2 and Mincle pathways to the immune response elicited by CFA. With this information, we approached the question of whether an adjuvant composed purely of synthetic mycobacterial ligands could generate similar immunity as the whole mycobacteria in CFA. We show that this is indeed the case with a synthetic adjuvant composed of just two MAMPs, *N*-glycolyl MDP and GlcC14C18.

CHAPTER II – Synthetic mycobacterial molecular patterns partially complete Freund's adjuvant

---

(This Chapter is adapted from an article published in *Scientific Reports*)

Jean-Yves Dubé [1,2,3], Fiona McIntosh [2,3], Juan G. Zarruk [4], Samuel David [4], Jérôme Nigou [5], Marcel A. Behr [1,2,3,6]

1. Department of Microbiology and Immunology, McGill University, Montreal, Quebec, Canada
2. Infectious diseases and Immunity in Global Health Program, Research Institute of the McGill University Health Centre, Montreal, Quebec, Canada
3. McGill International TB Centre, Montreal, Quebec, Canada
4. Centre for Research in Neuroscience, Research Institute of the McGill University Health Centre, Montreal, Quebec, Canada
5. Institut de Pharmacologie et de Biologie Structurale, Université de Toulouse, CNRS, Université Paul Sabatier, Toulouse, France.
6. Department of Medicine, McGill University Health Centre, Montreal, Quebec, Canada

1 – Abstract

Complete Freund's adjuvant (CFA) has historically been one of the most useful tools of immunologists. Essentially comprised of dead mycobacteria and mineral oil, we asked ourselves what is special about the mycobacterial part of this adjuvant, and could it be recapitulated synthetically? Here, we demonstrate the essentiality of *N*-glycolylated peptidoglycan plus trehalose dimycolate (both unique in mycobacteria) for the complete adjuvant effect using knockouts and chemical complementation. A combination of synthetic *N*-glycolyl muramyl dipeptide and minimal trehalose dimycolate motif GlcC14C18 was able to upregulate dendritic cell effectors, plus induce experimental autoimmunity qualitatively similar but quantitatively milder compared to CFA. This research outlines how to substitute CFA with a consistent, molecularly-defined adjuvant which may inform the design of immunotherapeutic agents and vaccines benefitting from cell-mediated immunity. We also anticipate using synthetic microbe-associated molecular patterns (MAMPs) to study mycobacterial immunity and immunopathogenesis.

2 – Introduction

Infection with *Mycobacterium tuberculosis*, or administration of bacille Calmette-Guérin (BCG), normally leads to cell-meditated immunity (CMI) to the corresponding bacterial antigens. The tuberculin skin test is positive when the immune response, a type IV hypersensitivity reaction or delayed-type hypersensitivity (DTH), occurs to tuberculin (a protein extract of *M. tuberculosis*). This "cutaneous sensitivity" was closely examined in the 1940s using complete Freund's adjuvant (CFA, heat-killed *M. tuberculosis* in mineral oil plus

surfactant) [320,321]. These studies provided the first direct evidence for the cellular nature of DTH by transfer from a CFA-immunized guinea pig to a naïve one only through the washed, heat-liable cellular fraction of peritoneal exudates [320,321]. It is now known that DTH is mediated specifically by antigen-sensitive T cells.

Today, CFA is a 'gold standard' adjuvant for eliciting CMI in research models of autoimmune disease. Notable is the experimental autoimmune encephalomyelitis (EAE) model of T-cell meditated destruction of myelin causing ascending paralysis, used most often to model multiple sclerosis [327,337]. CFA is not used in humans because of high reactogenicity [322]. We have asked ourselves: what was the impetus for Jules Freund to develop his eponymous adjuvant with *M. tuberculosis*? For those conducting TB research, it is well appreciated that handling *M. tuberculosis* (a slow growing, clumping, fastidious, and lethally pathogenic organism) is a significant task *per se*. So, why did Freund choose to incorporate these bacteria?

Effort has been made to describe the microbe-associated molecular patterns (MAMPs) in mycobacteria that drive the adjuvant effect. Evidence has pointed to mycobacterial peptidoglycan (PGN), specifically down to the molecular motif muramyl dipeptide (MDP) [108,338]. Mycobacteria are distinct in that they produce the *N*-glycolyl MDP motif in their cell wall [106,107,110] and this PGN modification has been shown to be more potent compared to the common *N*-acetyl MDP motif possessed by other bacteria [108,109]. MDP is thought to be recognized through the host molecule NOD2 [182], and mutations in NOD2 predispose humans to increased risk of mycobacterial and inflammatory diseases [255,284,370,371]. Alternatively, others have pointed to the mycobacterial cell wall lipid trehalose-6,6'-dimycolate (TDM) alone or synergistically with purified PGN [439]. TDM is recognized by the host with the C-type lectin Mincle in concert

with FcRγ and MCL [157,160]. TDM has been demonstrated in animal models to alone be sufficient for granuloma formation and immunopathological responses [157,466].

Both *N*-glycolyl MDP and TDM are MAMPs unique to mycobacteria. Their role in mycobacterial immune responses is supported by the literature and their host receptors are well-known. Additionally, *N*-glycolyl MDP is producible synthetically [108,344,467]. Recently a minimal motif of TDM called GlcC14C18 was produced synthetically and shown to retain adjuvancy but with minimal toxicity [428]. As a complex biologic, CFA is subjected to batch inconsistency. We hypothesized that it is possible to create an entirely synthetic CFA using a rational approach to identify essential MAMPs to replace the whole mycobacteria in the adjuvant. In this work, we establish the necessity for *N*-glycolylation of PGN, NOD2 and Mincle for full CFA adjuvancy. We also demonstrate that the mycobacteria in CFA can be replaced with synthetic *N*-glycolyl MDP and GlcC14C18 in combination to partially restore the adjuvant effect in both a murine model of antigen-specific T-cell immunity as well as the EAE model of autoimmune ascending paralysis.

3 – Results

3.1 – *N*-glycolylation of PGN by mycobacteria is required for complete adjuvancy

Previous work indicated mycobacteria required *N*-glycolylated PGN to elicit a maximal immune response during live infection [108,109]. To determine if CMI elicited from dead mycobacteria in the context of Freund's adjuvant similarly required *N*-glycolylated PGN, we prepared in-house complete Freund's adjuvant with heat-killed *M. tuberculosis* strain H37Rv,

and H37Rv Δ*namH*. NamH is the enzyme responsible for *N*-glycolylation of PGN units as they are being synthesized in the cytoplasm, and the Δ*namH* mutant was previously shown to be devoid of *N*-glycolylation [109] (fig. 1A). We next immunized mice against ovalbumin (OVA, an exemplary antigen) with our CFAs or incomplete Freund's adjuvant (IFA, lacks mycobacteria), and examined OVA-specific cytokine production by CD4+ T-cells from the draining lymph nodes seven days post-immunization (fig. 1B; gating in fig. S1A). Both mycobacteria and *namH* were required to generate the highest proportion of OVA-specific IFN-γ-producing CD4+ T cells (fig. 1C). OVA-specific IL-17A-producing cells required mycobacteria but did not significantly depend on *namH* (fig. 1D). Similar results were seen when examining total numbers of cytokine-producing CD4+ T cells in the lymph nodes (fig. S2A-B), and a closer analysis of the pooled data showed that *namH* contributes to about one third of mycobacteria-induced antigen-specific IFN-γ-producing Th cells (fig. S2C-D). The individual results of experiments are shown separately in fig. S2E; in all four cases we saw the same trends with IFN-γ. These results are consistent with the hypothesized role of mycobacteria being a key ingredient in CFA for eliciting CMI, and that mycobacterial PGN modification by NamH makes a more potent adjuvant.

3.2 – Host *Mincle* and *Nod2* are necessary for complete mycobacterial adjuvancy, but do not mediated the entire CFA effect.

Recognition of mycobacteria during live infection requires the host molecule NOD2 [189]. Because we hypothesize mycobacterial PGN plays a role in CFA adjuvancy, specifically the MDP motif where *N*-glycolylation occurs, we addressed whether the PGN/MDP sensor NOD2 is important for CFA adjuvancy in our OVA model. *Nod2*+/+ and *Nod2*-/- mice were immunized against OVA in the context of CFA or IFA of commercial provenance. A greater proportion of

OVA-specific IFN-γ-producing CD4+ cells was generated in CFA-immunized mice with *Nod2* than without (fig. 2A). An independently produced IFN-γ ELISpot of total lymph node cells supported the same conclusion (fig. S3A), as did another independent experiment using flow cytometry (fig. S3C). In the absence of *Nod2*, the proportion of OVA-specific IL-17A-producing cells was also impaired in CFA-immunized mice (fig. 2B and fig. S3C). With IFA as adjuvant, IFN-γ and IL-17A responses were *Nod2*-independent as expected (fig. 2A-B and S3A-C). Similar trends were observed with total cell numbers (fig. S3B-C and S4A-B). Together, these results corroborate the role for NOD2 and accordingly mycobacterial PGN in the ability of CFA to elicit CMI.

The adjuvant effect of mycobacteria declined partially with *Nod2* knock-out, but not completely. Therefore, there is clearly other mycobacterial MAMP recognition besides that through NOD2 which is important for the remainder CFA adjuvancy. Others have indicated that Mincle-mediated recognition of TDM contributes to mycobacterial adjuvancy [439]. We tested the dependence of our OVA-immunization model with *Mincle*-KO mice [433]. *Mincle*+/+ and *Mincle*-/- mice were immunized against OVA in the presence of CFA and IFA. Generation of CFA-elicited OVA-specific IFN-γ- and IL-17A-producing CD4+ T cells was partially dependent on *Mincle* (fig. 2C-D), while IFA-immunized mice showed *Mincle*-independent responses, as expected (fig. 2C-D). Similar trends were again observed with total cell numbers but did not reach statistical significance (fig. S4C-D). Un-pooled data showed the same trends in both experiments performed (fig. S3D). These results implicate Mincle and thus its main mycobacterial ligand, TDM, in CFA adjuvancy.

Both *Nod2* and *Mincle* were required for CFA adjuvancy in our model, but neither were responsible for the entire adjuvant effect. We asked what the sum of the immune responses

elicited by these PRRs is – if it appears these PRRs signal synergistically. We generated *Mincle-Nod2* double knock-out mice (DKO) and immunized them against OVA with CFA and IFA. The proportion of OVA-specific IFN-γ- and IL-17A-producing CD4+ T cells in CFA-immunized mice declined with DKO relative to WT mice, with no change in IFA-immunized mice (fig. 2E-F). However, the decrease when measuring IFN-γ did not appear obviously larger with DKO than what was observed with single-KO mice. Likewise, the decrease with IL-17A was intermediate, and similar trends were seen with total cell numbers (fig. S4E-F). The residual effect of CFA when both *Nod2* and *Mincle* are disrupted suggests that at least two mycobacterial MAMPs, *N*-glycolylated PGN as well as TDM, are essential, but insufficient, for the full adjuvant effect.

3.3 – Synthetic minimal structures of mycobacterial PGN and TDM work synergistically to stimulate dendritic cell effector functions.

To explore the effect of Mincle and NOD2 signalling on antigen presenting cells (necessary to generate antigen-specific T-cell immunity), we stimulated bone-marrow derived dendritic cells (BMDCs) from WT, *Mincle*-/-, *Nod2*-/- and DKO mice with synthetic versions of the respective PRR ligands. Recently, a rationally determined minimal chemical structure of TDM called GlcC14C18 was shown to retain activity as a Mincle agonist without the 'toxicity' associated with purified TDM [428]. Both synthetic *N*-glycolyl and *N*-acetyl MDP are commercially available. To elicit T-cell immunity, we would expect that mycobacterial MAMPs promote antigen presentation, co-stimulation and cytokine production by antigen presenting cells, the classical signals 1, 2 and 3, respectively.

After 24 hours of MAMP stimulation *in vitro*, we measured the proportion of cells in BMDC culture highly expressing MHC-II (fig. 3A-B). With WT cells, MDPs alone had little effect; GlcC14C18 alone increased the fraction of MHC-II^{hi} cells in WT BMDC cultures (fig. 3A). Combinations of GlcC14C18 with *N*-glycolyl MDP or *N*-acetyl MDP produced the largest responses. Knock-out of *Mincle* greatly reduced the effect of GlcC14C18 in *Mincle*-/- and DKO BMDCs, and knock-out of *Nod2* abrogated the effect of MDPs in *Nod2*-/- and DKO BMDCs. These results suggest these mycobacterial MAMPs can direct myeloid cells towards MHC-II^{hi} expression as expected for professional antigen presenting cells. Similar results were obtained at 48 hours of stimulation (fig. S5A).

On MHC-II^{hi} cells, we looked at the level of expression of MHC-II, CD40, CD80 and CD86 by median fluorescence intensity (MFI) after 24 hours of stimulation *in vitro* (fig. S5F-I). With WT cells and for all markers examined, MDPs alone were unable to substantially enhance expression over the control (fig. 3C-F). GlcC1418 alone increased marker expression, but GlcC14C18 together with *N*-glycolyl MDP synergistically produced the greatest responses. *N*-acetyl MDP was generally less efficacious than *N*-glycolyl MDP. Knockouts behaved as expected: cells without *Mincle* responded poorly to GlcC14C18; cells without *Nod2* failed to respond to MDPs (fig. 3C-F). I addition to 24-hour stimulation, cells were also collected after 48 hours of stimulation, yielding similar results (fig. S5B-I).

BMDCs from WT mice produced TNF in a dose-dependent manner in response to GlcC14C18, but not to MDPs alone (fig. 3G). When combined with limiting or saturating doses of GlcC14C18, *N*-glycolyl MDP synergistically elevated TNF production in a dose-dependent manner. *N*-acetyl MDP only significantly elevated TNF production at higher doses of GlcC14C18 plus MDP and worked less efficaciously than *N*-glycolyl MDP. In the absence of

functional *Mincle*, BMDCs did not respond to GlcC14C18 as expected. *Mincle*-/- BMDCs stimulated with GlcC14C18 and MDPs behaved like BMDCs exposed to MDP alone (little to no detectable TNF production). *Nod2*-/- BMDCs responded to GlcC14C18 but not to MDPs as expected. DKO BMDCs did not respond to either synthetic MAMP as expected. Overall, GlcC14C18 and *N*-glycolyl MDP combined, through *Mincle* and *Nod2* respectively, are sufficient to upregulate BMDC antigen presentation, co-stimulation and cytokine production.

3.4 – Synthetic mycobacterial NOD2 and Mincle ligands can complement IFA to increase antigen-specific T-cell responses.

As NOD2 and Mincle ligands worked synergistically in BMDCs *in vitro* to elicit effector functions in these antigen presenting cells, we hypothesized that IFA can be complemented with NOD2 and/or Mincle ligands to recapitulate at least a portion of the adjuvant effect of whole mycobacteria. Using minimal synthetic MAMPs for PGN (i.e. *N*-glycolyl MDP) and TDM (i.e. GlcC14C18), we complemented IFA to test if CMI could be achieved with a completely synthetic adjuvant containing these essential mycobacterial MAMPs. First, using 10 µg GlcC14C18 per mouse with varying doses of *N*-glycolyl MDP, we observed a dose dependent increase in the proportion and numbers of OVA-specific cytokine-producing CD4+ cells which was significantly greater than IFA alone at the highest dose (fig. 4A). Notably, previous attempts complementing IFA with only *N*-glycolyl MDP did not induce significant numbers of IFN-γ producing cells (fig. S6A-B).

Next, using 30 µg of *N*-glycolyl MDP per mouse and varying the dose of GlcC14C18, we similarly observed a dose dependent increase in the immune response; however this response did not surpass more than half of the level elicited with CFA by IFN-γ and IL-17A (fig. 4B). An

IFN-γ ELISpot performed in parallel provided a similar conclusion (fig. S6C-D). Together, these results show that mycobacterial adjuvancy in the context of CFA can be partially phenocopied synthetically with two mycobacterial MAMPs: namely *N*-glycolyl MDP and GlcC14C18.

3.5 – Synthetic mycobacterial MAMPs increase DC numbers and effectors in lymph nodes.

GlcC14C18 and *N*-glycolyl MDP together were sufficient to elicit antigen-specific T-cell responses. We next looked to see if this MAMP combination was associated with augmentation of DC effector functions *in vivo* as we had seen *in vitro* with BMDCs. Gating for DC subsets as well as other leukocytes in the lymph nodes is depicted in fig. S1B (guided by [468]). We looked in the lymph nodes at 4- and 7-days post-immunization. Both CD11b+ and CD11b- conventional DC (cDC) numbers were increased in the presence of IFA + 10 μg GlcC14C18 + 30 μg *N*-glycolyl MDP compared to IFA alone within 7 days, to levels similar to CFA (fig 5A-B). Trends suggest that early accumulation of cDCs could be driven by MDP alone, but GlcC14C18 together with *N*-glycolyl MDP were required to sustain numbers to day 7.

By MFI, expression levels of MHC-I and -II on both CD11b+ and CD11b- cDCs were not largely altered by MDP nor GlcC14C18 (fig. 5A-B). On CD11b+ cDCs, CD40 expression was elevated the highest and significantly with IFA + GlcC14C18 MDP at both 4 and 7 days. CD80 and CD86 expression were also highest with IFA + GlcC14C18 MDP, with statistical significance at day 4 but not day 7 when expression was possibly waning. On CD11b- cDCs, CD80 and CD86 expression behaved similarly to that on CD11b+ cDCs. CD40 expression of CD11b- cDCs was not statistically significantly greater with IFA + GlcC14C18 MDP compared

to IFA alone at both timepoints. Notably, IFA + GlcC14C18 MDP produced equal or greater costimulatory molecule expression compared to CFA in all cases.

In addition to increased numbers of cDCs in the lymph nodes of mice immunized with GlcC14C18 + *N*-glycolyl MDP, we observed that other leukocytes were substantially elevated in numbers after immunization with this adjuvant (fig. S7A-F). B cells, CD4+ and CD8+ T cells, plasmacytoid DCs, monocytes and PMNs were all increased by 7 days post-immunization relative to IFA, to levels similar to or greater than CFA. By day 7, while MDP alone was insufficient to elevate cell numbers over the IFA background, MDP in combination with GlcC14C18 enhanced numbers beyond the levels attained with GlcC14C18 alone. This provides evidence for synergy between these MAMPs *in vivo*.

3.6 – Synthetic mycobacterial MAMPs can induce EAE similar to CFA.

One of the common uses of CFA is in animal models of autoantigen-specific autoimmunity. To determine if our synthetic formulation can phenocopy the effect of whole mycobacteria to produce a more complex biological outcome such as autoimmunity (and thereby provide a further measure of the 'completeness' of the synthetic formula), we tested IFA + GlcC14C18 + *N*-glycolyl MDP against CFA in ability to induce relapsing-remitting EAE (RR-EAE). Briefly, mice were randomly immunized against myelin oligodendrocyte glycoprotein (MOG) synthetic peptide with CFA or IFA + 10 μg GlcC14C18 + 30 μg *N*-glycolyl MDP, and onset of RR-EAE was determined by clinically scoring ascending paralysis daily in a blinded manner (fig. 6A). Both CFA and IFA + GlcC14C18 + MDP produced RR-EAE that was indistinguishable except quantitatively: over the course of the experiment, the average EAE score was lower with the synthetic adjuvant compared to the CFA control (fig. 6B), with a

cumulative score suggesting about half the disease burden (58% of CFA cumulative score) (fig. 6C). Expectedly, lower EAE scores also corresponded with less weight-loss (fig. S8A). Of note, there were mice in the synthetic adjuvant group that reached the same scores as in the CFA group, but fewer (fig. S8B). Therefore, GlcC14C18 and *N*-glycolyl MDP were sufficient to recapitulate the adjuvant effect of the whole mycobacterial cell in EAE, albeit quantitatively less at the tested doses of MAMPs. Additionally, we had attempted RR-EAE with IFA + TDM + MDP previously, which produced a far less compelling phenocopy of CFA (fig. S8D-G). The IFA + GlcC14C18 + *N*-glycolyl MDP adjuvant has the advantage of being completely synthetic and more efficacious than the TDM-containing adjuvant.

To verify if there were overt qualitative histopathological differences in EAE between CFA and the synthetic adjuvant, we examined spinal cords from three mice from each adjuvant group, having EAE scores 2, 3 and 3.5 at harvest (disease profile of these mice in fig. S8C). Both cellular infiltrates and demyelination of the white matter looked equivalent between adjuvants upon visual inspection (fig. 7A). Mice with different EAE scores had correspondingly different areas of diseased tissue of the spinal cord (fig. 7B), but in comparing adjuvants there was no detectable difference in the area of diseased spinal cord tissue (with statistical power to detect as low as +/- 15% CFA levels) (fig. 7C). The main determining variable was EAE score, not adjuvant. Overall, we observed qualitatively similar autoimmune pathology using IFA + GlcC14C18 + *N*-glycolyl MDP compared to the gold standard CFA.

4 – Discussion

The ability of an adjuvant to elicit CMI can depend on ligand-receptor interactions, specifically MAMP-PRR interactions. It is well appreciated since the hypothesis of Charles Janeway Jr. that the host decision to mount an adaptive immune response requires genetically inborn sensors to detect the presence of microbial products, or microbes by association, and that this is the foundation of classical adjuvants including CFA [123]. These interactions can be thought of as an "arms race" between host and microbe, originating through antagonistic evolution in the case of immune evasion [469]. Additionally, we can imagine the case where a microbe might evolve to increase a specific PRR interaction that favours a specific active immunological environment necessary for its lifecycle. When mycobacteria interact with their host, either in the form of *M. tuberculosis* infection, BCG vaccination or immunization using CFA, CMI normally occurs. The immune response to mycobacteria has been attributed to its unique cell envelope, especially the MDP motif of PGN [108,109,189,338] and TDM [160,439]. We have shown in the context of both CFA-induced immunization and autoimmunity with wholly synthetic *N*-glycolyl MDP and TDM (GlcC14C18) that these MAMP-PRR pathways together contribute partially but significantly to the mycobacterial adjuvant effect.

There are other mycobacterial MAMPs previously identified (and likely more yet unidentified), plus a greater number of PRRs linked to these microbial products. However, most are not yet producible synthetically. Purified mannose-capped lipoarabinomannan (ManLAM) was recently shown to elicit EAE in mice, dependent on the host C-type lectin Dectin-2 (Clec4n), at a dose of 500 µg per animal [165]. Of note, we were not able yet to produce synthetic mimics of ManLAM that induce Dectin-2 signaling [166]. Similarly, purified TDM has been used to elicit EAE at 500 µg per mouse, mostly dependent on MCL (Clec4d) and partially on Mincle

(Clec4e) [160]. These findings support a role for mycobacterial MAMPs driving the CFA effect, but require purification of biologically-sourced MAMPs in high doses. When in combination, our synthetically pure MAMPs have shown clear activity *in vivo* beginning at 1-10 µg. Of note, with CFA we inject 50 µg of mycobacterial mass into mice.

TLR-2 has been documented to interact with multiple mycobacterial lipids [470]. The literature is inconsistent on whether or not TLR-2 promotes CFA-induced EAE [471-474]. Mycobacterial DNA was recently shown to signal through the cGAS/STING pathway after phagosomal disruption via ESX-1 [196,198]. In the context of Freund's adjuvant, it is not clear if heat-killed mycobacteria could have cytosolic access to activate cGAS/STING. The IFA fraction perhaps could deliver MAMPs across membranes. TLR-9 also senses DNA, and appears to play a role during *M. tuberculosis* infection in mice [219], and in humans [475]. TLR-9 was also shown to be necessary for full induction of EAE [471,473]. Although DNA is not unique to mycobacteria like TDM and *N*-glycolylated PGN, synthetic DNA is available and pursuing the role of DNA in mycobacterial adjuvancy interests us, perhaps as a third synthetic MAMP to work with MDP and GlcC14C18.

Mycobacteria are not completely unique in possessing MAMPs that elicit CMI. As an example, the TB vaccine candidate M72/AS01$_E$ utilizes monophosphoryl lipid A (MPLA), a TLR-4 agonist based on lipopolysaccharide (LPS), to elicit CMI. LPS is made in Gram-negative bacteria, not mycobacteria. We concede that many microbes likely contain MAMPs able to elicit CMI; here we have concerned ourselves primarily with the history of mycobacterial adjuvancy, CMI and Jules Freund. It is conceivable that a combination of MAMPs from different bacteria could elicit 'unnatural' immunity that may be beneficial to control certain infectious agents that otherwise evade natural immune responses.

We were able to show that *N*-glycolylation of *M. tuberculosis* PGN altered the adjuvancy of the mycobacterial cell in the context of CFA. This is consistent with our previous work on the increased potency of mycobacterial PGN in other contexts [108,109]. Interestingly, the benefit of *N*-glycolylation of PGN seemed primarily skewed toward IFN-γ production rather than IL-17A, while *Nod2*-KO showed a greater effect with IL-17A. This may indicate that mycobacteria retain *N*-glycolylation of PGN specifically to shift immune responses in a Th1 bias and should be further investigated during live infection. *Nod2* was necessary for full CFA adjuvancy by measures of IFN-γ and IL-17A, supporting the role for mycobacterial PGN. We were somewhat surprised that MDP emulsified by itself with IFA and antigen was insufficient to recapitulate the adjuvant effect of CFA. In a 1975 paper, *N*-acetyl MDP appeared sufficient in a guinea pig model to elicit DTH using OVA as antigen [338]. In 2009 using a very similar model to our current work, *N*-glycolyl MDP alone was sufficient to increase ELISpot IFN-γ to near CFA levels, while *N*-acetyl MDP failed [108]. One explanation is the possibility of contaminating MAMPs in certain preparations of OVA. OVA is known to often come with a dose of endotoxin which affects the immunological outcome of experiments [476]. In the current investigations we have used endotoxin-free/ultra-pure OVA. Much literature of *in vitro* experiments shows MDP requires another MAMP to produce measurable outputs like cytokine [108,348,349,477], although in few cases MDP was shown to elicit cellular responses by itself [348,477]. Responses measured from MDP alone may be unrepresentative of a cell's maximum capacity.

Other groups have supported a role for TDM in mycobacterial adjuvancy [160,439]. TDM together with purified PGN was shown to synergistically promote IL-17 production from OVA-specific (OT-II) CD4+ T cells adoptively transferred into congenic mice [439]. This and other work directed us to test Mincle-dependence of CFA and MDP synergy with the minimal TDM motif

GlcC14C18. *Mincle*-/- mice allowed us to infer that CFA adjuvancy required TDM for maximal induction of IFN-γ- and IL-17A-producing Th cells. TDM is thought to be the main Mincle ligand in mycobacteria; however, there are other ligands. Purified from H37Rv, trehalose-6,6'-monomycolate, glucose monomycolate, diacyl-trehalose and triacyl-trehalose were shown to stimulate mouse and human Mincle (plus glycerol monomycolate stimulates human Mincle only) [428]. It is possible that the phenotype of reduced immunity was because the sensing of these other MAMPs was decreased. Nevertheless, Mincle signalling was essential for full CFA adjuvancy.

Interestingly, simultaneous knock-out of both *Mincle* and *Nod2* resulted in incomplete abrogation of CFA adjuvancy. DKO mice more closely resembled single-KO from separate experiments, compared to controls, than IFA. This indicates two things: 1) that much of the adjuvancy of mycobacteria is not mediated through Mincle and NOD2, and therefore other mycobacterial MAMPs like those mentioned above may play a similarly important role as PGN and TDM; 2) that Mincle and NOD2 signalling might work synergistically, where in the absence of Mincle, NOD2 sensing of PGN is blunted as we have seen clearly *in vitro* with GlcC14C18 and *N*-glycolyl MDP, and therefore DKO resembles single knock-out of either receptor.

We demonstrated that GlcC14C18 plus *N*-glycolyl MDP synergistically were sufficient to promote DC effector functions *in vitro*. The GlcC14C18 plus *N*-glycolyl MDP adjuvant was also the most efficacious adjuvant to drive costimulatory molecule upregulation on cDCs *in vivo*, more than either MAMP alone. While either of these MAMPs by themselves failed to come close to the whole mycobacteria of CFA in our OVA model of CMI, together we showed they could produce about half the Th cell IFN-γ/IL-17A response and EAE disease burden as CFA. Resultingly, we are interested in further understanding the implications for MAMP signalling (which MAMPs synergize together; what redundancy exists; do different combinations alter the

Th type of CMI?). As the DKO data suggest, other mycobacterial MAMPs may be necessary to fully recapitulate the adjuvant effect of whole mycobacteria. An optimal dose of the two MAMPs may not have been reached, although additional dosing experiments (not shown) failed to find a clearly superior formulation than those presented here.

We chose to proceed primarily with the 10 µg GlcC14C18 + 30 µg *N*-glycolyl MDP doses because these quantities were sufficient for some biological activity on their own and/or in combination (fig. 4A-B, S6D and not shown). Detailed subset data also showed other biological synergy at the 10 µg / 30 µg dose (fig. S7). Mycobacteria are an estimated 30% PGN by mass, of which the MDP motif comprises about half, or 15% total mycobacterial mass [478]. Therefore, when injecting 50 ug of mycobacteria as CFA, we inject about 8 µg of MDP. The 10 µg / 30 µg dose did not quantitatively phenocopy the level of CMI from CFA in the OVA model, but we did not want to achieve this by using grossly unrepresentative quantities of MAMPs. Considering the DKO data showing *Mincle* and *Nod2* stimulation do not drive all of the CFA effect, we proceeded with tempered expectations for EAE. Nonetheless, we have demonstrated that synthetic TDM and *N*-glycolyl MDP signalling, unique to mycobacteria, enhance the adjuvancy of CFA. This partly corroborates the natural history of CFA in why it is a uniquely potent adjuvant. Remaining MAMPs, not necessarily unique to mycobacteria, might fill the difference.

With the wholly synthetic formulation of GlcC14C18 *N*-glycolyl MDP, we were able to induce RR-EAE in mice that was qualitatively indistinguishable from that induced with CFA, but milder overall (lower EAE scores on average). We selected spinal cords from mice having matched EAE scores between CFA and synthetic adjuvant groups; however, extrapolating the histopathological data to all the mice in our experiment, we would expect that the synthetic adjuvant produced less pathology in the spinal cord on average since EAE scores were lower on

average. The EAE result correlated with the incomplete complementation in the OVA model. EAE that failed with TDM plus MDP earlier was also less potent in the OVA model than the synthetic formulation (not shown), further indicating correlation between these readouts. CFA often needs to be 'titrated' to account for batch-dependent efficacy in our experience (not shown), and CFA with higher concentrations of mycobacteria (i.e. 4 mg/ml) is also used when a more severe, chronic progressive EAE is necessary for studies [331]. These facts point to dosing as a means of controlling the degree of EAE, which may work with the synthetic adjuvant. Other experimental uses of CFA include the collagen-induced arthritis (CIA) model and for producing specific antibodies. CIA takes longer and has a greater role for humoral immunity than EAE which is T-cell driven, (our interest was in CMI for this study) [479]. Wherever mycobacterial adjuvancy is useful, we suspect a synthetic adjuvant could be beneficial. Indeed, intravesical injection of BCG is used to treat bladder cancer (i.e. BCG can provide MAMP-driven protection, not simply antigen-specific protection). Furthermore, BCG administration to millions of babies each year can protect not just against childhood TB, but non-specifically against other diseases [297].

Our work demonstrates that mycobacterial NOD2 and Mincle ligands contribute to the adjuvant effect of the mycobacterial cell, and that a necessarily combinatorial formulation of synthetic MAMPs, *N*-glycolyl MDP and GlcC14C18, can partly recapitulate the adjuvant effect of whole mycobacteria to induce T-cell immunity and EAE. In addition to demonstrating the first entirely synthetic multi-MAMP mycobacterial adjuvant, we have outlined an approach to investigate the contribution of other MAMPs to adjuvant design. Moreover, the synthetic approach may be useful to probe mycobacterial immunity and immunopathogenesis.

5 – Methods

Mice

C57BL/6J ('wild-type') as well as *Nod2*-/- mice were obtained from Jackson laboratories and were bred or used immediately for experiments. *Mincle*-/- mice breeders were provided courtesy of the laboratory of Christine Wells [433]. Mice were genotyped to confirm absence of the *Dock2* mutation recently reported in *Nod2*-/- mice [480]. We crossed *Nod2*-/- and *Mincle*-/- mice to obtain double knock-out mice. All experiments used mice from 6 to 20 weeks of age. All protocols involving mice followed the guidelines of the Canadian Council on Animal Care (CCAC) and were approved by the ethics committees of the RI-MUHC.

Preparation of adjuvants and ovalbumin immunization

Complete and incomplete Freund's adjuvant were purchased from Sigma or InvivoGen. In some cases, IFA was made by the experimenter from purified mineral oil and mannide monooleate (Sigma). Adjuvants were prepared on the day of immunization by emulsifying CFA (1 mg/ml *M. tuberculosis*) or IFA with a PBS solution containing 1 mg/ml ovalbumin (Endofit brand, InvivoGen) in a 1:1 ratio. Emulsification was accomplished using all-plastic syringes and repeated passage through an 18-G blunt-end needle. Where IFA was complemented with mycobacterial components: MDP (InvivoGen) was diluted in the PBS fraction of the adjuvant before emulsification; TDM (Sigma) or GlcC14C18 [428] were dissolved in the IFA fraction before emulsification as described previously [439]; heat-killed mycobacteria in saline were diluted in PBS and added to the PBS fraction of the adjuvant before emulsification for mice to receive an

equivalent of 10^8 CFU. To make heat-killed mycobacteria, cultures were grown to equivalent 600-nm absorbance at mid-log phase, were pelleted and washed three times with saline, then heat-killed at 100°C for 30 minutes and frozen at -80°C until use. Mice were injected subcutaneously with 100 µl adjuvant-antigen emulsions in the tail 1-2 cm from the body, towards the body, for sufficient and consistent drainage to the inguinal lymph nodes. Four or seven days after injection mice were euthanized and organs were harvested for analysis.

ELISpot and flow cytometry of lymph node cells

Lymph nodes extracted from immunized mice were gently crushed over 70-µm cell strainers to release the cells therein. Cell concentrations were determined by counting with a haemocytometer or with a BD Accuri C6 flow cytometer. Lymph node cells (LNCs) were washed in culture medium, counted and cultured in 100 µl RPMI + 10% FBS (R10) at 250,000 or 500,000 cells per well in IFNγ ELISpot plates (R&D Systems) with or without 100 µg OVA for ~40 hours at 37°C 5% CO_2 before developing the ELISpot plates. For flow cytometry analysis of OVA-specific cytokine production, washed LNCs were cultured at 6 million cells per ml in 200 µl R10 with or without 200 µg OVA for ~40 hours at 37°C 5% CO_2, Brefeldin A (GolgiPlug, BD) was added for an additional 5 hours, and then cells were stained and fixed (BD fixation/permeabilization solution) for flow cytometry on ice. Intracellular staining was performed on the same or the next day using BD Perm/Wash buffer. See Table S1 for antibody probes used. For flow cytometry of leukocyte subsets, 3 million LNCs were taken immediately after harvest for extracellular staining and fixing. See Table S2 for antibody probes used. A BD LSRFortessa X-20 was used for cellular phenotyping.

Bone marrow-derived dendritic cells (BMDCs)

Bone marrow was extracted from mice by flushing femora and tibiae with PBS + 2% BSA + 2% glucose using a 25-G syringe. Red blood cells were lysed and remaining bone marrow cells were filtered through 70 µm cell strainer. Cells were cultured at 500,000 cells / ml R10 with 20 ng/ml murine rGM-CSF (PeproTech); cells were fed on day 3 with R10 + rGM-CSF, and on day 6 with R10 alone. On day 7, loosely adherent cells were harvested by gentle pipetting and used in assays. These cells were ~60% CD11c+ MHC-II+ as we obtain routinely. To assess cytokine production, 100,000 BMDCs were transferred per well to 96-well plates precoated with GlcC14C18 (by dissolving in isopropanol and drying) and containing MDP in a final volume of 200 µl. BMDCs were incubated with stimulants for 6 hours at 37°C, 5% CO_2 before supernatant was removed and stored at -80°C for later ELISA analysis (mouse TNF ELISA from ThermoScientific). To assess surface marker expression, 300,000 BMDCs were transferred per FACS tube precoated with 50 ng GlcC14C18 (by dissolving in isopropanol and drying) and containing 100 ng/ml MDP in a final volume of 200 µl. BMDCs were incubated with stimulants for 24 or 48 hours at 37°C, 5% CO_2 before staining and fixing for flow cytometry analysis. See Table S3 for antibodies used in flow cytometry.

Relapsing-remitting experimental autoimmune encephalomyelitis (RR-EAE)

Adjuvants were prepared similarly as above, but with myelin oligodendrocyte glycoprotein (MOG) used as antigen. Briefly, PBS solution containing 1 mg/ml MOG +/- 600 µg/ml *N*-glycolyl MDP was emulsified with CFA (1 mg/ml *M. tuberculosis*) / IFA plus 200 µg/ml

GlcC14C18 (or 20 μg/ml TDM) by back-and-forth extrusion through an 18 G two-way needle with two all-plastic syringes. 8-12 week-old female C57BL/6 mice (Charles River) were induced for RR-EAE by a standard protocol: briefly, on day 0, pertussis toxin (PT) (200 ng) was administered i.v. in the tail vein, and mice were immunized with 50 μg MOG by bilateral s.c. injection in the back towards the tail with 100 μl total of an emulsification of CFA or IFA plus mycobacterial MAMPs (adjuvant group was randomized within and across cages). On day 2, mice received a second equivalent dose of PT i.v.. After about one week, EAE was scored blinded (i.e. the scorer did not know the adjuvant received by the mouse) every day according to these cumulative criteria: 0, no paralysis (normal); 0.5, partial tail weakness observed as < 50% of tail dragging when mouse walks; 1, tail paralysis observed as >50% of tail dragging as mouse walks; 2, slow righting reflex (delay < 5 seconds) when mouse is flipped; 3, very slow or absent righting reflex (> 5 seconds) or inability to bear weight with back legs observed as dragging hindquarters when walking; 3.5, partial paralysis of one or both hind limbs; 4, complete paralysis of one or both hindlimbs; 4.5, complete paralysis of one or both hind limbs plus trunk weakness; 5, weakness or paralysis of forelimbs; 6, found dead. Mice were weighed every other day during scoring. Mice reaching a score of 5 were euthanized within 24 hours. Blinding was accomplished by having one person inject the mice and another person score/weigh the mice, unaware of experimental group.

Histopathology

At the end of EAE scoring, the experiment was un-blinded and three mice from each group with matching scores were selected. These six mice were anesthetized with peritoneal ketamine injection, were perfused with PBS and formalin, and then spinal cords were extracted,

equilibrated in sucrose and then frozen in OTC compound (VWR). Frozen tissue was sectioned 14-nm thick onto slides and then stained (Nissl or Luxol fast blue). Sections of good quality (20 per mouse, 5 cervical, 5 upper thoracic, 5 lower thoracic and 5 lumbar) were randomly selected and photographed with a Nikon Eclipse NI microscope. Randomized (blinded) Nissl stain photographs were used to quantify the area of disease in the spinal cord by subtracting the total 2D area of each tissue section with the area without cellular infiltration in white matter (thus, the difference of areas is the area with cellular infiltration). This was divided by the total area to determine the fraction or percent of diseased area.

Software, data analysis and statistics

Flow cytometry data was acquired using FACSDiva software (BD). FCS files were analyzed using FlowJo V10 (BD). Digital microscopy images were analyzed with ImageJ (NIH). Graphs were generated and routine statistical testing was accomplished with GraphPad Prism 8.1.1 (GraphPad Software Inc.; https://www.graphpad.com/). Assessment for normal data, then parametric or non-parametric analyses were applied, as indicated. Sample-size and power calculations were performed manually using Microsoft Excel. Manuscript figures were assembled with Microsoft PowerPoint.

6 – Acknowledgements

We would like to thank the Containment Level 3 platform of the Research Institute of the McGill University Health Centre (RI-MUHC) for providing the needed facilities and intellectual support. We thank the Immunophenotyping platform of the RI-MUHC for cytometers and

advice. We are very grateful to Christine Wells (University of Melbourne, Australia) for providing *Mincle*-KO mice and to Alexiane Decout for preparing GlcC14C18. For tutelage and technical assistance, J.Y.D. is thankful to Damien Montamat-Sicotte, Ourania Tsatas, Sarah Danchuk, Iain Roe, Andréanne Lupien, Nimara Asbah, and Daniel Houle. J.Y.D. was personally supported by the Canadian Institutes of Health Research (CIHR) Canada Graduate Scholarship – Master's Program, Fonds de Recherche du Québec – Santé (FRQ-S) Doctoral Training Award, RI-MUHC studentships (Master's and Ph.D.) and scholarships from the McGill Department of Microbiology and Immunology. Research activities were funded by CIHR foundation grant held by M.B. and a CIHR grant held by S.D.

Additional Information

Competing interests: the authors have none.

Author Contributions

Conceptualization, J.Y.D. and M.B.; Methodology, J.Y.D. and J.G.Z.; Investigation, J.Y.D., F.M. and J.G.Z.; Resources, S.D., J.N. and M.B.; Writing – Original Draft, J.Y.D. and M.B.; Writing – Review & Editing, J.Y.D., F.M., J.G.Z., S.D., J.N. and M.B.; Visualization, J.Y.D.; Supervision, S.D. and M.B.; Funding acquisition, J.Y.D., S.D. and M.B.

7 – Figures

Chapter II, Figure 1. CFA-dependent cell-mediated immune responses as a function of mycobacterial *namH*.

A, PGN of wild-type H37Rv *M. tuberculosis* (left) and PGN of the Δ*namH* mutant (right). The MDP motif is drawn in red, and the site of *N*-glcolylation is in bold font. With NamH, *N*-glycolylation was shown on ~70% of muramic acid residues, with *N*-acetylation on the remaining ~30% [106,109]. **B**, immunization scheme (relevant to figs. 1, 2 and 4): mice were immunized with adjuvant emulsion containing OVA by s.c. injection at the base of the tail, and after seven days, inguinal (draining) lymph nodes were harvested. Lymph node cells were cultured *ex vivo* with or without OVA to examine the OVA-specific cytokine response by flow cytometry or ELISpot. **C-D**, Proportion of cytokine-producing CD4+CD8- lymph node cells of mice immunized against OVA with heat-killed *M. tuberculosis* strain H37Rv, H37Rv Δ*namH*, or IFA alone, seven days prior. Shown are data pooled from four separate experiments with averages +/- SEM. p-values were calculated with two-tailed student's *t*-tests. *$p<0.05$. For IFA + H37Rv, IFA + H37Rv Δ*namH*, and IFA alone, sample size N = 31, 27 and 16 mice, respectively. Each plotted point represents the result obtained from an individual mouse.

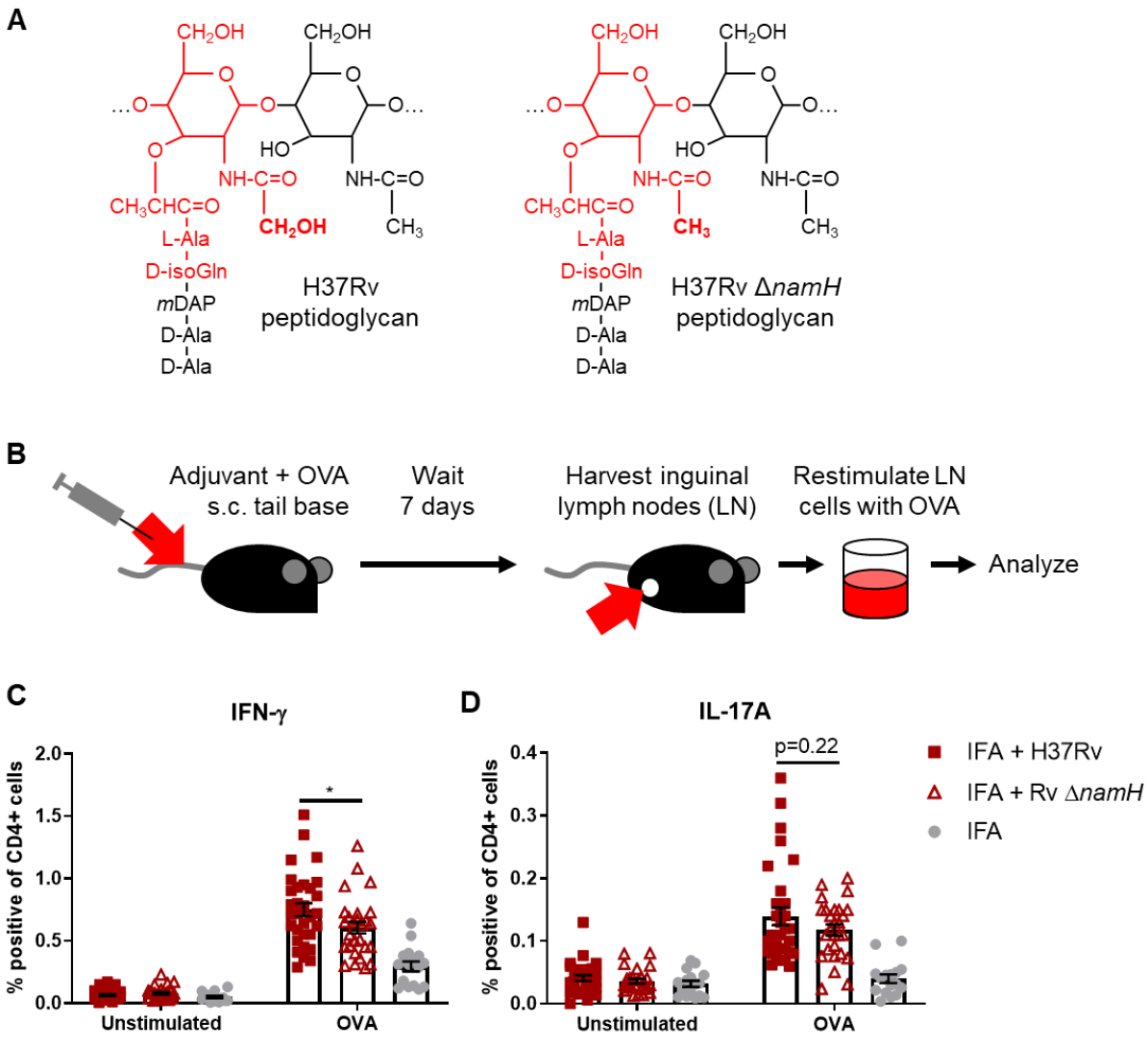
A
H37Rv peptidoglycan
H37Rv ΔnamH peptidoglycan
B
Adjuvant + OVA s.c. tail base
Wait 7 days
Harvest inguinal lymph nodes (LN)
Restimulate LN cells with OVA
Analyze
C
IFN-γ
% positive of CD4+ cells
Unstimulated
OVA
*
D
IL-17A
p=0.22
IFA + H37Rv
IFA + Rv ΔnamH
IFA

Chapter II, Figure 2. CFA-dependent cell-mediated immune responses as a function of host *Nod2* and *Mincle*.

Proportion of cytokine-producing CD4+CD8- lymph node cells of mice immunized against OVA with CFA or IFA seven days prior. **A-B**, *Nod2*+/+ vs. *Nod2*-/- mice, data representative of two independent experiments with averages +/- SEM. p-values were calculated with two-tailed student's *t*-tests. *p<0.05; **p<0.01. For CFA *Nod2*+/+, CFA *Nod2*-/-, IFA *Nod2*+/+ and IFA *Nod2*-/-, sample size N = 12, 13, 9 and 7 mice, respectively. **C-D**, *Mincle*+/+ vs. *Mincle*-/- mice, data pooled from two independent experiments with averages +/- SEM. p-values were calculated with two-tailed student's *t*-tests. *p<0.05; **p<0.01. For CFA *Mincle*+/+, CFA *Mincle*-/-, IFA *Mincle*+/+ and IFA *Mincle*-/-, sample size N = 14, 16, 15 and 11 mice, respectively. **E-F**, WT (*Mincle*+/+*Nod2*+/+) vs. DKO (*Mincle*-/-*Nod2*-/-) mice with averages +/- SEM. p-values were calculated with two-tailed student's *t*-tests. *p<0.05; **p<0.01. For CFA WT, CFA DKO, IFA WT and IFA DKO, sample size N = 10, 7, 7 and 7 mice, respectively.

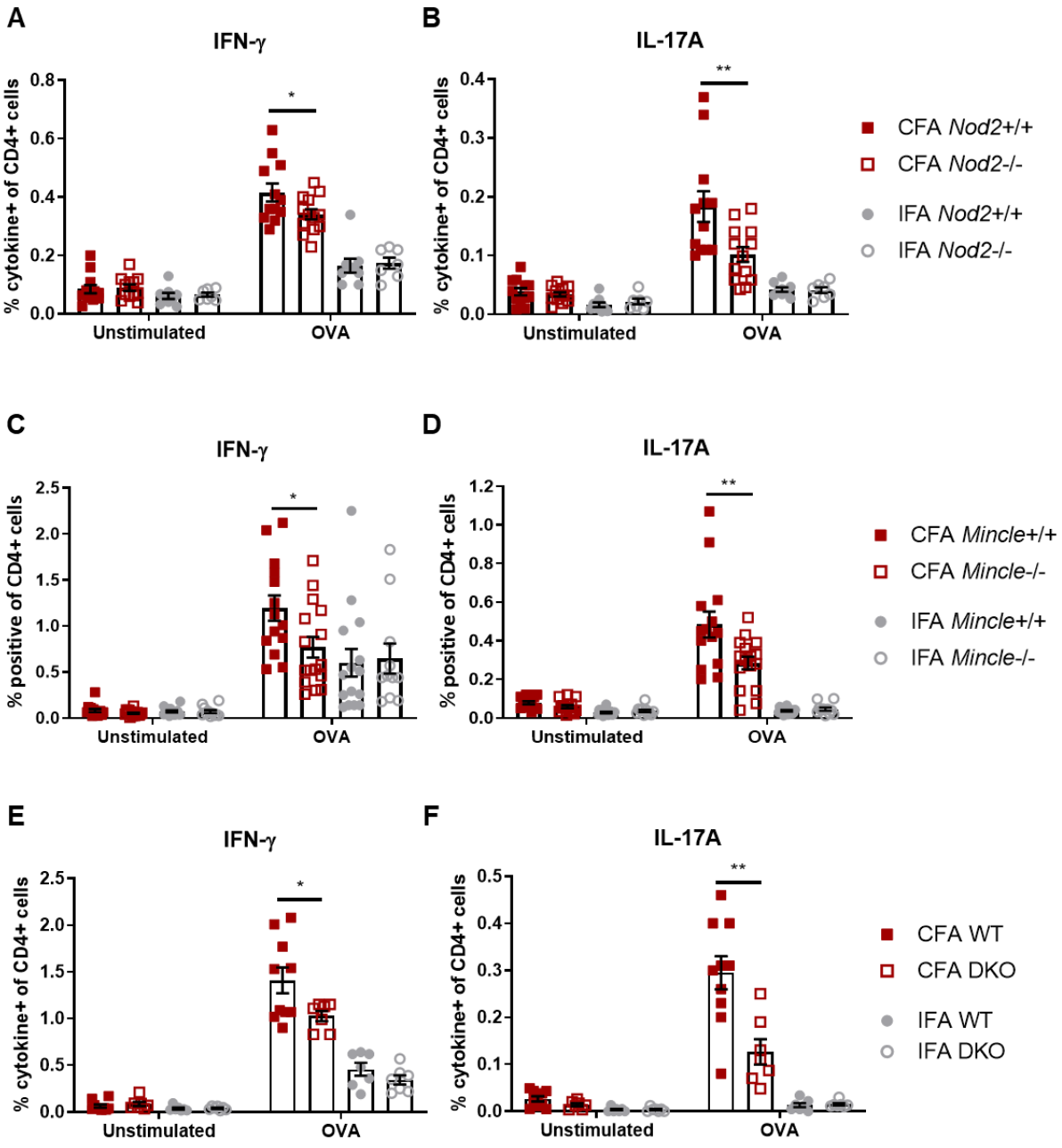
A
IFN-γ
% cytokine+ of CD4+ cells
0.8
0.6
0.4
0.2
0.0
*
Unstimulated
OVA
B
IL-17A
% cytokine+ of CD4+ cells
0.4
0.3
0.2
0.1
0.0
**
Unstimulated
OVA
CFA Nod2+/+
CFA Nod2-/-
IFA Nod2+/+
IFA Nod2-/-
C
IFN-γ
% positive of CD4+ cells
2.5
2.0
1.5
1.0
0.5
0.0
*
Unstimulated
OVA
D
IL-17A
% positive of CD4+ cells
1.2
1.0
0.8
0.6
0.4
0.2
0.0
**
Unstimulated
OVA
CFA Mincle+/+
CFA Mincle-/-
IFA Mincle+/+
IFA Mincle-/-
E
IFN-γ
% cytokine+ of CD4+ cells
2.5
2.0
1.5
1.0
0.5
0.0
*
Unstimulated
OVA
F
IL-17A
% cytokine+ of CD4+ cells
0.5
0.4
0.3
0.2
0.1
0.0
**
Unstimulated
OVA
CFA WT
CFA DKO
IFA WT
IFA DKO

Chapter II, Figure 3. MHC-II expression, costimulatory molecule upregulation and TNF production and by BMDCs stimulated with GlcC14C18 and MDPs.

A, percentage of cells expressing MHC-II at high levels (according to gate in panel B) after 24 hours of stimulation with the indicated MAMPs. **B**, gating of MHC-II^{hi} cells amongst live single CD11b+CD11c+ cells. **C**-**F**, median fluorescence intensity of **C**, MHC-II; **D**, CD40; **E**, CD80; **F**, CD86 on CD11b+CD11c+MHC-II^{hi} cells after 24 hours of stimulation with the indicated MAMPs (use legend of panel A). Shown are averages +/- SD of 3 individually stimulated and assayed cultures. To compare the combination of GlcC14C18+*N*-glycolyl MDP to unstimulated control, GlcC14C18 alone and GlcC14C18+*N*-acetyl MDP with WT cells, p-values were calculated using Dunnett's T3 multiple comparisons test; $p<0.05$; $^{**}p<0.01$; $^{***}p<0.001$; $^{****}p<0.0001$; ns, not significant, $p>0.05$. **G**, Supernatant TNF after 6-hour stimulation with GlcC14C18 and MDPs. Shown are averages +/- SD of 3-6 individually stimulated and assayed culture wells. To determine which MDP dose elicited significantly more TNF over background dose of GlcC14C18, p-values were calculated with Dunnett's multiple comparisons test. The *, # and & symbols were used for the 17, 50 and 150 ng GlcC14C18 doses respectively, where $^{*}p<0.05$; $^{**}p<0.01$; $^{***}p<0.001$ (for clarity, non-significant p-values are not noted).

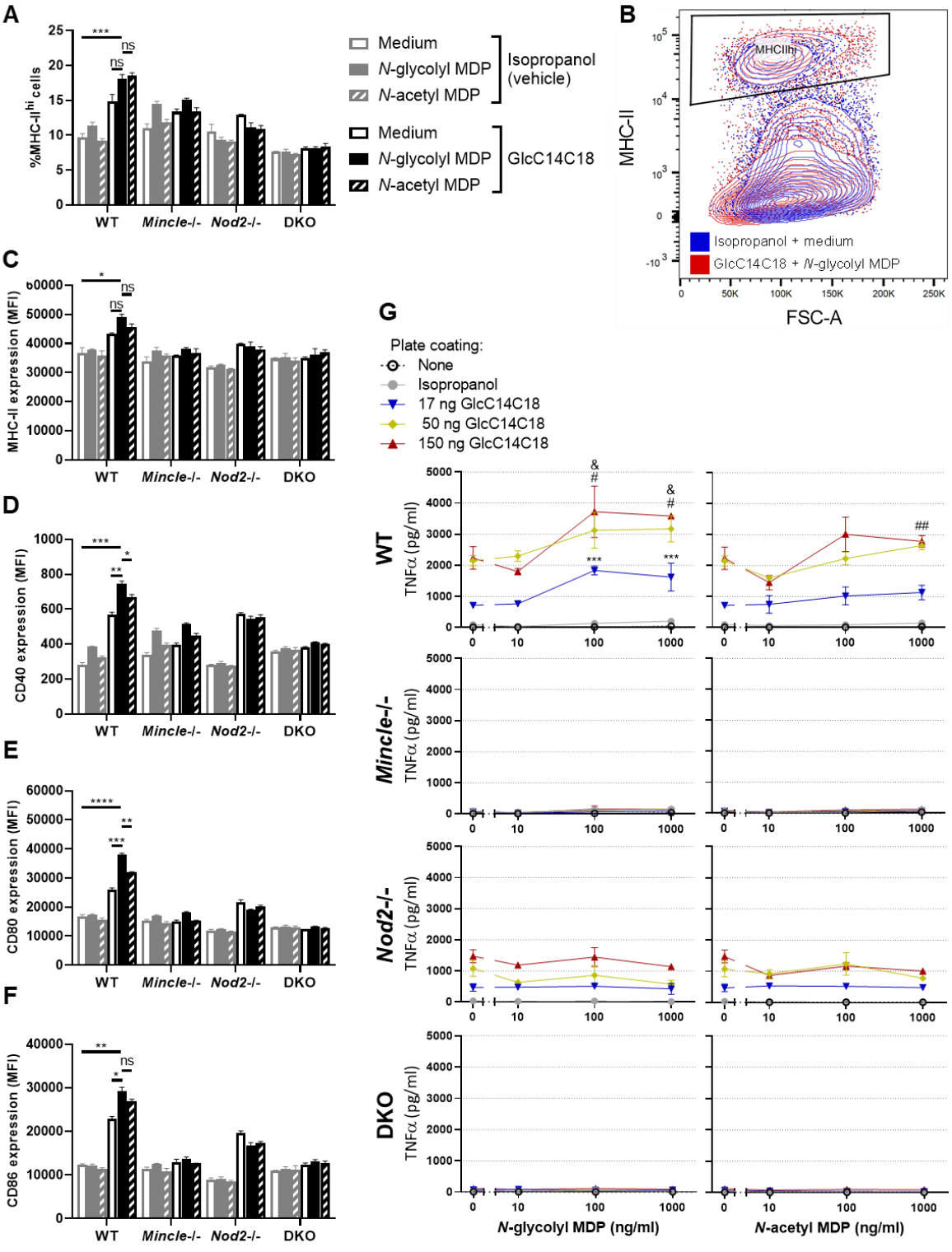
A
%MHC-II^hi cells
Medium
N-glycolyl MDP
N-acetyl MDP
Isopropanol (vehicle)
Medium
N-glycolyl MDP
N-acetyl MDP
GlcC14C18
WT
Mincle-/-
Nod2-/-
DKO
B
MHC-II
FSC-A
MHCIIhi
Isopropanol + medium
GlcC14C18 + N-glycolyl MDP
C
MHC-II expression (MFI)
D
CD40 expression (MFI)
E
CD80 expression (MFI)
F
CD86 expression (MFI)
G
Plate coating:
None
Isopropanol
17 ng GlcC14C18
50 ng GlcC14C18
150 ng GlcC14C18
WT
Mincle-/-
Nod2-/-
DKO
TNFα (pg/ml)
N-glycolyl MDP (ng/ml)
N-acetyl MDP (ng/ml)

Chapter II, Figure 4. Complementation of IFA with synthetic mycobacterial MAMPs.

Proportion of cytokine-producing CD4+CD8- lymph node cells of WT mice immunized against OVA seven days prior. **A**, *N*-glycolyl MDP dose-dependent response with 10 µg GlcC14C18: IFA (N=4), IFA + 10 µg GlcC14C18 (N=7), IFA + 10 µg GlcC14C18 + 1 µg *N*-glycolyl MDP (N=6), and IFA + 10 µg GlcC14C18 + 3 µg *N*-glycolyl MDP (N=7). Shown are data from individual mice, with averages +/- SEM. p-values were calculated with Welch's two-tailed student's *t*-tests. *p<0.05; **p<0.01. **B**, GlcC14C18 dose-dependent response with 30 µg *N*-glycolyl MDP: IFA + 30 µg *N*-glycolyl MDP (N=6), IFA + 30 µg *N*-glycolyl MDP + 10 µg GlcC14C18 (N=7), IFA + 30 µg *N*-glycolyl MDP + 30 µg GlcC14C18 (N=7), and CFA (N=7). Shown are data from individual mice, with averages +/- SEM. In comparing IFA + 30 µg *N*-glycolyl MDP to IFA + *N*-glycolyl MDP + 10 or 30 µg GlcC14C18, p-values were calculated using Dunnett's T3 multiple comparisons test. *p<0.05; **p<0.01; ns, not significant, p>0.05.

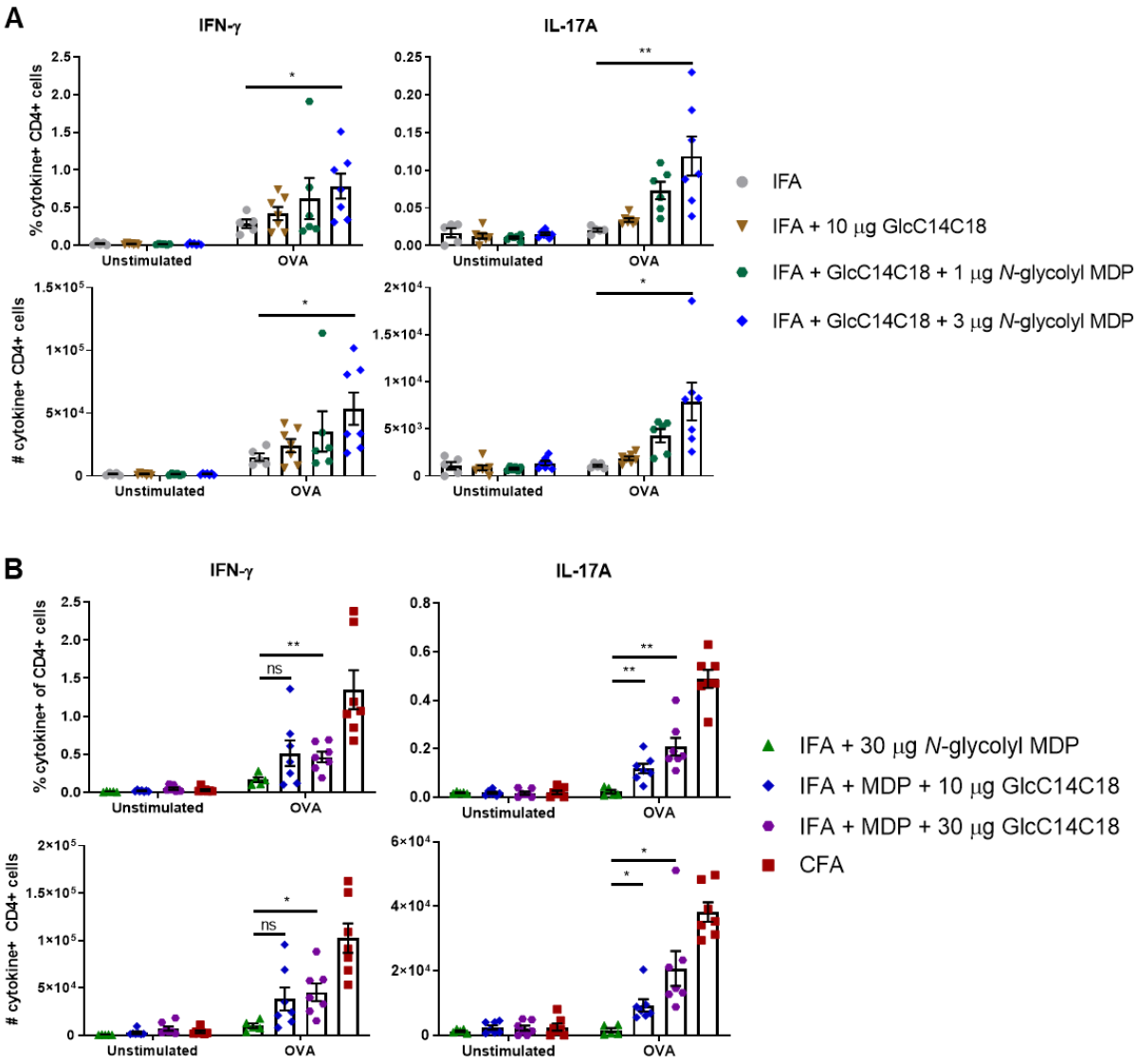
A
IFN-γ
IL-17A
% cytokine+ CD4+ cells
# cytokine+ CD4+ cells
Unstimulated
OVA
IFA
IFA + 10 μg GlcC14C18
IFA + GlcC14C18 + 1 μg N-glycolyl MDP
IFA + GlcC14C18 + 3 μg N-glycolyl MDP
B
IFN-γ
IL-17A
% cytokine+ of CD4+ cells
# cytokine+ CD4+ cells
ns
Unstimulated
OVA
IFA + 30 μg N-glycolyl MDP
IFA + MDP + 10 μg GlcC14C18
IFA + MDP + 30 μg GlcC14C18
CFA

Chapter II, Figure 5. Dynamics of cDCs in lymph nodes after immunization with synthetic mycobacterial MAMPs.

A, CD11b+ cDC quantities and median fluorescence intensity of MHC-I, MHC-II, CD40, CD80 and CD86 in mice immunized with the indicated adjuvants after 4 or 7 days. **B**, CD11b- cDC quantities and median fluorescence intensity of MHC-I, MHC-II, CD40, CD80 and CD86 in mice immunized with the indicated adjuvants after 4 or 7 days. For all adjuvant groups, N=8 mice (each plotted point represents data from an individual mouse). Shown are averages +/- SEM. To determine if IFA + GlcC14C18 + *N*-glycolyl MDP altered cDC parameters compared to IFA alone, p-values were calculated using Dunnett's T3 multiple comparisons test correcting for multiple timepoints and cDC type (CD11b+/-). *$p<0.05$; **$p<0.01$; ns, not significant, $p>0.05$.

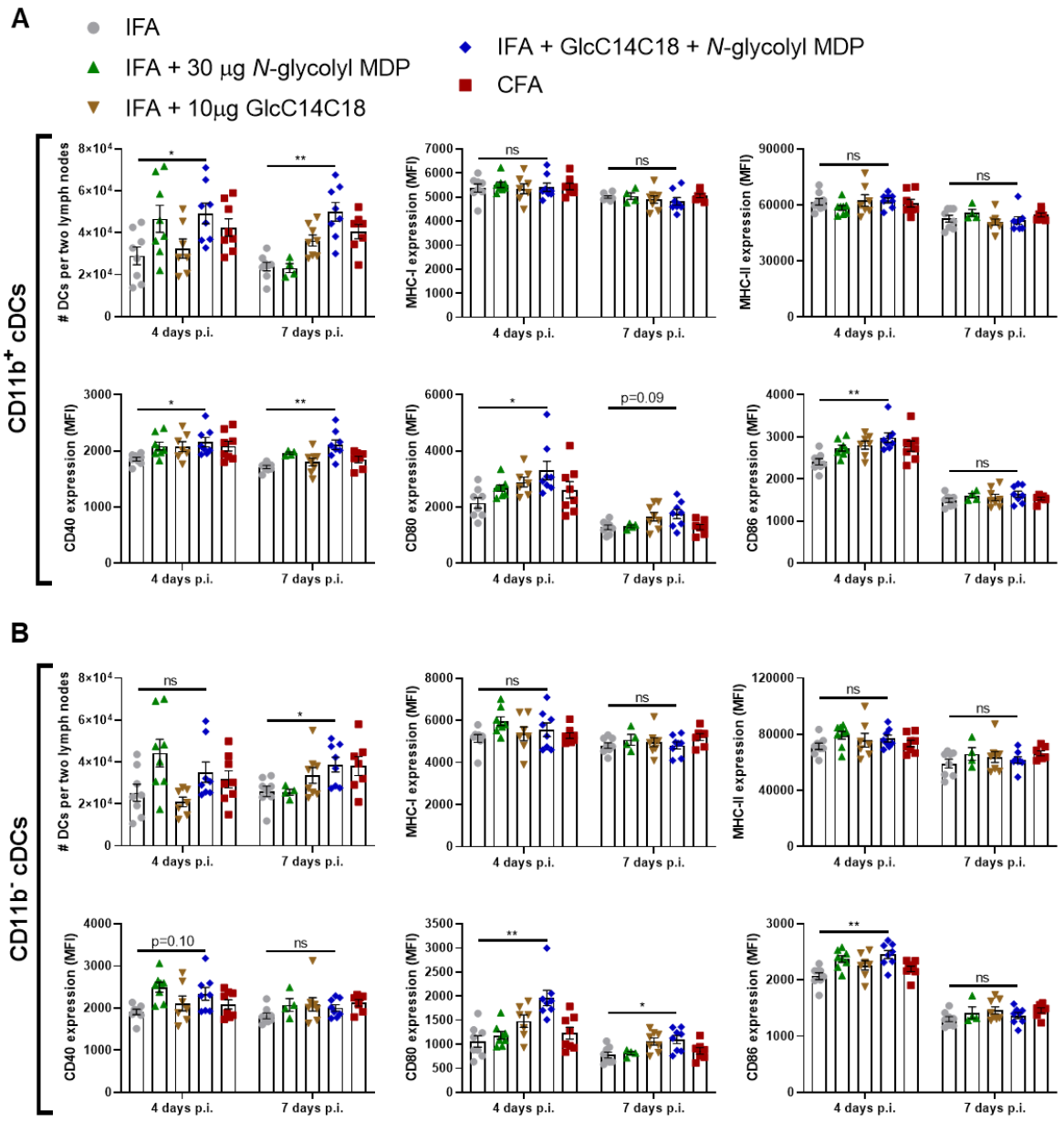
A
IFA
IFA + 30 µg N-glycolyl MDP
IFA + 10µg GlcC14C18
IFA + GlcC14C18 + N-glycolyl MDP
CFA
CD11b+ cDCs
DCs per two lymph nodes
MHC-I expression (MFI)
MHC-II expression (MFI)
CD40 expression (MFI)
CD80 expression (MFI)
CD86 expression (MFI)
4 days p.i.
7 days p.i.
ns
p=0.09
B
CD11b- cDCs
p=0.10

Chapter II, Figure 6. RR-EAE induced by IFA+GlcC14C18+MDP.

A, experimental timeline. **B**, average EAE score +/- SEM over time of mice induced with CFA (N=15) or IFA + 10 µg GlcC14C18 + 30 µg *N*-glycolyl MDP (N=15). Mice were euthanized on day 28 post injection. **C**, Cumulative EAE score, obtained by adding the EAE score of each mouse over each of the 28 days. Lines represent averages +/- SEM. p-value was calculated with two-tailed student's *t*-test. **p = 0.0022.

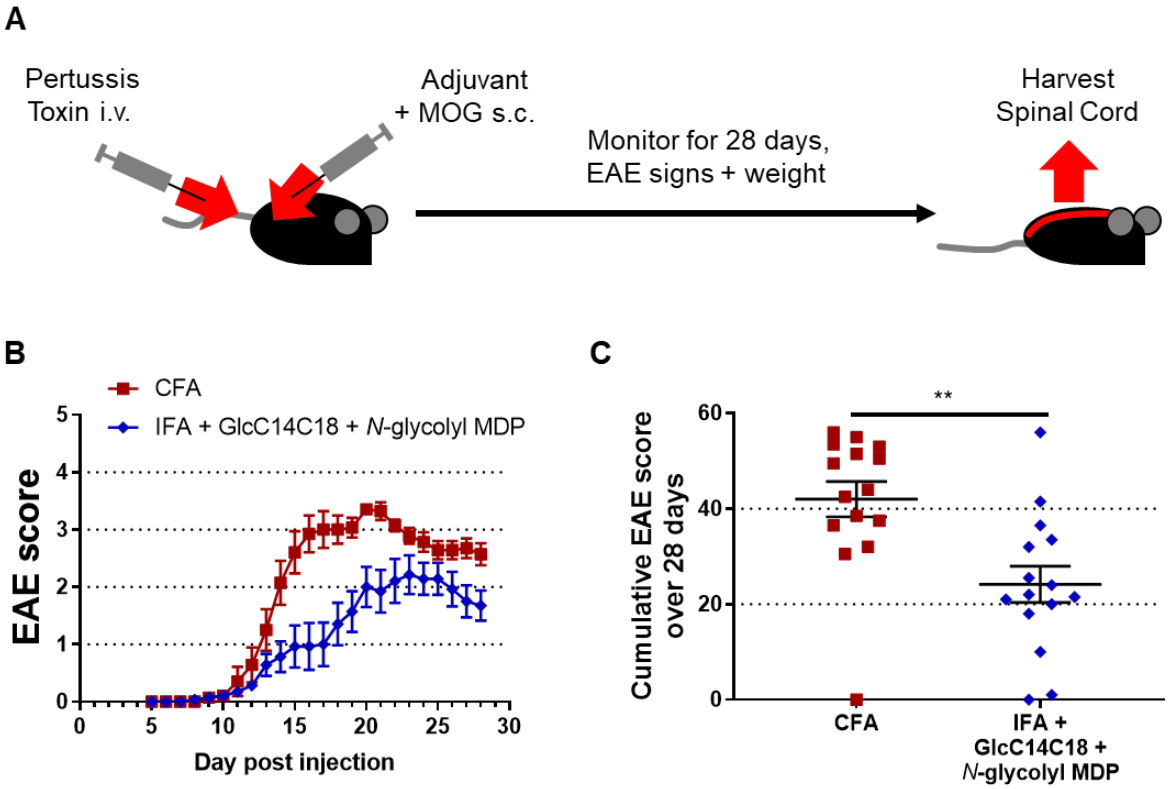
A
Pertussis
Toxin i.v.
Adjuvant
+ MOG s.c.
Monitor for 28 days,
EAE signs + weight
Harvest
Spinal Cord
B
CFA
IFA + GlcC14C18 + N-glycolyl MDP
EAE score
Day post injection
C
Cumulative EAE score
over 28 days
**
CFA
IFA +
GlcC14C18 +
N-glycolyl MDP

Chapter II, Figure 7. Spinal cord pathology in RR-EAE mice induced by IFA+GlcC14C18+MDP.

A, Nissl and Luxol fast blue (LFB) stains of spinal cord sections from RR-EAE-induced mice at day 28 post injection, having an EAE score of 3.5 upon euthanasia. Red boxes highlight cellular infiltration and spatially associated demyelination of the white matter seen by Nissl and LFB staining, respectively. **B**, Quantitative spinal cord pathology per EAE score upon euthanasia. Statistical significance was determined by Tukey's multiple comparisons test. *$p<0.05$ and ****$p<0.0001$. N=40 for each group (20 from CFA and 20 from synthetic adjuvant of equivalent EAE scores). Lines indicate averages +/- SEM **C**, Quantitative spinal cord pathology per adjuvant. Statistical significance was tested with two-tailed unpaired Welch's *t*-test; a power calculation for given variances and N=60 per group indicated an ability to discern +/- 15% difference vs. CFA control. Lines indicate averages +/- SEM.

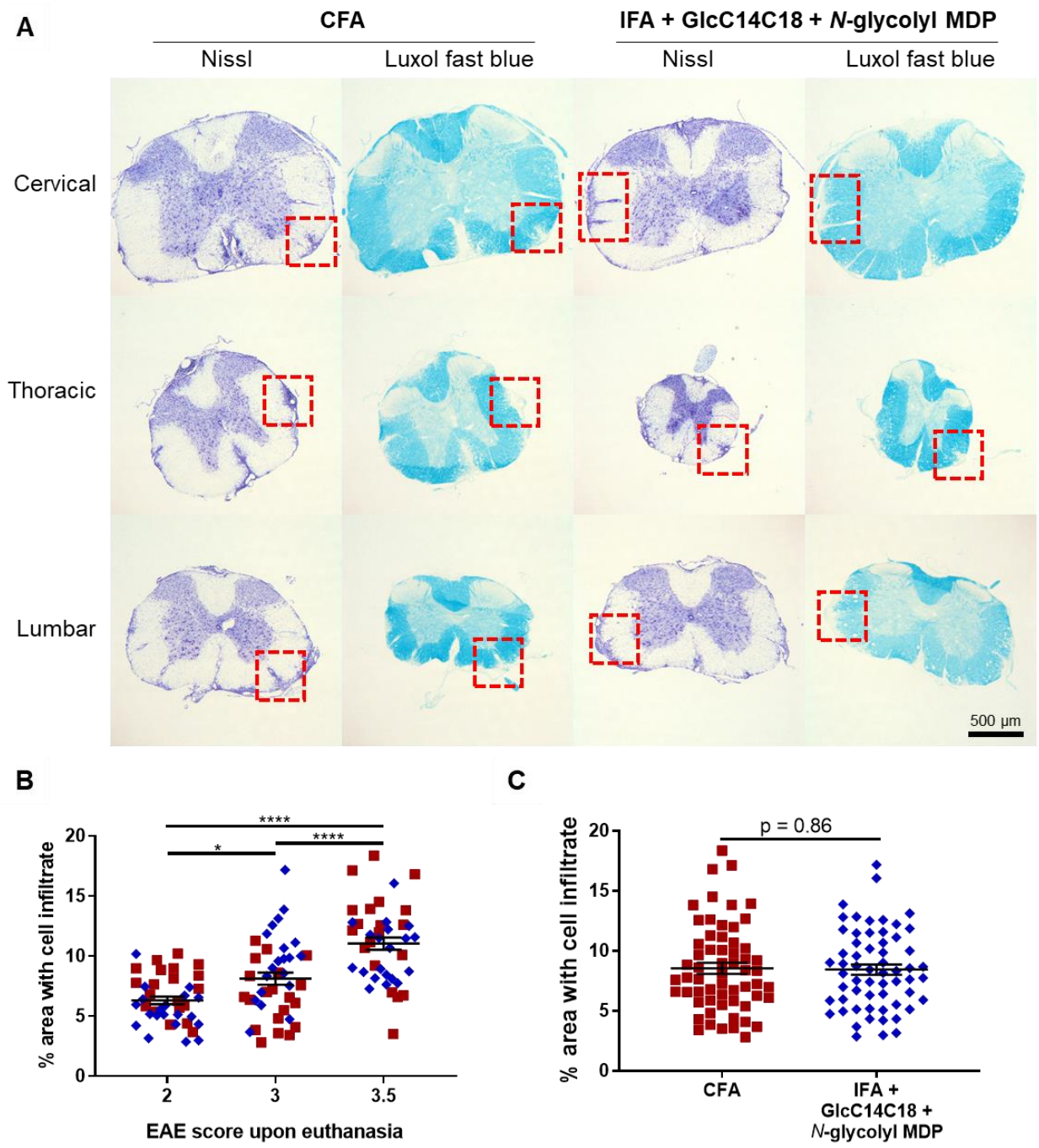
A
CFA
IFA + GlcC14C18 + N-glycolyl MDP
Nissl
Luxol fast blue
Nissl
Luxol fast blue
Cervical
Thoracic
Lumbar
500 µm
B
****
*
****
% area with cell infiltrate
20
15
10
5
0
2
3
3.5
EAE score upon euthanasia
C
p = 0.86
% area with cell infiltrate
20
15
10
5
0
CFA
IFA +
GlcC14C18 +
N-glycolyl MDP

8 – Supplemental Figures

Chapter II, Figure S1. Flow cytometry gating strategies for lymph node cells.

A, gating to quantify cytokine-producing CD4+CD8- T cells. Shown are representative gating and data from an OVA-stimulated sample (CFA-immunized WT mouse). For comparison, cytokine production for the corresponding unstimulated sample is included. **B**, gating to identify lymph node cell subsets. Shown is gating on a representative sample (CFA-immunized WT mouse). pDCs are B220+Ly6C+MHC-II+CD11b-CD11c+ cells. B cells are B220+Ly6C-CD11b-CD11c-CD4-CD8a- cells. cDCs are B220-MHC-II^{hi}Ly6C-CD11c+ cells (analyzed subsets are CD11b+/-). CD4+ T cells are B220-CD11b-CD4+CD8a- cells. CD8+ T cells are B220-CD11b-CD4-CD8a+ cells. Monocytes are B220-CD11b+Ly6C+SSC^{lo} cells. PMNs are B220-CD11b+Ly6C^{med}SSC^{hi} CD11c- cells.

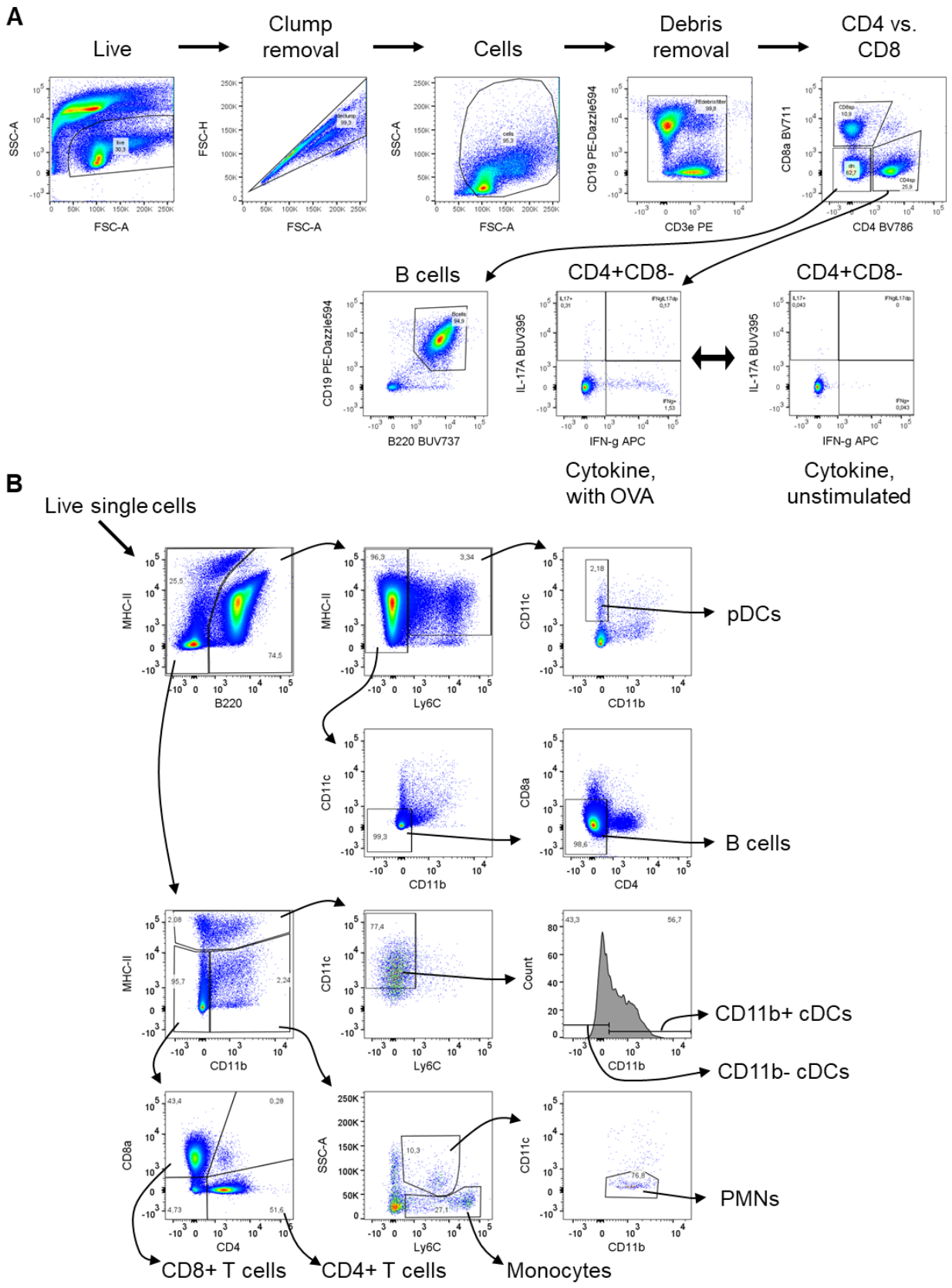
A
Live
Clump removal
Cells
Debris removal
CD4 vs. CD8
SSC-A
FSC-A
FSC-H
CD19 PE-Dazzle594
CD3e PE
CD8a BV711
CD4 BV786
B cells
CD4+CD8-
CD4+CD8-
B220 BUV737
IL-17A BUV395
IFN-g APC
Cytokine, with OVA
Cytokine, unstimulated
B
Live single cells
MHC-II
B220
Ly6C
CD11c
CD11b
pDCs
B cells
CD4
CD8a
Count
CD11b+ cDCs
CD11b- cDCs
PMNs
CD8+ T cells
CD4+ T cells
Monocytes

Chapter II, Figure S2. Addition data on CFA-dependent cell-mediated immune responses as a function of mycobacterial *namH*.

These data are from the same experiments shown in fig. 1C (refer to fig. 1C legend for details). **A-B**, Total numbers (from two lymph nodes) of cytokine-producing CD4+CD8- lymph node cells of mice immunized against OVA with H37Rv, H37Rv Δ*namH*, or IFA alone. Shown are averages +/- SEM. p-values were calculated with two-tailed student's *t*-tests. **p<0.01. **C-D**, Contribution of *namH* to the mycobacterial portion of OVA-specific IFN-γ elicited by CFA. **C**, result was obtained from %IFN-γ+ data by subtracting the average IFA background from all CFA data, and plotting the results as % of IFA+H37Rv 'wild-type'. **D**, result was obtained from # IFN-γ+ data by subtracting the average IFA background from all CFA data, and plotting the results as % of IFA+H37Rv 'wild-type'. Shown are averages +/- SEM. p-values were calculated with two-tailed student's t-tests. *p<0.05. **E**, results separated by experimental run for the data presented in fig. 1C and fig. S2A-B. Shown are averages +/- SEM.

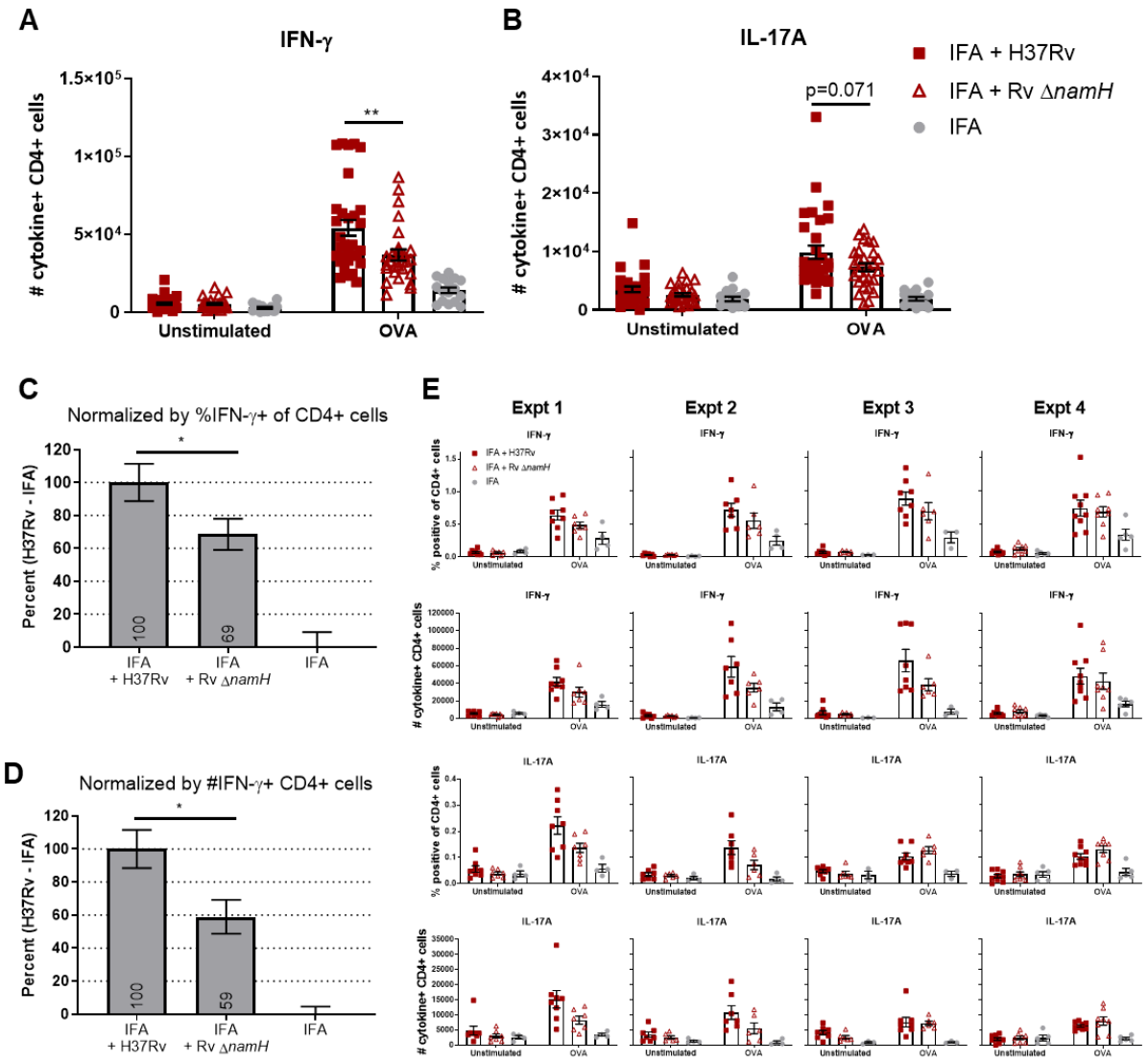
A
IFN-γ
cytokine+ CD4+ cells
1.5×10^5
1×10^5
5×10^4
0
**
Unstimulated
OVA
B
IL-17A
cytokine+ CD4+ cells
4×10^4
3×10^4
2×10^4
1×10^4
0
p=0.071
Unstimulated
OVA
IFA + H37Rv
IFA + Rv ΔnamH
IFA
C
Normalized by %IFN-γ+ of CD4+ cells
Percent (H37Rv - IFA)
120
100
80
60
40
20
0
*
100
69
IFA + H37Rv
IFA + Rv ΔnamH
IFA
D
Normalized by #IFN-γ+ CD4+ cells
Percent (H37Rv - IFA)
120
100
80
60
40
20
0
*
100
59
IFA + H37Rv
IFA + Rv ΔnamH
IFA
E
Expt 1
Expt 2
Expt 3
Expt 4
IFN-γ
IL-17A
% positive of CD4+ cells
# cytokine+ CD4+ cells
Unstimulated
OVA

Chapter II, Figure S3. Additional data on CFA-dependent immune responses as a function of *Nod2* and *Mincle*.

A-B, IFN-γ ELISpot of inguinal lymph node cells mice immunized against OVA seven days prior, produced in an independent experiment. **A**, number of IFN-γ spot-forming cells per one million cells. **B**, total number of IFN-γ spot-forming cells per two inguinal lymph nodes. Shown are averages +/- SEM. p-values were calculated with two-tailed student's *t*-tests. *p<0.05. For CFA *Nod2*+/+, CFA *Nod2*-/-, IFA *Nod2*+/+ and IFA *Nod2*-/-, N = 6, 8, 6 and 6 mice, respectively. **C**, flow cytometry of inguinal lymph node cells mice immunized against OVA seven days prior, produced in an independent experiment similar to that in fig. 2A-B. **D**, results separated by experimental run for the data presented in fig. 2C-D and fig. S4C-D. Shown are averages +/- SEM.

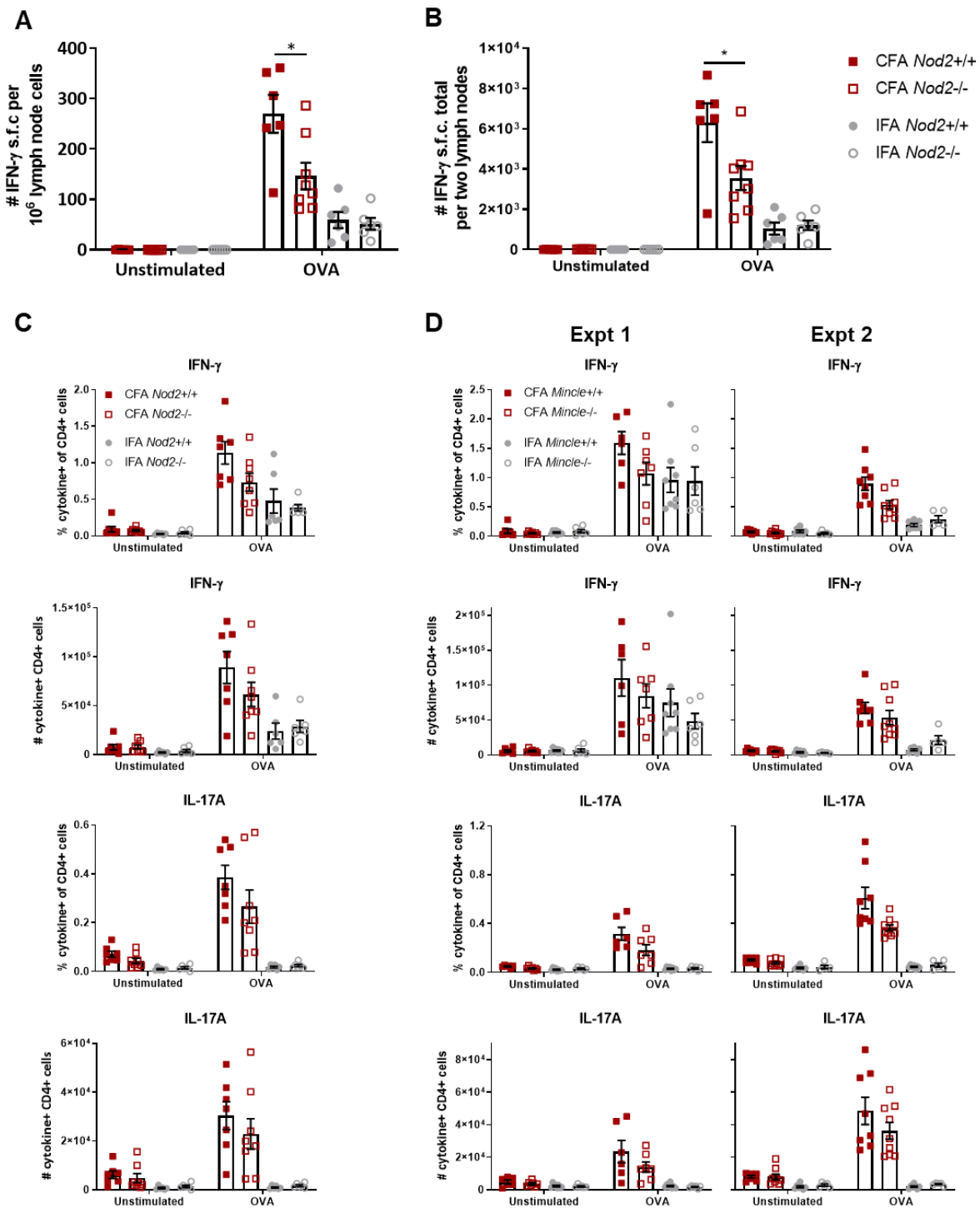
A
IFN-γ s.f.c per 10^6 lymph node cells
400
300
200
100
0
*
Unstimulated
OVA
B
IFN-γ s.f.c. total per two lymph nodes
1×10^4
8×10^3
6×10^3
4×10^3
2×10^3
0
*
Unstimulated
OVA
CFA Nod2+/+
CFA Nod2-/-
IFA Nod2+/+
IFA Nod2-/-
C
IFN-γ
% cytokine+ of CD4+ cells
2.0
1.5
1.0
0.5
0.0
CFA Nod2+/+
CFA Nod2-/-
IFA Nod2+/+
IFA Nod2-/-
Unstimulated
OVA
IFN-γ
cytokine+ CD4+ cells
1.5×10^5
1×10^5
5×10^4
0
Unstimulated
OVA
IL-17A
% cytokine+ of CD4+ cells
0.6
0.4
0.2
0.0
Unstimulated
OVA
IL-17A
cytokine+ CD4+ cells
6×10^4
4×10^4
2×10^4
0
Unstimulated
OVA
D
Expt 1
Expt 2
IFN-γ
% cytokine+ of CD4+ cells
2.5
2.0
1.5
1.0
0.5
0.0
CFA Mincle+/+
CFA Mincle-/-
IFA Mincle+/+
IFA Mincle-/-
Unstimulated
OVA
IFN-γ
cytokine+ CD4+ cells
2×10^5
1.5×10^5
1×10^5
5×10^4
0
Unstimulated
OVA
IL-17A
% cytokine+ of CD4+ cells
1.2
0.8
0.4
0.0
Unstimulated
OVA
IL-17A
cytokine+ CD4+ cells
8×10^4
6×10^4
4×10^4
2×10^4
0
Unstimulated
OVA

Chapter II, Figure S4. CFA-dependent cell-mediated immune responses as a function of host *Nod2* and *Mincle* expressed in total cell numbers

These data are from the same experiments shown in fig. 2 (refer to fig. 2 legend for details). **A-F**, Total numbers (from two lymph nodes) of cytokine-producing CD4+CD8- lymph node cells of mice immunized against OVA with the indicated adjuvant as a function of: **A-B**, *Nod2*; **C-D**, *Mincle*; **E-F**, *Mincle* and *Nod2* together. Shown are averages +/- SEM. p-values were calculated with two-tailed student's *t*-tests. *$p<0.05$; ns, not significant, $p>0.05$.

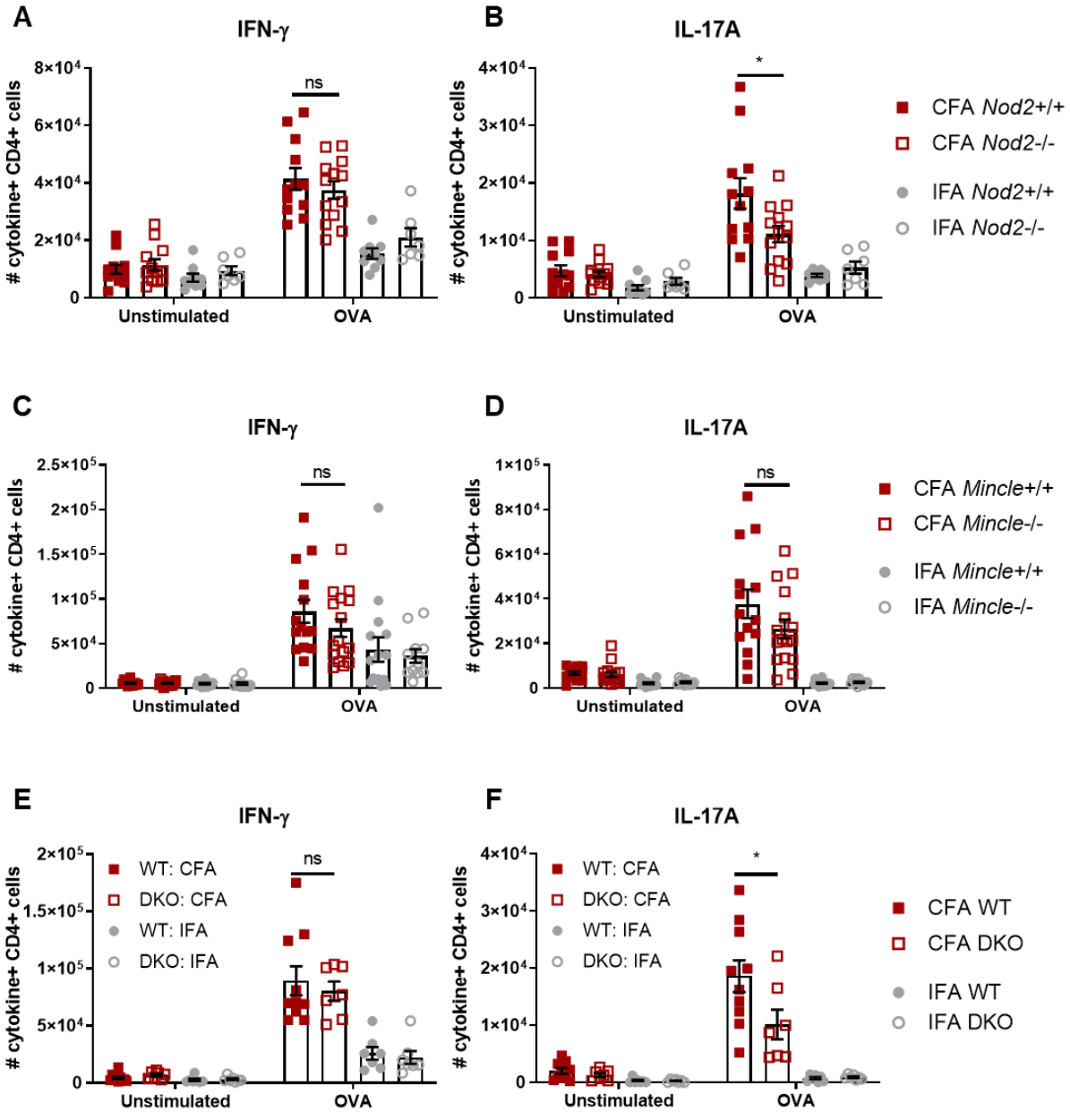
A
IFN-γ
cytokine+ CD4+ cells
8×10⁴
6×10⁴
4×10⁴
2×10⁴
0
ns
Unstimulated
OVA
B
IL-17A
4×10⁴
3×10⁴
2×10⁴
1×10⁴
0
*
Unstimulated
OVA
CFA Nod2+/+
CFA Nod2-/-
IFA Nod2+/+
IFA Nod2-/-
C
IFN-γ
2.5×10⁵
2×10⁵
1.5×10⁵
1×10⁵
5×10⁴
0
ns
Unstimulated
OVA
D
IL-17A
1×10⁵
8×10⁴
6×10⁴
4×10⁴
2×10⁴
0
ns
Unstimulated
OVA
CFA Mincle+/+
CFA Mincle-/-
IFA Mincle+/+
IFA Mincle-/-
E
IFN-γ
2×10⁵
1.5×10⁵
1×10⁵
5×10⁴
0
WT: CFA
DKO: CFA
WT: IFA
DKO: IFA
ns
Unstimulated
OVA
F
IL-17A
4×10⁴
3×10⁴
2×10⁴
1×10⁴
0
WT: CFA
DKO: CFA
WT: IFA
DKO: IFA
*
Unstimulated
OVA
CFA WT
CFA DKO
IFA WT
IFA DKO

Chapter II, Figure S5. Additional data on MHC-II expression and costimulatory molecule upregulation by BMDCs stimulated with GlcC14C18 and MDPs.

A, percentage of cells expressing MHC-II at high levels (according to gate in fig. 3B) after 48 hours of stimulation with the indicated MAMPs. **B-E**, median fluorescence intensity of **B**, MHC-II; **C**, CD40; **D**, CD80; **E**, CD86 on CD11b+CD11c+MHC-II^{hi} cells after 48 hours of stimulation with the indicated MAMPs (use legend of panel A). Shown are averages +/- SD of 3 individually stimulated and assayed cultures. **F-I**, histograms of CD11b+CD11c+MHC-II^{hi} cells demonstrating expression levels of **F**, MHC-II; **G**, CD40; **H**, CD80; **I**, CD86, for both timepoints (FMOC is not shown for MHC-II because the analysis required MHC-II gating).

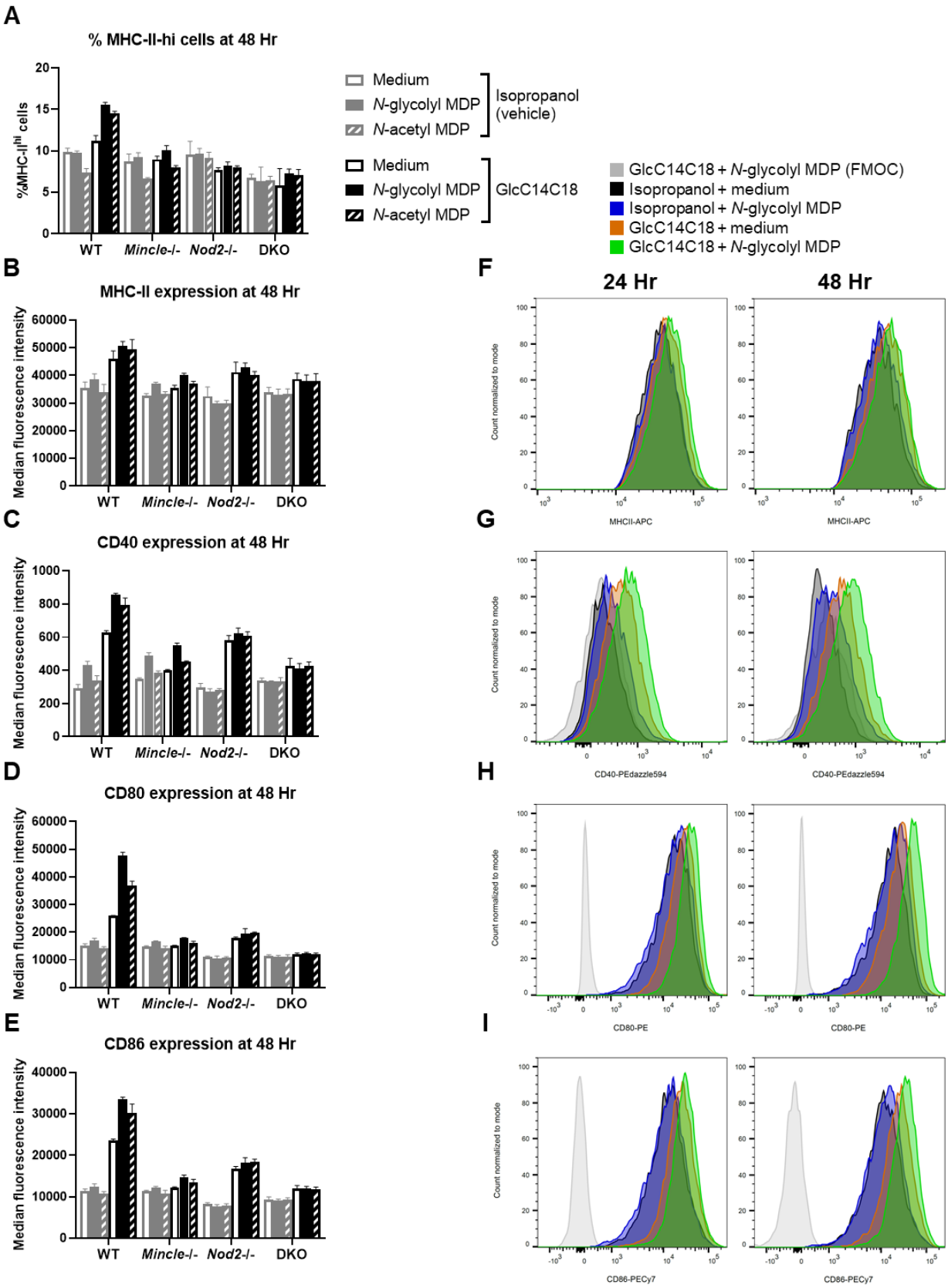
A
% MHC-II-hi cells at 48 Hr
%MHC-II^hi cells
WT
Mincle-/-
Nod2-/-
DKO
Medium
N-glycolyl MDP
N-acetyl MDP
Isopropanol (vehicle)
Medium
N-glycolyl MDP
N-acetyl MDP
GlcC14C18
GlcC14C18 + N-glycolyl MDP (FMOC)
Isopropanol + medium
Isopropanol + N-glycolyl MDP
GlcC14C18 + medium
GlcC14C18 + N-glycolyl MDP
B
MHC-II expression at 48 Hr
Median fluorescence intensity
C
CD40 expression at 48 Hr
D
CD80 expression at 48 Hr
E
CD86 expression at 48 Hr
F
24 Hr
48 Hr
Count normalized to mode
MHCII-APC
G
CD40-PEdazzle594
H
CD80-PE
I
CD86-PECy7

Chapter II, Figure S6. Synthetic adjuvant-dependent IFN-γ responses compared to CFA by ELISpot.

A-B, IFN-γ ELISpot of inguinal lymph node cells of mice immunized against OVA with the indicated adjuvant seven days prior. **A**, number of IFN-γ spot-forming cells per one million cells. **B**, total number of IFN-γ spot-forming cells per two inguinal lymph nodes. Data was pooled from two independent experiments. Shown are averages +/- SEM, where for IFA, IFA + 3 µg *N*-glycolyl MDP, IFA + 10 µg *N*-glycolyl MDP, IFA + 30 µg *N*-glycolyl MDP, IFA + 100 µg *N*-glycolyl MDP and CFA, N = 11, 6, 12, 11, 6 and 11 mice, respectively. **C-D**, These data are from the same mice used in fig. 4B (refer to fig. 4B legend for details). **C**, number of IFN-γ spot-forming cells per one million cells. **D**, total number of IFN-γ spot-forming cells per two inguinal lymph nodes. Shown are averages +/- SEM. In comparing IFA + 30 µg MDP to IFA + MDP + 10 or 30 µg GlcC14C18, p-values were calculated using Dunnett's T3 multiple comparisons test. *$p<0.05$; **$p<0.01$; ns, not significant, $p>0.05$.

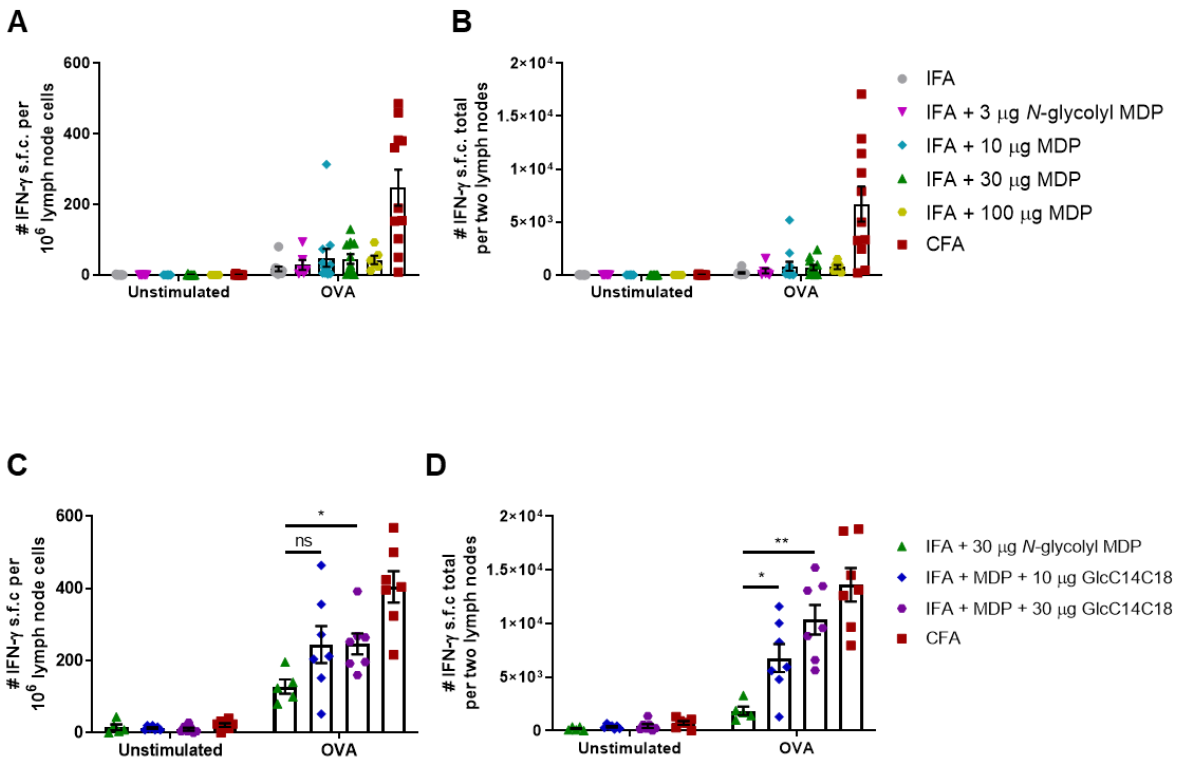
A
B
C
D
IFN-γ s.f.c. per 10^6 lymph node cells
IFN-γ s.f.c. total per two lymph nodes
Unstimulated
OVA
ns
*
**
IFA
IFA + 3 μg N-glycolyl MDP
IFA + 10 μg MDP
IFA + 30 μg MDP
IFA + 100 μg MDP
CFA
IFA + 30 μg N-glycolyl MDP
IFA + MDP + 10 μg GlcC14C18
IFA + MDP + 30 μg GlcC14C18

Chapter II, Figure S7. Lymph node cell subset numbers after immunization with synthetic adjuvants.

These data are from the same mice used in fig. 5 (refer to fig. 5 legend for details of the experiment). **A-F,** From two inguinal lymph nodes at 4 or 7 days post-immunization, shown are total numbers of extracted **A**, B cells; **B**, CD4+ T cells; **C**, CD8+ T cells; **D**, plasmacytoid dendritic cells (pDCs); **E**, monocytes; **F**, polymorphonuclear cells (PMNs). Data are graphed as averages +/- SEM.

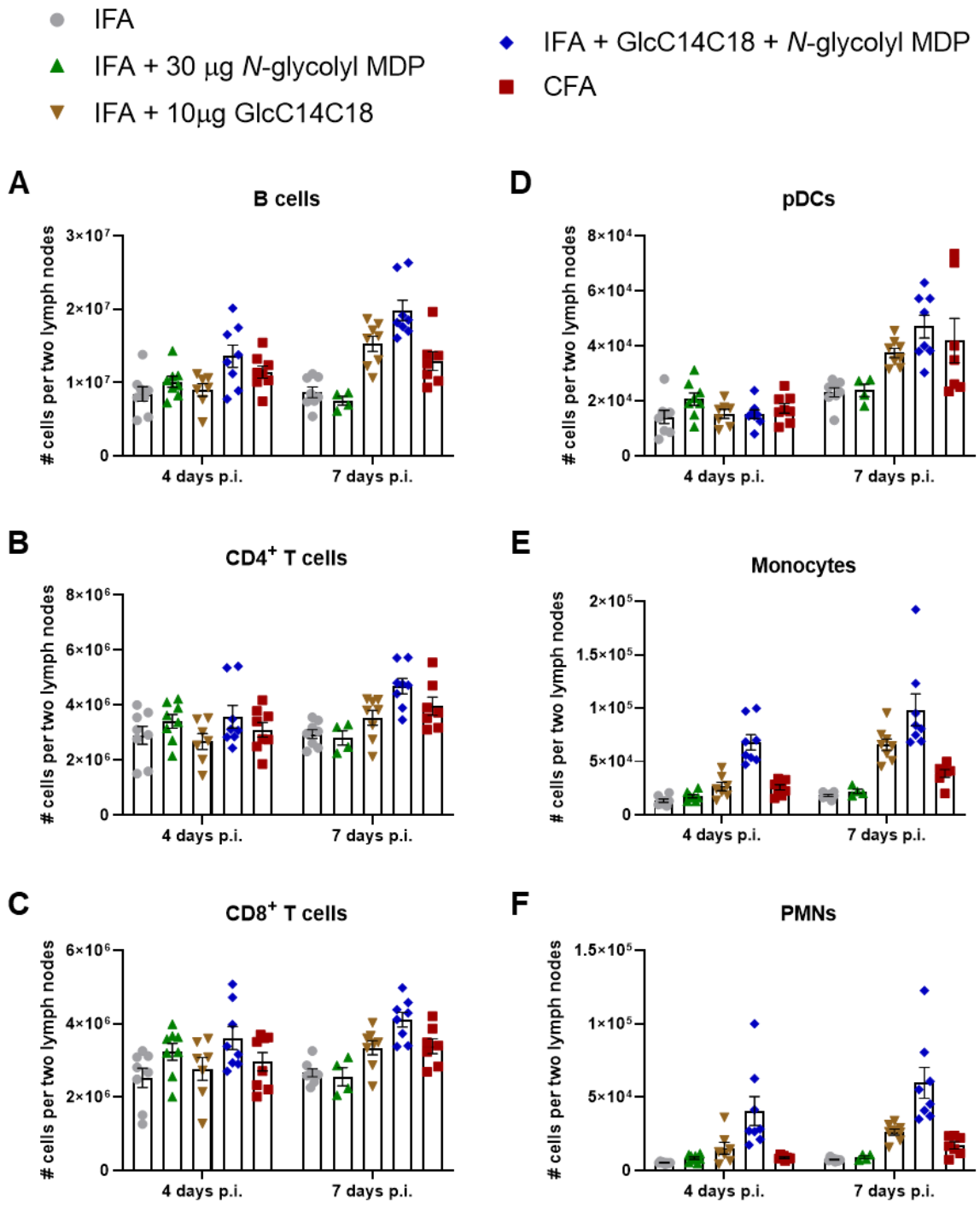
IFA
IFA + 30 µg N-glycolyl MDP
IFA + 10µg GlcC14C18
IFA + GlcC14C18 + N-glycolyl MDP
CFA
A
B cells
cells per two lymph nodes
3×10^7
2×10^7
1×10^7
0
4 days p.i.
7 days p.i.
B
CD4+ T cells
8×10^6
6×10^6
4×10^6
2×10^6
C
CD8+ T cells
D
pDCs
8×10^4
6×10^4
4×10^4
2×10^4
E
Monocytes
2×10^5
1.5×10^5
1×10^5
5×10^4
F
PMNs

Chapter II, Figure S8. Additional statistics for RR-EAE.

These data are from the same set shown in fig. 5 (refer to fig. 5 legend for details). **A**, average weight of mice over time +/- SEM. **B**, maximum EAE score reached on any day by mice, as of day 28. **C**, disease course of mice selected for spinal cord histopathology. **D-G**, Statistics for RR-EAE induced by IFA+TDM+MDP. **D**, average EAE score +/- SEM over time of mice induced with CFA (N=13) or IFA + 1 µg TDM + 30 µg *N*-glycolyl MDP (N=13). Mice were euthanized on day 27 post injection. **E**, cumulative EAE score, obtained by adding the EAE score of each mouse over each of the 27 days. Lines represent averages +/- SEM. **F**, average weight of mice over time +/- SEM. **G**, maximum EAE score reached on any day by mice, as of day 27.

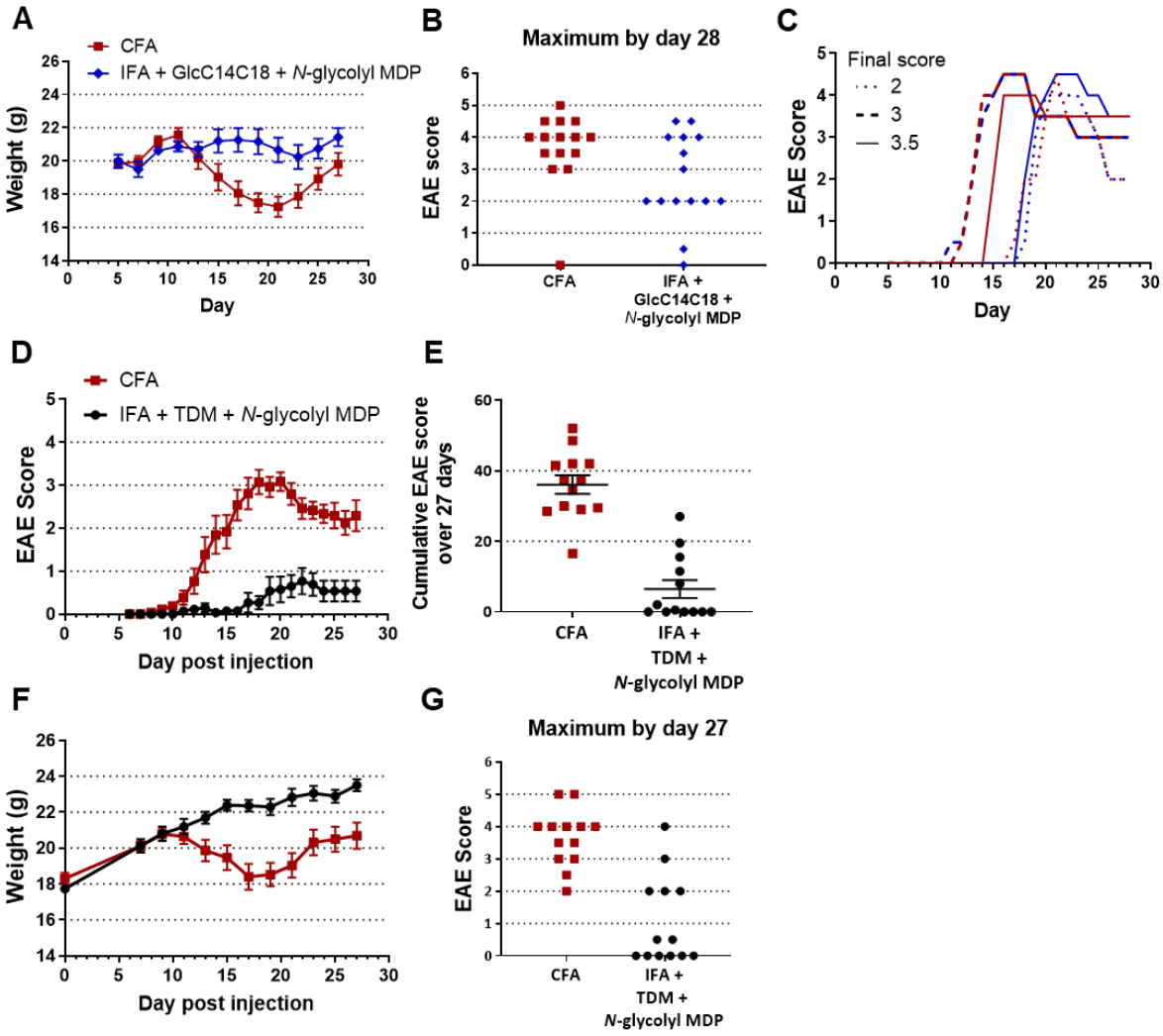
A
CFA
IFA + GlcC14C18 + N-glycolyl MDP
Weight (g)
Day
B
Maximum by day 28
EAE score
CFA
IFA + GlcC14C18 + N-glycolyl MDP
C
Final score
2
3
3.5
EAE Score
Day
D
CFA
IFA + TDM + N-glycolyl MDP
EAE Score
Day post injection
E
Cumulative EAE score over 27 days
CFA
IFA + TDM + N-glycolyl MDP
F
Weight (g)
Day post injection
G
Maximum by day 27
EAE Score
CFA
IFA + TDM + N-glycolyl MDP

9 – Supplemental Tables

Chapter II, Table S1. Flow cytometry antibodies for lymph node cell cytokines

Target	Supplier	Clone	Fluorochrome*
CD3ε	BD	145-2C11	PE
CD4	BD	GK1.5	BV786
CD8α	BD	53-6.7	BV711
CD19	Biolegend	6D5	PE-Dazzle594
B220/CD45R	BD	RA3-6B2	BUV737
IFN-γ	Biolegend	XMG1.2	APC
IL-2	BD	JES6-5H4	BV605
IL-4	eBiosciences	BVD6-24G2	PE-Cy7
IL-17A	BD	TC11-18H10	BUV395
IL-10	BD	JES5-16E3	FITC

*Viability dye: LIVE/DEAD™ Fixable Violet Dead Cell Stain (ThermoFisher Scientific)

Chapter II, Table S2. Flow cytometry antibodies for lymph node cell DC and subset analysis

Target	Supplier	Clone	Fluorochrome*
B220/CD45R	BD	RA3-6B2	BUV737
CD4	BD	GK1.5	BV786
CD8α	BD	53-6.7	BV711
CD11b	Biolegend	M1/70	BV605
CD11c	BD	HL3	FITC
CD40	Biolegend	3/23	PE-Dazzle594
CD80	Biolegend	16-10A1	PE
CD86	Biolegend	GL1	PE-Cy7
CD209	BD	5H10	BUV395
F4/80	Biolegend	BM8	APC
Ly6C	Biolegend	HK1.4	APC-Cy7
MHC-I (H-2K^b)	Biolegend	AF6-88.5	BV510
MHC-II (I-A^b)	Biolegend	AF6-120.1	PerCP-Cy5.5

*Viability dye: LIVE/DEAD™ Fixable Violet Dead Cell Stain (ThermoFisher Scientific)

Chapter II, Table S3. Flow cytometry antibodies for BMDCs

Target	Supplier	Clone	Fluorochrome*
CD11b	Biolegend	M1/70	PerCP-Cy5.5
CD11c	BD	HL3	FITC
CD40	Biolegend	3/23	PE-Dazzle594
CD80	Biolegend	16-10A1	PE
CD86	Biolegend	GL1	PE-Cy7
MHC-II (I-A^b)	Biolegend	AF6-120.1	APC

*Viability dye: LIVE/DEAD™ Fixable Violet Dead Cell Stain (ThermoFisher Scientific)

PREFACE TO CHAPTER III

In Chapter I, the importance of PRRs during *Mtb* infection was demonstrated to be generally limited to altered immunity with few reports of PRR KOs in mice resulting in significant loss of bacterial control resulting in premature death. In Chapter II, we showed that NOD2 and Mincle were essential for a complete immune response to mycobacteria, that these PRR pathways synergize and that together they can recapitulate about half of the mycobacterial adjuvant effect. Therefore, with two PRRs known to be important, and cooperative, for the mycobacterial immune response, in Chapter III we test whether double knockout (DKO) of *Mincle* and *Nod2* during live mycobacterial infection results in significant loss of bacterial control due to doubly defective immunity. The absence of NOD2 was associated with altered immunity during disparate mycobacterial infections and reduced survival particularly during *Mtb* infection, regardless of *Mincle* status, demonstrating a distinct role for *Nod2* in the host response to mycobacteria that was more important than Mincle.

CHAPTER III – Respective and combined disruption of *Mincle* and *Nod2* distinctly alter mycobacterial immunity and resistance

---

(This Chapter is adapted from a manuscript in preparation)

Jean-Yves Dubé[*, †, ‡], Fiona McIntosh [†, ‡], Shannon C. Duffy [*, †, ‡], Marcel A. Behr [*, †, ‡, §]

*****, Department of Microbiology and Immunology, McGill University.

†, Infectious diseases and Immunity in Global Health Program, Research Institute of the McGill University Health Centre.

‡, McGill International TB Centre.

§, Department of Medicine, McGill University Health Centre, Montréal, Canada.

1 – Abstract

Pattern recognition receptors Mincle and NOD2 have been implicated in mycobacterial immunity. However, attempts to find associations between polymorphisms in these genes and mycobacterial diseases have yielded varied results and knockout (KO) animal infection studies have had mild phenotypes. Genetic susceptibility to infectious diseases can be polygenic. We hypothesized that murine double knockout (DKO) of two immunologically important factors *Mincle* and *Nod2* would result in exacerbation of altered immunity to mycobacterial infection. To test this hypothesis, we monitored immune responses, bacterial burden and survival following *ex vivo* and *in vivo* infections with *Mycobacterium tuberculosis* and *Mycobacterium avium* subspecies *paratuberculosis*. Immune responses were blunted with *Mincle* and/or *Nod2* disruptions, yet DKO phenocopied *Nod2*-KO mice in terms of reduced survival with *Mtb*; in contrast, *Mincle*-KO survival was intermediate between *Nod2*-disrupted and wildtype mice. *Mtb*-related death, exclusively in mice with disrupted *Nod2*, was accompanied by greater pulmonary cell death and large necrotic foci. Despite the differences in survival across groups, bacterial burdens were little changed with *Mincle* and/or *Nod2* disruptions. Disparate infection with *Map* also exhibited impaired immunity with limited differences in bacterial control, showing that the roles of these pattern recognition receptors during mycobacterial infection may not be species specific. In conclusion, while both Mincle and NOD2 contribute to immune responsiveness during mycobacterial infection, their disruption, alone and together, does not result in a clear difference in bacterial burden. The importance of these receptors in resistance to mycobacterial infection requires analysis of immunophenotypes and their consequences on host pathology.

2 – Introduction

Each year, *Mycobacterium tuberculosis* (*Mtb*) causes tuberculosis (TB) in about 10 million people and results in the death of over a million (WHO). Other species in the *Mtb* complex as well as non-tuberculous mycobacteria cause disease in livestock and occasionally in humans too. For example, *Mycobacterium avium* subspecies *paratuberculosis* (*Map*) is the etiologic agent of Johne's disease, a lethal wasting illness affecting ruminants including cattle. Many aspects of immunity have been linked to susceptibility to mycobacterial infection (e.g. HIV status, host genetics). Therefore, understanding which immune mechanisms are important for host control or tolerance of mycobacteria is needed to guide the development of immunotherapeutic agents and vaccines.

Pattern recognition receptors (PRRs) help to initiate innate immunity and instruct the development of adaptive immunity to pathogens. They are a collection of genetically inborn sensors that detect microbe-associated molecular patterns (MAMPs) to initiate the inflammatory response at the cellular level (e.g. through NF-κB and MAPK pathways). One such PRR is Macrophage-Inducible C-type Lectin (Mincle), which binds to the mycobacterial outer membrane lipid trehalose 6,6'-dimycolate (TDM, aka cord factor) [157]. TDM is an abundant glycolipid in the outer membrane of mycobacteria and has been posited as both a host-beneficial MAMP as well as a virulence factor of pathogenic mycobacteria [481]. *Mincle*-/- mice have altered immunity to mycobacteria [157,460,461,482], although whether Mincle polymorphisms are associated with human mycobacterial infection is only starting to emerge: at least two such studies reported statistically significant associations [435,483].

Another PRR of interest is Nucleotide-binding Oligomerization Domain-containing 2 (NOD2), which is a cytoplasmic molecule essential for the recognition of the bacterial

peptidoglycan through the muropeptide moiety [182,183,347]. NOD2 has been implicated in mycobacterial immunity through chemical, immunologic and epidemiologic evidence: 1) mycobacteria contain a distinct NOD2 agonist in that they possess *N*-glycolylated muropeptides while other bacteria are *N*-acetylated [106,107]; 2) *N*-glycolylation of the muropeptide was shown to be a more potent activator of innate immune cells [108,187] and *Nod2*-/- mice have altered (decreased) immune responses to mycobacteria [188,189]; 3) polymorphisms in NOD2 have been associated with mycobacterial infection and disease [255,388,392]. NOD2 variation is also associated with predisposition to Crohn's disease [368-370], for which *Map* has long been hypothesized to contribute [52].

We have recently shown that both *Mincle* and *Nod2* are essential to the immune response elicited by Freund's adjuvant, a mycobacterial adjuvant, and that Mincle and NOD2 ligands together account for about 30-50% of the cellular immune response to dead *Mtb* [187]. However, *Nod2*-/- mouse studies have shown only modestly reduced *Mtb* control[188,189] and survival [189]. *Mincle*-/- mice were shown to have little difference from WT in terms of *Mtb* burden and survival analysis has not been reported [460,461]. The importance of PRRs during *Mtb* infection may indeed be restricted to specific phenotypes due their nature as redundant sensors of infection, in contrast to the essentiality of unique immune effectors [484]. Therefore, we hypothesized that simultaneous loss of *Mincle and Nod2* could result in a greater degree of altered immunity leading to a larger impairment in bacterial control and survival. The 'double-knockout' simulates a genetic 'two-hit' scenario which could explain why some loss-of-function polymorphisms do not appear to have complete disease phenotype penetrance.

To address this, we used *Mincle*-/-*Nod2*-/- (double knockout, DKO) mice previously generated [187] (with the corresponding single knockouts, SKO) to model genetic susceptibility to

mycobacterial disease during infection with *Mtb* and *Map*. Our data show that DKO mice had defective mycobacterial immunity similar to *Nod2*-/- mice, but that these immunological defects appeared limited in terms of bacterial control. DKO and *Nod2*-/- mice had similarly shortened survival during *Mtb* infection, and although mortality occurred late it was occasionally accompanied by necrotic foci in the lungs not seen in NOD2-competent animals. In contrast, for *Mincle*-KO the immunologic phenotypes and survival data were intermediate between WT and *Nod2*-KO. Our data indicate that PRRs like Mincle and NOD2 are largely dispensable for control of mycobacterial burden and that the absence of NOD2 is more important than Mincle for dictating the ultimate host response to mycobacterial infection.

3 – Materials and Methods

Mice

Nod2-/- mice were initially obtained from Jackson laboratories. *Mincle*-/- mice breeders were generously provided by the laboratory of Christine Wells [433]. Imported mice were genotyped to confirm that the *Dock2* mutation reported in certain *Nod2*-/- mice was not present [480]. All mice were obtained by crossing *Nod2*-/- and *Mincle*-/- mice (both C57BL/6 background) to generate double heterozygotes which were mated to regenerate single *Nod2* and *Mincle* knockouts as well as 'wild-type' (WT, *Mincle*+/+*Nod2*+/+) and 'double knockout' (DKO, *Mincle*-/-*Nod2*-/-). Homozygotic mice were then used as breeders to sustain the colony. For *Mtb* experiments, all mice were from 2 to 4 months of age at the start of the experiment. For intraperitoneal *Map* infection, mice were from 2 to 8 months of age at the start of the experiment. Mice were age and sex matched where applicable across groups in all experiments All protocols requiring mice

adhered to the guidelines of the Canadian Council on Animal Care (CCAC) and were authorized by the RI-MUHC animal resource division.

Bacteria

Mtb H37Rv and *Map* K10 were grown at 37°C in complete 7H9 medium (Middlebrook 7H9 (BD), ADC (BD), 0.2% glycerol (Sigma), 0.05% Tween-80 (Sigma)). *Map* was also supplemented with 1 μg/ml ferric mycobactin J (Allied Monitor, Missouri USA). Cultures in mid-log phase were used for experiments. *Mtb* culture used in aerosol experiments was aliquoted into 7H9 complete medium with 20% glycerol at OD-600 ~ 0.5, frozen at -80°C and thawed immediately before use. For plating on solid media, we used complete 7H10 (Middlebrook 7H10 (BD), OADC (BD), 0.5% glycerol (Sigma)) including PANTA (BD) and, for *Map* experiments, 1 μg/ml ferric mycobactin J.

Bone marrow-derived macrophage (BMDM) infection

Bone marrow was extracted from murine tibiae and femora and differentiated into macrophages with recombinant M-CSF (100 U/ml) (Peprotech) over 7 days as previously described [485]. After differentiation, BMDMs were lifted using CellStripper Solution (Corning) and replated into 96-well plates at 200,000 cells per well for *Mtb* infection. BMDMs were cultured in R10 (RPMI 1640 media supplemented with non-essential amino acids, 10 mM HEPES, 10% FBS and, while not being infected, Penicillin/Streptomycin (Wisent)). *Mtb* was resuspended in R10 at an OD-600 of 0.2 and 100 μl of this (approximately 2 million CFU) was added to BMDMs (t = 0). After four hours, extracellular bacteria were removed by washing wells three times with R10 after which R10 was restored. Supernatant was harvested and frozen at -80°C at the indicated

timepoints, and was later thawed, filter sterilized and subjected to ELISA analysis (ThermoFisher). In the case of heat-killed bacteria, *Mtb* was heated at 80^{o}C for 30 minutes before being added to BMDMs, no washing was performed and supernatant was harvested the following day only.

Mtb aerosol infections

Mice were infected by aerosol using an ONARES device (New Jersey, USA) over 15 minutes with an *Mtb* suspension in PBS + 0.05% Tween-80 at OD-600 = 0.04. This method routinely resulted in a low dose *Mtb* infection (< 60 CFU total in both lungs one day after infection). Actual day 1 pulmonary loads are indicated in figures and/or legends.

Mtb survival

Mice infected with *Mtb* were weighed and periodically examined every 1-4 weeks with a body score system (4 = normal; 3 = slight hunch; 2 = hunch plus less active or reduced grooming; 2- = 2 with slow gait and very bad posture; 1 = hardly moving, dehydrated, thin and ungroomed). Endpoints were set to determine whether mice were imminently dying of *Mtb* infection and/or required compassionate euthanasia: body score under 2; body score of 2 with relatively low and rapidly dropping weight (such that death is likely within a week); body score of 3 with extremely low (<20 g) and steadily dropping weight (losing >1g/week for last 2 weeks); non-TB ailment normally requiring euthanasia (e.g. serious wound).

Map infection

Mice were infected with *Map* as described previously in an established model [486-488]. Briefly, *Map* culture was grown to OD-600 ~ 0.5 (equivalent to 10^8 CFU/ml), centrifuged and washed with PBS, and then resuspended in PBS + 0.1% Tween-80 (Sigma) at 1/5 the original volume. Mice were injected intraperitoneally with 200 µl of this bacterial suspension to receive an equivalent of ~ 10^8 CFU total. At the indicated timepoints, mice were euthanized and organs were harvested for CFU enumeration or immunophenotyping.

Enumeration of organ CFUs

Lungs, spleens and livers were removed from mice after euthanasia and processed immediately, except in the case of survival studies with *Mtb*, in which case organs were frozen at -80°C for later processing together once all mice were euthanized. Organs were placed in 1 ml complete 7H9 and were homogenized with an Omni Tissue Homogenizer TH (Omni International) for 30 seconds. Homogenate was serially diluted and plated. After approximately 3 and 5 weeks for *Mtb* and *Map*, respectively, CFUs were enumerated from culture plates.

Lung cell preparation for flow cytometry

Three minutes before euthanasia by cervical dislocation, mice were injected intravenously with 5 µg of anti-CD45-FITC (BD) antibody to stain circulatory leukocytes for later differentiation from parenchymal leukocytes. Right lungs were harvested, sliced into small pieces in RPMI-1640 medium and digested in 150 U/ml collagenase (purified from *Clostridium histolyticum*, Sigma) for 1 hour at 37°C. Digested lung tissue was pressed through a 100 µM cell strainer,

treated with red blood cell lysis buffer (Roche), and resuspended in a small volume of RPMI-1640 medium. 20% of this suspension was taken for flow cytometry staining.

Splenocyte preparation for flow cytometry

Spleens harvested from *Map* infected mice were immediately weighed and placed in RPMI-1640 medium. Spleens were next pressed through a 100 μM cell strainer, treated with red blood cell lysis buffer (Roche), and resuspended in 5 ml of R10. Cell concentrations were estimated by counting with a hemocytometer and set to 20 million cells per ml. Approximately 2 million cells were immediately stained and fixed for flow cytometry analysis. Another 2 million cells were cultured *ex vivo* in 142 μl R10 in the presence of 5 μg soluble *Map* lysate (or 8 μl equivalent PBS volume control) for 21 hours at 37°C 5% CO_2, after which 2 μg of Brefeldin A (Sigma) in 50 μl R10 were added and cells were incubated for another 5 hours before staining and fixing for flow cytometry. Soluble *Map* lysate was prepared from a logarithmically growing culture of *Map*, which was centrifuged and washed three times with PBS, subjected to lysis by bead beating with silica beads (MP Biomedicals, FastPrep-24), and the supernatant passed through a 0.2 μm filter and stored at -80°C until needed.

Flow cytometry analysis

Cells were washed in PBS then stained with LIVE/DEAD™ fixable violet dead cell stain (ThermoFisher Scientific). Next, cells were washed with FACS buffer (PBS, 5% BSA, 2mM EDTA), Fc receptors were blocked with TruStain FcX (Biolegend), and then cells were incubated with antibody cocktail prepared in a 1:1 mix of FACS buffer and BD Horizon™ Brilliant Stain Buffer. Cells were washed in FACS buffer, fixed in BD fixation/permeabilization

solution, washed in FACS buffer and stored at 4°C until analysis. Where intracellular staining was performed, after fixation, cells were washed twice with BD Perm/Wash™ buffer, incubated with antibody cocktail for 30 minutes, then washed twice again with BD Perm/Wash™ buffer and once more with FACS buffer and stored at 4°C until analysis. Equal numbers of Precision Count Beads™ (Biolegend) were added to samples just before analysis to determine total cell numbers per organ. A BD Fortessa X-20 cytometer was used for all experiments. Flow cytometry data were collected with FACSDivaTM software (BD) and FCS files were analyzed using FlowJo V10 (BD). Antibody probes from BD included (target, clone, fluorochrome): B220, RA3-6B2, BUV737; CD3ε, 145-2C11, PE; CD8α, 53-6.7, BV711; CD11c, HL3, BUV395; CD44, IM7, BUV395; CD45, 30-F11, FITC; Siglec-F, E50-2440, BV786; IL-2, JES6-5H4, BV605; IL-10, JES5-16E3, FITC; IL-17A, TC11-18H10, BV786. Antibody probes from Biolegend included (target, clone, fluorochrome): CD4, GK1.5, BV510 or BV786; CD11b, M1/70, PE-Cy7 or PerCP-Cy5.5; CD19, 6D5, PE-Dazzle594; CD44, IM7, BV510; F4/80, BM8, APC; Ly6C, HK1.4, APC-Cy7; Ly6G, 1A8, PerCP-Cy5.5; MHC-II (I-A^b), AF6-120.1, APC or AlexaFluor488; IFN-γ, XMG1.2, APC; IL-4, 11B11, PE-Cy7; TNF, MP6-XT22, APC-Cy7.

Histology

For short-term (3-6 week) timepoints, the accessory (post-caval) lobe of the right lung was harvested and placed immediately in 10% formalin for storage until H&E processing. For survival experiments, after CO_2 asphyxiation lungs were injected with 10% formalin through an intratracheal catheter *in situ* as described elsewhere [489]. Briefly, a reservoir of formalin was maintained 25 cm above the mouse to provide a standardized pressure to the injection. A fluid line from this reservoir was fitted with an intravenous catheter which was inserted into an

incision made in the trachea. Silk thread was tied around the trachea to seal the catheter in place, after which the stopcock was opened to allow formalin into the lungs at constant pressure which was maintained for about 20 minutes. After *in situ* fixation, lungs were stored in 10% formalin until H&E processing. All tissue processing post fixation (embedding, cutting and staining) was performed by the Histology Core of McGill University.

Digital images of H&E- and Ziehl–Neelsen-stained sections were generated with a Nikon Eclipse microscope or a Leica Aperio AT Turbo digital pathology scanner at 40X. For 3-6 week timepoints, one representative image of each accessory lobe was obtained for blinded ranking. For survival experiments, three representative images per mouse's lungs were obtained for pixel counting. To quantify the relative two-dimensional alveolar airspace and nuclei-occupied area, a Python code was written. Briefly, reading the H&E section in RGB colour code per pixel, the program called a pixel tissue if it was predominantly red, nuclei if it was predominantly blue, or elsewise it was airspace, and then the % of the airspace and nuclei were calculated over the total area denominator (equal to the sum of tissue, nuclei and airspace pixels; irrelevant areas were cut out). Calculations, image processing, and the GUI utilized the NumPy (**https://numpy.org/**), scikit-image (**https://scikit-image.org/**) and Pygame (**https://www.pygame.org/news**) Python modules, respectively. Digitally scanned slides containing whole lung sections were examined and analyzed with QuPath [490] to quantify cell death by manually annotating lesions with cell death to calculate its area relative to the total lung area analyzed.

Data management and statistical analyses

Numerical data were collected with Microsoft Excel. All graphs were generated with GraphPad Prism v9 (GraphPad Software Inc.). Determinations of data normalcy and statistical significance

were performed with the assistance of GraphPad. Figures were completed in Microsoft PowerPoint. The manuscript was written with Microsoft Word.

4 – Results

4.1 – *Mincle-Nod2* DKO resulted in altered immunity and a small difference in bacterial control during *Mtb* infection.

Given the roles ascribed to Mincle and NOD2 individually in the immune response to *Mtb* [188,189,460,461], we first sought to demonstrate whether knockout of these PRRs individually and together alter the immune response in macrophages, which play a major role in *Mtb*'s lifecycle and are known to express both these receptors. Bone-marrow derived macrophages responded to heat-killed *Mtb* by releasing TNFα, with cytokine production dependent on *Mincle* and *Nod2* (fig. 1A). DKO of both PRRs resulted in similar or lower TNFα compared to SKOs. Heat-killed bacteria retain MAMPs but may lack virulence activities of live bacteria, thus we infected WT, SKOs and DKO BMDMs with live *Mtb* and monitored the immune response by TNFα production over 3 days (fig. 1B). TNFα was produced most abundantly in WT BMDMs, and reduced in *Mincle*-KO; *Nod2*-KO and DKO cells produced the least and appeared to phenocopy each other. Thus, the macrophage response to *Mtb* (live or dead) is dependent on *Mincle* and *Nod2*, with NOD2 exerting the larger effect in terms of TNFα.

We next sought to determine if the immune defect observed in DKO cells translates into reduced *Mtb* control during infection in a whole animal. WT and DKO mice were infected with *Mtb* by aerosol and lungs were harvested at 3- and 6-weeks post-infection to examine pulmonary bacterial burden and pathology. We observed a small (less than one log) increase in bacterial

burden in DKO mice compared to WT reaching significance at 6 weeks (fig. 1C). Additionally, blinded ranking of H&E-stained sections of lungs resulted in DKO mice ranking with higher pathology at 6 weeks post-infection (fig. 1D). DKO mice tended to have less alveolar airspace than WT, but inflammation was not accompanied by large numbers of nuclei suggestive of lymphocyte infiltration (fig. 1E). Previous studies had shown *Mincle* and *Nod2* SKOs had reduced lymphocyte immunity and/or similarly small increases in bacterial burden compared to WT during mycobacterial infection [189,461,482]. These results with DKO mice showed a comparable reduction of *Mtb* control and adaptive immunity.

4.2 – Impact of *Mincle* and *Nod2* DKO during *Mtb* infection was similar to SKOs in terms of bacterial burden and adaptive immunity.

To address whether DKO of *Mincle* and *Nod2* results in a greater impairment in *Mtb* control and adaptive immunity than WT and SKOs, we infected all four genotypes with *Mtb* by aerosol and, at 3- and 6-weeks post-infection, examined lung, spleen and liver bacterial burden, plus conducted flow cytometry on lung homogenates to determine the state of leukocytes in the lung parenchyma and associated vasculature (using intravenous CD45 staining just prior to euthanasia; fig. S1A for gating). Bacterial burden tended to be greater in all three organs in *Nod2*-KO and DKO mice at 3 and/or 6 weeks, compared to WT and *Mincle*-KO, but did not attain statistical significance given the multiple comparisons and small effect (less than one log difference as in fig. 1C) (fig. 2A).

At 3 weeks, when the bacterial burden was comparable or slightly higher in the DKO than WT, there was a trend to reduced lymphocyte ($CD4^+$ T cells, $CD8^+$ T cells and B cells) numbers in DKO mice, in both the lung parenchyma and vasculature (fig. 2B). This difference

was not apparent by 6 weeks. SKOs appeared to have slightly reduced T cell numbers at 3 weeks too, but similarly converged to WT at 6 weeks. None of these trends were statistically significant. With other markers included in the flow cytometry panel, we were able to provide descriptive data on other cell types in the lung. Alveolar macrophage numbers remained similar across the different genotypes (fig. S1B). At 3 weeks post infection, there were slight trends of decreased neutrophils and Ly6C^{lo} monocytes in the lung parenchyma of DKO compared to WT (fig. S1C). Again, these were small, less than one log differences. Additionally, like lymphocytes, any trends observed in these cells at 3 weeks were unseen by 6 weeks post infection. Thus, it appears that *Nod2*-KO and DKO mice might have an impairment in the timeliness of mounting an adaptive immune response, associated with increased bacterial burden compared to WT, but comparable numbers of lymphocytes are eventually elicited. Importantly, DKO mice did not respond differently from *Nod2*-KO mice. We had also collected accessory lobes at these timepoints for H&E staining, but no differences were observed here at six weeks post infection (not shown).

4.3 – NOD2 was more important to survival than Mincle in *Mtb*-infected mice.

Nod2-KO mice had been shown to have reduced survival during *Mtb* infection compared to WT mice in one previous study [189]. We could not find any published work presenting a survival curve for *Mtb* infection in *Mincle*-KO mice. Thus, as an unbiased readout of the importance of these PRRs during *Mtb* infection, we tested both SKO and DKO mice for comparison to WT. We infected WT, *Mincle*-KO, *Nod2*-KO and DKO mice with *Mtb* by aerosol and monitored these mice over the course of a year. Mice were euthanized when they reached a predefined endpoint (see methods). Median survival times of *Mincle*-KO, *Nod2*-KO and DKO

groups were 324, 291 and 281 days, respectively. The experiment was ended at day 363 with more than half of WT mice surviving (fig. 3A), but median survival is projected at approximately 400 days assuming a linear regression model for death rate (not shown). Compared to WT, the probabilities that SKO and DKO groups had significantly reduced survival are p = 0.0497, 0.0161 and 0.0016 for *Mincle*-KO, *Nod2*-KO and DKO, respectively (Bonferroni-corrected threshold for three comparisons is 0.0167). *Nod2*-KO and DKO curves closely followed each other. The weight of the mice was measured throughout the experiment, and mice dying of *Mtb* infection lost much of their body mass in the weeks prior to death, which is reflected in our data (fig. 3B). Mass of male and female mice are plotted separately in fig. S2A. By weight, DKO and *Nod2*-KO groups were ill earlier than *Mincle*-KO and WT groups. A separate, earlier survival experiment was conducted comparing only WT and DKO mice yielding a similar result (median survival of 287 days for DKO, fig. S2B).

4.4 – Absence of *Nod2* was associated with altered immunity near *Mtb*-related mortality.

Over the course of the survival experiments, spleens, livers and lungs were taken at euthanasia. CFUs from spleens and livers were plotted to determine if death in KO mice was associated with greater extrapulmonary bacterial burden. Comparing spleen *Mtb* burden at death in WT, *Mincle*-KO, *Nod2*-KO and DKO mice, there was a trend to greater CFUs in KO mice than WT; however, when plotted over time it appears that the many WT mice with lower spleen *Mtb* burden were those euthanized not because of TB *per se* but because the experiment had ended (fig. S3A). Thus, elevated splenic dissemination of *Mtb* was associated with TB death, not necessarily KOs. Statistically greater splenic burden was shown in the earlier experiment comparing only WT and DKO mice during survival (fig. S3B). In both experiments this

elevated burden represents a less than one log departure from WT. The same analysis applied to liver *Mtb* burden at death did not result in a statistically significant difference between groups in either experiment, although KOs again trended with higher values (fig. S3C-D). Thus, when mice were dying of *Mtb* infection, they had an approximately half-log elevation in dissemination of *Mtb* which is insufficient to explain their morbidity.

Lungs that were taken at euthanasia were formalin fixed *in situ* and subsequently stained with H&E. This was done to determine whether the pulmonary pathology associated with death from *Mtb* infection differed across the genotypes. We examined the range of pathology over the four genotypes: all contained some alveoli free of inflammation as well as other sites of acute and chronic inflammation. With all genotypes we also observed lymphocytic foci, cell death, cholesterol accumulation and keratinization (not shown). Interestingly, we only observed large, necrotizing foci in *Nod2*-KO and DKO lungs although these were in a minority of mice (3 of 12 *Nod2*-KO mice, and 1 of 14 DKO mice) (fig. 4A). These necrotizing foci where about half a millimetre in diameter, circumscribed with a cuff of foamy macrophages and having a centre containing cell debris mixed with variable numbers of relatively intact foamy macrophages, PMNs and possibly a few lymphocytes. Some of these lesions contained keratinization. We also found ample quantities of acid-fast bacilli in these necrotic foci upon examination of the corresponding Ziehl–Neelsen-stained sections (fig. 4B). This prompted us to measure whether there was more cell death overall in the lungs of mice deficient in *Nod2*. The number of lesions containing dead cells was not significantly different between genotypes (fig. S3E). However, a larger proportion of the lung volume contained dead cells in *Nod2* and DKO mice compared to WT and *Mincle*-KO mice (fig. 4C). This did not appear to be driven by the timing of euthanasia (fig. S3F). There were more large lesions (>0.2 mm^2) containing cell death in *Nod2*-deficient

mice compared to *Nod2*-competent mice (fig. 4D) which may explain the phenotype of greater cell death overall and is compatible with the generation of large necrotic foci.

To further quantitation of these H&E lung sections, we used pixel counting to calculate the relative amount of alveolar airspace (i.e. whitish pixels) and nuclei (i.e. bluish pixels) (fig. S3G). We did not detect a difference in the available airspace across genotypes in the two experiments (fig. S3H-I). There was a trend for elevated numbers of nuclei in DKO mice among the four genotypes which may have been related to the time of euthanasia (fig. S3J). The difference in nuclei between WT and DKO mice was significant in the earlier experiment (fig. S3K). Thus, there was greater immunopathology in the lungs of *Nod2*-deficient mice characterized by more necrosis and leukocyte infiltration and this was associated with hastened mortality.

4.5 – Mincle and NOD2 disruption caused early altered immunity during *Map* infection while bacterial control was maintained.

During *Mtb* infection, we observed immunopathological changes associated with minimal differences in bacterial control upon PRR perturbation. Because Mincle and NOD2 ligands of *Mtb* are a common feature of mycobacteria, we wanted to ascertain whether Mincle and NOD2 sensing are similarly important in a contrasting, non-*Mtb* mycobacterial infection. *Map* is a non-tuberculous veterinary pathogen for which there is a previously established murine intraperitoneal infection model [486-488]. Mice infected intraperitoneally with ~10^8 CFU of *Map* developed splenomegaly early in infection which subsided from 3 to 12 weeks post infection. Interestingly, splenomegaly was visibly, additively and significantly milder with PRR disruption (fig. 5A). At 3 and 6 weeks post infection, *Nod2*-KO and DKO mice tended to have greater

concentrations of *Map* in the spleen and liver compared to WT and *Mincle*-KO but this was not statistically significant (fig. 5B-C). Accounting for variable splenomegaly, the CFU total in the spleen was also not significant (fig. S4A).

To investigate whether milder splenomegaly in PRR mutants was the result of a specific leukocyte deficiency, we analyzed the cellular contents of spleens at 3 weeks post infection where splenomegaly and differences between genotypes were most pronounced. There did not appear to be less lymphocytes in the spleens of KO mice compared to WT (fig. 5D). Trends with less myeloid subsets in DKO compared to WT were not significant (fig. 5D).

Previous studies had demonstrated functional lymphocyte defects during mycobacterial infection or immunization in *Nod2*-KO and *Mincle*-KO [108,187,189]. Thus, we tested the response of lymphocytes to soluble *Map* lysate (containing *Map* antigens) isolated from the spleen of *Map* infected mice at 3 weeks post infection. Although not statistically significant, $CD4^+$ T cells from *Nod2*-KO and DKO mice produced less IFN-γ, TNF, IL-2, IL-4 and IL-10 compared to WT and Mincle-KO mice when stimulated with Map lysate (fig. 6A-E). The effect was interestingly most pronounced for *Nod2*-KO IL-10. There was no significant difference between groups in terms of Map-specific IFN-γ-producing $CD8^+$ T cells. (fig. S4B). Polyfunctional Th1 cells producing IL-2 tended to be less frequent in *Nod2*-KO and DKO cells compared to WT (fig. 6F) (values for PBS control in fig. S4C) (gating in fig. S4D). While the effect was not large enough to be demonstrable statistically, these results are consistent with defective lymphocyte function in the absence of *Nod2* during mycobacterial infection.

5 – Discussion

The PRRs Mincle and NOD2 uniquely interact with mycobacteria and have been shown to synergistically drive immunological functions [108,157,187]. In this study, we used measures of the immune response, bacterial control and survival to examine the course of *Mtb* infection, and infection with the disparate mycobacterium *Map*, in mice defective for Mincle and/or NOD2. Despite their established immunological roles, these PRRs contributed little to mycobacterial control. Both PRRs were important to prevent premature death in *Mtb* infected mice. Because *Nod2*-KO and DKO mice had very similar reduced survival times, while *Mincle*-KO mice survived longer, it appears that absence of *Nod2* was the 'dominant' driver of hastened mortality in DKO mice, and the added *Mincle* defect was unimportant. The *Nod2*-deficient death phenotype was associated with increased cell death in the lungs with distinct necrotic foci.

In humans, one study found a significant association between *NOD2* loss-of-function mutations and an increased risk of necrotizing enterocolitis or focal intestinal perforation in very low-birth-weight infants [491], suggesting NOD2 deficiency is related to necrotic pathology in humans. Murine *Nod2* and MDP treatment promoted the formation of necrotic zones in a murine model of atherosclerosis however [492], so the relationship between NOD2 and necrosis seems complex. The necrotic foci seen in *Nod2* deficient mice were reminiscent of similar pathology in the Kramnik mouse [85,493], the susceptibility of which has been attributed to the *Sst1* locus and excess type I IFN production [270]. However, NOD2 signaling contributed to type I IFN production [97], so how the absence of *Nod2* lead to the formation of necrotic foci is not so easily explainable. Perhaps the amount of type I IFN in space and time is a critical element for these outcomes, or that excess type I IFN precipitates a common secondary effect that leads to runaway necrosis. Heterozygous deficiency in IL-1R antagonist or anti-IL-1R antagonist

treatment ameliorated morbidity and lung pathology in mice with the susceptible *Sst1* allele [270]. IL-1 signaling contributed to PGE2 production, and PGE2 was protective against *Mtb* in IL-1 signaling-deficient mice [494]. Thus, roles for NOD2 in IL-1 and PGE2 pathways should be further explored in late *Mtb* infection. When infected with *Mtb*, human PBMCs with functional NOD2 produced more IL-1 than human PBMCs containing the NOD2 3020insC mutation [495]. MDP also promoted PGE2 production by monocytes and macrophages [496,497]. The balance of immune mediators like type I IFN, IL-1 and PGE2 may play a key role in pulmonary cell death during *Mtb* infection.

Extensive necrosis was not seen in *Nod2*-deficient mouse lungs at early timepoints (3 and 6 weeks post infection) (fig. 1E and not shown). The phenotype of large necrotic foci was late, appearing in mice euthanized at 223, 275, 307 (*Nod2*-KO) and 254 (DKO) days post infection, and occurred in a minority of the animals. It will be challenging to directly study the mechanisms of this phenomenon with this model. A 10X higher-dose aerosol may increase the rate of death in *Nod2*-KO mice [189], but could overlook the phenotype that occurred with our more epidemiologically relevant dose of *Mtb* if time is needed for the pathology to develop. At 6 weeks post infection, DKO mouse lungs were more congested than WT controls but without lymphocytic clusters (fig. 1E), consistent with what has been demonstrated before with *Nod2*-KO mice [189]. Our trend of decreased lymphocytes in *Nod2*-KO and DKO mouse lungs at three weeks post infection with *Mtb* is similar to results with *Nod2*-KO mouse lungs at 4 weeks post infection with BCG Russia [189]. We did not observe a difference in splenic lymphocyte numbers during high-dose *Map* infection across genotypes, but the trend of reduced *Map*-specific cytokine production and polyfunctionality in *Nod2* deficient mice still suggests a defective lymphocyte response. The defect in innate immunity caused by *Nod2* mutation results in altered

instruction of the adaptive immune response [187,189], but while the innate defect is undoubtedly present throughout the course of the infection (and therefore well deserves attention), we are only certain the adaptive defect is present early. NOD2 deficiency may also impair macrophage production of nitric oxide as well as secreted immune mediators [188].

Throughout this study, what had not shone through is the importance of Mincle. *Mincle*-KO mice demonstrated a null or intermediate phenotype between WT and *Nod2*-deficient animals. Such intermediate trends were occasionally observed for measures of immunity, but bacterial loads were similar to WT except at *Mtb*-related death. Most noteworthy was the slight reduction in survival with *Mtb* for *Mincle*-KO mice compared to WT, which to our knowledge has not been published before. Previous *Mincle*-KO studies of *Mtb* infection did not present survival data but had only reported bacteriologic and immunologic changes which were minor, not long-lasting or inconsistent between studies [460,461]. Administration of TDM or synthetic TDM analogues has been shown to produce distinct, robust biologic effects [157,187] but this is dependent on an arbitrarily selected dose which may not be representative of the amount of immune-available material from the millions of bacilli in a mouse. Interestingly, as *Nod2*-KO and DKO mice phenocopied each other in terms of survival with *Mtb*, NOD2 appears to be dominant over Mincle in this system. This result suggests Mincle is dispensable in the absence of NOD2 (i.e. Mincle-NOD2 synergy) or NOD2 deficiency simply leads to death before Mincle deficiency has an effect.

NOD2 polymorphisms are strongly associated with Crohn's disease yet a long-hypothesized role for *Map* in Crohn's disease remains unproven. Unlike *Mtb*, *Map* lacks a functioning Esx-1 secretion system that enables the bacteria to disrupt the phagosomal membrane and access the host cytosolic compartment. However, *Map* is still pathogenic in cattle

and a long list of other hosts. *Map* burden remained within one log from 3 to 12 weeks in mice, even as the appearance of the internal organs returned to normal. This persistence might permit the development of an altered pathologic response in a genetically susceptible host, however, the intraperitoneal infection route that we used is unable to produce detectable pathology in the gastrointestinal tract. Future work can test whether *Map* can precipitate inflammatory pathology in the intestines of *Nod2*-KO mouse using an experimental model that is more relevant to Crohn's disease. The trend we observed of reduced IL-10-producing *Map*-specific CD4+ T cells in *Nod2*-KO mice should also be sought in such a model [498]. Associations of *NOD2* polymorphisms and TB have not been as strong, but future studies exploring how altered immunity in NOD2-deficient hosts leads to distinct disease states will inform the definitions of TB endophenotypes which can be tested for associations with *NOD2* polymorphisms at large. Our work has asserted that NOD2 is indeed important in *Mtb* infection through reduced survival associated with distinct pathology. Defining the mechanisms of these NOD2 phenotypes will inform our understanding of human mycobacterial diseases.

6 – Acknowledgements

We are grateful for the Containment Level 3 platform of the Research Institute of the McGill University Health Centre (RI-MUHC). We thank the Immunophenotyping and Histology platforms of the RI-MUHC, and the Histology Core of McGill University for tissue processing. We greatly appreciate the generosity of Christine Wells (University of Melbourne, Australia) for providing *Mincle*-KO mice. We thank Richard Fraser of the McGill department of Pathology for guiding us with histopathological analyses. For advice and assistance in

experiments, J.Y.D. would like to thank Andréanne Lupien, Helena Strand Clemmensen and Sarah Danchuck.

J.Y.D. was personally supported by the Canadian Institutes of Health Research (CIHR) Canada Graduate Scholarship – Master's Program, Fonds de Recherche du Québec – Santé (FRQ-S) Doctoral Training Award, RI-MUHC studentships (Master's and Ph.D.) and scholarships from the McGill Department of Microbiology and Immunology. Research activities were funded by a CIHR foundation grant held by M.A.B. (FDN-148362).

Additional Information

The authors have no competing interests.

Author Contributions

Conceptualization, J.Y.D. and M.A.B.; Methodology, J.Y.D., F.M. and S.C.D.; Investigation, J.Y.D., F.M. and S.C.D.; Resources, M.A.B.; Writing – Original Draft, J.Y.D. and M.A.B.; Writing – Review & Editing, J.Y.D., F.M., S.C.D. and M.A.B.; Visualization, J.Y.D.; Supervision, M.A.B.; Funding acquisition, J.Y.D. and M.A.B.

7 – Figures

Chapter III, Figure 1. Effect of *Mincle* and *Nod2* disruptions on the macrophage and pulmonary immune response to *Mtb*.

A, TNFα in supernatant of BMDM culture after incubation with heat-killed *Mtb* (HK H37Rv) or medium control for 20 hours. Mean +/- standard deviation of four individually treated culture wells. **$p < 0.01$ with one-way ANOVA on HK H37Rv treated BMDMs. **B**, TNFα in supernatant of BMDM culture after infection with live *Mtb*. Mean +/- standard deviation of eight (t = 4 hours) or four (all other timepoints) individually infected culture wells. **C**, total *Mtb* burden in both lungs of WT and DKO mice. N = 2 mice per group on day 1, while N = 4 to 6 mice per group for days 26 and 42 post infection. *$p < 0.05$ with Dunnett's T3 multiple comparisons test over days 26 and 42; ns, not significant, $p > 0.05$. **D**, rank of pathology on H&E lung sections at 42 days post infection. Ranking was obtained from the median rank of seven blinded individuals. *$p < 0.05$ with one-tailed Mann Whitney test. **E**, representative H&E sections from WT (rank 5) and DKO (rank 10) mice.

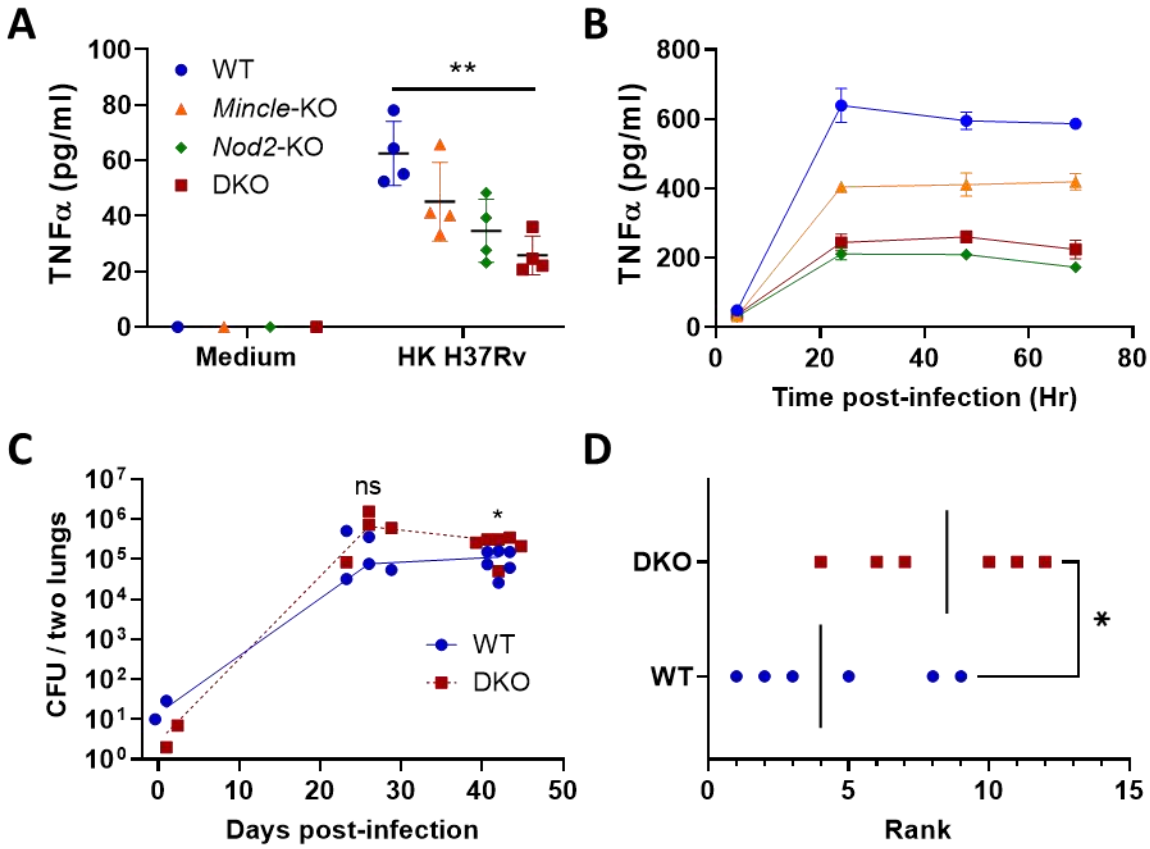
A
TNFα (pg/ml)
WT
Mincle-KO
Nod2-KO
DKO
**
Medium
HK H37Rv
B
TNFα (pg/ml)
Time post-infection (Hr)
C
CFU / two lungs
ns
*
WT
DKO
Days post-infection
D
DKO
WT
*
Rank

E

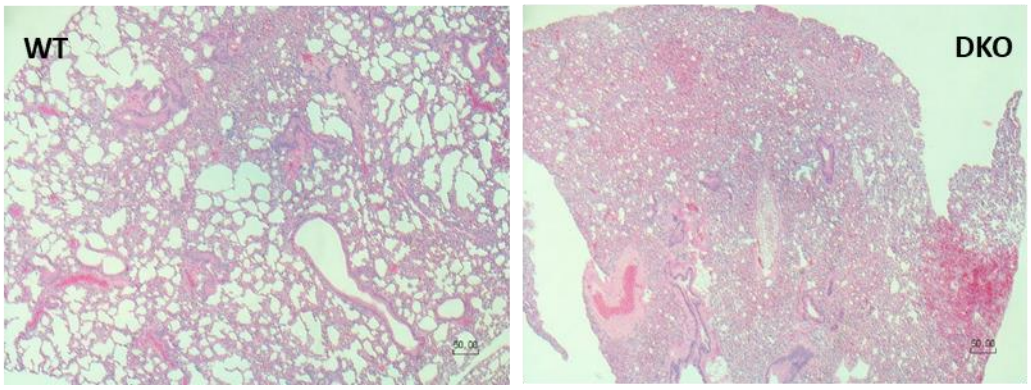
WT
DKO

Chapter III, Figure 2. *Mtb* control and lymphocyte recruitment in mice lacking *Mincle* and *Nod2* singly and in combination.

A, *Mtb* CFU burden per gram of left lung (left), spleen (middle) and liver (right) for the indicated timepoint. Median day 1 pulmonary *Mtb* load was 15 CFU. **B**, Absolute numbers of pulmonary lymphocytes at the indicated timepoints post *Mtb* infection. Using intravenous anti-CD45-FITC staining just prior to euthanasia, parenchymal (CD45-FITC$^-$) or vascular (CD45-FITC$^+$) location was determined. Shown are medians for N = 5 to 7 mice per group per timepoint; mice are represented by individual points on the graphs. No statistically significant differences were found between genotypes for the given variables and timepoints.

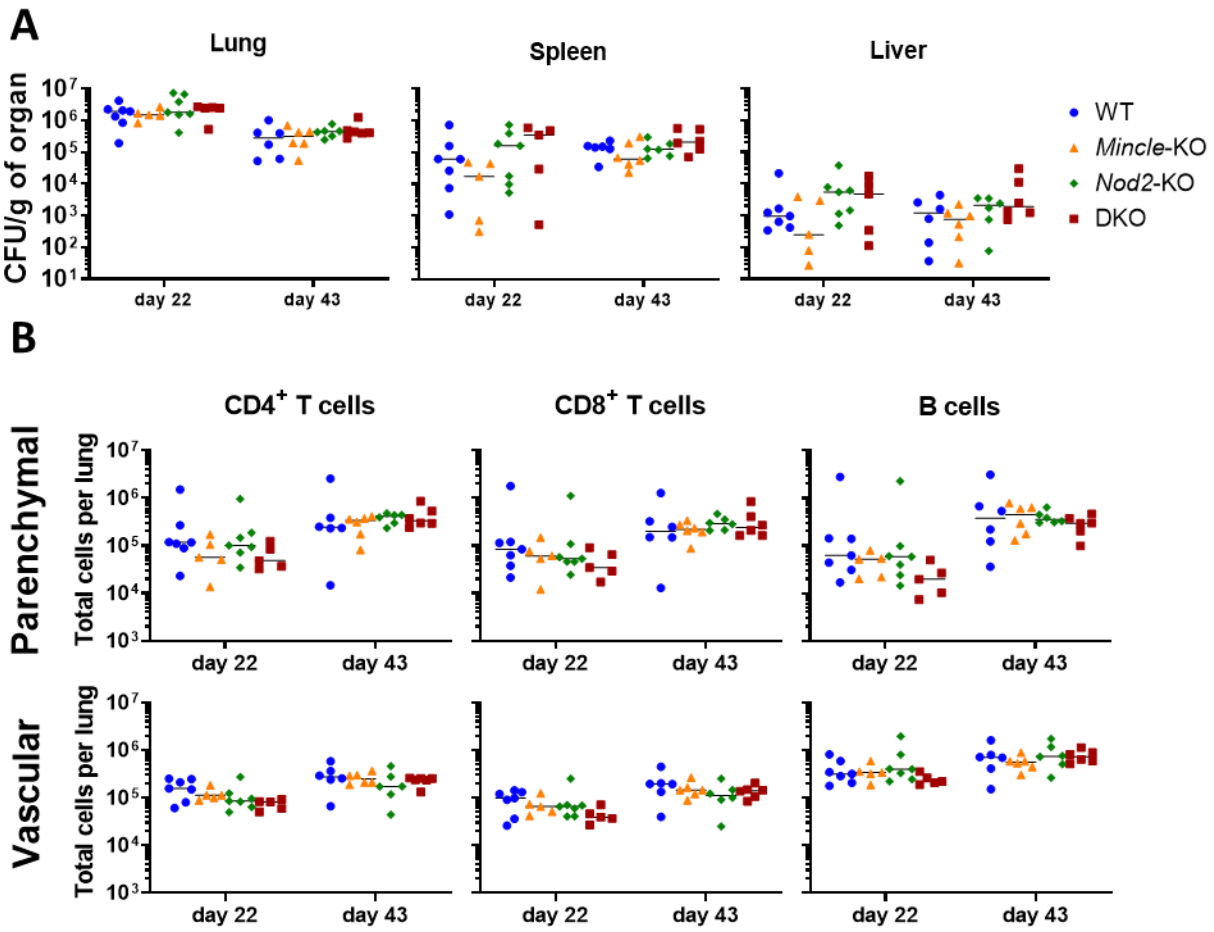
A
Lung
Spleen
Liver
CFU/g of organ
day 22
day 43
WT
Mincle-KO
Nod2-KO
DKO
B
CD4+ T cells
CD8+ T cells
B cells
Parenchymal
Vascular
Total cells per lung

Chapter III, Figure 3. Survival of *Mincle* and *Nod2* deficient mice infected with *Mtb*.

A, percent survival of *Mtb*-infected mice of the indicated genotype over time. Log-rank (Mantel-Cox) test p values generated from comparing to the WT group are reported next to legend. The Bonferrroni-corrected threshold for three such comparisons is 0.0167. **B**, percent weight from 6 days post infection over time for the indicated genotype (male and female mice combined); median (lines) +/- interquartile range (shading) are shown. Euthanized mice received a weight of 0. Weight in grams is plotted in fig. S2A. Median day 1 pulmonary *Mtb* load was 31 CFU. N = 12, 8, 12 and 14 for WT, *Mincle*-KO, *Nod2*-KO and DKO, respectively.

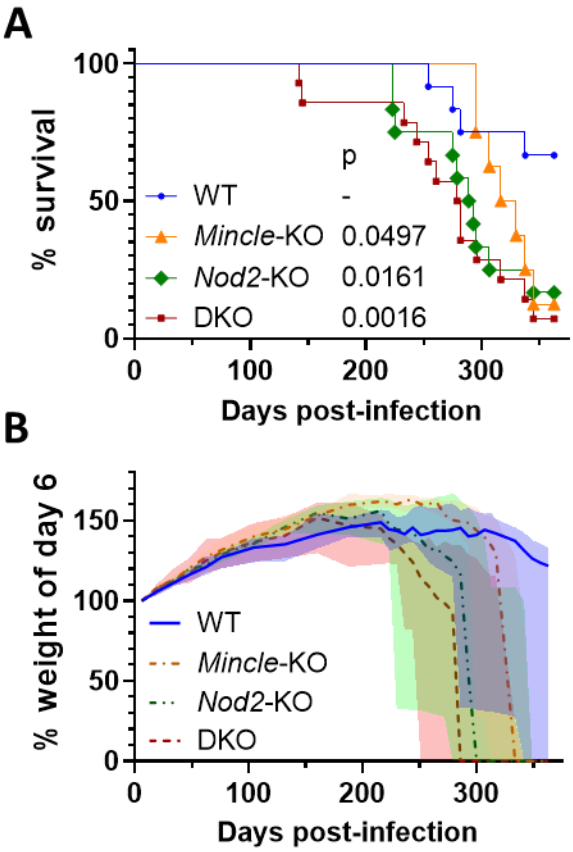
A
100
50
0
% survival
p
WT -
Mincle-KO 0.0497
Nod2-KO 0.0161
DKO 0.0016
0
100
200
300
Days post-infection
B
150
100
50
0
% weight of day 6
WT
Mincle-KO
Nod2-KO
DKO
0
100
200
300
Days post-infection

Chapter III, Figure 4. Pulmonary pathology at death in *Mincle* and *Nod2* deficient mice infected with *Mtb*.

A, images of largest lesions containing cell death, each from a different mouse: one WT (largest lesion in all WT mice), two *Mincle*-KO, three *Nod2*-KO (all representative necrotic foci) and three DKO (top, necrotic focus, middle, diffuse necrosis, bottom, airway filled with inflammatory infiltrate containing dead cell debris). Scale bars, 100 μm. **B**, Ziehl–Neelsen stained lung section containing large necrotic focus, from *Nod2*-KO mouse shown in A (center). **C**, percentage of lung space containing dead cells with medians. Kruskal-Wallis test was used determine statistical significance; *$p < 0.05$. **D**, sizes of individual lesions containing dead cells, separated by mouse according to genotype (colour/shape coded) and in order of survival time (left to right, shortest to longest). Dotted line, to delineate lesions larger than 0.2 mm^2. N = 11, 7, 12 and 14 for WT, *Mincle*-KO, *Nod2*-KO and DKO, respectively.

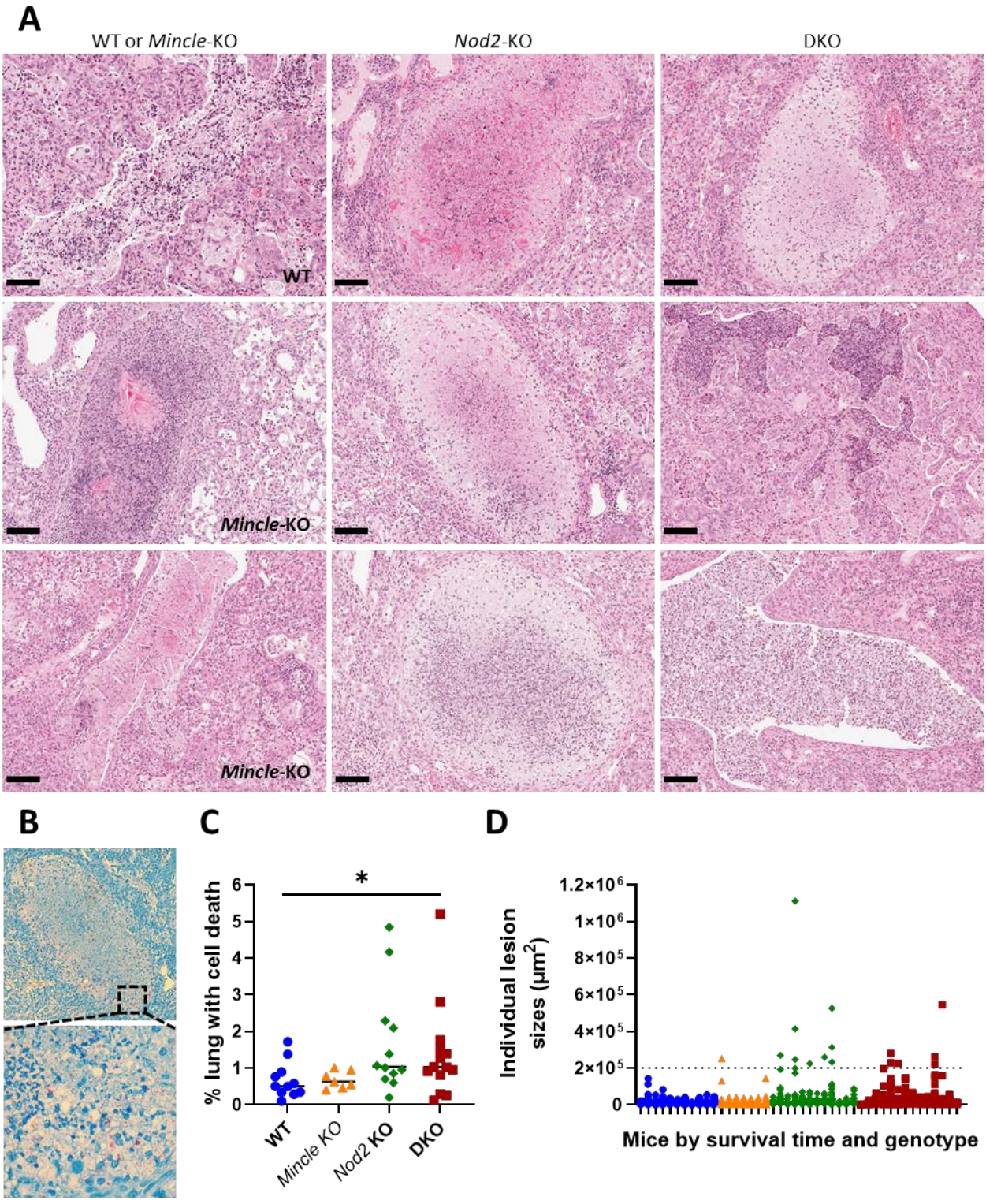
A
WT or Mincle-KO
Nod2-KO
DKO
WT
Mincle-KO
Mincle-KO
B
C
% lung with cell death
*
WT
Mincle KO
Nod2 KO
DKO
D
Individual lesion sizes (µm²)
1.2×10⁶
1×10⁶
8×10⁵
6×10⁵
4×10⁵
2×10⁵
0
Mice by survival time and genotype

Chapter III, Figure 5. Control of *Map* infection in *Mincle* and *Nod2* deficient mice.

A, mass of spleens upon euthanasia at the indicated timepoint. Shown are medians of N = 5 to 13 mice per group per timepoint (data for day 21 were combined from two independent experiments). Welch's ANOVA was performed at each timepoint; *$p < 0.05$. **B-C**, *Map* CFU burden per gram of spleen (B) and liver (C) at the indicated timepoint. Shown are medians of N = 5 to 7 mice per group. Kruskal-Wallis test was performed at each timepoint for each organ; ns, not significant ($p > 0.05$). **D**, flow cytometry enumeration of leukocyte subsets in the spleens of *Map* infected mice at 3 weeks post infection. Populations were identified with t-SNE similarly to fig. S1. Shown are medians of N = 6 to 8 mice per group; mice are represented by individual points on the graphs. No statistically significant differences were found.

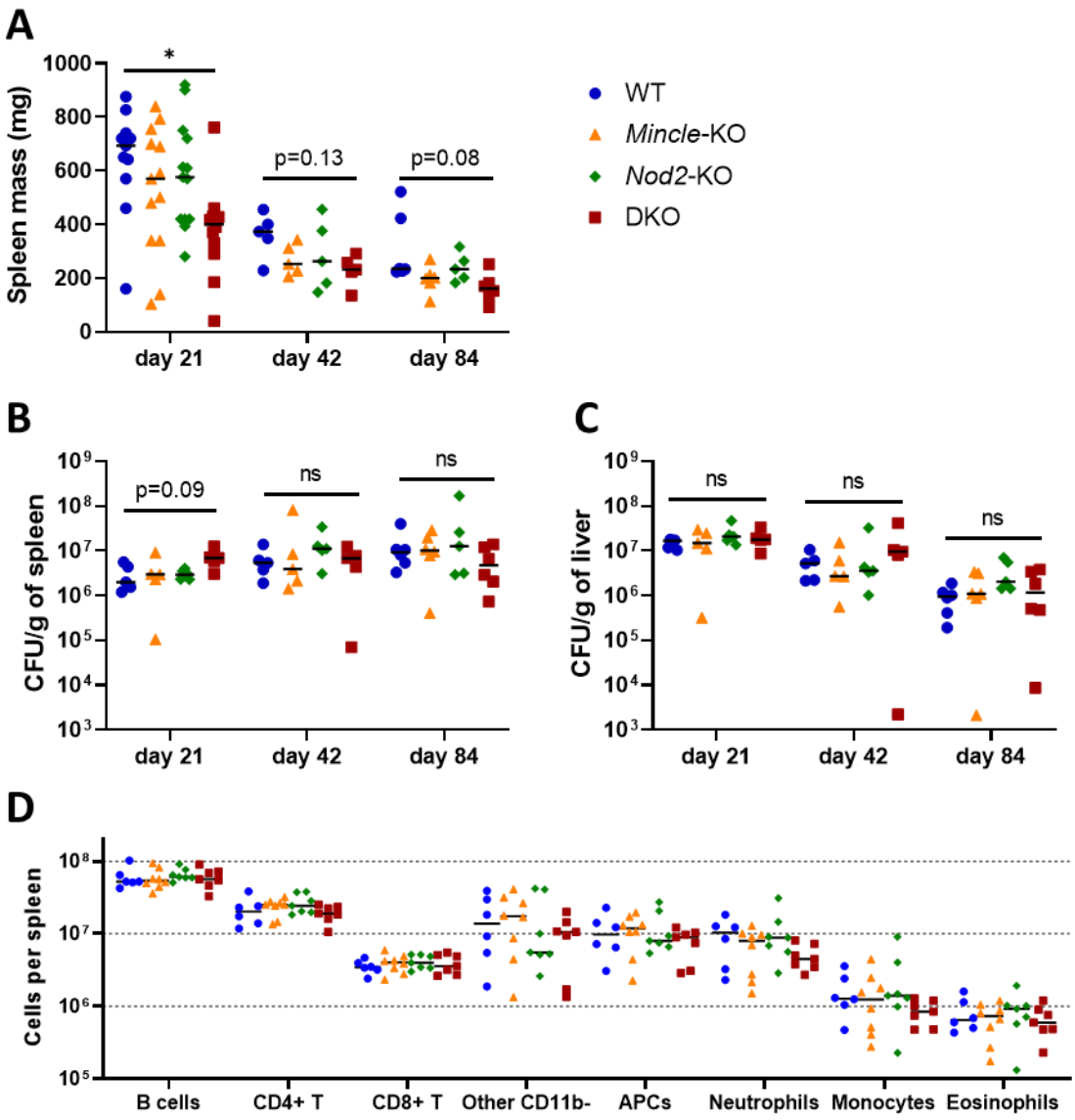
A
Spleen mass (mg)
1000
800
600
400
200
0
*
p=0.13
p=0.08
day 21
day 42
day 84
WT
Mincle-KO
Nod2-KO
DKO
B
CFU/g of spleen
p=0.09
ns
ns
C
CFU/g of liver
ns
ns
ns
D
Cells per spleen
B cells
CD4+ T
CD8+ T
Other CD11b-
APCs
Neutrophils
Monocytes
Eosinophils

Chapter III, Figure 6. *Map*-specific $CD4^+$ T cell response elicited during *Map* infection in *Mincle* and *Nod2* deficient mice.

A-F, Flow cytometry enumeration of total numbers of splenic $CD4^+$ T cells ($CD11b^-CD19^-CD3\varepsilon^+CD44^+CD4^+CD8\alpha^-$) expressing different cytokines from mice infected with *Map* three weeks prior. **A-E**, IFN-γ+, TNF+, IL-2+, IL-4+ or IL-10+ cells after incubation with soluble *Map* lysate or equivalent volume of PBS. **F**, Map lysate-stimulated $CD4^+$ T cells expressing combinations of Th1 cytokines IFN-γ, TNF and/or IL-2 (PBS control shown in fig. S4C). No cytokine positive cells were found where points are plotted on top of the x axis (at 10 cells per spleen). Shown are medians of N = 6 to 7 mice per group; mice are represented by individual points on the graphs. No statistically significant differences were found.

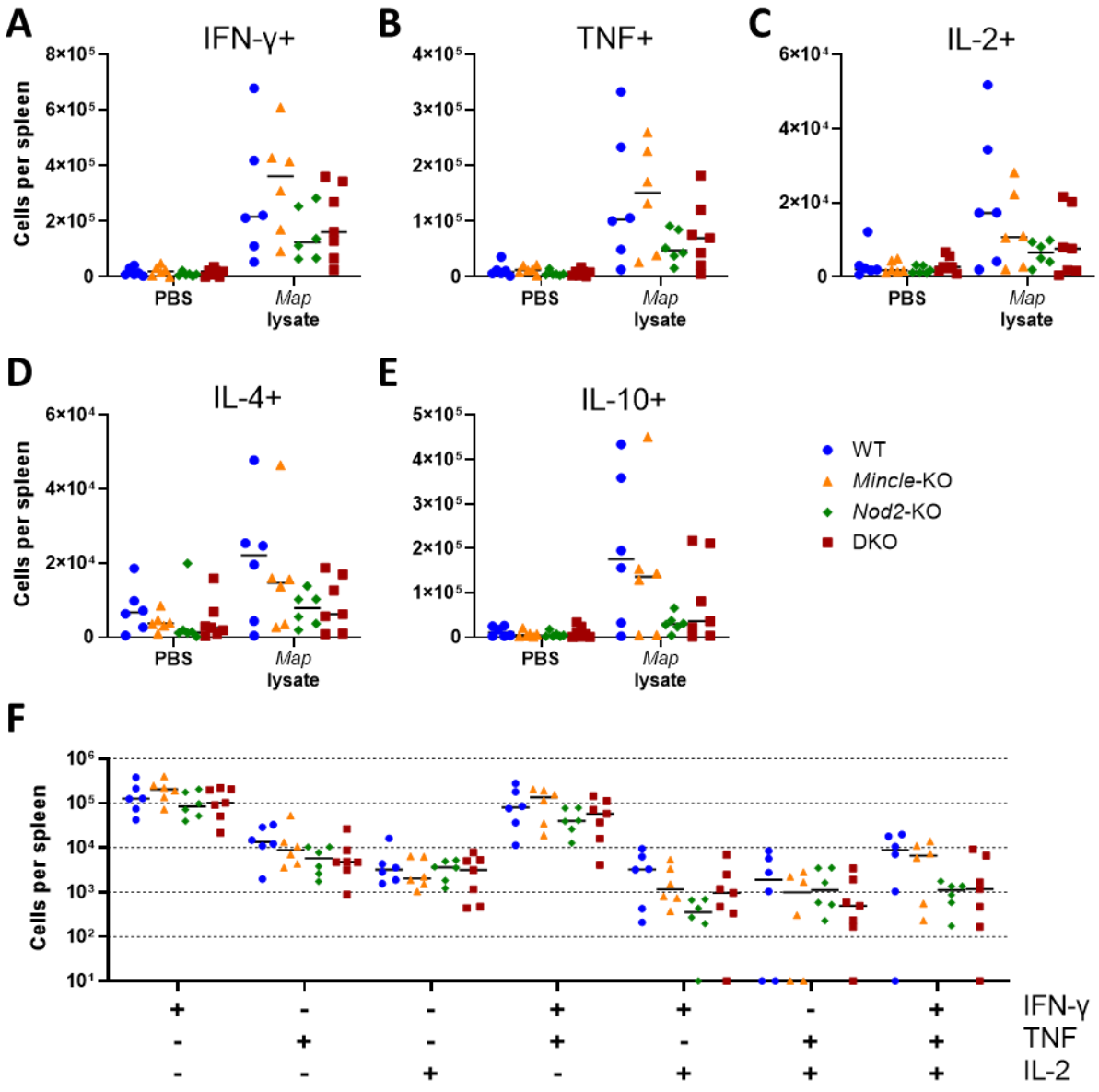
A
IFN-γ+
B
TNF+
C
IL-2+
D
IL-4+
E
IL-10+
Cells per spleen
PBS
Map lysate
WT
Mincle-KO
Nod2-KO
DKO
F
IFN-γ
TNF
IL-2

8 – Supplemental Figures

Chapter III, Figure S1. Flow cytometry of lung cells of *Mtb*-infected *Mincle* and *Nod2* deficient mice.

A, gating strategy used to enumerate lung cell types. After gating on single, live cells, downsampling and concatenation were performed to put all samples through t-SNE. Populations in the two t-SNE generated dimensions were identified and gated by checking expression of characteristic markers. Per population, gating of CD45-FITC positive and negative cells was performed separately to account for autofluorescence of difference leukocyte types. Total numbers of events in each final gate were exported and proportioned based on the number of counting beads passed with the cells to determine total cell type numbers per lung. **B**, total alveolar macrophage numbers per lung (none were considered vascular). **C**, total numbers of parenchymal and vascular cells of the indicated phenotype. Shown are medians for N = 5 to 7 mice per group per timepoint; mice are represented by individual points on the graphs. No statistically significant differences were found between genotypes for the given variables and timepoints.

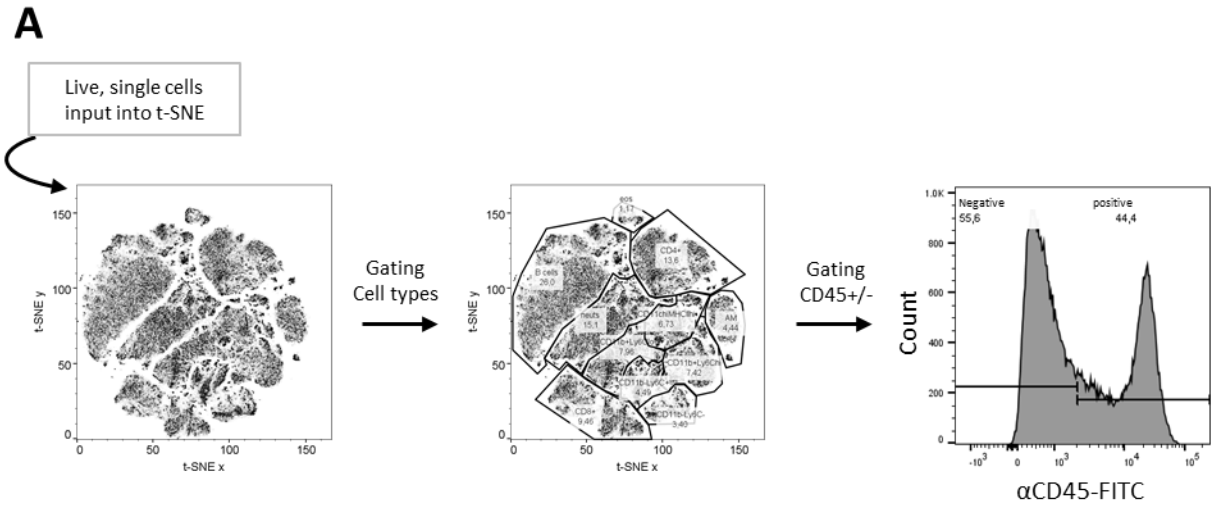
A
Live, single cells
input into t-SNE
t-SNE y
t-SNE x
Gating
Cell types
Gating
CD45+/-
Count
Negative
55,6
positive
44,4
αCD45-FITC

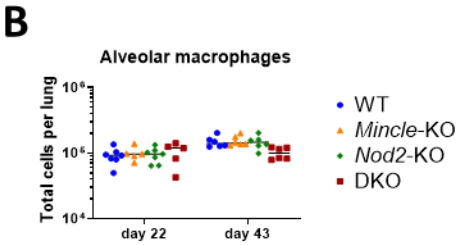
B
Alveolar macrophages
Total cells per lung
day 22
day 43
WT
Mincle-KO
Nod2-KO
DKO

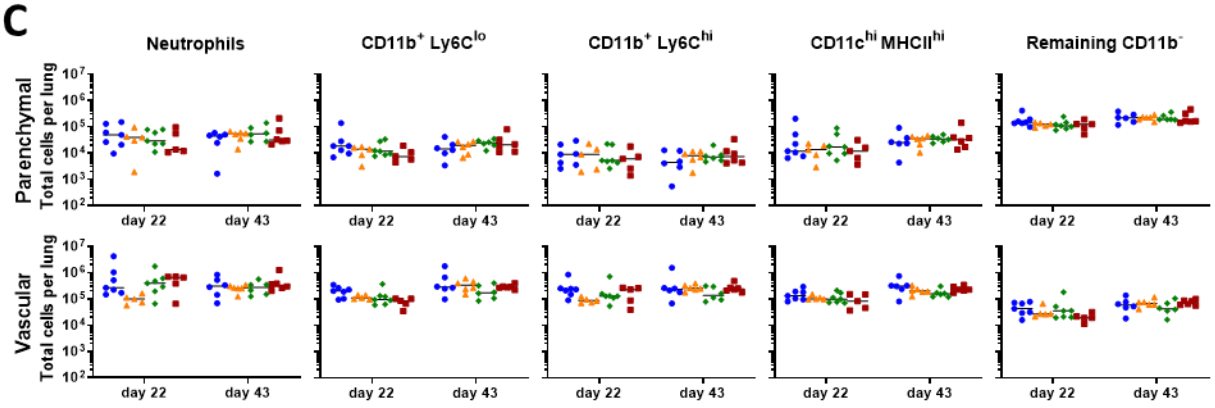
C
Neutrophils
CD11b+ Ly6Clo
CD11b+ Ly6Chi
CD11chi MHCIIhi
Remaining CD11b-
Parenchymal
Vascular
Total cells per lung
day 22
day 43

Chapter III, Figure S2. Survival and weight of *Mincle* and *Nod2* deficient mice infected with *Mtb*.

A, weight in grams of mice subjected to survival challenge shown in fig. 3. **B**, independent experiment comparing just WT and DKO mice: median day 1 pulmonary *Mtb* load was 29 CFU. Shown are percent survival (top), weight in grams (middle) and percent weight from two days post infection (bottom) over time. **$p < 0.01$ by log-rank (Mantel-Cox) test. All mice were female. Median (lines) +/- interquartile range (shading) are shown for weight and percent weight. N = 14 and 16 for WT and DKO, respectively.

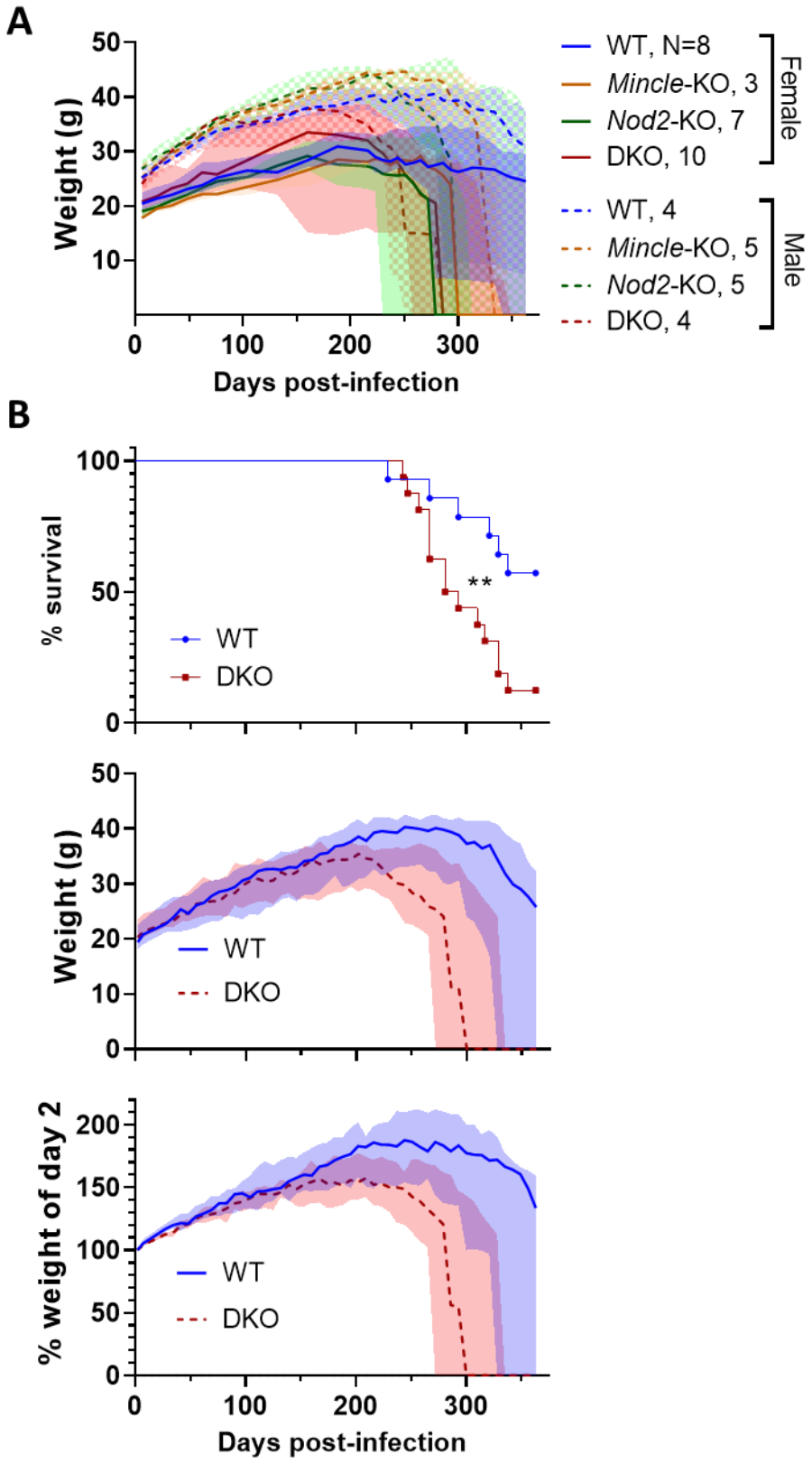
A
Weight (g)
50
40
30
20
10
0
100
200
300
Days post-infection
WT, N=8
Mincle-KO, 3
Nod2-KO, 7
DKO, 10
Female
WT, 4
Mincle-KO, 5
Nod2-KO, 5
DKO, 4
Male
B
% survival
100
50
0
**
WT
DKO
Weight (g)
50
40
30
20
10
0
WT
DKO
% weight of day 2
200
150
100
50
0
WT
DKO
0
100
200
300
Days post-infection

Chapter III, Figure S3. Quantitation of extrapulmonary bacterial burdens and pulmonary pathology associated with death in *Mtb*-infected *Mincle* and *Nod2* deficient mice.

A, C, spleen and liver *Mtb* CFUs per gram of organ harvested upon endpoint euthanasia from survival challenge in fig. 3. **B, D**, spleen and liver *Mtb* CFUs per gram of organ harvested upon endpoint euthanasia from survival challenge in fig. S2B. Linear regressions of bacterial burden over time of euthanasia were calculated per group to highlight slope lines' deviation from zero (left graph of panels). Assuming the date of euthanasia is not confounding, groups were compared by Welch's ANOVA (A and C) or Welch's t-test (B and D); ns, $p > 0.05$; *$p < 0.05$ (right graph of panels). Shown are averages of N = 7 to 14 mice per group; mice are represented by individual points on the graphs. **E**, Number of lesions containing dead cells per area of lung plotted with medians. Kruskal-Wallis test was used determine statistical significance; ns, $p > 0.05$. **F**, percentage of lung space containing dead cells plotted over time per group with linear regressions. No slopes were significantly non-zero. **G**, Example of Python code processing used to quantify tissue (red), nuclei (blue) and alveolar airspace (white); details in Methods. **H, J**, alveolar airspace and nuclei in lung sections harvested upon endpoint euthanasia from survival challenge in fig. 3. **I, K**, alveolar airspace and nuclei in lung sections harvested upon endpoint euthanasia from survival challenge in fig. S2B. Linear regressions of indicated variable over time of euthanasia were calculated per group to highlight slope lines' deviation from zero (left graph of panels). Assuming the date of euthanasia is not confounding, groups were compared by Welch's ANOVA (A and C) or Welch's t-test (B and D); ns, $p > 0.05$; *$p < 0.05$ (right graph of panels). Shown are averages of N = 7 to 14 mice per group; mice are represented by individual points on the graphs.

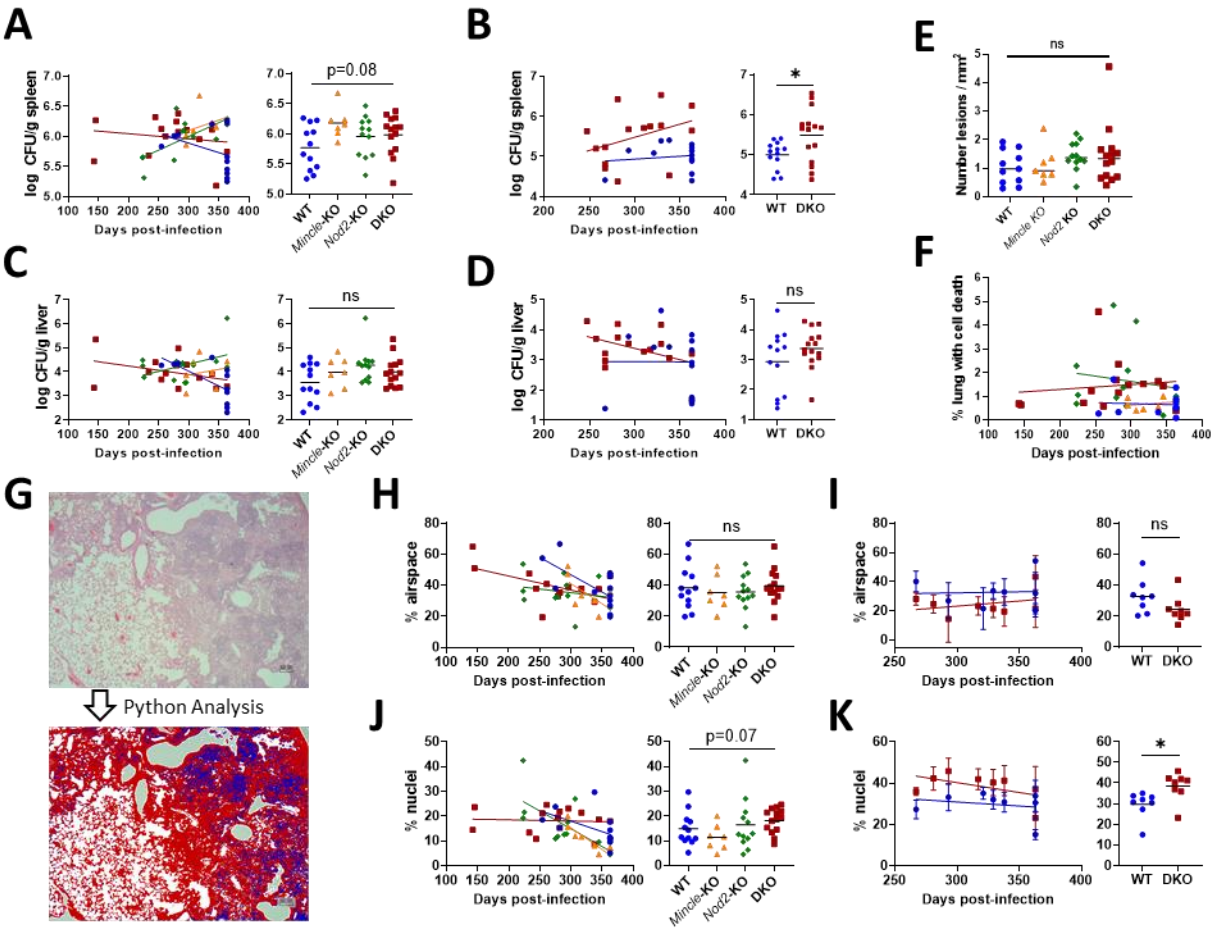
A
log CFU/g spleen
Days post-infection
p=0.08
WT
Mincle-KO
Nod2-KO
DKO
B
log CFU/g spleen
Days post-infection
*
WT
DKO
E
Number lesions / mm²
ns
WT
Mincle KO
Nod2 KO
DKO
C
log CFU/g liver
Days post-infection
ns
D
log CFU/g liver
Days post-infection
ns
F
% lung with cell death
Days post-infection
G
Python Analysis
H
% airspace
Days post-infection
ns
I
% airspace
Days post-infection
ns
J
% nuclei
Days post-infection
p=0.07
K
% nuclei
Days post-infection
*

Chapter III, Figure S4. Bacterial control and immunity during *Map* infection in *Mincle* and *Nod2* deficient mice.

A, Total Map burden per spleen of infected mice. Complementary data to that in fig, 5B. Kruskal-Wallis test was performed at each timepoint; ns, not significant ($p > 0.05$). **B**, Flow cytometry enumeration of total numbers of splenic $CD8^+$ T cells ($CD11b^-CD19^-CD3\varepsilon^+$ $CD4^-$ $CD8\alpha^+$) expressing IFN-γ after incubation with soluble *Map* lysate or equivalent volume of PBS, from mice infected with *Map* three weeks prior. **C**, PBS controls for data in fig. 6F. No cytokine positive cells were found where points are plotted on top of the x axis (at 10 cells per spleen). Shown are medians of N = 5 to 7 mice per group; mice are represented by individual points on the graphs. **D**, gating strategy to identify cytokine positive $CD4^+$ T cells ($CD11b^-CD19^-$ $CD3\varepsilon^+CD44^+CD4^+CD8\alpha^-$), generated with representative samples. *Map* lysate treatment is shown with red histograms and PBS control is shown with blue histograms.

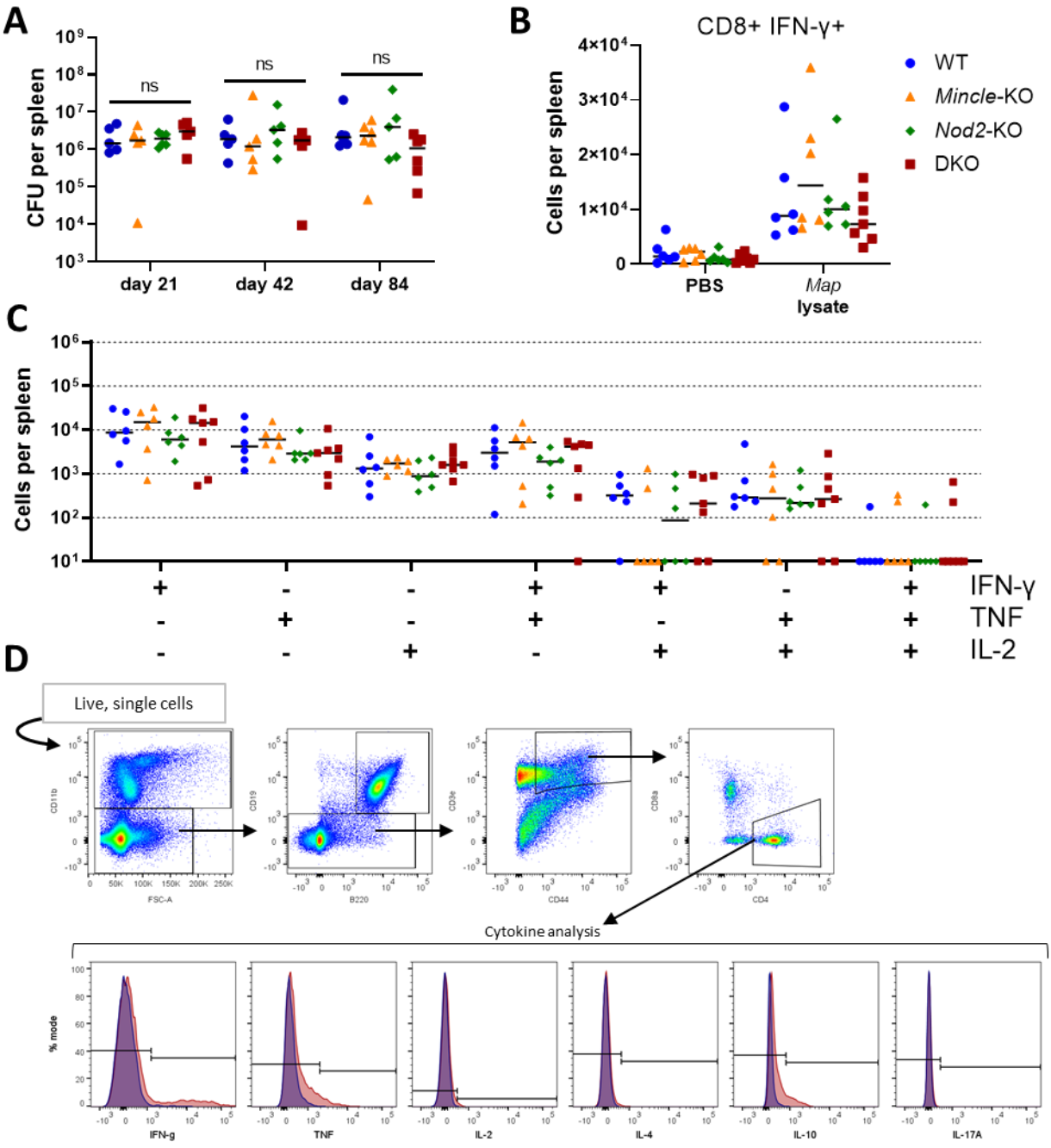
A
CFU per spleen
ns
ns
ns
day 21
day 42
day 84
B
CD8+ IFN-γ+
Cells per spleen
WT
Mincle-KO
Nod2-KO
DKO
PBS
Map lysate
C
Cells per spleen
IFN-γ
TNF
IL-2
D
Live, single cells
Cytokine analysis
% mode
IFN-g
TNF
IL-2
IL-4
IL-10
IL-17A

CHAPTER IV – DISCUSSION

We studied the importance of the NOD2 and Mincle pathways to the mycobacteria-host interaction using models of immunity and infection. In my first study, NOD2 and Mincle were essential for the immune response elicited by the mycobacteria in CFA, and ligands of these PRRs, when combined, were sufficient to partially recreate the adjuvant effect by direct measures of T-cell activity as well as EAE. With this insight into the importance of these PRR pathways and their cooperation in mycobacterial immunity, we sought to examine their roles more closely during live mycobacterial infection in the second study. There, we observed that deficiency in NOD2 and Mincle, even together, had but a modest effect on bacterial control in the presence of altered immunity. Nevertheless, NOD2 deficiency resulted in premature death from *Mtb* associated with distinct pulmonary necrosis.

As reviewed in Chapter I, many PRR KOs have produced significant immunophenotypes with little or no change in survival and bacterial burden [484]. This conclusion is consistent with the results of our infections of NOD2- and Mincle-deficient animals. As studies on PRRs continue, the immunological phenotypes specific to different PRR pathways during mycobacterial infection should be defined and compared to assist our understanding of the mycobacterial immune response and correlates of protection. As exists for *M. leprae*, endophenotypes based on the inflammatory state of the host should be defined for *Mtb*, tested for associations with PRR polymorphisms and mechanistically explored in animal models.

That *NOD2* SNPs have currently been strongly associated with *M. leprae*, of all mycobacteria, is a curious development: *namH* is a non-functional pseudogene and there is no *N*-

glycolylation of PGN in *M. leprae* [106,110]. Although it has not yet been tested, *M. leprae* would be expected to signal less strongly through NOD2 as has been shown with *namH*-mutant *M. smegmatis* and *Mtb* [108,109]. All known *M. leprae*-associated *NOD2* SNPs are non-coding or synonymous [284,388-391], so their function is unclear but possibly related to the expression level of NOD2, in which case the system may be more vulnerable to a weaker (*N*-acetyl) MDP ligand. In our adjuvant studies, we did not see a role for NOD2 outside of MDP sensing: the responses to IFA and GlcC14C18 were *Nod2*-independent, while MDP responses were fully *Nod2*-dependent. Other groups have proposed NOD2 possesses functions beyond MDP sensing (e.g. cellular stress [499]), which may contribute to a SNP-associated phenotype. We cannot determine whether MDP-independent functions of NOD2 contributed to the phenotypes presented in our infection studies in Chapter III. We sought to simulate NOD2 loss-of-function during *Mtb* infection using murine *Nod2*-KO alleles, which we accomplished.

We demonstrated that NOD2 signalling promotes CMI in Chapter II. Favouring humoral immunity (i.e. a change in Th1/Th2 balance) is associated with multibacillary leprosy, which is more contagious [27]. NOD2 polymorphisms were more strongly associated with multibacillary than paucibacillary infection, and with type II (antibody-mediated) than type I (DTH) lepra reactions [284,388]. Therefore, weakened NOD2 signalling, and thus weakened CMI, seems to favour *M. leprae* transmission. This contrasts with *Mtb*, which is more transmissible in those with cavitary disease which requires CMI [72,83]. This differential requirement of CMI for transmission may explain the evolutionary decay of *namH* in *M. leprae* (and *M. lepromatosis*) in contrast to *Mtb*.

The importance of NOD2 during NTM infection in humans has not been established. A few case reports have been published on *NOD2* mutations in patients with *M. abscessus* or MAC

infection [500], but controlled genetic studies associating *NOD2* with these bacteria have not been performed. In mice, absence of *Nod2* during *M. abscessus* infection resulted in higher bacterial burden during clearance (up to 10-fold more in KO), worse pulmonary histopathology and reduced cytokine production compared to WT [501]. These results are comparable with both *Mtb* and *Map* data in Chapter III. Macrophage experiments have shown that NOD2 is important for the recognition of a range of bacteria with NamH, from *Map* and *M. smegmatis* to *Nocardia asteroides* and *Rhodococcus equi*, where NOD2 signalling was almost nil with *M. smegmatis namH* knockout in the same study [108]. Supporting the role for the NamH-NOD2 axis in immune responses, Jules Freund himself tested *N. asteroides* in place of *Mtb* during the development of CFA to successfully sensitize animals to foreign and self antigens [502].

NamH is a non-essential modifier of PGN. Its modification of the MDP motif may be regulated, and this regulation may be connected to pathogenesis in *Mtb*. The requirement for molecular oxygen for NamH-mediated *N*-glycolylation [106,107] is interesting , as *Mtb* experiences different concentrations of O_2 in different zones of pulmonary lesions [81]. Indeed, *Mtb* cultured *in vitro* under hypoxic conditions for weeks upregulates *namH* (*Rv3818*) expression upon returning to an O_2-replete growth environment [503]. *Mtb* performs immune invasion but also elicits CMI in the course of its lifecycle, and therefore understanding the regulation and timing of *namH* expression my be informative about the role of NOD2 sensing during *Mtb* infection.

Like *N*-glycolylated PGN, TDM is present in many mycobacteria, while various trehalose lipids (which are also Mincle agonists) are present in *Corynebacterium*, *Nocardia* and *Rhodococcus* spp. [427,428]. Therefore, Mincle is likely involved in the immune response to these various actinobacteria. However, Mincle offered little resistance to infection in our studies of disparate mycobacteria, despite its importance for adjuvancy. Thus, Mincle sensing of trehalose

lipids may not be a critical factor in host resistance during actinobacterial infections. This difference in importance is perhaps reflected in the current paucity of literature on Mincle in comparison to NOD2 at the level of human genetic studies, where a larger genetic effect is easier to detect statistically. It is rather paradoxical that the receptor for this abundant glycolipid famed for its distinct immunologic effects has failed to demonstrate a significant role in survival or bacterial control. A recent study using single-cell RNA seq demonstrated that Mincle expression is uneven across subsets of murine pulmonary interstitial and alveolar macrophages during *Mtb* infection. Expression was greater in cells with a proinflammatory phenotype, expected to be competent killers of *Mtb*, which suggests *Mtb* killing would occur without Mincle if Mincle is unnecessary for their existence and effector functions. Indeed, in the same study analogous proinflammatory AMs were already present in uninfected humans. NOD2 expression was not reported in the study [504].

We have studied *Mtb* infection as a function of Mincle, but did not explore *Mtb* infection as a function of TDM *per se*. Delipidation of *Mtb* with petroleum ether, which primarily extracts TDM without significantly reducing viability, promotes macrophage migration, lysosome targeting and killing of the bacteria, while simultaneously reducing cytokine responses [417,505,506]. A TDM-poor *Mtb* mutant (lacking mycolyltransferase Ag85a) also had impaired survival in macrophages, associated with increased phagosomal maturation and killing, and was more immunogenic [507]. How much these phenotypes are dependent on Mincle is unknown but could be investigated. Lastly, the extent to which MCL sensing of TDM can promote immunity in the absence of Mincle is not clear but does not appear to be nil [160]. In one study, MCL KO during *Mtb* infection with 100 CFU resulted in 20% mortality in the first few weeks following infection while WT all survived, but no further mortality occurred until the end of the experiment at 10

weeks [224]. This may be a result of delayed adaptive immunity failing to catch up to and control a high bacterial inoculum.

Mtb infection as a function of MDP has been previously explored: KO of *namH* did not result in a significant difference in survival in immunocompetent mice, but *Rag1*-KO mice survived 40% (2 weeks) longer with the *namH* mutant than with WT *Mtb* [109]. Therefore, in the absence of CMI (T cells), increased NOD2 sensing of *Mtb* was harmful, possibly through immunopathology not examined in the study. The *namH* mutant was not attenuated for growth *in vitro* nor *in vivo* and was not associated in altered immunity at three weeks post infection of immunocompetent mice [109]. Incorporated into CFA, we showed that the same *namH* mutant was defective in producing antigen-specific IFN-γ-producing T cells at one week post immunization. A *namH* mutant of *M. smegmatis* produced reduced amounts of Th1 cytokines 14 days after infection upon restimulation with autologous bacteria [108]. In our *Mtb* infections, trends of lymphocyte defects in *Nod2*-KO mice at 3 weeks post infection disappeared by 6 weeks. A previous report showed a reduction in pulmonary lymphocytes at 4 weeks post BCG infection in *Nod2*-KO mice compared to WT [189]. The enhancement of CMI through *Mtb* NamH may only be short-lived since *N*-acetyl MDP (and thus NOD2 signalling) is still present.

In Chapter II, we alluded to the idea that a defined cocktail of synthetic MAMPs could copy or improve upon mycobacterial reagents. Our work focused on CFA, while BCG is the most common mycobacterial product used in medicine. We demonstrated the sufficiency of a multi-MAMP adjuvant to generate antigen-specific CMI, and thus expect that a similar synthetic adjuvant could recapitulate this activity of BCG (after careful antigen selection [96]). Recent work has suggested that part of the utility of BCG is in its capacity to generate trained innate immunity [297,304]. NOD2 has been identified to promote this response with BCG [297], but no similar reports

exist for Mincle. However, fungal cell wall β-glucan is a well-defined inducer of trained innate immunity. The CLR Dectin-1 senses β-glucan [508,509], and thus by analogy a CLR like Mincle may be able to generate similar immune responses with TDM [510]. Mincle and Dectin-1 signalling differ at least in that Dectin-1 has its own cytoplasmic ITAM while Mincle requires the ITAM of FcRγ, but both CLRs subsequently signal to the SYK-CARD9 pathway [438].

BCG is a safe, well-studied, century-old vaccine. Any BCG replacement would have to exceed the protective effect of BCG, not just demonstrate non-inferiority. A novel genetically engineered BCG vaccine for TB is attempting to do that [94]. While NOD2 and Mincle offered modest resistance to *Mtb* infection in our experiments, the immunotherapeutic capacity through targeting these receptors during *Mtb* infection was not tested. Unlike BCG, *Mtb* antagonizes trained innate immunity using RD-1[305], and thus experiments targeting NOD2 and Mincle positively in *Mtb* infection should be done. Besides TB, a mycobacterial MAMP cocktail may apply to the treatment of bladder cancer analogous to BCG. Assuming the utility of mycobacterial therapies are largely determined by MAMPs, *Mip* can also be compared against a MAMP adjuvant where applicable (e.g. leprosy adjunctive therapy). Future studies should investigate the potential of NOD2 plus CLR/Mincle signalling together in the induction of trained innate immunity, especially as we have shown the potential for synergy.

Final Conclusions

Through my investigations, we know that mycobacterial adjuvancy can be recapitulated synthetically using combinations of MAMPs inspired by PRR pathways essential to the immune mycobacterial response. Interestingly, while NOD2 and Mincle are important in the process of mycobacteria-stimulated CMI, these PRRs serve subtle, unequal purposes during *Mtb* infection. I have demonstrated that NOD2 is necessary to prevent premature TB death associated with increased pulmonary necrosis, the precise mechanism of which will need further study. The results of my work indicate that the NOD2 and Mincle pathways can be exploited together in immunotherapeutic reagents, while uncovering the precise roles of these PRRs in disease will require a greater exploration of the pathological phenomena associated with PRR dysfunction.

BIBLIOGRAPHY

1 DeLeo, F. R. & Hinnebusch, B. J. A plague upon the phagocytes. *Nat. Med.* **11**, 927-928, doi:10.1038/nm0905-927 (2005).

2 Henderson, D. A. The eradication of smallpox--an overview of the past, present, and future. *Vaccine* **29 Suppl 4**, D7-9, doi:10.1016/j.vaccine.2011.06.080 (2011).

3 Riedel, S. Edward Jenner and the history of smallpox and vaccination. *Proc. (Bayl. Univ. Med. Cent.)* **18**, 21-25, doi:10.1080/08998280.2005.11928028 (2005).

4 Spreeuwenberg, P., Kroneman, M. & Paget, J. Reassessing the Global Mortality Burden of the 1918 Influenza Pandemic. *Am. J. Epidemiol.* **187**, 2561-2567, doi:10.1093/aje/kwy191 (2018).

5 Vincent, A. T. *et al.* The Mycobacterial Cell Envelope: A Relict From the Past or the Result of Recent Evolution? *Frontiers in Microbiology* **9**, doi:10.3389/fmicb.2018.02341 (2018).

6 Lehmann, K. B. & Neumann, R. Atlas und Grundriss der Bakteriologie und Lehrbuch der speziellen bakteriologischen Diagnostik. (1896).

7 Koch, R. Die Aetiologie der Tuberculose. *Berliner Klinische Wochenschrift* **15**, 287-296, doi:10.1016/s0174-3031(82)80099-1 (1882).

8 Supply, P. *et al.* Genomic analysis of smooth tubercle bacilli provides insights into ancestry and pathoadaptation of *Mycobacterium tuberculosis*. *Nat. Genet.* **45**, 172-179, doi:10.1038/ng.2517 (2013).

9 Dulberger, C. L., Rubin, E. J. & Boutte, C. C. The mycobacterial cell envelope — a moving target. *Nature Reviews Microbiology* **18**, 47-59, doi:10.1038/s41579-019-0273-7 (2020).

10 Willey, J. M., Sherwood, L., Woolverton, C. J. & Prescott, L. M. *Prescott's microbiology*. 8th ed. edn, 37 (McGraw-Hill, 2011).

11 Kalscheuer, R. *et al.* The *Mycobacterium tuberculosis* capsule: a cell structure with key implications in pathogenesis. *Biochem. J.* **476**, 1995-2016, doi:10.1042/bcj20190324 (2019).

12 Lemassu, A. *et al.* Extracellular and surface-exposed polysaccharides of non-tuberculous mycobacteria. *Microbiology (Reading)* **142 (Pt 6)**, 1513-1520, doi:10.1099/13500872-142-6-1513 (1996).

13 Fraenkel, A. R. Koch, Ueber Tuberculose. *Dtsch. Med. Wochenschr.* **15**, 210-211 (1882).

14 Sakula, A. Robert Koch: centenary of the discovery of the tubercle bacillus, 1882. *Thorax* **37**, 246-251, doi:10.1136/thx.37.4.246 (1982).

15 Garnier, T. *et al.* The complete genome sequence of *Mycobacterium bovis*. *Proc. Natl. Acad. Sci. U. S. A.* **100**, 7877-7882, doi:10.1073/pnas.1130426100 (2003).

16 Cá, B. *et al.* Experimental Evidence for Limited *in vivo* Virulence of *Mycobacterium africanum*. *Front Microbiol* **10**, 2102, doi:10.3389/fmicb.2019.02102 (2019).

17 de Jong, B. C. *et al.* Differences between tuberculosis cases infected with *Mycobacterium africanum*, West African type 2, relative to Euro-American *Mycobacterium tuberculosis*: an update. *FEMS Immunol. Med. Microbiol.* **58**, 102-105, doi:10.1111/j.1574-695X.2009.00628.x (2010).

18 Ngabonziza, J. C. S. *et al.* A sister lineage of the *Mycobacterium tuberculosis* complex discovered in the African Great Lakes region. *Nature Communications* **11**, 2917, doi:10.1038/s41467-020-16626-6 (2020).

19 Coscolla, M. *et al.* Phylogenomics of *Mycobacterium africanum* reveals a new lineage and a complex evolutionary history. *Microb Genom* **7**, doi:10.1099/mgen.0.000477 (2021).

20 Bottai, D. *et al.* TbD1 deletion as a driver of the evolutionary success of modern epidemic *Mycobacterium tuberculosis* lineages. *Nature Communications* **11**, 684, doi:10.1038/s41467-020-14508-5 (2020).

21 Cole, S. T. *et al.* Deciphering the biology of *Mycobacterium tuberculosis* from the complete genome sequence. *Nature* **393**, 537-544, doi:10.1038/31159 (1998).

22 Steenken, W., Oatway, W. H. & Petroff, S. A. BIOLOGICAL STUDIES OF THE TUBERCLE BACILLUS : III. DISSOCIATION AND PATHOGENICITY OF THE R AND S VARIANTS OF THE HUMAN TUBERCLE BACILLUS (H(37)). *J. Exp. Med.* **60**, 515-540, doi:10.1084/jem.60.4.515 (1934).

23 Calmette, A. Preventive Vaccination Against Tuberculosis with BCG. *Proc. R. Soc. Med.* **24**, 1481-1490 (1931).

24 van Ingen, J. *et al.* Characterization of *Mycobacterium orygis* as *M. tuberculosis* complex subspecies. *Emerg. Infect. Dis.* **18**, 653-655, doi:10.3201/eid1804.110888 (2012).

25 Duffy, S. C. *et al.* Reconsidering *Mycobacterium bovis* as a proxy for zoonotic tuberculosis: a molecular epidemiological surveillance study. *Lancet Microbe* **1**, e66-e73, doi:10.1016/s2666-5247(20)30038-0 (2020).

26 Franco-Paredes, C. *et al.* Cutaneous Mycobacterial Infections. *Clin. Microbiol. Rev.* **32**, doi:10.1128/cmr.00069-18 (2018).

27 Khadilkar, S. V., Patil, S. B. & Shetty, V. P. Neuropathies of leprosy. *J. Neurol. Sci.* **420**, 117288, doi:10.1016/j.jns.2020.117288 (2021).

28 Fava, V. M. *et al.* A genome wide association study identifies a lncRna as risk factor for pathological inflammatory responses in leprosy. *PLoS Genet* **13**, e1006637, doi:10.1371/journal.pgen.1006637 (2017).

29 Schuenemann, V. J. *et al.* Genome-wide comparison of medieval and modern *Mycobacterium leprae*. *Science* **341**, 179-183, doi:10.1126/science.1238286 (2013).

30 Krause-Kyora, B. *et al.* Ancient DNA study reveals HLA susceptibility locus for leprosy in medieval Europeans. *Nature Communications* **9**, 1569, doi:10.1038/s41467-018-03857-x (2018).

31 Cole, S. T. *et al.* Massive gene decay in the leprosy bacillus. *Nature* **409**, 1007-1011, doi:10.1038/35059006 (2001).

32 Truman, R. W. *et al.* Probable Zoonotic Leprosy in the Southern United States. *N. Engl. J. Med.* **364**, 1626-1633, doi:10.1056/NEJMoa1010536 (2011).

33 Han, X. Y. *et al.* A new *Mycobacterium* species causing diffuse lepromatous leprosy. *Am. J. Clin. Pathol.* **130**, 856-864, doi:10.1309/ajcpp72fjzzrrvmm (2008).

34 Avanzi, C. *et al.* Red squirrels in the British Isles are infected with leprosy bacilli. *Science* **354**, 744-747, doi:10.1126/science.aah3783 (2016).

35 Schilling, A.-K. *et al.* British Red Squirrels Remain the Only Known Wild Rodent Host for Leprosy Bacilli. *Frontiers in Veterinary Science* **6**, doi:10.3389/fvets.2019.00008 (2019).

36 Veyrier, F., Pletzer, D., Turenne, C. & Behr, M. A. Phylogenetic detection of horizontal gene transfer during the step-wise genesis of *Mycobacterium tuberculosis*. *BMC Evol. Biol.* **9**, 196, doi:10.1186/1471-2148-9-196 (2009).

37 Buhler, V. B. & Pollak, A. Human infection with atypical acid-fast organisms; report of two cases with pathologic findings. *Am. J. Clin. Pathol.* **23**, 363-374, doi:10.1093/ajcp/23.4.363 (1953).

38 Hanks, J. H. *et al. Mycobacterium Kansasii* Hauduroy Subcommittee on Mycobacteria, American Society for Microbiology. *J. Bacteriol.* **83**, 931-932, doi:10.1128/jb.83.4.931-932.1962 (1962).

39 Ghanem, M. *et al.* Heterologous Production of 1-Tuberculosinyladenosine in *Mycobacterium kansasii* Models Pathoevolution towards the Transcellular Lifestyle of *Mycobacterium tuberculosis*. *mBio* **11**, e02645-02620, doi:10.1128/mBio.02645-20 (2020).

40 Luo, T. *et al.* Population genomics provides insights into the evolution and adaptation to humans of the waterborne pathogen *Mycobacterium kansasii*. *Nat Commun* **12**, 2491, doi:10.1038/s41467-021-22760-6 (2021).

41 Aronson, J. D. Spontaneous Tuberculosis in Salt Water Fish. *The Journal of Infectious Diseases* **39**, 315-320 (1926).

42 Aubry, A., Chosidow, O., Caumes, E., Robert, J. & Cambau, E. Sixty-three Cases of *Mycobacterium marinum* Infection: Clinical Features, Treatment, and Antibiotic Susceptibility of Causative Isolates. *Arch. Intern. Med.* **162**, 1746-1752, doi:10.1001/archinte.162.15.1746 (2002).

43 Ramakrishnan, L. Revisiting the role of the granuloma in tuberculosis. *Nature Reviews Immunology* **12**, 352-366, doi:10.1038/nri3211 (2012).

44 Conrad, W. H. *et al.* Mycobacterial ESX-1 secretion system mediates host cell lysis through bacterium contact-dependent gross membrane disruptions. *Proceedings of the National Academy of Sciences* **114**, 1371-1376, doi:10.1073/pnas.1620133114 (2017).

45 Zingue, D., Panda, A. & Drancourt, M. A protocol for culturing environmental strains of the Buruli ulcer agent, *Mycobacterium ulcerans*. *Sci. Rep.* **8**, 6778, doi:10.1038/s41598-018-25278-y (2018).

46 van der Werf, T. S., Stinear, T., Stienstra, Y., van der Graaf, W. T. & Small, P. L. Mycolactones and *Mycobacterium ulcerans* disease. *Lancet* **362**, 1062-1064, doi:10.1016/s0140-6736(03)14417-0 (2003).

47 Turenne, C. Y., Wallace, R., Jr. & Behr, M. A. *Mycobacterium avium* in the postgenomic era. *Clin. Microbiol. Rev.* **20**, 205-229, doi:10.1128/cmr.00036-06 (2007).

48 Marochi-Telles, J. P., Muniz, R., Jr., Sztajnbok, J. & Cosme-de Oliveira, A. Disseminated *Mycobacterium avium* on HIV/AIDS: Historical and Current Literature Review. *AIDS Rev* **22**, 9-15, doi:10.24875/AIDSRev.20000104 (2020).

49 Diel, R., Lipman, M. & Hoefsloot, W. High mortality in patients with *Mycobacterium avium* complex lung disease: a systematic review. *BMC Infect. Dis.* **18**, 206, doi:10.1186/s12879-018-3113-x (2018).

50 Twort, F. W. & Ingram, G. L. Y. A Method for Isolating and Cultivating the *Mycobacterium enteritidis chronicae pseudotuberculosae bovi*s, Johne, and some Experiments on the Preparation of a Diagnostic Vaccine for Pseudo-tuberculous Enteritis

of Bovines. *Proceedings of the Royal Society of London. Series B, Containing Papers of a Biological Character* **84**, 517-542 (1912).

51 Gill, C. O., Saucier, L. & Meadus, W. J. *Mycobacterium avium* subsp. *paratuberculosis* in dairy products, meat, and drinking water. *J. Food Prot.* **74**, 480-499, doi:10.4315/0362-028x.Jfp-10-301 (2011).

52 Dalziel, T. K. Chronic Interstitial Enteritis. *The British Medical Journal* **2**, 1068-1070 (1913).

53 Crohn, B. B., Ginzburg, L. & Oppenheimer, G. D. REGIONAL ILEITIS: A PATHOLOGIC AND CLINICAL ENTITY. *J. Am. Med. Assoc.* **99**, 1323-1329, doi:10.1001/jama.1932.02740680019005 (1932).

54 Vinh, D. C. & Behr, M. A. Crohn's as an immune deficiency: from apparent paradox to evolving paradigm. *Expert Rev. Clin. Immunol.* **9**, 17-30, doi:10.1586/eci.12.87 (2013).

55 Talwar, G. P. Towards development of a vaccine against leprosy. Introduction. *Lepr. India* **50**, 492-497 (1978).

56 Saini, V. *et al.* Polyphasic Taxonomic Analysis Establishes *Mycobacterium indicus pranii* as a Distinct Species. *PLoS One* **4**, e6263, doi:10.1371/journal.pone.0006263 (2009).

57 Tortoli, E. *et al.* Emended description of *Mycobacterium abscessus*, *Mycobacterium abscessus* subsp. *abscessus* and *Mycobacterium abscessus* subsp. *bolletii* and designation of *Mycobacterium abscessus* subsp. *massiliense* comb. nov. *Int J Syst Evol Microbiol* **66**, 4471-4479, doi:10.1099/ijsem.0.001376 (2016).

58 Victoria, L., Gupta, A., Gómez, J. L. & Robledo, J. *Mycobacterium abscessus* complex: A Review of Recent Developments in an Emerging Pathogen. *Frontiers in Cellular and Infection Microbiology* **11**, doi:10.3389/fcimb.2021.659997 (2021).

59 Alvarez & Tavel. Recherches sur le bacille de Lustgarten. *Archives de physiologie normale et pathologique 6*, 303-321 (1885).

60 Hippocrates & Adams, F. e. The genuine works of Hippocrates. *London: The Sydenham Society*, 353-355 (1849).

61 Herodotus, De Sélincourt, A. & Marincola, J. *The Histories*. Further revised edn, 444 (Penguin Books, 2003).

62 Hershkovitz, I. *et al.* Detection and molecular characterization of 9,000-year-old *Mycobacterium tuberculosis* from a Neolithic settlement in the Eastern Mediterranean. *PLoS One* **3**, e3426, doi:10.1371/journal.pone.0003426 (2008).

63 Nerlich, A. G., Haas, C. J., Zink, A., Szeimies, U. & Hagedorn, H. G. Molecular evidence for tuberculosis in an ancient Egyptian mummy. *The Lancet* **350**, 1404, doi:10.1016/S0140-6736(05)65185-9 (1997).

64 Salo, W. L., Aufderheide, A. C., Buikstra, J. & Holcomb, T. A. Identification of *Mycobacterium tuberculosis* DNA in a pre-Columbian Peruvian mummy. *Proc. Natl. Acad. Sci. U. S. A.* **91**, 2091-2094, doi:10.1073/pnas.91.6.2091 (1994).

65 Menardo, F., Duchêne, S., Brites, D. & Gagneux, S. The molecular clock of *Mycobacterium tuberculosis*. *PLoS Pathog.* **15**, e1008067, doi:10.1371/journal.ppat.1008067 (2019).

66 Bos, K. I. *et al.* Pre-Columbian mycobacterial genomes reveal seals as a source of New World human tuberculosis. *Nature* **514**, 494-497, doi:10.1038/nature13591 (2014).

67 Behr, M. A., Edelstein, P. H. & Ramakrishnan, L. Revisiting the timetable of tuberculosis. *BMJ* **362**, k2738, doi:10.1136/bmj.k2738 (2018).

68 Lillebaek, T. *et al.* Molecular evidence of endogenous reactivation of *Mycobacterium tuberculosis* after 33 years of latent infection. *J. Infect. Dis.* **185**, 401-404, doi:10.1086/338342 (2002).

69 Lillebaek, T. *et al.* Substantial molecular evolution and mutation rates in prolonged latent *Mycobacterium tuberculosis* infection in humans. *Int. J. Med. Microbiol.* **306**, 580-585, doi:10.1016/j.ijmm.2016.05.017 (2016).

70 Khanna, K. & Sabharwal, S. Spinal tuberculosis: a comprehensive review for the modern spine surgeon. *Spine J* **19**, 1858-1870, doi:10.1016/j.spinee.2019.05.002 (2019).

71 Grzybowski, S. & Allen, E. A. History and importance of scrofula. *The Lancet* **346**, 1472-1474, doi:https://doi.org/10.1016/S0140-6736(95)92478-7 (1995).

72 Drobniewski, F. A., Pozniak, A. L. & Uttley, A. H. Tuberculosis and AIDS. *J. Med. Microbiol.* **43**, 85-91, doi:10.1099/00222615-43-2-85 (1995).

73 Geremew, D. *et al.* Tuberculosis and its association with CD4+ T cell count among adult HIV positive patients in Ethiopian settings: a systematic review and meta-analysis. *BMC Infect. Dis.* **20**, 325, doi:10.1186/s12879-020-05040-4 (2020).

74 Cohen, S. B. *et al.* Alveolar Macrophages Provide an Early *Mycobacterium tuberculosis* Niche and Initiate Dissemination. *Cell Host Microbe* **24**, 439-446.e434, doi:10.1016/j.chom.2018.08.001 (2018).

75 Plumlee, C. R. *et al.* Ultra-low Dose Aerosol Infection of Mice with *Mycobacterium tuberculosis* More Closely Models Human Tuberculosis. *Cell Host Microbe* **29**, 68-82.e65, doi:10.1016/j.chom.2020.10.003 (2021).

76 Lin, P. L. *et al.* Sterilization of granulomas is common in active and latent tuberculosis despite within-host variability in bacterial killing. *Nat. Med.* **20**, 75-79, doi:10.1038/nm.3412 (2014).

77 Wolf, A. J. *et al. Mycobacterium tuberculosis* infects dendritic cells with high frequency and impairs their function in vivo. *J. Immunol.* **179**, 2509-2519, doi:10.4049/jimmunol.179.4.2509 (2007).

78 Behr, M. A. & Waters, W. R. Is tuberculosis a lymphatic disease with a pulmonary portal? *The Lancet Infectious Diseases* **14**, 250-255, doi:10.1016/s1473-3099(13)70253-6 (2014).

79 Lozza, L. *et al.* Communication between Human Dendritic Cell Subsets in Tuberculosis: Requirements for Naive CD4+ T Cell Stimulation. *Front. Immunol.* **5**, doi:10.3389/fimmu.2014.00324 (2014).

80 Wolf, A. J. *et al.* Initiation of the adaptive immune response to *Mycobacterium tuberculosis* depends on antigen production in the local lymph node, not the lungs. *J. Exp. Med.* **205**, 105-115, doi:10.1084/jem.20071367 (2008).

81 Sarathy, J. P. & Dartois, V. Caseum: a Niche for *Mycobacterium tuberculosis* Drug-Tolerant Persisters. *Clin. Microbiol. Rev.* **33**, doi:10.1128/cmr.00159-19 (2020).

82 Marakalala, M. J. *et al.* Inflammatory signaling in human tuberculosis granulomas is spatially organized. *Nat. Med.* **22**, 531-538, doi:10.1038/nm.4073 (2016).

83 Ehlers, S. & Schaible, U. E. The granuloma in tuberculosis: dynamics of a host-pathogen collusion. *Front. Immunol.* **3**, 411-411, doi:10.3389/fimmu.2012.00411 (2013).

84 Lenaerts, A., Barry III, C. E. & Dartois, V. Heterogeneity in tuberculosis pathology, microenvironments and therapeutic responses. *Immunol. Rev.* **264**, 288-307, doi:https://doi.org/10.1111/imr.12252 (2015).

85 Driver, E. R. *et al.* Evaluation of a mouse model of necrotic granuloma formation using C3HeB/FeJ mice for testing of drugs against *Mycobacterium tuberculosis*. *Antimicrob. Agents Chemother.* **56**, 3181-3195, doi:10.1128/aac.00217-12 (2012).

86 Yang, H., Kruh-Garcia, N. A. & Dobos, K. M. Purified protein derivatives of tuberculin - past, present, and future. *FEMS Immunol. Med. Microbiol.* **66**, 273-280, doi:10.1111/j.1574-695X.2012.01002.x (2012).

87 Farhat, M., Greenaway, C., Pai, M. & Menzies, D. False-positive tuberculin skin tests: what is the absolute effect of BCG and non-tuberculous mycobacteria? *Int. J. Tuberc. Lung Dis.* **10**, 1192-1204 (2006).

88 Rendon, A. *et al.* Classification of drugs to treat multidrug-resistant tuberculosis (MDR-TB): evidence and perspectives. *J. Thorac. Dis.* **8**, 2666-2671, doi:10.21037/jtd.2016.10.14 (2016).

89 Turner, C. T. *et al.* Blood transcriptional biomarkers for active pulmonary tuberculosis in a high-burden setting: a prospective, observational, diagnostic accuracy study. *Lancet Respir Med* **8**, 407-419, doi:10.1016/s2213-2600(19)30469-2 (2020).

90 Gupta, R. K. *et al.* Concise whole blood transcriptional signatures for incipient tuberculosis: a systematic review and patient-level pooled meta-analysis. *Lancet Respir Med* **8**, 395-406, doi:10.1016/s2213-2600(19)30282-6 (2020).

91 McShane, H. *et al.* BCG: myths, realities, and the need for alternative vaccine strategies. *Tuberculosis (Edinb)* **92**, 283-288, doi:10.1016/j.tube.2011.12.003 (2012).

92 Tameris, M. D. *et al.* Safety and efficacy of MVA85A, a new tuberculosis vaccine, in infants previously vaccinated with BCG: a randomised, placebo-controlled phase 2b trial. *The Lancet* **381**, 1021-1028, doi:https://doi.org/10.1016/S0140-6736(13)60177-4 (2013).

93 Tait, D. R. *et al.* Final Analysis of a Trial of M72/AS01E Vaccine to Prevent Tuberculosis. *N. Engl. J. Med.* **381**, 2429-2439, doi:10.1056/NEJMoa1909953 (2019).

94 Loxton, A. G. *et al.* Safety and Immunogenicity of the Recombinant *Mycobacterium bovis* BCG Vaccine VPM1002 in HIV-Unexposed Newborn Infants in South Africa. *Clin. Vaccine Immunol.* **24**, doi:10.1128/cvi.00439-16 (2017).

95 Krug, S., Parveen, S. & Bishai, W. R. Host-Directed Therapies: Modulating Inflammation to Treat Tuberculosis. *Front. Immunol.* **12**, 660916, doi:10.3389/fimmu.2021.660916 (2021).

96 Clemmensen, H. S. *et al. In Vivo* Antigen Expression Regulates CD4 T Cell Differentiation and Vaccine Efficacy against *Mycobacterium tuberculosis* Infection. *mBio* **12**, e00226-00221, doi:10.1128/mBio.00226-21 (2021).

97 Pandey, A. K. *et al.* NOD2, RIP2 and IRF5 play a critical role in the type I interferon response to *Mycobacterium tuberculosis*. *PLoS Pathog.* **5**, e1000500, doi:10.1371/journal.ppat.1000500 (2009).

98 Camacho, L. R., Ensergueix, D., Perez, E., Gicquel, B. & Guilhot, C. Identification of a virulence gene cluster of *Mycobacterium tuberculosis* by signature-tagged transposon mutagenesis. *Mol. Microbiol.* **34**, 257-267, doi:10.1046/j.1365-2958.1999.01593.x (1999).

99 Cox, J. S., Chen, B., McNeil, M. & Jacobs, W. R., Jr. Complex lipid determines tissue-specific replication of *Mycobacterium tuberculosis* in mice. *Nature* **402**, 79-83, doi:10.1038/47042 (1999).

100 Cambier, C. J. *et al.* Mycobacteria manipulate macrophage recruitment through coordinated use of membrane lipids. *Nature* **505**, 218-222, doi:10.1038/nature12799 (2014).

101 Quigley, J. *et al.* The Cell Wall Lipid PDIM Contributes to Phagosomal Escape and Host Cell Exit of *Mycobacterium tuberculosis*. *mBio* **8**, e00148-00117, doi:10.1128/mBio.00148-17 (2017).

102 Pethe, K. *et al.* Isolation of *Mycobacterium tuberculosis* mutants defective in the arrest of phagosome maturation. *Proc. Natl. Acad. Sci. U. S. A.* **101**, 13642-13647, doi:10.1073/pnas.0401657101 (2004).

103 Layre, E. *et al.* Molecular profiling of *Mycobacterium tuberculosis* identifies tuberculosinyl nucleoside products of the virulence-associated enzyme Rv3378c. *Proc. Natl. Acad. Sci. U. S. A.* **111**, 2978-2983, doi:10.1073/pnas.1315883111 (2014).

104 Buter, J. *et al. Mycobacterium tuberculosis* releases an antacid that remodels phagosomes. *Nat. Chem. Biol.* **15**, 889-899, doi:10.1038/s41589-019-0336-0 (2019).

105 Ruhl, C. R. *et al. Mycobacterium tuberculosis* Sulfolipid-1 Activates Nociceptive Neurons and Induces Cough. *Cell* **181**, 293-305 e211, doi:10.1016/j.cell.2020.02.026 (2020).

106 Raymond, J. B., Mahapatra, S., Crick, D. C. & Pavelka, M. S., Jr. Identification of the *namH* gene, encoding the hydroxylase responsible for the *N*-glycolylation of the

mycobacterial peptidoglycan. *J. Biol. Chem.* **280**, 326-333, doi:10.1074/jbc.M411006200 (2005).

107 Essers, L. & Schoop, H. J. Evidence for the incorporation of molecular oxygen, a pathway in biosynthesis of *N*-glycolylmuramic acid in *Mycobacterium phlei*. *Biochim. Biophys. Acta* **544**, 180-184 (1978).

108 Coulombe, F. *et al.* Increased NOD2-mediated recognition of *N*-glycolyl muramyl dipeptide. *J. Exp. Med.* **206**, 1709-1716, doi:10.1084/jem.20081779 (2009).

109 Hansen, J. M. *et al. N*-glycolylated peptidoglycan contributes to the immunogenicity but not pathogenicity of *Mycobacterium tuberculosis*. *J. Infect. Dis.* **209**, 1045-1054, doi:10.1093/infdis/jit622 (2014).

110 Mahapatra, S., Crick, D. C., McNeil, M. R. & Brennan, P. J. Unique structural features of the peptidoglycan of *Mycobacterium leprae*. *J. Bacteriol.* **190**, 655-661, doi:10.1128/JB.00982-07 (2008).

111 Houben, R. M. & Dodd, P. J. The Global Burden of Latent Tuberculosis Infection: A Re-estimation Using Mathematical Modelling. *PLoS Med.* **13**, e1002152, doi:10.1371/journal.pmed.1002152 (2016).

112 Gagneux, S. Host-pathogen coevolution in human tuberculosis. *Philos. Trans. R. Soc. Lond. B Biol. Sci.* **367**, 850-859, doi:10.1098/rstb.2011.0316 (2012).

113 Boisson-Dupuis, S. *et al.* Tuberculosis and impaired IL-23-dependent IFN-γ immunity in humans homozygous for a common *TYK2* missense variant. *Sci Immunol* **3**, doi:10.1126/sciimmunol.aau8714 (2018).

114 Kerner, G. *et al.* Human ancient DNA analyses reveal the high burden of tuberculosis in Europeans over the last 2,000 years. *Am. J. Hum. Genet.* **108**, 517-524, doi:10.1016/j.ajhg.2021.02.009 (2021).

115 Kerner, G. *et al.* Homozygosity for TYK2 P1104A underlies tuberculosis in about 1% of patients in a cohort of European ancestry. *Proc. Natl. Acad. Sci. U. S. A.* **116**, 10430-10434, doi:10.1073/pnas.1903561116 (2019).

116 Möller, M. *et al.* Genetic Resistance to *Mycobacterium tuberculosis* Infection and Disease. *Front. Immunol.* **9**, doi:10.3389/fimmu.2018.02219 (2018).

117 Luo, Y. *et al.* Early progression to active tuberculosis is a highly heritable trait driven by 3q23 in Peruvians. *Nat Commun* **10**, 3765, doi:10.1038/s41467-019-11664-1 (2019).

118 Napier, G. *et al.* Robust barcoding and identification of *Mycobacterium tuberculosis* lineages for epidemiological and clinical studies. *Genome Med.* **12**, 114, doi:10.1186/s13073-020-00817-3 (2020).

119 Ernst, J. D. Antigenic Variation and Immune Escape in the MTBC. *Adv. Exp. Med. Biol.* **1019**, 171-190, doi:10.1007/978-3-319-64371-7_9 (2017).

120 Kroon, E. E. *et al.* An observational study identifying highly tuberculosis-exposed, HIV-1-positive but persistently TB, tuberculin and IGRA negative persons with *M. tuberculosis* specific antibodies in Cape Town, South Africa. *EBioMedicine* **61**, 103053, doi:10.1016/j.ebiom.2020.103053 (2020).

121 Joosten, S. A. *et al.* Harnessing donor unrestricted T-cells for new vaccines against tuberculosis. *Vaccine* **37**, 3022-3030, doi:10.1016/j.vaccine.2019.04.050 (2019).

122 Ruibal, P., Voogd, L., Joosten, S. A. & Ottenhoff, T. H. M. The role of donor-unrestricted T-cells, innate lymphoid cells, and NK cells in anti-mycobacterial immunity. *Immunol. Rev.*, doi:10.1111/imr.12948 (2021).

123 Janeway, C. A. Approaching the Asymptote? Evolution and Revolution in Immunology. *Cold Spring Harb. Symp. Quant. Biol.* **54**, 1-13 (1989).

124 Lemaitre, B., Nicolas, E., Michaut, L., Reichhart, J. M. & Hoffmann, J. A. The dorsoventral regulatory gene cassette *spätzle*/*Toll*/*cactus* controls the potent antifungal response in Drosophila adults. *Cell* **86**, 973-983, doi:10.1016/s0092-8674(00)80172-5 (1996).

125 Medzhitov, R., Preston-Hurlburt, P. & Janeway, C. A., Jr. A human homologue of the *Drosophila* Toll protein signals activation of adaptive immunity. *Nature* **388**, 394-397, doi:10.1038/41131 (1997).

126 Poltorak, A. *et al.* Defective LPS signaling in C3H/HeJ and C57BL/10ScCr mice: mutations in *Tlr4* gene. *Science* **282**, 2085-2088, doi:10.1126/science.282.5396.2085 (1998).

127 Qureshi, S. T. *et al.* Endotoxin-tolerant mice have mutations in Toll-like receptor 4 (*Tlr4*). *J. Exp. Med.* **189**, 615-625, doi:10.1084/jem.189.4.615 (1999).

128 Means, T. K. *et al.* The CD14 ligands lipoarabinomannan and lipopolysaccharide differ in their requirement for Toll-like receptors. *J. Immunol.* **163**, 6748-6755 (1999).

129 Means, T. K. *et al.* Human toll-like receptors mediate cellular activation by *Mycobacterium tuberculosis*. *J. Immunol.* **163**, 3920-3927 (1999).

130 Brightbill, H. D. *et al.* Host defense mechanisms triggered by microbial lipoproteins through toll-like receptors. *Science* **285**, 732-736, doi:10.1126/science.285.5428.732 (1999).

131 Jones, B. W. *et al.* Different Toll-like receptor agonists induce distinct macrophage responses. *J. Leukoc. Biol.* **69**, 1036-1044 (2001).

132 Gilleron, M., Quesniaux, V. F. & Puzo, G. Acylation state of the phosphatidylinositol hexamannosides from *Mycobacterium bovis* bacillus Calmette Guerin and *Mycobacterium tuberculosis* H37Rv and its implication in Toll-like receptor response. *J. Biol. Chem.* **278**, 29880-29889, doi:10.1074/jbc.M303446200 (2003).

133 Gehring, A. J., Dobos, K. M., Belisle, J. T., Harding, C. V. & Boom, W. H. *Mycobacterium tuberculosis* LprG (*Rv1411c*): a novel TLR-2 ligand that inhibits human macrophage class II MHC antigen processing. *J. Immunol.* **173**, 2660-2668, doi:10.4049/jimmunol.173.4.2660 (2004).

134 Pecora, N. D., Gehring, A. J., Canaday, D. H., Boom, W. H. & Harding, C. V. *Mycobacterium tuberculosis* LprA is a lipoprotein agonist of TLR2 that regulates innate immunity and APC function. *J. Immunol.* **177**, 422-429, doi:10.4049/jimmunol.177.1.422 (2006).

135 Drage, M. G. *et al.* TLR2 and its co-receptors determine responses of macrophages and dendritic cells to lipoproteins of *Mycobacterium tuberculosis*. *Cell. Immunol.* **258**, 29-37, doi:10.1016/j.cellimm.2009.03.008 (2009).

136 Prados-Rosales, R. *et al.* Mycobacteria release active membrane vesicles that modulate immune responses in a TLR2-dependent manner in mice. *J. Clin. Invest.* **121**, 1471-1483, doi:10.1172/jci44261 (2011).

137 Blanc, L. *et al. Mycobacterium tuberculosis* inhibits human innate immune responses via the production of TLR2 antagonist glycolipids. *Proc. Natl. Acad. Sci. U. S. A.* **114**, 11205-11210, doi:10.1073/pnas.1707840114 (2017).

138 Cehovin, A. *et al.* Comparison of the moonlighting actions of the two highly homologous chaperonin 60 proteins of *Mycobacterium tuberculosis*. *Infect. Immun.* **78**, 3196-3206, doi:10.1128/iai.01379-09 (2010).

139 Bai, W. *et al.* TLR3 regulates mycobacterial RNA-induced IL-10 production through the PI3K/AKT signaling pathway. *Cell. Signal.* **26**, 942-950, doi:10.1016/j.cellsig.2014.01.015 (2014).

140 Keegan, C. *et al.* Mycobacterium tuberculosis Transfer RNA Induces IL-12p70 via Synergistic Activation of Pattern Recognition Receptors within a Cell Network. *J. Immunol.* **200**, 3244-3258, doi:10.4049/jimmunol.1701733 (2018).

141 Pawar, K., Shigematsu, M., Sharbati, S. & Kirino, Y. Infection-induced 5'-half molecules of tRNAHisGUG activate Toll-like receptor 7. *PLoS Biol.* **18**, e3000982, doi:10.1371/journal.pbio.3000982 (2020).

142 Matsumoto, S. *et al.* DNA augments antigenicity of mycobacterial DNA-binding protein 1 and confers protection against *Mycobacterium tuberculosis* infection in mice. *J. Immunol.* **175**, 441-449, doi:10.4049/jimmunol.175.1.441 (2005).

143 Ruiz, A., Guzmán-Beltrán, S., Carreto-Binaghi, L. E., Gonzalez, Y. & Juárez, E. DNA from virulent *M. tuberculosis* induces TNF-α production and autophagy in M1 polarized macrophages. *Microb. Pathog.* **132**, 166-177, doi:10.1016/j.micpath.2019.04.041 (2019).

144 Fitzgerald, K. A. & Kagan, J. C. Toll-like Receptors and the Control of Immunity. *Cell* **180**, 1044-1066, doi:10.1016/j.cell.2020.02.041 (2020).

145 Brown, G. D., Willment, J. A. & Whitehead, L. C-type lectins in immunity and homeostasis. *Nature Reviews Immunology* **18**, 374-389, doi:10.1038/s41577-018-0004-8 (2018).

146 Schlesinger, L. S. Macrophage phagocytosis of virulent but not attenuated strains of *Mycobacterium tuberculosis* is mediated by mannose receptors in addition to complement receptors. *J. Immunol.* **150**, 2920-2930 (1993).

147 Schlesinger, L. S., Hull, S. R. & Kaufman, T. M. Binding of the terminal mannosyl units of lipoarabinomannan from a virulent strain of *Mycobacterium tuberculosis* to human macrophages. *J. Immunol.* **152**, 4070-4079 (1994).

148 Rajaram, M. V. *et al. Mycobacterium tuberculosis* activates human macrophage peroxisome proliferator-activated receptor gamma linking mannose receptor recognition to regulation of immune responses. *J. Immunol.* **185**, 929-942, doi:10.4049/jimmunol.1000866 (2010).

149 Guirado, E. *et al.* Deletion of PPARγ in lung macrophages provides an immunoprotective response against *M. tuberculosis* infection in mice. *Tuberculosis (Edinb)* **111**, 170-177, doi:10.1016/j.tube.2018.06.012 (2018).

150 Tailleux, L. *et al.* DC-SIGN is the major *Mycobacterium tuberculosis* receptor on human dendritic cells. *J. Exp. Med.* **197**, 121-127, doi:10.1084/jem.20021468 (2003).

151 Maeda, N. *et al.* The cell surface receptor DC-SIGN discriminates between *Mycobacterium* species through selective recognition of the mannose caps on lipoarabinomannan. *J. Biol. Chem.* **278**, 5513-5516, doi:10.1074/jbc.C200586200 (2003).

152 Driessen, N. N. *et al.* Role of phosphatidylinositol mannosides in the interaction between mycobacteria and DC-SIGN. *Infect. Immun.* **77**, 4538-4547, doi:10.1128/iai.01256-08 (2009).

153 Geurtsen, J. *et al.* Identification of mycobacterial alpha-glucan as a novel ligand for DC-SIGN: involvement of mycobacterial capsular polysaccharides in host immune modulation. *J. Immunol.* **183**, 5221-5231, doi:10.4049/jimmunol.0900768 (2009).

154 Koppel, E. A. *et al.* Identification of the mycobacterial carbohydrate structure that binds the C-type lectins DC-SIGN, L-SIGN and SIGNR1. *Immunobiology* **209**, 117-127, doi:10.1016/j.imbio.2004.03.003 (2004).

155 Gringhuis, S. I. *et al.* C-type lectin DC-SIGN modulates Toll-like receptor signaling via Raf-1 kinase-dependent acetylation of transcription factor NF-kappaB. *Immunity* **26**, 605-616, doi:10.1016/j.immuni.2007.03.012 (2007).

156 Gringhuis, S. I., den Dunnen, J., Litjens, M., van der Vlist, M. & Geijtenbeek, T. B. Carbohydrate-specific signaling through the DC-SIGN signalosome tailors immunity to *Mycobacterium tuberculosis*, HIV-1 and *Helicobacter pylori*. *Nat. Immunol.* **10**, 1081-1088, doi:10.1038/ni.1778 (2009).

157 Ishikawa, E. *et al.* Direct recognition of the mycobacterial glycolipid, trehalose dimycolate, by C-type lectin Mincle. *J. Exp. Med.* **206**, 2879-2888, doi:10.1084/jem.20091750 (2009).

158 Ostrop, J. *et al.* Contribution of MINCLE-SYK Signaling to Activation of Primary Human APCs by Mycobacterial Cord Factor and the Novel Adjuvant TDB. *J. Immunol.* **195**, 2417-2428, doi:10.4049/jimmunol.1500102 (2015).

159 Dorhoi, A. *et al.* The adaptor molecule CARD9 is essential for tuberculosis control. *J. Exp. Med.* **207**, 777-792, doi:10.1084/jem.20090067 (2010).

160 Miyake, Y. *et al.* C-type lectin MCL is an FcRγ-coupled receptor that mediates the adjuvanticity of mycobacterial cord factor. *Immunity* **38**, 1050-1062, doi:10.1016/j.immuni.2013.03.010 (2013).

161 Miyake, Y., Oh-hora, M. & Yamasaki, S. C-Type Lectin Receptor MCL Facilitates Mincle Expression and Signaling through Complex Formation. *The Journal of Immunology* **194**, 5366-5374, doi:10.4049/jimmunol.1402429 (2015).

162 Kerscher, B. *et al.* Mycobacterial receptor, Clec4d (CLECSF8, MCL), is coregulated with Mincle and upregulated on mouse myeloid cells following microbial challenge. *Eur. J. Immunol.* **46**, 381-389, doi:10.1002/eji.201545858 (2016).

163 Rothfuchs, A. G. *et al.* Dectin-1 interaction with *Mycobacterium tuberculosis* leads to enhanced IL-12p40 production by splenic dendritic cells. *J. Immunol.* **179**, 3463-3471, doi:10.4049/jimmunol.179.6.3463 (2007).

164 Das, R. *et al.* Macrophage migration inhibitory factor (MIF) is a critical mediator of the innate immune response to *Mycobacterium tuberculosis*. *Proc. Natl. Acad. Sci. U. S. A.* **110**, E2997-3006, doi:10.1073/pnas.1301128110 (2013).

165 Yonekawa, A. *et al.* Dectin-2 is a direct receptor for mannose-capped lipoarabinomannan of mycobacteria. *Immunity* **41**, 402-413, doi:10.1016/j.immuni.2014.08.005 (2014).

166 Decout, A. *et al.* Deciphering the molecular basis of mycobacteria and lipoglycan recognition by the C-type lectin Dectin-2. *Sci. Rep.* **8**, 16840, doi:10.1038/s41598-018-35393-5 (2018).

167 Toyonaga, K. *et al.* C-Type Lectin Receptor DCAR Recognizes Mycobacterial Phosphatidyl-Inositol Mannosides to Promote a Th1 Response during Infection. *Immunity* **45**, 1245-1257, doi:10.1016/j.immuni.2016.10.012 (2016).

168 Downing, J. F., Pasula, R., Wright, J. R., Twigg, H. L., 3rd & Martin, W. J., 2nd. Surfactant protein a promotes attachment of *Mycobacterium tuberculosis* to alveolar macrophages during infection with human immunodeficiency virus. *Proc. Natl. Acad. Sci. U. S. A.* **92**, 4848-4852, doi:10.1073/pnas.92.11.4848 (1995).

169 Gaynor, C. D., McCormack, F. X., Voelker, D. R., McGowan, S. E. & Schlesinger, L. S. Pulmonary surfactant protein A mediates enhanced phagocytosis of *Mycobacterium tuberculosis* by a direct interaction with human macrophages. *J. Immunol.* **155**, 5343-5351 (1995).

170 Pasula, R., Wright, J. R., Kachel, D. L. & Martin, W. J., 2nd. Surfactant protein A suppresses reactive nitrogen intermediates by alveolar macrophages in response to *Mycobacterium tuberculosis*. *J. Clin. Invest.* **103**, 483-490, doi:10.1172/jci2991 (1999).

171 Sidobre, S., Nigou, J., Puzo, G. & Rivière, M. Lipoglycans are putative ligands for the human pulmonary surfactant protein A attachment to mycobacteria. Critical role of the lipids for lectin-carbohydrate recognition. *J. Biol. Chem.* **275**, 2415-2422, doi:10.1074/jbc.275.4.2415 (2000).

172 Ragas, A., Roussel, L., Puzo, G. & Rivière, M. The *Mycobacterium tuberculosis* cell-surface glycoprotein apa as a potential adhesin to colonize target cells via the innate immune system pulmonary C-type lectin surfactant protein A. *J. Biol. Chem.* **282**, 5133-5142, doi:10.1074/jbc.M610183200 (2007).

173 Ferguson, J. S., Voelker, D. R., McCormack, F. X. & Schlesinger, L. S. Surfactant protein D binds to *Mycobacterium tuberculosis* bacilli and lipoarabinomannan via carbohydrate-lectin interactions resulting in reduced phagocytosis of the bacteria by macrophages. *J. Immunol.* **163**, 312-321 (1999).

174 Ferguson, J. S., Voelker, D. R., Ufnar, J. A., Dawson, A. J. & Schlesinger, L. S. Surfactant protein D inhibition of human macrophage uptake of *Mycobacterium tuberculosis* is independent of bacterial agglutination. *J. Immunol.* **168**, 1309-1314, doi:10.4049/jimmunol.168.3.1309 (2002).

175 Ferguson, J. S. *et al.* Surfactant protein D increases fusion of *Mycobacterium tuberculosis*-containing phagosomes with lysosomes in human macrophages. *Infect. Immun.* **74**, 7005-7009, doi:10.1128/iai.01402-06 (2006).

176 Garred, P., Harboe, M., Oettinger, T., Koch, C. & Svejgaard, A. Dual role of mannan-binding protein in infections: another case of heterosis? *Eur. J. Immunogenet.* **21**, 125-131, doi:10.1111/j.1744-313x.1994.tb00183.x (1994).

177 Luo, F. *et al.* Ficolin-2 defends against virulent *Mycobacteria tuberculosis* infection *in vivo*, and its insufficiency is associated with infection in humans. *PLoS One* **8**, e73859, doi:10.1371/journal.pone.0073859 (2013).

178 Bartlomiejczyk, M. A., Swierzko, A. S., Brzostek, A., Dziadek, J. & Cedzynski, M. Interaction of lectin pathway of complement-activating pattern recognition molecules with mycobacteria. *Clin. Exp. Immunol.* **178**, 310-319, doi:10.1111/cei.12416 (2014).

179 Polotsky, V. Y., Belisle, J. T., Mikusova, K., Ezekowitz, R. A. & Joiner, K. A. Interaction of human mannose-binding protein with *Mycobacterium avium*. *J. Infect. Dis.* **175**, 1159-1168, doi:10.1086/520354 (1997).

180 Świerzko, A. S. *et al.* Mycobacterial antigen 85 complex (Ag85) as a target for ficolins and mannose-binding lectin. *Int. J. Med. Microbiol.* **306**, 212-221, doi:10.1016/j.ijmm.2016.04.004 (2016).

181 Zhong, Y., Kinio, A. & Saleh, M. Functions of NOD-Like Receptors in Human Diseases. *Front. Immunol.* **4**, 333, doi:10.3389/fimmu.2013.00333 (2013).

182 Girardin, S. E. *et al.* Nod2 is a general sensor of peptidoglycan through muramyl dipeptide (MDP) detection. *J. Biol. Chem.* **278**, 8869-8872, doi:10.1074/jbc.C200651200 (2003).

183 Inohara, N. *et al.* Host recognition of bacterial muramyl dipeptide mediated through NOD2. Implications for Crohn's disease. *J. Biol. Chem.* **278**, 5509-5512, doi:10.1074/jbc.C200673200 (2003).

184 Chamaillard, M. *et al.* An essential role for NOD1 in host recognition of bacterial peptidoglycan containing diaminopimelic acid. *Nat. Immunol.* **4**, 702-707, doi:10.1038/ni945 (2003).

185 Girardin, S. E. *et al.* Nod1 detects a unique muropeptide from gram-negative bacterial peptidoglycan. *Science* **300**, 1584-1587, doi:10.1126/science.1084677 (2003).

186 Lee, J. Y. *et al.* The role of nucleotide-binding oligomerization domain 1 during cytokine production by macrophages in response to *Mycobacterium tuberculosis* infection. *Immunobiology* **221**, 70-75, doi:10.1016/j.imbio.2015.07.020 (2016).

187 Dubé, J.-Y. *et al.* Synthetic mycobacterial molecular patterns partially complete Freund’s adjuvant. *Sci. Rep.* **10**, 5874, doi:10.1038/s41598-020-62543-5 (2020).

188 Gandotra, S., Jang, S., Murray, P. J., Salgame, P. & Ehrt, S. Nucleotide-binding oligomerization domain protein 2-deficient mice control infection with *Mycobacterium tuberculosis*. *Infect. Immun.* **75**, 5127-5134, doi:10.1128/IAI.00458-07 (2007).

189 Divangahi, M. *et al.* NOD2-Deficient Mice Have Impaired Resistance to *Mycobacterium tuberculosis* Infection through Defective Innate and Adaptive Immunity. *J. Immunol.* **181**, 7157-7165, doi:10.4049/jimmunol.181.10.7157 (2008).

190 Landes, M. B., Rajaram, M. V., Nguyen, H. & Schlesinger, L. S. Role for NOD2 in *Mycobacterium tuberculosis*-induced iNOS expression and NO production in human macrophages. *J. Leukoc. Biol.* **97**, 1111-1119, doi:10.1189/jlb.3A1114-557R (2015).

191 Ferwerda, G. *et al.* NOD2 and toll-like receptors are nonredundant recognition systems of *Mycobacterium tuberculosis*. *PLoS Pathog.* **1**, 279-285, doi:10.1371/journal.ppat.0010034 (2005).

192 Beckwith, K. S. *et al.* Plasma membrane damage causes NLRP3 activation and pyroptosis during *Mycobacterium tuberculosis* infection. *Nat Commun* **11**, 2270, doi:10.1038/s41467-020-16143-6 (2020).

193 Saiga, H. *et al.* Critical role of AIM2 in *Mycobacterium tuberculosis* infection. *Int. Immunol.* **24**, 637-644, doi:10.1093/intimm/dxs062 (2012).

194 Watson, R. O., Manzanillo, P. S. & Cox, J. S. Extracellular *M. tuberculosis* DNA targets bacteria for autophagy by activating the host DNA-sensing pathway. *Cell* **150**, 803-815, doi:10.1016/j.cell.2012.06.040 (2012).

195 van der Vaart, M. *et al.* The DNA damage-regulated autophagy modulator DRAM1 links mycobacterial recognition via TLR-MYD88 to autophagic defense [corrected]. *Cell Host Microbe* **15**, 753-767, doi:10.1016/j.chom.2014.05.005 (2014).

196 Collins, A. C. *et al.* Cyclic GMP-AMP Synthase Is an Innate Immune DNA Sensor for *Mycobacterium tuberculosis*. *Cell Host Microbe* **17**, 820-828, doi:10.1016/j.chom.2015.05.005 (2015).

197 Wassermann, R. *et al. Mycobacterium tuberculosis* Differentially Activates cGAS- and Inflammasome-Dependent Intracellular Immune Responses through ESX-1. *Cell Host Microbe* **17**, 799-810, doi:10.1016/j.chom.2015.05.003 (2015).

198 Watson, Robert O. *et al.* The Cytosolic Sensor cGAS Detects *Mycobacterium tuberculosis* DNA to Induce Type I Interferons and Activate Autophagy. *Cell Host & Microbe* **17**, 811-819, doi:10.1016/j.chom.2015.05.004 (2015).

199 Dey, B. *et al.* A bacterial cyclic dinucleotide activates the cytosolic surveillance pathway and mediates innate resistance to tuberculosis. *Nat. Med.* **21**, 401-406, doi:10.1038/nm.3813 (2015).

200 Yan, S. *et al.* Deficiency of the AIM2-ASC Signal Uncovers the STING-Driven Overreactive Response of Type I IFN and Reciprocal Depression of Protective IFN-γ Immunity in Mycobacterial Infection. *J. Immunol.* **200**, 1016-1026, doi:10.4049/jimmunol.1701177 (2018).

201 Patten, D. A. & Shetty, S. More Than Just a Removal Service: Scavenger Receptors in Leukocyte Trafficking. *Front. Immunol.* **9**, 2904, doi:10.3389/fimmu.2018.02904 (2018).

202 Pombinho, R., Sousa, S. & Cabanes, D. Scavenger Receptors: Promiscuous Players during Microbial Pathogenesis. *Crit. Rev. Microbiol.* **44**, 685-700, doi:10.1080/1040841X.2018.1493716 (2018).

203 Zimmerli, S., Edwards, S. & Ernst, J. D. Selective receptor blockade during phagocytosis does not alter the survival and growth of *Mycobacterium tuberculosis* in human

macrophages. *Am. J. Respir. Cell Mol. Biol.* **15**, 760-770, doi:10.1165/ajrcmb.15.6.8969271 (1996).

204 Bowdish, D. M. *et al.* MARCO, TLR2, and CD14 are required for macrophage cytokine responses to mycobacterial trehalose dimycolate and *Mycobacterium tuberculosis*. *PLoS Pathog.* **5**, e1000474, doi:10.1371/journal.ppat.1000474 (2009).

205 Benard, E. L., Roobol, S. J., Spaink, H. P. & Meijer, A. H. Phagocytosis of mycobacteria by zebrafish macrophages is dependent on the scavenger receptor Marco, a key control factor of pro-inflammatory signalling. *Dev. Comp. Immunol.* **47**, 223-233, doi:10.1016/j.dci.2014.07.022 (2014).

206 Khan, A. *et al.* Mesenchymal stem cells internalize *Mycobacterium tuberculosis* through scavenger receptors and restrict bacterial growth through autophagy. *Sci. Rep.* **7**, 15010, doi:10.1038/s41598-017-15290-z (2017).

207 Shi, S. *et al.* Expression of many immunologically important genes in *Mycobacterium tuberculosis*-infected macrophages is independent of both TLR2 and TLR4 but dependent on IFN-alphabeta receptor and STAT1. *J. Immunol.* **175**, 3318-3328, doi:10.4049/jimmunol.175.5.3318 (2005).

208 Ozeki, Y. *et al.* Macrophage scavenger receptor down-regulates mycobacterial cord factor-induced proinflammatory cytokine production by alveolar and hepatic macrophages. *Microb. Pathog.* **40**, 171-176, doi:10.1016/j.micpath.2005.12.006 (2006).

209 Schäfer, G., Guler, R., Murray, G., Brombacher, F. & Brown, G. D. The role of scavenger receptor B1 in infection with *Mycobacterium tuberculosis* in a murine model. *PLoS One* **4**, e8448, doi:10.1371/journal.pone.0008448 (2009).

210 Khan, H. S. *et al.* Identification of scavenger receptor B1 as the airway microfold cell receptor for *Mycobacterium tuberculosis*. *Elife* **9**, doi:10.7554/eLife.52551 (2020).

211 Philips, J. A., Rubin, E. J. & Perrimon, N. *Drosophila* RNAi screen reveals CD36 family member required for mycobacterial infection. *Science* **309**, 1251-1253, doi:10.1126/science.1116006 (2005).

212 Dodd, C. E., Pyle, C. J., Glowinski, R., Rajaram, M. V. & Schlesinger, L. S. CD36-Mediated Uptake of Surfactant Lipids by Human Macrophages Promotes Intracellular Growth of *Mycobacterium tuberculosis*. *J. Immunol.* **197**, 4727-4735, doi:10.4049/jimmunol.1600856 (2016).

213 Hawkes, M. *et al.* CD36 deficiency attenuates experimental mycobacterial infection. *BMC Infect. Dis.* **10**, 299, doi:10.1186/1471-2334-10-299 (2010).

214 Sattler, N. *et al.* Functions of the Dictyostelium LIMP-2 and CD36 homologues in bacteria uptake, phagolysosome biogenesis and host cell defence. *J. Cell Sci.* **131**, doi:10.1242/jcs.218040 (2018).

215 Flynn, J. L., Gideon, H. P., Mattila, J. T. & Lin, P. L. Immunology studies in non-human primate models of tuberculosis. *Immunol. Rev.* **264**, 60-73, doi:10.1111/imr.12258 (2015).

216 Wieland, C. W., van der Windt, G. J., Wiersinga, W. J., Florquin, S. & van der Poll, T. CD14 contributes to pulmonary inflammation and mortality during murine tuberculosis. *Immunology* **125**, 272-279, doi:10.1111/j.1365-2567.2008.02840.x (2008).

217 Sever-Chroneos, Z., Tvinnereim, A., Hunter, R. L. & Chroneos, Z. C. Prolonged survival of scavenger receptor class A-deficient mice from pulmonary *Mycobacterium*

tuberculosis infection. *Tuberculosis (Edinb)* **91 Suppl 1**, S69-74, doi:10.1016/j.tube.2011.10.014 (2011).

218 Sugawara, I. *et al.* Mycobacterial infection in TLR2 and TLR6 knockout mice. *Microbiol. Immunol.* **47**, 327-336, doi:10.1111/j.1348-0421.2003.tb03404.x (2003).

219 Bafica, A. *et al.* TLR9 regulates Th1 responses and cooperates with TLR2 in mediating optimal resistance to *Mycobacterium tuberculosis*. *J. Exp. Med.* **202**, 1715-1724, doi:10.1084/jem.20051782 (2005).

220 Fremond, C. M. *et al.* IL-1 receptor-mediated signal is an essential component of MyD88-dependent innate response to *Mycobacterium tuberculosis* infection. *J. Immunol.* **179**, 1178-1189, doi:10.4049/jimmunol.179.2.1178 (2007).

221 Hölscher, C. *et al.* Containment of aerogenic *Mycobacterium tuberculosis* infection in mice does not require MyD88 adaptor function for TLR2, -4 and -9. *Eur. J. Immunol.* **38**, 680-694, doi:10.1002/eji.200736458 (2008).

222 Fremond, C. M. *et al.* Fatal *Mycobacterium tuberculosis* infection despite adaptive immune response in the absence of MyD88. *J. Clin. Invest.* **114**, 1790-1799, doi:10.1172/jci21027 (2004).

223 Sugawara, I., Yamada, H., Mizuno, S., Takeda, K. & Akira, S. Mycobacterial infection in MyD88-deficient mice. *Microbiol. Immunol.* **47**, 841-847, doi:10.1111/j.1348-0421.2003.tb03450.x (2003).

224 Wilson, G. J. *et al.* The C-type lectin receptor CLECSF8/CLEC4D is a key component of anti-mycobacterial immunity. *Cell Host Microbe* **17**, 252-259, doi:10.1016/j.chom.2015.01.004 (2015).

225 Marakalala, M. J. *et al.* The Syk/CARD9-coupled receptor Dectin-1 is not required for host resistance to *Mycobacterium tuberculosis* in mice. *Microbes Infect* **13**, 198-201, doi:10.1016/j.micinf.2010.10.013 (2011).

226 Court, N. *et al.* Partial redundancy of the pattern recognition receptors, scavenger receptors, and C-type lectins for the long-term control of *Mycobacterium tuberculosis* infection. *J. Immunol.* **184**, 7057-7070, doi:10.4049/jimmunol.1000164 (2010).

227 Tanne, A. *et al.* A murine DC-SIGN homologue contributes to early host defense against *Mycobacterium tuberculosis*. *J. Exp. Med.* **206**, 2205-2220, doi:10.1084/jem.20090188 (2009).

228 Lemos, M. P., McKinney, J. & Rhee, K. Y. Dispensability of surfactant proteins A and D in immune control of *Mycobacterium tuberculosis* infection following aerosol challenge of mice. *Infect. Immun.* **79**, 1077-1085, doi:10.1128/iai.00286-10 (2011).

229 Mayer-Barber, K. D. *et al.* Cutting Edge: Caspase-1 Independent IL-1β Production Is Critical for Host Resistance to *Mycobacterium tuberculosis* and Does Not Require TLR Signaling In Vivo. *The Journal of Immunology* **184**, 3326-3330, doi:10.4049/jimmunol.0904189 (2010).

230 McElvania Tekippe, E. *et al.* Granuloma formation and host defense in chronic *Mycobacterium tuberculosis* infection requires PYCARD/ASC but not NLRP3 or caspase-1. *PLoS One* **5**, e12320, doi:10.1371/journal.pone.0012320 (2010).

231 Marinho, F. V. *et al.* The cGAS/STING Pathway Is Important for Dendritic Cell Activation but Is Not Essential to Induce Protective Immunity against *Mycobacterium tuberculosis* Infection. *J. Innate Immun.* **10**, 239-252, doi:10.1159/000488952 (2018).

232 Hu, C., Mayadas-Norton, T., Tanaka, K., Chan, J. & Salgame, P. *Mycobacterium tuberculosis* infection in complement receptor 3-deficient mice. *J. Immunol.* **165**, 2596-2602, doi:10.4049/jimmunol.165.5.2596 (2000).

233 Melo, M. D., Catchpole, I. R., Haggar, G. & Stokes, R. W. Utilization of CD11b knockout mice to characterize the role of complement receptor 3 (CR3, CD11b/CD18) in the growth of *Mycobacterium tuberculosis* in macrophages. *Cell. Immunol.* **205**, 13-23, doi:10.1006/cimm.2000.1710 (2000).

234 Quintana-Murci, L. Human Immunology through the Lens of Evolutionary Genetics. *Cell* **177**, 184-199, doi:10.1016/j.cell.2019.02.033 (2019).

235 Zeberg, H. & Paabo, S. The major genetic risk factor for severe COVID-19 is inherited from Neanderthals. *Nature* **587**, 610-612, doi:10.1038/s41586-020-2818-3 (2020).

236 Barreiro, L. B. & Quintana-Murci, L. From evolutionary genetics to human immunology: how selection shapes host defence genes. *Nat Rev Genet* **11**, 17-30, doi:10.1038/nrg2698 (2010).

237 Barreiro, L. B. *et al.* Evolutionary dynamics of human Toll-like receptors and their different contributions to host defense. *PLoS Genet* **5**, e1000562, doi:10.1371/journal.pgen.1000562 (2009).

238 Ferwerda, B. *et al.* TLR4 polymorphisms, infectious diseases, and evolutionary pressure during migration of modern humans. *Proc Natl Acad Sci U S A* **104**, 16645-16650, doi:10.1073/pnas.0704828104 (2007).

239 Pisitkun, P. *et al.* Autoreactive B cell responses to RNA-related antigens due to TLR7 gene duplication. *Science* **312**, 1669-1672, doi:10.1126/science.1124978 (2006).

240 Krieg, A. M. & Vollmer, J. Toll-like receptors 7, 8, and 9: linking innate immunity to autoimmunity. *Immunol Rev* **220**, 251-269, doi:10.1111/j.1600-065X.2007.00572.x (2007).

241 Celhar, T., Magalhaes, R. & Fairhurst, A. M. TLR7 and TLR9 in SLE: when sensing self goes wrong. *Immunol Res* **53**, 58-77, doi:10.1007/s12026-012-8270-1 (2012).

242 Mathieson, I. *et al.* Genome-wide patterns of selection in 230 ancient Eurasians. *Nature* **528**, 499-503, doi:10.1038/nature16152 (2015).

243 Wong, S. H. *et al.* Leprosy and the adaptation of human toll-like receptor 1. *PLoS Pathog* **6**, e1000979, doi:10.1371/journal.ppat.1000979 (2010).

244 Ma, X. *et al.* Full-exon resequencing reveals toll-like receptor variants contribute to human susceptibility to tuberculosis disease. *PLoS One* **2**, e1318, doi:10.1371/journal.pone.0001318 (2007).

245 Uciechowski, P. *et al.* Susceptibility to tuberculosis is associated with TLR1 polymorphisms resulting in a lack of TLR1 cell surface expression. *J. Leukoc. Biol.* **90**, 377-388, doi:10.1189/jlb.0409233 (2011).

246 Hawn, T. R. *et al.* A common human TLR1 polymorphism regulates the innate immune response to lipopeptides. *Eur. J. Immunol.* **37**, 2280-2289, doi:10.1002/eji.200737034 (2007).

247 Marques Cde, S. *et al.* Toll-like receptor 1 N248S single-nucleotide polymorphism is associated with leprosy risk and regulates immune activation during mycobacterial infection. *J Infect Dis* **208**, 120-129, doi:10.1093/infdis/jit133 (2013).

248 Mortaz, E. *et al.* Interaction of Pattern Recognition Receptors with *Mycobacterium Tuberculosis*. *J. Clin. Immunol.* **35**, 1-10, doi:10.1007/s10875-014-0103-7 (2015).

249 Jin, X., Yin, S., Zhang, Y. & Chen, X. Association between TLR2 Arg677Trp polymorphism and tuberculosis susceptibility: A meta-analysis. *Microb Pathog* **144**, 104173, doi:10.1016/j.micpath.2020.104173 (2020).

250 Cubillos-Angulo, J. M. *et al.* Polymorphisms in *TLR4* and *TNFA* and Risk of *Mycobacterium tuberculosis* Infection and Development of Active Disease in Contacts of Tuberculosis Cases in Brazil: A Prospective Cohort Study. *Clin. Infect. Dis.* **69**, 1027-1035, doi:10.1093/cid/ciy1001 (2019).

251 Graustein, A. D. *et al.* TLR9 gene region polymorphisms and susceptibility to tuberculosis in Vietnam. *Tuberculosis (Edinb)* **95**, 190-196, doi:10.1016/j.tube.2014.12.009 (2015).

252 Velez, D. R. *et al.* Variants in toll-like receptors 2 and 9 influence susceptibility to pulmonary tuberculosis in Caucasians, African-Americans, and West Africans. *Hum Genet* **127**, 65-73, doi:10.1007/s00439-009-0741-7 (2010).

253 Vasseur, E. *et al.* The evolutionary landscape of cytosolic microbial sensors in humans. *Am J Hum Genet* **91**, 27-37, doi:10.1016/j.ajhg.2012.05.008 (2012).

254 Wang, C. *et al.* NOD2 polymorphisms and pulmonary tuberculosis susceptibility: a systematic review and meta-analysis. *Int J Biol Sci* **10**, 103-108, doi:10.7150/ijbs.7585 (2013).

255 Austin, C. M., Ma, X. & Graviss, E. A. Common nonsynonymous polymorphisms in the *NOD2* gene are associated with resistance or susceptibility to tuberculosis disease in African Americans. *J. Infect. Dis.* **197**, 1713-1716, doi:10.1086/588384 (2008).

256 Hui, K. Y. *et al.* Functional variants in the *LRRK2* gene confer shared effects on risk for Crohn's disease and Parkinson's disease. *Sci. Transl. Med.* **10**, doi:10.1126/scitranslmed.aai7795 (2018).

257 Ravimohan, S. *et al.* Common Variation in NLRP3 Is Associated With Early Death and Elevated Inflammasome Biomarkers Among Advanced HIV/TB Co-infected Patients in Botswana. *Open Forum Infect Dis* **5**, ofy075, doi:10.1093/ofid/ofy075 (2018).

258 Barreiro, L. B. *et al.* The heritage of pathogen pressures and ancient demography in the human innate-immunity CD209/CD209L region. *Am J Hum Genet* **77**, 869-886, doi:10.1086/497613 (2005).

259 Barreiro, L. B. *et al.* Promoter variation in the DC-SIGN-encoding gene CD209 is associated with tuberculosis. *PLoS Med.* **3**, e20, doi:10.1371/journal.pmed.0030020 (2006).

260 Vannberg, F. O. *et al.* CD209 genetic polymorphism and tuberculosis disease. *PLoS One* **3**, e1388, doi:10.1371/journal.pone.0001388 (2008).

261 Ben-Ali, M. *et al.* Promoter and neck region length variation of DC-SIGN is not associated with susceptibility to tuberculosis in Tunisian patients. *Hum. Immunol.* **68**, 908-912, doi:10.1016/j.humimm.2007.09.003 (2007).

262 Kobayashi, K. *et al.* Association of CD209 polymorphisms with tuberculosis in an Indonesian population. *Hum. Immunol.* **72**, 741-745, doi:10.1016/j.humimm.2011.04.004 (2011).

263 da Silva, R. C. *et al.* Association of CD209 and CD209L polymorphisms with tuberculosis infection in a Northeastern Brazilian population. *Mol. Biol. Rep.* **41**, 5449-5457, doi:10.1007/s11033-014-3416-y (2014).

264 Xu, D. D. *et al.* Association of the FCN2 Gene Single Nucleotide Polymorphisms with Susceptibility to Pulmonary Tuberculosis. *PLoS One* **10**, e0138356, doi:10.1371/journal.pone.0138356 (2015).

265 Li, Y. *et al.* Association of ficolin-1 and ficolin-3 gene variation and pulmonary tuberculosis susceptibility in a Chinese population. *J Clin Lab Anal* **35**, e23732, doi:10.1002/jcla.23732 (2021).

266 Juffermans, N. P. *et al.* Interleukin-1 signaling is essential for host defense during murine pulmonary tuberculosis. *J. Infect. Dis.* **182**, 902-908, doi:10.1086/315771 (2000).

267 Sugawara, I., Yamada, H., Hua, S. & Mizuno, S. Role of interleukin (IL)-1 type 1 receptor in mycobacterial infection. *Microbiol. Immunol.* **45**, 743-750, doi:10.1111/j.1348-0421.2001.tb01310.x (2001).

268 Yamada, H., Mizumo, S., Horai, R., Iwakura, Y. & Sugawara, I. Protective Role of Interleukin-1 in Mycobacterial Infection in IL-1 α/β Double-Knockout Mice. *Lab. Invest.* **80**, 759-767, doi:10.1038/labinvest.3780079 (2000).

269 Bourigault, M. L. *et al.* Relative contribution of IL-1α, IL-1β and TNF to the host response to *Mycobacterium tuberculosis* and attenuated *M. bovis* BCG. *Immun Inflamm Dis* **1**, 47-62, doi:10.1002/iid3.9 (2013).

270 Ji, D. X. *et al.* Type I interferon-driven susceptibility to *Mycobacterium tuberculosis* is mediated by IL-1Ra. *Nat Microbiol* **4**, 2128-2135, doi:10.1038/s41564-019-0578-3 (2019).

271 Flynn, J. L. *et al.* Tumor necrosis factor-alpha is required in the protective immune response against *Mycobacterium tuberculosis* in mice. *Immunity* **2**, 561-572, doi:10.1016/1074-7613(95)90001-2 (1995).

272 Drennan, M. B. *et al.* Toll-like receptor 2-deficient mice succumb to *Mycobacterium tuberculosis* infection. *Am. J. Pathol.* **164**, 49-57, doi:10.1016/s0002-9440(10)63095-7 (2004).

273 Segueni, N. *et al.* Innate myeloid cell TNFR1 mediates first line defence against primary *Mycobacterium tuberculosis* infection. *Sci. Rep.* **6**, 22454, doi:10.1038/srep22454 (2016).

274 Keane, J. *et al.* Tuberculosis associated with infliximab, a tumor necrosis factor alpha-neutralizing agent. *N. Engl. J. Med.* **345**, 1098-1104, doi:10.1056/NEJMoa011110 (2001).

275 Cooper, A. M. *et al.* Disseminated tuberculosis in interferon gamma gene-disrupted mice. *J. Exp. Med.* **178**, 2243-2247, doi:10.1084/jem.178.6.2243 (1993).

276 Flynn, J. L. *et al.* An essential role for interferon gamma in resistance to *Mycobacterium tuberculosis* infection. *J. Exp. Med.* **178**, 2249-2254, doi:10.1084/jem.178.6.2249 (1993).

277 Sakai, S. *et al.* CD4 T Cell-Derived IFN-gamma Plays a Minimal Role in Control of Pulmonary *Mycobacterium tuberculosis* Infection and Must Be Actively Repressed by PD-1 to Prevent Lethal Disease. *PLoS Pathog.* **12**, e1005667, doi:10.1371/journal.ppat.1005667 (2016).

278 Cooper, A. M., Magram, J., Ferrante, J. & Orme, I. M. Interleukin 12 (IL-12) is crucial to the development of protective immunity in mice intravenously infected with *Mycobacterium tuberculosis*. *J. Exp. Med.* **186**, 39-45, doi:10.1084/jem.186.1.39 (1997).

279 Döffinger, R. *et al.* Inherited disorders of IL-12- and IFNgamma-mediated immunity: a molecular genetics update. *Mol. Immunol.* **38**, 903-909, doi:10.1016/s0161-5890(02)00017-2 (2002).

280 MacMicking, J. D. *et al.* Identification of nitric oxide synthase as a protective locus against tuberculosis. *Proceedings of the National Academy of Sciences* **94**, 5243-5248, doi:10.1073/pnas.94.10.5243 (1997).

281 Jung, Y. J., LaCourse, R., Ryan, L. & North, R. J. Virulent but not avirulent *Mycobacterium tuberculosis* can evade the growth inhibitory action of a T helper 1-dependent, nitric oxide Synthase 2-independent defense in mice. *J. Exp. Med.* **196**, 991-998, doi:10.1084/jem.20021186 (2002).

282 Fava, V. M., Dallmann-Sauer, M. & Schurr, E. Genetics of leprosy: today and beyond. *Hum Genet* **139**, 835-846, doi:10.1007/s00439-019-02087-5 (2020).

283 Zhang, F. *et al.* Identification of two new loci at IL23R and RAB32 that influence susceptibility to leprosy. *Nat Genet* **43**, 1247-1251, doi:10.1038/ng.973 (2011).

284 Zhang, F. R. *et al.* Genomewide association study of leprosy. *N. Engl. J. Med.* **361**, 2609-2618, doi:10.1056/NEJMoa0903753 (2009).

285 Fava, V. M. *et al.* Reply to Zhang et al.: The differential role of LRRK2 variants in nested leprosy phenotypes. *Proc Natl Acad Sci U S A* **117**, 10124-10125, doi:10.1073/pnas.2002654117 (2020).

286 Fava, V. M. *et al.* Association of *TNFSF8* regulatory variants with excessive inflammatory responses but not leprosy *per se*. *J. Infect. Dis.* **211**, 968-977, doi:10.1093/infdis/jiu566 (2015).

287 Fava, V. M., Sales-Marques, C., Alcais, A., Moraes, M. O. & Schurr, E. Age-Dependent Association of TNFSF15/TNFSF8 Variants and Leprosy Type 1 Reaction. *Front Immunol* **8**, 155, doi:10.3389/fimmu.2017.00155 (2017).

288 Fava, V. M. *et al.* Pleiotropic effects for Parkin and LRRK2 in leprosy type-1 reactions and Parkinson's disease. *Proc. Natl. Acad. Sci. U. S. A.* **116**, 15616-15624, doi:10.1073/pnas.1901805116 (2019).

289 Lange, C. *et al.* Perspective for Precision Medicine for Tuberculosis. *Front. Immunol.* **11**, 566608, doi:10.3389/fimmu.2020.566608 (2020).

290 DiNardo, A. R. *et al.* Gene expression signatures identify biologically and clinically distinct tuberculosis endotypes. *medRxiv*, 2020.2005.2013.20100776, doi:10.1101/2020.05.13.20100776 (2021).

291 Singh, A. K., Netea, M. G. & Bishai, W. R. BCG turns 100: its nontraditional uses against viruses, cancer, and immunologic diseases. *J. Clin. Invest.* **131**, doi:10.1172/jci148291 (2021).

292 Mahairas, G. G., Sabo, P. J., Hickey, M. J., Singh, D. C. & Stover, C. K. Molecular analysis of genetic differences between *Mycobacterium bovis* BCG and virulent *M. bovis*. *J. Bacteriol.* **178**, 1274-1282, doi:doi:10.1128/jb.178.5.1274-1282.1996 (1996).

293 Behr, M. A. *et al.* Comparative Genomics of BCG Vaccines by Whole-Genome DNA Microarray. *Science* **284**, 1520-1523, doi:10.1126/science.284.5419.1520 (1999).

294 Charlet, D. *et al.* Reduced expression of antigenic proteins MPB70 and MPB83 in *Mycobacterium bovis* BCG strains due to a start codon mutation in sigK. *Mol. Microbiol.* **56**, 1302-1313, doi:10.1111/j.1365-2958.2005.04618.x (2005).

295 Ladel, C. H., Blum, C., Dreher, A., Reifenberg, K. & Kaufmann, S. H. Protective role of gamma/delta T cells and alpha/beta T cells in tuberculosis. *Eur. J. Immunol.* **25**, 2877-2881, doi:10.1002/eji.1830251025 (1995).

296 Mangtani, P. *et al.* Protection by BCG Vaccine Against Tuberculosis: A Systematic Review of Randomized Controlled Trials. *Clin. Infect. Dis.* **58**, 470-480, doi:10.1093/cid/cit790 (2013).

297 Kleinnijenhuis, J. *et al.* Bacille Calmette-Guerin induces NOD2-dependent nonspecific protection from reinfection via epigenetic reprogramming of monocytes. *Proc. Natl. Acad. Sci. U. S. A.* **109**, 17537-17542, doi:10.1073/pnas.1202870109 (2012).

298 Aaby, P. *et al.* Randomized Trial of BCG Vaccination at Birth to Low-Birth-Weight Children: Beneficial Nonspecific Effects in the Neonatal Period? *The Journal of Infectious Diseases* **204**, 245-252, doi:10.1093/infdis/jir240 (2011).

299 Biering-Sørensen, S. *et al.* Small Randomized Trial Among Low–birth-weight Children Receiving Bacillus Calmette-Guérin Vaccination at First Health Center Contact. *The Pediatric Infectious Disease Journal* **31**, 306-308, doi:10.1097/INF.0b013e3182458289 (2012).

300 Aaby, P. & Benn, C. S. BCG: new life for a centenarian vaccine. *The Lancet Infectious Diseases* **21**, 897-898, doi:10.1016/S1473-3099(20)30714-3 (2021).

301 Prentice, S. *et al.* BCG-induced non-specific effects on heterologous infectious disease in Ugandan neonates: an investigator-blind randomised controlled trial. *The Lancet Infectious Diseases* **21**, 993-1003, doi:10.1016/S1473-3099(20)30653-8 (2021).

302 van Puffelen, J. H. *et al.* Trained immunity as a molecular mechanism for BCG immunotherapy in bladder cancer. *Nat Rev Urol* **17**, 513-525, doi:10.1038/s41585-020-0346-4 (2020).

303 Kleinnijenhuis, J. *et al.* Long-lasting effects of BCG vaccination on both heterologous Th1/Th17 responses and innate trained immunity. *J. Innate Immun.* **6**, 152-158, doi:10.1159/000355628 (2014).

304 Kaufmann, E. *et al.* BCG Educates Hematopoietic Stem Cells to Generate Protective Innate Immunity against Tuberculosis. *Cell* **172**, 176-190.e119, doi:10.1016/j.cell.2017.12.031 (2018).

305 Khan, N. *et al. M. tuberculosis* Reprograms Hematopoietic Stem Cells to Limit Myelopoiesis and Impair Trained Immunity. *Cell* **183**, 752-770.e722, doi:10.1016/j.cell.2020.09.062 (2020).

306 Nath, I. A vaccine for leprosy. *Nat. Med.* **4**, 548-550, doi:10.1038/nm0598-548 (1998).

307 Sharma, S. K. *et al.* Efficacy and Safety of *Mycobacterium indicus pranii* as an adjunct therapy in Category II pulmonary tuberculosis in a randomized trial. *Sci. Rep.* **7**, 3354, doi:10.1038/s41598-017-03514-1 (2017).

308 Mayosi, B. M. *et al.* Prednisolone and *Mycobacterium indicus pranii* in tuberculous pericarditis. *N. Engl. J. Med.* **371**, 1121-1130, doi:10.1056/NEJMoa1407380 (2014).

309 Sur, P. K. & Dastidar, A. G. Role of mycobacterium w as adjuvant treatment of lung cancer (non-small cell lung cancer). *J. Indian Med. Assoc.* **101**, 118, 120 (2003).

310 Subramaniam, M. *et al.* Anti-Cancer Effects of Synergistic Drug–Bacterium Combinations on Induced Breast Cancer in BALB/c Mice. *Biomolecules* **9**, 626 (2019).

311 Freund, J., Casals, J. & Hosmer, E. P. Sensitization and Antibody Formation after Injection of Tubercle Bacilli and Paraffin Oil. *Proc. Soc. Exp. Biol. Med.* **37**, 509-513, doi:10.3181/00379727-37-9625 (1937).

312 Opie, E. L. & Freund, J. AN EXPERIMENTAL STUDY OF PROTECTIVE INOCULATION WITH HEAT KILLED TUBERCLE BACILLI. *J. Exp. Med.* **66**, 761-788, doi:10.1084/jem.66.6.761 (1937).

313 Freund, J. & Opie, E. L. SENSITIZATION AND ANTIBODY FORMATION WITH INCREASED RESISTANCE TO TUBERCULOUS INFECTION INDUCED BY HEAT KILLED TUBERCLE BACILLI. *J. Exp. Med.* **68**, 273-298, doi:10.1084/jem.68.2.273 (1938).

314 Freund, J. & Thomson, K. J. A SIMPLE, RAPID TECHNIC OF PREPARING WATER-IN-OIL EMULSIONS OF PENICILLIN, DRUGS AND BIOLOGICS. *Science* **101**, 468-469, doi:10.1126/science.101.2627.468-a (1945).

315 Freund, J., Sommer, H. E. & Walter, A. W. IMMUNIZATION AGAINST MALARIA: VACCINATION OF DUCKS WITH KILLED PARASITES INCORPORATED WITH ADJUVANTS. *Science* **102**, 200-202, doi:10.1126/science.102.2643.200 (1945).

316 Freund, J., Thomson, K. J., Sommer, H. E., Walter, A. W. & Schenkein, E. L. IMMUNIZATION OF RHESUS MONKEYS AGAINST MALARIAL INFECTION (P. KNOWLESI) WITH KILLED PARASITES AND ADJUVANTS. *Science* **102**, 202-204, doi:10.1126/science.102.2643.202 (1945).

317 Freund, J., Stern, E. R. & Pisani, T. M. Isoallergic encephalomyelitis and radiculitis in guinea pigs after one injection of brain and Mycobacteria in water-in-oil emulsion. *J. Immunol.* **57**, 179-194 (1947).

318 Freund, J. & McDermott, K. Sensitization to Horse Serum by Means of Adjuvants. *Proc. Soc. Exp. Biol. Med.* **49**, 548-553, doi:10.3181/00379727-49-13625 (1942).

319 Freund, J., Lipton, M. M. & Thompson, G. E. Aspermatogenesis in the guinea pig induced by testicular tissue and adjuvants. *J. Exp. Med.* **97**, 711-726, doi:10.1084/jem.97.5.711 (1953).

320 Chase, M. W. & Landsteiner, K. Experiments on Transfer of Cutaneous Sensitivity to Simple Compounds. *Proc. Soc. Exp. Biol. Med.* **49**, 688-690 (1942).

321 Chase, M. W. The Cellular Transfer of Cutaneous Hypersensitivity to Tuberculin. *Proc. Soc. Exp. Biol. Med.* **59**, 134-135 (1945).

322 Vogel, F. R. Improving Vaccine Performance with Adjuvants. *Clin. Infect. Dis.* **30**, S266–270 (2000).

323 Courtenay, J. S., Dallman, M. J., Dayan, A. D., Martin, A. & Mosedale, B. Immunisation against heterologous type II collagen induces arthritis in mice. *Nature* **283**, 666-668, doi:10.1038/283666a0 (1980).

324 Caspi, R. R. *et al.* A new model of autoimmune disease. Experimental autoimmune uveoretinitis induced in mice with two different retinal antigens. *J. Immunol.* **140**, 1490-1495 (1988).

325 Lee, J. M. & Olitsky, P. K. Simple method for enhancing development of acute disseminated encephalomyelitis in mice. *Proc. Soc. Exp. Biol. Med.* **89**, 263-266, doi:10.3181/00379727-89-21778 (1955).

326 Freund, J. The mode of action of immunologic adjuvants. *Bibl. Tuberc.*, 130-148 (1956).

327 Baxter, A. G. The origin and application of experimental autoimmune encephalomyelitis. *Nat. Rev. Immunol.* **7**, 904-912 (2007).

328 Lachance, D. H. *et al.* An outbreak of neurological autoimmunity with polyradiculoneuropathy in workers exposed to aerosolised porcine neural tissue: a descriptive study. *Lancet Neurol.* **9**, 55-66, doi:10.1016/s1474-4422(09)70296-0 (2010).

329 Kabat, E. A., Wolf, A. & Bezer, A. E. Rapid Production of Acute Disseminated Encephalomyelitis in Rhesus Monkeys by Injection of Brain Tissue With Adjuvants. *Science* **104**, 362-363, doi:10.1126/science.104.2703.362 (1946).

330 Morgan, I. M. ALLERGIC ENCEPHALOMYELITIS IN MONKEYS IN RESPONSE TO INJECTION OF NORMAL MONKEY NERVOUS TISSUE. *J. Exp. Med.* **85**, 131-140, doi:10.1084/jem.85.1.131 (1947).

331 Berard, J. L., Wolak, K., Fournier, S. & David, S. Characterization of relapsing-remitting and chronic forms of experimental autoimmune encephalomyelitis in C57BL/6 mice. *Glia* **58**, 434-445, doi:10.1002/glia.20935 (2010).

332 Linthicum, D. S., Munoz, J. J. & Blaskett, A. Acute experimental autoimmune encephalomyelitis in mice. I. Adjuvant action of *Bordetella pertussis* is due to vasoactive amine sensitization and increased vascular permeability of the central nervous system. *Cell. Immunol.* **73**, 299-310, doi:10.1016/0008-8749(82)90457-9 (1982).

333 Shive, C. L., Hofstetter, H., Arredondo, L., Shaw, C. & Forsthuber, T. G. The enhanced antigen-specific production of cytokines induced by pertussis toxin is due to clonal expansion of T cells and not to altered effector functions of long-term memory cells. *Eur. J. Immunol.* **30**, 2422-2431, doi:10.1002/1521-4141(2000)30:8<2422::Aid-immu2422>3.0.Co;2-h (2000).

334 Hofstetter, H. H., Shive, C. L. & Forsthuber, T. G. Pertussis toxin modulates the immune response to neuroantigens injected in incomplete Freund's adjuvant: induction of Th1

cells and experimental autoimmune encephalomyelitis in the presence of high frequencies of Th2 cells. *J. Immunol.* **169**, 117-125, doi:10.4049/jimmunol.169.1.117 (2002).

335 Kerfoot, S. M. *et al.* TLR4 contributes to disease-inducing mechanisms resulting in central nervous system autoimmune disease. *J. Immunol.* **173**, 7070-7077, doi:10.4049/jimmunol.173.11.7070 (2004).

336 Waldner, H., Collins, M. & Kuchroo, V. K. Activation of antigen-presenting cells by microbial products breaks self tolerance and induces autoimmune disease. *J. Clin. Invest.* **113**, 990-997, doi:10.1172/jci19388 (2004).

337 Constantinescu, C. S., Farooqi, N., O'Brien, K. & Gran, B. Experimental autoimmune encephalomyelitis (EAE) as a model for multiple sclerosis (MS). *Br. J. Pharmacol.* **164**, 1079-1106, doi:10.1111/bph.2011.164.issue-4 (2011).

338 Adam, A., Ellouz, F., Ciorbaru, R., Petit, J. F. & Lederer, E. Peptidoglycan adjuvants: minimal structure required for activity. *Z. Immunitatsforsch. Exp. Klin. Immunol.* **149**, 341-348 (1975).

339 Guryanova, S. V. & Khaitov, R. M. Strategies for Using Muramyl Peptides - Modulators of Innate Immunity of Bacterial Origin - in Medicine. *Front. Immunol.* **12**, 607178, doi:10.3389/fimmu.2021.607178 (2021).

340 Abrahams, K. A. & Besra, G. S. Mycobacterial cell wall biosynthesis: a multifaceted antibiotic target. *Parasitology* **145**, 116-133, doi:10.1017/s0031182016002377 (2018).

341 Rubino, S. J. *et al.* Identification of a synthetic muramyl peptide derivative with enhanced Nod2 stimulatory capacity. *Innate Immun.* **19**, 493-503, doi:10.1177/1753425912471691 (2013).

342 Chen, K. T. *et al.* Synthesis of Diverse *N*-Substituted Muramyl Dipeptide Derivatives and Their Use in a Study of Human NOD2 Stimulation Activity. *Chemistry (Easton)* **21**, 11984-11988, doi:10.1002/chem.201501557 (2015).

343 Melnyk, J. E., Mohanan, V., Schaefer, A. K., Hou, C. W. & Grimes, C. L. Peptidoglycan Modifications Tune the Stability and Function of the Innate Immune Receptor Nod2. *J. Am. Chem. Soc.* **137**, 6987-6990, doi:10.1021/jacs.5b01607 (2015).

344 Xing, S. & Gleason, J. L. A robust synthesis of *N*-glycolyl muramyl dipeptide *via* azidonitration/reduction. *Org. Biomol. Chem.* **13**, 1515-1520, doi:10.1039/c4ob02147a (2015).

345 Ogawa, C., Liu, Y. J. & Kobayashi, K. S. Muramyl dipeptide and its derivatives: peptide adjuvant in immunological disorders and cancer therapy. *Curr Bioact Compd* **7**, 180-197, doi:10.2174/157340711796817913 (2011).

346 Grimes, C. L., Podolsky, D. K. & O'Shea, E. K. Synthesis of biologically active biotinylated muramyl dipeptides. *Bioorg. Med. Chem. Lett.* **20**, 6061-6063, doi:10.1016/j.bmcl.2010.08.056 (2010).

347 Grimes, C. L., Ariyananda Lde, Z., Melnyk, J. E. & O'Shea, E. K. The innate immune protein Nod2 binds directly to MDP, a bacterial cell wall fragment. *J. Am. Chem. Soc.* **134**, 13535-13537, doi:10.1021/ja303883c (2012).

348 Kobayashi, K. S. *et al.* Nod2-dependent regulation of innate and adaptive immunity in the intestinal tract. *Science* **307**, 731-734, doi:10.1126/science.1104911 (2005).

349 Wolfert, M. A., Murray, T. F., Boons, G. J. & Moore, J. N. The origin of the synergistic effect of muramyl dipeptide with endotoxin and peptidoglycan. *J. Biol. Chem.* **277**, 39179-39186, doi:10.1074/jbc.M204885200 (2002).

350 Davis, K. M., Nakamura, S. & Weiser, J. N. Nod2 sensing of lysozyme-digested peptidoglycan promotes macrophage recruitment and clearance of *S. pneumoniae* colonization in mice. *J. Clin. Invest.* **121**, 3666-3676, doi:10.1172/jci57761 (2011).

351 Nakamura, N. *et al.* Endosomes are specialized platforms for bacterial sensing and NOD2 signalling. *Nature* **509**, 240-244, doi:10.1038/nature13133 (2014).

352 Ismair, M. G. *et al.* hPepT1 selectively transports muramyl dipeptide but not Nod1-activating muramyl peptides. *Can. J. Physiol. Pharmacol.* **84**, 1313-1319, doi:10.1139/y06-076 (2006).

353 Charrière, G. M. *et al.* Identification of *Drosophila* Yin and PEPT2 as evolutionarily conserved phagosome-associated muramyl dipeptide transporters. *J. Biol. Chem.* **285**, 20147-20154, doi:10.1074/jbc.M110.115584 (2010).

354 Marina-García, N. *et al.* Clathrin- and dynamin-dependent endocytic pathway regulates muramyl dipeptide internalization and NOD2 activation. *J. Immunol.* **182**, 4321-4327, doi:10.4049/jimmunol.0802197 (2009).

355 Lee, J. *et al.* pH-dependent internalization of muramyl peptides from early endosomes enables Nod1 and Nod2 signaling. *J. Biol. Chem.* **284**, 23818-23829, doi:10.1074/jbc.M109.033670 (2009).

356 Schaefer, A. K. *et al.* Membrane Association Dictates Ligand Specificity for the Innate Immune Receptor NOD2. *ACS Chem. Biol.* **12**, 2216-2224, doi:10.1021/acschembio.7b00469 (2017).

357 Dixon, C. L. & Fairn, G. D. *S*-palmitoylation of NOD2 controls its localization to the plasma membrane. *J. Lipid Res.* **62**, doi:10.1016/j.jlr.2021.100097 (2021).

358 Lu, Y. *et al.* Palmitoylation of NOD1 and NOD2 is required for bacterial sensing. *Science* **366**, 460-467, doi:10.1126/science.aau6391 (2019).

359 Lauro, M. L., D'Ambrosio, E. A., Bahnson, B. J. & Grimes, C. L. Molecular Recognition of Muramyl Dipeptide Occurs in the Leucine-rich Repeat Domain of Nod2. *ACS Infect Dis* **3**, 264-270, doi:10.1021/acsinfecdis.6b00154 (2017).

360 Mo, J. *et al.* Pathogen sensing by nucleotide-binding oligomerization domain-containing protein 2 (NOD2) is mediated by direct binding to muramyl dipeptide and ATP. *J. Biol. Chem.* **287**, 23057-23067, doi:10.1074/jbc.M112.344283 (2012).

361 Guan, R. *et al.* Structural basis for peptidoglycan binding by peptidoglycan recognition proteins. *Proc. Natl. Acad. Sci. U. S. A.* **101**, 17168-17173, doi:10.1073/pnas.0407856101 (2004).

362 Guan, R. *et al.* Crystal structure of human peptidoglycan recognition protein I alpha bound to a muramyl pentapeptide from Gram-positive bacteria. *Protein Sci.* **15**, 1199-1206, doi:10.1110/ps.062077606 (2006).

363 Sharma, P. *et al.* Multiligand specificity of pathogen-associated molecular pattern-binding site in peptidoglycan recognition protein. *J. Biol. Chem.* **286**, 31723-31730, doi:10.1074/jbc.M111.264374 (2011).

364 Duerr, C. U. *et al.* Control of intestinal Nod2-mediated peptidoglycan recognition by epithelium-associated lymphocytes. *Mucosal Immunol.* **4**, 325-334, doi:10.1038/mi.2010.71 (2011).

365 Faustin, B. *et al.* Reconstituted NALP1 Inflammasome Reveals Two-Step Mechanism of Caspase-1 Activation. *Mol. Cell* **25**, 713-724, doi:https://doi.org/10.1016/j.molcel.2007.01.032 (2007).

366 Reubold, T. F., Hahne, G., Wohlgemuth, S. & Eschenburg, S. Crystal structure of the leucine-rich repeat domain of the NOD-like receptor NLRP1: implications for binding of muramyl dipeptide. *FEBS Lett.* **588**, 3327-3332, doi:10.1016/j.febslet.2014.07.017 (2014).

367 Verschoor, C. P. *et al.* Circulating muramyl dipeptide is negatively associated with interleukin-10 in the frail elderly. *Inflammation* **38**, 272-277, doi:10.1007/s10753-014-0030-z (2015).

368 Hampe, J. *et al.* Association between insertion mutation in NOD2 gene and Crohn's disease in German and British populations. *Lancet* **357**, 1925-1928, doi:10.1016/s0140-6736(00)05063-7 (2001).

369 Hugot, J. P. *et al.* Association of NOD2 leucine-rich repeat variants with susceptibility to Crohn's disease. *Nature* **411**, 599-603, doi:10.1038/35079107 (2001).

370 Ogura, Y. *et al.* A frameshift mutation in NOD2 associated with susceptibility to Crohn's disease. *Nature* **411**, 603-606, doi:10.1038/35079114 (2001).

371 Miceli-Richard, C. *et al.* CARD15 mutations in Blau syndrome. *Nat. Genet.* **29**, 19-20, doi:10.1038/ng720 (2001).

372 Behr, M. A., Semret, M., Poon, A. & Schurr, E. Crohn's disease, mycobacteria, and NOD2. *Lancet Infect. Dis.* **4**, 136-137, doi:10.1016/s1473-3099(04)00935-1 (2004).

373 Sechi, L. A. *et al. Mycobacterium avium* sub. *paratuberculosis* in tissue samples of Crohn's disease patients. *New Microbiol.* **27**, 75-77 (2004).

374 Ferwerda, G. *et al.* Mycobacterium paratuberculosis is recognized by Toll-like receptors and NOD2. *J. Leukoc. Biol.* **82**, 1011-1018, doi:10.1189/jlb.0307147 (2007).

375 Zanello, G. *et al.* The Cytosolic Microbial Receptor Nod2 Regulates Small Intestinal Crypt Damage and Epithelial Regeneration following T Cell–Induced Enteropathy. *The Journal of Immunology* **197**, 345-355, doi:10.4049/jimmunol.1600185 (2016).

376 Mukherjee, T. *et al.* NOD1 and NOD2 in inflammation, immunity and disease. *Arch. Biochem. Biophys.* **670**, 69-81, doi:10.1016/j.abb.2018.12.022 (2019).

377 Berrebi, D. *et al.* Card15 gene overexpression in mononuclear and epithelial cells of the inflamed Crohn's disease colon. *Gut* **52**, 840-846, doi:10.1136/gut.52.6.840 (2003).

378 Ogura, Y. *et al.* Expression of NOD2 in Paneth cells: a possible link to Crohn's ileitis. *Gut* **52**, 1591-1597, doi:10.1136/gut.52.11.1591 (2003).

379 Tanabe, T. *et al.* Regulatory regions and critical residues of NOD2 involved in muramyl dipeptide recognition. *EMBO J.* **23**, 1587-1597, doi:10.1038/sj.emboj.7600175 (2004).

380 Cuthbert, A. P. *et al.* The contribution of NOD2 gene mutations to the risk and site of disease in inflammatory bowel disease. *Gastroenterology* **122**, 867-874, doi:10.1053/gast.2002.32415 (2002).

381 Lesage, S. *et al.* CARD15/NOD2 mutational analysis and genotype-phenotype correlation in 612 patients with inflammatory bowel disease. *Am. J. Hum. Genet.* **70**, 845-857, doi:10.1086/339432 (2002).

382 Pascoe, L., Zouali, H., Sahbatou, M. & Hugot, J.-P. Estimating the odds ratios of Crohn disease for the main CARD15/NOD2 mutations using a conditional maximum likelihood method in pedigrees collected via affected family members. *Eur. J. Hum. Genet.* **15**, 864-871, doi:10.1038/sj.ejhg.5201839 (2007).

383 Dugan, J. *et al.* Blau syndrome-associated *Nod2* mutation alters expression of full-length NOD2 and limits responses to muramyl dipeptide in knock-in mice. *J. Immunol.* **194**, 349-357, doi:10.4049/jimmunol.1402330 (2015).

384 Martin, T. M. *et al.* The NOD2 defect in Blau syndrome does not result in excess interleukin-1 activity. *Arthritis Rheum.* **60**, 611-618, doi:10.1002/art.24222 (2009).

385 Son, S. *et al.* Altered cytokine profiles of mononuclear cells after stimulation in a patient with Blau syndrome. *Rheumatol. Int.* **30**, 1121-1124, doi:10.1007/s00296-009-1342-4 (2010).

386 Galozzi, P. *et al. Ex vivo* and *in vitro* production of pro-inflammatory cytokines in Blau syndrome. *Reumatismo* **66**, 277-284, doi:10.4081/reumatismo.2014.772 (2015).

387 Okafuji, I. *et al.* Role of the NOD2 genotype in the clinical phenotype of Blau syndrome and early-onset sarcoidosis. *Arthritis Rheum.* **60**, 242-250, doi:10.1002/art.24134 (2009).

388 Berrington, W. R. *et al.* Common polymorphisms in the *NOD2* gene region are associated with leprosy and its reactive states. *J. Infect. Dis.* **201**, 1422-1435, doi:10.1086/651559 (2010).

389 Leturiondo, A. L. *et al.* Association of NOD2 and IFNG single nucleotide polymorphisms with leprosy in the Amazon ethnic admixed population. *PLoS Negl. Trop. Dis.* **14**, e0008247, doi:10.1371/journal.pntd.0008247 (2020).

390 Sales-Marques, C. *et al.* NOD2 and CCDC122-LACC1 genes are associated with leprosy susceptibility in Brazilians. *Hum. Genet.* **133**, 1525-1532, doi:10.1007/s00439-014-1502-9 (2014).

391 Sales-Marques, C. *et al.* Genetic polymorphisms of the *IL6* and *NOD2* genes are risk factors for inflammatory reactions in leprosy. *PLoS Negl. Trop. Dis.* **11**, e0005754, doi:10.1371/journal.pntd.0005754 (2017).

392 Hall, N. B. *et al.* Polymorphisms in *TICAM2* and *IL1B* are associated with TB. *Genes Immun.* **16**, 127-133, doi:10.1038/gene.2014.77 (2015).

393 Lécine, P. *et al.* The NOD2-RICK complex signals from the plasma membrane. *J. Biol. Chem.* **282**, 15197-15207, doi:10.1074/jbc.M606242200 (2007).

394 Ogura, Y. *et al.* Nod2, a Nod1/Apaf-1 family member that is restricted to monocytes and activates NF-kappaB. *J. Biol. Chem.* **276**, 4812-4818, doi:10.1074/jbc.M008072200 (2001).

395 Park, J. H. *et al.* RICK/RIP2 mediates innate immune responses induced through Nod1 and Nod2 but not TLRs. *J. Immunol.* **178**, 2380-2386, doi:10.4049/jimmunol.178.4.2380 (2007).

396 Trindade, B. C. & Chen, G. Y. NOD1 and NOD2 in inflammatory and infectious diseases. *Immunol. Rev.* **297**, 139-161, doi:10.1111/imr.12902 (2020).

397 Sabbah, A. *et al.* Activation of innate immune antiviral responses by NOD2. *Nat. Immunol.* **10**, 1073-1080, doi:10.1038/ni.1782 (2009).

398 Morosky, S. A., Zhu, J., Mukherjee, A., Sarkar, S. N. & Coyne, C. B. Retinoic acid-induced gene-I (RIG-I) associates with nucleotide-binding oligomerization domain-2 (NOD2) to negatively regulate inflammatory signaling. *J. Biol. Chem.* **286**, 28574-28583, doi:10.1074/jbc.M111.227942 (2011).

399 Shaw, M. H. *et al.* T cell-intrinsic role of Nod2 in promoting type 1 immunity to Toxoplasma gondii. *Nat. Immunol.* **10**, 1267-1274, doi:10.1038/ni.1816 (2009).

400 Caetano, B. C. *et al.* Intrinsic expression of Nod2 in CD4+ T lymphocytes is not necessary for the development of cell-mediated immunity and host resistance to Toxoplasma gondii. *Eur. J. Immunol.* **41**, 3627-3631, doi:10.1002/eji.201141876 (2011).

401 Cooney, R. *et al.* NOD2 stimulation induces autophagy in dendritic cells influencing bacterial handling and antigen presentation. *Nat. Med.* **16**, 90-97, doi:10.1038/nm.2069 (2010).

402 Travassos, L. H. *et al.* Nod1 and Nod2 direct autophagy by recruiting ATG16L1 to the plasma membrane at the site of bacterial entry. *Nat. Immunol.* **11**, 55-62, doi:10.1038/ni.1823 (2010).

403 Hampe, J. *et al.* A genome-wide association scan of nonsynonymous SNPs identifies a susceptibility variant for Crohn disease in *ATG16L1*. *Nat. Genet.* **39**, 207-211, doi:10.1038/ng1954 (2007).

404 Rioux, J. D. *et al.* Genome-wide association study identifies new susceptibility loci for Crohn disease and implicates autophagy in disease pathogenesis. *Nat. Genet.* **39**, 596-604, doi:10.1038/ng2032 (2007).

405 Zhang, Q. *et al.* Commensal bacteria direct selective cargo sorting to promote symbiosis. *Nat. Immunol.* **16**, 918-926, doi:10.1038/ni.3233 (2015).

406 Yan, R. & Liu, Z. LRRK2 enhances Nod1/2-mediated inflammatory cytokine production by promoting Rip2 phosphorylation. *Protein Cell* **8**, 55-66, doi:10.1007/s13238-016-0326-x (2017).

407 Wang, H. *et al.* Rip2 Is Required for Nod2-Mediated Lysozyme Sorting in Paneth Cells. *J. Immunol.* **198**, 3729-3736, doi:10.4049/jimmunol.1601583 (2017).

408 Barrett, J. C. *et al.* Genome-wide association defines more than 30 distinct susceptibility loci for Crohn's disease. *Nat. Genet.* **40**, 955-962, doi:10.1038/ng.175 (2008).

409 Fava, V. M. *et al.* A Missense *LRRK2* Variant Is a Risk Factor for Excessive Inflammatory Responses in Leprosy. *PLoS Negl. Trop. Dis.* **10**, e0004412, doi:10.1371/journal.pntd.0004412 (2016).

410 Liu, T. C. *et al. LRRK2* but not *ATG16L1* is associated with Paneth cell defect in Japanese Crohn's disease patients. *JCI Insight* **2**, e91917, doi:10.1172/jci.insight.91917 (2017).

411 Rivas, M. A. *et al.* Insights into the genetic epidemiology of Crohn's and rare diseases in the Ashkenazi Jewish population. *PLoS Genet* **14**, e1007329, doi:10.1371/journal.pgen.1007329 (2018).

412 Keestra-Gounder, A. M. *et al.* NOD1 and NOD2 signalling links ER stress with inflammation. *Nature* **532**, 394-397, doi:10.1038/nature17631 (2016).

413 Singh, K. *et al.* Parkin targets NOD2 to regulate astrocyte endoplasmic reticulum stress and inflammation. *Glia* **66**, 2427-2437, doi:10.1002/glia.23482 (2018).

414 Pham, O. H. *et al.* NOD1/NOD2 and RIP2 Regulate Endoplasmic Reticulum Stress-Induced Inflammation during Chlamydia Infection. *mBio* **11**, doi:10.1128/mBio.00979-20 (2020).

415 Fritz, T., Niederreiter, L., Adolph, T., Blumberg, R. S. & Kaser, A. Crohn's disease: NOD2, autophagy and ER stress converge. *Gut* **60**, 1580-1588, doi:10.1136/gut.2009.206466 (2011).

416 Dubos, R. J. CELLULAR STRUCTURES AND FUNCTIONS CONCERNED IN PARASITISM. *Bacteriol. Rev.* **12**, 173-194, doi:10.1128/br.12.3.173-194.1948 (1948).

417 Bloch, H. Studies on the virulence of tubercle bacilli; isolation and biological properties of a constituent of virulent organisms. *J. Exp. Med.* **91**, 197-218, pl, doi:10.1084/jem.91.2.197 (1950).

418 Noll, H., Bloch, H., Asselineau, J. & Lederer, E. The chemical structure of the cord factor of *Mycobacterium tuberculosis*. *Biochim. Biophys. Acta* **20**, 299-309, doi:10.1016/0006-3002(56)90289-x (1956).

419 Behling, C. A., Bennett, B., Takayama, K. & Hunter, R. L. Development of a trehalose 6,6'-dimycolate model which explains cord formation by *Mycobacterium tuberculosis*. *Infect. Immun.* **61**, 2296-2303, doi:doi:10.1128/iai.61.6.2296-2303.1993 (1993).

420 van Dissel, J. T. *et al.* A novel liposomal adjuvant system, CAF01, promotes long-lived *Mycobacterium tuberculosis*-specific T-cell responses in human. *Vaccine* **32**, 7098-7107, doi:10.1016/j.vaccine.2014.10.036 (2014).

421 Abraham, S. *et al.* Safety and immunogenicity of the chlamydia vaccine candidate CTH522 adjuvanted with CAF01 liposomes or aluminium hydroxide: a first-in-human, randomised, double-blind, placebo-controlled, phase 1 trial. *Lancet Infect. Dis.* **19**, 1091-1100, doi:10.1016/s1473-3099(19)30279-8 (2019).

422 Dejon-Agobe, J. C. *et al.* Controlled Human Malaria Infection of Healthy Adults With Lifelong Malaria Exposure to Assess Safety, Immunogenicity, and Efficacy of the Asexual Blood Stage Malaria Vaccine Candidate GMZ2. *Clin. Infect. Dis.* **69**, 1377-1384, doi:10.1093/cid/ciy1087 (2019).

423 Nouatin, O. *et al.* Effect of immune regulatory pathways after immunization with GMZ2 malaria vaccine candidate in healthy lifelong malaria-exposed adults. *Vaccine* **38**, 4263-4272, doi:10.1016/j.vaccine.2020.04.046 (2020).

424 Fay, A. *et al.* Two Accessory Proteins Govern MmpL3 Mycolic Acid Transport in Mycobacteria. *mBio* **10**, doi:10.1128/mBio.00850-19 (2019).

425 Batt, S. M., Minnikin, D. E. & Besra, G. S. The thick waxy coat of mycobacteria, a protective layer against antibiotics and the host's immune system. *Biochem. J.* **477**, 1983-2006, doi:10.1042/bcj20200194 (2020).

426 Abrahams, K. A. & Besra, G. S. Synthesis and recycling of the mycobacterial cell envelope. *Curr. Opin. Microbiol.* **60**, 58-65, doi:10.1016/j.mib.2021.01.012 (2021).

427 Kugler, J. H., Le Roes-Hill, M., Syldatk, C. & Hausmann, R. Surfactants tailored by the class *Actinobacteria*. *Front Microbiol* **6**, 212, doi:10.3389/fmicb.2015.00212 (2015).

428 Decout, A. *et al.* Rational design of adjuvants targeting the C-type lectin Mincle. *Proc. Natl. Acad. Sci. U. S. A.* **114**, 2675-2680, doi:10.1073/pnas.1612421114 (2017).

429 Schoenen, H. *et al.* Cutting edge: Mincle is essential for recognition and adjuvanticity of the mycobacterial cord factor and its synthetic analog trehalose-dibehenate. *J. Immunol.* **184**, 2756-2760, doi:10.4049/jimmunol.0904013 (2010).

430 Matsumoto, M. *et al.* A novel LPS-inducible C-type lectin is a transcriptional target of NF-IL6 in macrophages. *J. Immunol.* **163**, 5039-5048 (1999).

431 Yamasaki, S. *et al.* Mincle is an ITAM-coupled activating receptor that senses damaged cells. *Nat. Immunol.* **9**, 1179-1188, doi:10.1038/ni.1651 (2008).

432 Bugarcic, A. *et al.* Human and mouse macrophage-inducible C-type lectin (Mincle) bind *Candida albicans*. *Glycobiology* **18**, 679-685, doi:10.1093/glycob/cwn046 (2008).

433 Wells, C. A. *et al.* The macrophage-inducible C-type lectin, mincle, is an essential component of the innate immune response to *Candida albicans*. *J. Immunol.* **180**, 7404-7413, doi:10.4049/jimmunol.180.11.7404 (2008).

434 Yamasaki, S. *et al.* C-type lectin Mincle is an activating receptor for pathogenic fungus, *Malassezia*. *Proc. Natl. Acad. Sci. U. S. A.* **106**, 1897-1902, doi:10.1073/pnas.0805177106 (2009).

435 Kabuye, D., Chu, Y., Lao, W., Jin, G. & Kang, H. Association between *CLEC4E* gene polymorphism of mincle and pulmonary tuberculosis infection in a northern Chinese population. *Gene* **710**, 24-29, doi:10.1016/j.gene.2019.05.011 (2019).

436 Feinberg, H. *et al.* Mechanism for recognition of an unusual mycobacterial glycolipid by the macrophage receptor mincle. *J. Biol. Chem.* **288**, 28457-28465, doi:10.1074/jbc.M113.497149 (2013).

437 Ivashkiv, L. B. Cross-regulation of signaling by ITAM-associated receptors. *Nat. Immunol.* **10**, 340-347, doi:10.1038/ni.1706 (2009).

438 Ruland, J. & Hartjes, L. CARD–BCL-10–MALT1 signalling in protective and pathological immunity. *Nature Reviews Immunology* **19**, 118-134, doi:10.1038/s41577-018-0087-2 (2019).

439 Shenderov, K. *et al.* Cord factor and peptidoglycan recapitulate the Th17-promoting adjuvant activity of mycobacteria through Mincle/CARD9 signaling and the inflammasome. *J. Immunol.* **190**, 5722-5730, doi:10.4049/jimmunol.1203343 (2013).

440 Hsu, Y. M. *et al.* The adaptor protein CARD9 is required for innate immune responses to intracellular pathogens. *Nat. Immunol.* **8**, 198-205, doi:10.1038/ni1426 (2007).

441 Reiling, N. *et al.* Cutting edge: Toll-like receptor (TLR)2- and TLR4-mediated pathogen recognition in resistance to airborne infection with *Mycobacterium tuberculosis*. *J. Immunol.* **169**, 3480-3484, doi:10.4049/jimmunol.169.7.3480 (2002).

442 Báfica, A., Scanga, C. A., Schito, M. L., Hieny, S. & Sher, A. Cutting edge: in vivo induction of integrated HIV-1 expression by mycobacteria is critically dependent on Toll-like receptor 2. *J. Immunol.* **171**, 1123-1127, doi:10.4049/jimmunol.171.3.1123 (2003).

443 Tjärnlund, A., Guirado, E., Julián, E., Cardona, P. J. & Fernández, C. Determinant role for Toll-like receptor signalling in acute mycobacterial infection in the respiratory tract. *Microbes Infect* **8**, 1790-1800, doi:10.1016/j.micinf.2006.02.017 (2006).

444 Carlos, D. *et al.* TLR2-dependent mast cell activation contributes to the control of *Mycobacterium tuberculosis* infection. *Microbes Infect* **11**, 770-778, doi:10.1016/j.micinf.2009.04.025 (2009).

445 Teixeira-Coelho, M. *et al.* TLR2 deficiency by compromising p19 (IL-23) expression limits Th 17 cell responses to *Mycobacterium tuberculosis*. *Int. Immunol.* **23**, 89-96, doi:10.1093/intimm/dxq459 (2011).

446 Choi, H. H. *et al.* Effects of mycobacterial infection on proliferation of hematopoietic precursor cells. *Microbes Infect* **13**, 1252-1260, doi:10.1016/j.micinf.2011.08.001 (2011).

447 McBride, A., Bhatt, K. & Salgame, P. Development of a secondary immune response to *Mycobacterium tuberculosis* is independent of Toll-like receptor 2. *Infect. Immun.* **79**, 1118-1123, doi:10.1128/iai.01076-10 (2011).

448 McBride, A., Konowich, J. & Salgame, P. Host defense and recruitment of $Foxp3^{+}$ T regulatory cells to the lungs in chronic *Mycobacterium tuberculosis* infection requires Toll-like receptor 2. *PLoS Pathog.* **9**, e1003397, doi:10.1371/journal.ppat.1003397 (2013).

449 Konowich, J. *et al.* Divergent Functions of TLR2 on Hematopoietic and Nonhematopoietic Cells during Chronic *Mycobacterium tuberculosis* Infection. *J. Immunol.* **198**, 741-748, doi:10.4049/jimmunol.1601651 (2017).

450 Gopalakrishnan, A., Dietzold, J., Verma, S., Bhagavathula, M. & Salgame, P. Toll-like Receptor 2 Prevents Neutrophil-Driven Immunopathology during Infection with *Mycobacterium tuberculosis* by Curtailing CXCL5 Production. *Infect. Immun.* **87**, doi:10.1128/iai.00760-18 (2019).

451 Blumenthal, A. *et al.* RP105 facilitates macrophage activation by *Mycobacterium tuberculosis* lipoproteins. *Cell Host Microbe* **5**, 35-46, doi:10.1016/j.chom.2008.12.002 (2009).

452 Abel, B. *et al.* Toll-like receptor 4 expression is required to control chronic *Mycobacterium tuberculosis* infection in mice. *J. Immunol.* **169**, 3155-3162, doi:10.4049/jimmunol.169.6.3155 (2002).

453 Kamath, A. B., Alt, J., Debbabi, H. & Behar, S. M. Toll-like receptor 4-defective C3H/HeJ mice are not more susceptible than other C3H substrains to infection with *Mycobacterium tuberculosis*. *Infect. Immun.* **71**, 4112-4118, doi:10.1128/iai.71.7.4112-4118.2003 (2003).

454 Shim, T. S., Turner, O. C. & Orme, I. M. Toll-like receptor 4 plays no role in susceptibility of mice to *Mycobacterium tuberculosis* infection. *Tuberculosis (Edinb)* **83**, 367-371, doi:10.1016/s1472-9792(03)00071-4 (2003).

455 Branger, J. *et al.* Toll-like receptor 4 plays a protective role in pulmonary tuberculosis in mice. *Int. Immunol.* **16**, 509-516, doi:10.1093/intimm/dxh052 (2004).

456 Park, J. *et al.* Toll-like receptor 4 signaling-mediated responses are critically engaged in optimal host protection against highly virulent *Mycobacterium tuberculosis* K infection. *Virulence* **11**, 430-445, doi:10.1080/21505594.2020.1766401 (2020).

457 Branger, J. *et al.* Lipopolysaccharide binding protein-deficient mice have a normal defense against pulmonary mycobacterial infection. *Clin. Immunol.* **116**, 174-181, doi:10.1016/j.clim.2005.03.014 (2005).

458 Gopalakrishnan, A., Dietzold, J. & Salgame, P. Vaccine-mediated immunity to experimental *Mycobacterium tuberculosis* is not impaired in the absence of Toll-like receptor 9. *Cell. Immunol.* **302**, 11-18, doi:10.1016/j.cellimm.2015.12.009 (2016).

459 Wieland, C. W. *et al.* Mice lacking SIGNR1 have stronger T helper 1 responses to *Mycobacterium tuberculosis*. *Microbes Infect* **9**, 134-141, doi:10.1016/j.micinf.2006.10.018 (2007).

460 Heitmann, L., Schoenen, H., Ehlers, S., Lang, R. & Holscher, C. Mincle is not essential for controlling *Mycobacterium tuberculosis* infection. *Immunobiology* **218**, 506-516, doi:10.1016/j.imbio.2012.06.005 (2013).

461 Lee, W. B. *et al.* Neutrophils Promote Mycobacterial Trehalose Dimycolate-Induced Lung Inflammation via the Mincle Pathway. *PLoS Pathog.* **8**, e1002614, doi:10.1371/journal.ppat.1002614 (2012).

462 Walter, K., Hölscher, C., Tschopp, J. & Ehlers, S. NALP3 is not necessary for early protection against experimental tuberculosis. *Immunobiology* **215**, 804-811, doi:10.1016/j.imbio.2010.05.015 (2010).

463 Dorhoi, A. *et al.* Activation of the NLRP3 inflammasome by *Mycobacterium tuberculosis* is uncoupled from susceptibility to active tuberculosis. *Eur. J. Immunol.* **42**, 374-384, doi:10.1002/eji.201141548 (2012).

464 Allen, I. C. *et al.* Characterization of NLRP12 during the *In Vivo* Host Immune Response to *Klebsiella pneumoniae* and *Mycobacterium tuberculosis*. *PLoS One* **8**, e60842, doi:10.1371/journal.pone.0060842 (2013).

465 Hu, S. *et al.* NLRC3 negatively regulates CD4+ T cells and impacts protective immunity during *Mycobacterium tuberculosis* infection. *PLoS Pathog.* **14**, e1007266, doi:10.1371/journal.ppat.1007266 (2018).

466 Bekierkunst, A. Acute Granulomatous Response Produced in Mice by Trehalose-6,6-Dimycolate. *J. Bacteriol.* **96**, 958-961 (1968).

467 Shigeru, K. *et al.* Synthesis of Muramyl Dipeptide Analogs with Enhanced Adjuvant Activity. *Bull. Chem. Soc. Japan* **53**, 2570-2577 (1980).

468 Merad, M., Sathe, P., Helft, J., Miller, J. & Mortha, A. The dendritic cell lineage: ontogeny and function of dendritic cells and their subsets in the steady state and the inflamed setting. *Annu. Rev. Immunol.* **31**, 563-604, doi:10.1146/annurev-immunol-020711-074950 (2013).

469 Odendall, C. & Kagan, J. C. Host-Encoded Sensors of Bacteria: Our Windows into the Microbial World. *MicrobiolSpectrum* **7** (2019).

470 Stamm, C. E., Collins, A. C. & Shiloh, M. U. Sensing of *Mycobacterium tuberculosis* and consequences to both host and bacillus. *Immunol. Rev.* **264**, 204-219, doi:10.1111/imr.12263 (2015).

471 Prinz, M. *et al.* Innate immunity mediated by TLR9 modulates pathogenicity in an animal model of multiple sclerosis. *J. Clin. Invest.* **116**, 456-464, doi:10.1172/JCI26078 (2006).

472 Reynolds, J. M. *et al.* Toll-like receptor 2 signaling in CD4(+) T lymphocytes promotes T helper 17 responses and regulates the pathogenesis of autoimmune disease. *Immunity* **32**, 692-702, doi:10.1016/j.immuni.2010.04.010 (2010).

473 Miranda-Hernandez, S. *et al.* Role for MyD88, TLR2 and TLR9 but not TLR1, TLR4 or TLR6 in experimental autoimmune encephalomyelitis. *J. Immunol.* **187**, 791-804, doi:10.4049/jimmunol.1001992 (2011).

474 Shaw, P. J. *et al.* Signaling via the RIP2 adaptor protein in central nervous system-infiltrating dendritic cells promotes inflammation and autoimmunity. *Immunity* **34**, 75-84, doi:10.1016/j.immuni.2010.12.015 (2011).

475 Chen, Z. *et al.* Association between toll-like receptors 9 (TLR9) gene polymorphism and risk of pulmonary tuberculosis: meta-analysis. *BMC Pulm. Med.* **15**, 57, doi:10.1186/s12890-015-0049-4 (2015).

476 Eisenbarth, S. C. *et al.* Lipopolysaccharide-enhanced, toll-like receptor 4-dependent T helper cell type 2 responses to inhaled antigen. *J. Exp. Med.* **196**, 1645-1651, doi:10.1084/jem.20021340 (2002).

477 Khan, N. *et al.* Signaling through NOD-2 and TLR-4 Bolsters the T cell Priming Capability of Dendritic cells by Inducing Autophagy. *Sci. Rep.* **6**, 19084, doi:10.1038/srep19084 (2016).

478 Allison, D. G. & Lambert, P. A. in *Molecular Medical Microbiology* Ch. 32, 583-598 (2015).

479 Brand, D. D., Latham, K. A. & Rosloniec, E. F. Collagen-induced arthritis. *Nat. Protoc.* **2**, 1269-1275, doi:10.1038/nprot.2007.173 (2007).

480 Wong, S. Y. *et al.* B Cell Defects Observed in *Nod2* Knockout Mice Are a Consequence of a *Dock2* Mutation Frequently Found in Inbred Strains. *J. Immunol.* **201**, 1442-1451, doi:10.4049/jimmunol.1800014 (2018).

481 Lang, R. Recognition of the mycobacterial cord factor by Mincle: relevance for granuloma formation and resistance to tuberculosis. *Front. Immunol.* **4**, 5, doi:10.3389/fimmu.2013.00005 (2013).

482 Behler, F. *et al.* Role of Mincle in alveolar macrophage-dependent innate immunity against mycobacterial infections in mice. *J. Immunol.* **189**, 3121-3129, doi:10.4049/jimmunol.1201399 (2012).

483 Olvany, J. M. *et al.* CLEC4E (Mincle) genetic variation associates with pulmonary tuberculosis in Guinea-Bissau (West Africa). *Infect. Genet. Evol.* **85**, 104560, doi:10.1016/j.meegid.2020.104560 (2020).

484 Dubé, J.-Y., Fava, V. M., Schurr, E. & Behr, M. A. Underwhelming or Misunderstood? Genetic Variability of Pattern Recognition Receptors in Immune Responses and Resistance to *Mycobacterium tuberculosis*. *Front. Immunol.* **12**, doi:10.3389/fimmu.2021.714808 (2021).

485 Zhang, X., Goncalves, R. & Mosser, D. M. The isolation and characterization of murine macrophages. *Curr. Protoc. Immunol.* **Chapter 14**, Unit 14.11, doi:10.1002/0471142735.im1401s83 (2008).

486 Scandurra, G. M. *et al.* Assessment of live candidate vaccines for paratuberculosis in animal models and macrophages. *Infect. Immun.* **78**, 1383-1389, doi:10.1128/iai.01020-09 (2010).

487 Hines, M. E. *et al.* Experimental challenge models for Johne's disease: A review and proposed international guidelines. *Vet. Microbiol.* **122**, 197-222, doi:https://doi.org/10.1016/j.vetmic.2007.03.009 (2007).

488 Stabel, J. R. & Ackermann, M. R. Temporal *Mycobacterium paratuberculosis* infection in T-cell receptor (TCR)-alpha and TCR-delta-deficient mice. *Vet. Immunol. Immunopathol.* **89**, 127-132, doi:10.1016/s0165-2427(02)00167-8 (2002).

489 Limjunyawong, N., Mock, J. & Mitzner, W. Instillation and Fixation Methods Useful in Mouse Lung Cancer Research. *JoVE*, e52964, doi:doi:10.3791/52964 (2015).

490 Bankhead, P. *et al.* QuPath: Open source software for digital pathology image analysis. *Sci. Rep.* **7**, 16878, doi:10.1038/s41598-017-17204-5 (2017).

491 Härtel, C. *et al.* NOD2 Loss-of-Function Mutations and Risks of Necrotizing Enterocolitis or Focal Intestinal Perforation in Very Low-birth-weight Infants. *Inflamm. Bowel Dis.* **22**, 249-256, doi:10.1097/mib.0000000000000658 (2016).

492 Johansson, M. E. *et al.* Innate immune receptor NOD2 promotes vascular inflammation and formation of lipid-rich necrotic cores in hypercholesterolemic mice. *Eur. J. Immunol.* **44**, 3081-3092, doi:10.1002/eji.201444755 (2014).

493 Kramnik, I., Dietrich, W. F., Demant, P. & Bloom, B. R. Genetic control of resistance to experimental infection with virulent *Mycobacterium tuberculosis*. *Proc. Natl. Acad. Sci. U. S. A.* **97**, 8560-8565, doi:10.1073/pnas.150227197 (2000).

494 Mayer-Barber, K. D. *et al.* Host-directed therapy of tuberculosis based on interleukin-1 and type I interferon crosstalk. *Nature* **511**, 99-103, doi:10.1038/nature13489 (2014).

495 Kleinnijenhuis, J. *et al.* Transcriptional and inflammasome-mediated pathways for the induction of IL-1beta production by *Mycobacterium tuberculosis*. *Eur. J. Immunol.* **39**, 1914-1922, doi:10.1002/eji.200839115 (2009).

496 Liu, F. *et al.* T cell-derived soluble glycoprotein GPIbα mediates PGE(2) production in human monocytes activated with the vaccine adjuvant MDP. *Sci Signal* **12**, doi:10.1126/scisignal.aat6023 (2019).

497 Bansal, K. & Balaji, K. N. Intracellular pathogen sensor NOD2 programs macrophages to trigger Notch1 activation. *J. Biol. Chem.* **286**, 5823-5835, doi:10.1074/jbc.M110.192393 (2011).

498 Ip, W. K. E., Hoshi, N., Shouval, D. S., Snapper, S. & Medzhitov, R. Anti-inflammatory effect of IL-10 mediated by metabolic reprogramming of macrophages. *Science* **356**, 513-519, doi:10.1126/science.aal3535 (2017).

499 Pei, G. *et al.* Cellular stress promotes NOD1/2-dependent inflammation via the endogenous metabolite sphingosine-1-phosphate. *The EMBO Journal* **40**, e106272, doi:https://doi.org/10.15252/embj.2020106272 (2021).

500 Gonzalez-Mancera, M. S., Forghani, I. & Mirsaeidi, M. Missense (p.Glu778Lys) and (p.Gly908Arg) variants of NOD2 gene are associated with recurrent pulmonary non-tuberculous mycobacterial infections. *Scand. J. Immunol.* **92**, e12935, doi:https://doi.org/10.1111/sji.12935 (2020).

501 Lee, J. Y. *et al.* Nucleotide-Binding Oligomerization Domain 2 Contributes to Limiting Growth of *Mycobacterium abscessus* in the Lung of Mice by Regulating Cytokines and

Nitric Oxide Production. *Front. Immunol.* **8**, 1477, doi:10.3389/fimmu.2017.01477 (2017).

502 Freund, J. & Lipton, M. M. Potentiating effect of *Nocardia asteroides* on sensitization to picryl chloride and on production of isoallergic encephalomyelitis. *Proc. Soc. Exp. Biol. Med.* **68**, 373-377, doi:10.3181/00379727-68-16490 (1948).

503 Du, P., Sohaskey, C. D. & Shi, L. Transcriptional and Physiological Changes during *Mycobacterium tuberculosis* Reactivation from Non-replicating Persistence. *Front Microbiol* **7**, 1346, doi:10.3389/fmicb.2016.01346 (2016).

504 Pisu, D. *et al.* Single cell analysis of M. tuberculosis phenotype and macrophage lineages in the infected lung. *J. Exp. Med.* **218**, doi:10.1084/jem.20210615 (2021).

505 Indrigo, J., Hunter, R. L. & Actor, J. K. Influence of trehalose 6,6'-dimycolate (TDM) during mycobacterial infection of bone marrow macrophages. *Microbiology (Reading)* **148**, 1991-1998, doi:10.1099/00221287-148-7-1991 (2002).

506 Indrigo, J., Hunter, R. L. & Actor, J. K. Cord factor trehalose 6,6'-dimycolate (TDM) mediates trafficking events during mycobacterial infection of murine macrophages. *Microbiology (Reading)* **149**, 2049-2059, doi:10.1099/mic.0.26226-0 (2003).

507 Katti, M. K. *et al.* The Delta *fbpA* mutant derived from *Mycobacterium tuberculosis* H37Rv has an enhanced susceptibility to intracellular antimicrobial oxidative mechanisms, undergoes limited phagosome maturation and activates macrophages and dendritic cells. *Cell. Microbiol.* **10**, 1286-1303, doi:10.1111/j.1462-5822.2008.01126.x (2008).

508 Brown, G. D. & Gordon, S. Immune recognition. A new receptor for beta-glucans. *Nature* **413**, 36-37, doi:10.1038/35092620 (2001).

509 Quintin, J. *et al. Candida albicans* infection affords protection against reinfection via functional reprogramming of monocytes. *Cell Host Microbe* **12**, 223-232, doi:10.1016/j.chom.2012.06.006 (2012).

510 Del Fresno, C., Iborra, S., Saz-Leal, P., Martínez-López, M. & Sancho, D. Flexible Signaling of Myeloid C-Type Lectin Receptors in Immunity and Inflammation. *Front. Immunol.* **9**, 804, doi:10.3389/fimmu.2018.00804 (2018).